Carl von Ossietzky
Universität
Oldenburg

The effect of amyloid-beta species and N,N-Diethyltryptamine on ageing

Von der Fakultät für Medizin und Gesundheitswissenschaften
der Carl von Ossietzky Universität Oldenburg

Doctor Rerum Naturalium (Dr. rer. nat.)

angenommene Dissertation

von Herrn
Michiel Van Bulck
geboren am **08.10.1991** in **Belgien**

Betreuender Gutachterin: **Prof. Dr. Anja U. Bräuer**

Weitere Gutachterin/Gutachter:
Prof. Dr. Angela Kuhla
Prof. Dr. Christoph Siegfried Herrmann

Tag der Disputation: **22.10.2025**

Table of content

Abbreviations

%	percentage
°C	degree Celsius
µL	microlitre
µm	micrometre
µM	micromolar
$\mu m^2/s$	micrometre square per second
µT	microtesla
3-HAA	3-hydroxyanthranilic acid
3-HAAO	3-hydroxyanthranilate 3,4-dioxygenase
3-HKYN	3-hydroxykynurenine
5-HIAA	5-hydroxyindole acetic acid
5-HT	5-hydroxytryptamine or serotonin
5-HTP	5-hydroxytryptophan
5-HTR	serotonin receptors
5-MeO-DMT	5-methoxy-N,N-dimethyltryptamines
AICD	intracellular APP domain
ApoE-ε4	apolipoprotein-E-ε4
APP	amyloid precursor protein
aSMase	acidic sphingomyelinase
Aß	amyloid-Beta
$Aß_{(1-40)}$	amyloid-Beta with 40 amino acids
$Aß_{(1-42)}$	amyloid-Beta with 42 amino acids
AU	arbitrary unit
Axialdiff	axial diffusion
BACE-1	β-secretase
BBB	blood-brain barrier
BDNF	brain-derived neurotrophic factor
BHT	butylhydroxytoluol
BPSD	behavioural and psychological symptoms of dementia
Brdu	5-bromo2-deoxyuridine
C1P	ceramide-1-phosphates
C1PP	ceramide phosphate phosphatase
C83	83 amino acid fragment
C99	CTF-β
Ca^{2+}	calcium
CDP-DAG	cytidine diphosphate-DAG
Cer	ceramides
CerK	ceramide kinase
CerS	ceramide synthase
CGT	ceramide galactosyltransferase
$CHCl_3$	Chloroform

CLQ	clorgyline hydrochloride
cm	centimetre
cPLA2	cytosolic phospholipase A2
Cr	creatine
CSF	cerebrospinal fluid
CTF-α	α-cleaved C-terminal fragment
CTRL	control
DAG	diacylglycerol
DAPI	4',6-diamino-2-phenylindole
ddH_2O	double-distilled water
DEGS	DHCer desaturase
DET	N,N-diethyltryptamines
DHCer	dihydroceramides
DHSM	dihydrosphingomyelins
DIV	days *in vitro*
DMEM	Dubecco's modified Eagle's medium
DMSO	dimethylsulfoxide
DMT	N,N-dimethyltryptamines
DPT	N,N-dipropyltryptamines
DTI	diffusion tensor imaging
E	embryonic
EPI	echo planar imaging
ER	endoplasmic reticulum
ERK	extracellular signal-regulated kinase
FA	fractional anisotropy diffusion
FBS	foetal bovine serum
FOV	field of view acquisition matrix
G/cm	Gauss per centimetre
G3P	glycerol-3-phosphate
GABA	γ-aminobutyric acid
GalCer	galactosyl ceramides
GDP	guanosine diphosphate
GlcCer	glucosyl ceramides
Gln	glutamine
Glu	glutamate
GM4	Neu5Acα2-3GalβCer
GPC	glycerophosphocholine
GSK-3	glycogen synthase kinase 3
GTP	guanosine triphosphate
h	hour
H_2O	water
hAPP SWe/Ldn	human APP Swedish/London

HBSS	Hanks' balanced salt solution
HCl	hydrochloric acid
HexCer	monohexosylceramides
HMG-CoA	3-hydroxy-3-methylglutaryl-coenzyme A
HPTLC	high-performance thin layer chromatography
HS	horse serum
Hz	Hertz
ICC	immunocytochemistry
IDO	indoleamine-2,3-dioxygenase
IHC	immunohistochemistry
iPLA2	Ca^{2+} independent Phospholipase A2
KAT	kynurenine aminotransferases
kg	kilogram
kHz	kilohertz
KMO	kynurenine 3-monooxygenase
KYNA	kynurenic acid
L	Litre
LacCer	lactosylceramides
LPA	lysophosphatidic acid
LPC	lysophosphatidylcholines
LPE	lysophosphatidylethanolamines
LPG	lysophosphatidylglycerols
LPLAT	lysoglycerophospholipid acyltransferase
LPS	lysophosphatidylserines
LTP	long term potentiation
Lyso-PAF	lyso-platelet-activating factor
M	molar
MAO	monoamine oxidase
MAO-A	monoamine oxidase A
MAO-B	monoamine oxidase B
MD	mean diffusion
MDD	major depressive disorders
mg	milligram
min	minutes
mL	millilitre
mm	millimetre
mm^3	cubic millimetre
$_{Mo/Hu}$APP695swe	chimeric mouse/human amyloid precursor protein
MRI	magnetic resonance imaging
MS	mass spectrometry
ms	millisecond
MS/MS	tandem mass spectrometry (tandem MS)

MT	magnetisation transfer
NAA	N-acetyl aspartate
NAAG	N-acetyl-aspartyl-glutamate
NAD+	nicotinamide adenine dinucleotide
NEP	neprylisins
ng	nanogram
NGS	normal goat serum
NH_3	ammonia
nM	nanomolar
NMDA	N-methyl-D-aspartic acid
nmol	nanomole
NSC	neuronal stem cells
nSMase	neutral sphingomyelinase
PA	phosphatidic acid
PAF	platelet-activating factor
PB	phosphate buffer
PBS	phosphate-buffered saline
PC	phosphatidylcholines
PCh	phosphocholine
PCr	phosphocreatine
PE	phosphatidylethanolamines
PFA	paraformaldehyde
PG	phosphatidylglycerols
PI	phosphatidylinositols
PIP	phosphatidylinositol phosphates
PKC	protein kinase C
PLA2	phospholipase A2
PLC	phospholipase C
PLL	poly-L-lysine
ppm	parts per million
PRESS	point-resolved spatially spectroscopy
PS	phosphatidylserines
PSD-95	postsynaptic density protein 95
PSEN-1	presenilin-1
PSEN1dE9	mutant human presenilin 1
PSEN-2	presenilin-2
QUINA	quinolinic acid
RAC1	ras-related C3 botulinum toxin substrate 1
Radialdiff	radial diffusion
RARE	rapid acquisition with relaxation enhancement
RELN	Reelin
RF	retention factors

ROI	region of interest
ROS	reactive oxygen species
RP	reverse-phase
s/mm^2	seconds per square millimetre
Sa	sphinganines
Sa1P	sphinganine-1-Phosphates
sAPPα	soluble APPα
sAPPβ	soluble APPβ
SD	standard deviation
SERT	serotonin reuptake transporters
SM	sphingomyelins
SMase	sphingomyelinase
SMDase	sphingomylin deacylase
SMS	sphingomyelin synthase
So	sphingosines
So1P	sphingosine-1-Phosphates
SPC	sphingosylphosphorylcholines
SphK 1	sphingosine kinase 1
SphK 2	sphingosine kinase 2
SPL	sphingosine-1-phosphate lyase
sPLA2	secreted Phospholipase A2
SR	sigma receptors
SR1	sigma-1 receptors
TAAR	trace amine-associated receptors
TCA	citric acid cycle
TE	time to echo
Tg	transgenic, carrying $_{Mo/Hu}$APP695swe/PSEN1dE9
TNF-α	tumour necrose factor-α
TPH	Trp hydroxylase
TR	repetition time
Trp	tryptophan
U/mL	units per millilitre
UGCG	uridine diphosphate glucose ceramide glucosyltransferase
v/v	volume per volume
Vglut-1	vesicular glutamate transport 1
WT	wild-type, carrying only endogenous mouse APP and PSEN-1

List of figures and supplementary figures

List of tables and supplementary tables

Summary

Ageing and its related disorders, like Alzheimer's disease (AD), are becoming a significant burden on contemporary society. Both are characterised by a gradual decline in cognitive abilities. An early effect involving physiological and pathological ageing is a change in neuroplasticity in the adult brain. These alterations are due to neuroinflammatory triggers such as abnormal aggregation of amyloid-beta (Aβ) species and metabolic factors in both the extracellular and intracellular environment of brain cells.

In the development of AD, two primary Aβ species, $Aβ_{(1–40)}$ and $Aβ_{(1–42)}$, are implicated, $Aβ_{(1–42)}$ being more toxic than $Aβ_{(1–40)}$. These Aβ species were reported to target synapses and aggregate preferentially within them. Reelin (RELN), a large extracellular matrix glycoprotein crucial for hippocampal neurogenesis and synaptic plasticity, provides neuroprotection against Aβ-induced toxicity. A longitudinal study of AD rodents has not fully elucidated the relationship between RELN and neuroinflammation. To address this gap, we conducted preliminary observations of specific regions on brain slices and neurosphere cultures using immunofluorescence imaging. In a longitudinal study in a 2-to-12-month AD mice model, we looked for microgliosis and RELN. Additionally, we examined adult neurogenesis in neurospheres from a group of approximately 16-month-old wild-type and transgenic mice. Our observation revealed a possible dysregulation of RELN in aged and transgenic animals, as well as an impairment in adult neurogenesis. Understanding the role of RELN in providing neuroprotection against Aβ-induced toxicity in AD not only sheds light on the mechanisms of neurodegeneration but also bridges the gap to exploring how Aβ species influence synaptic function and lipid metabolism in neuronal cells.

Aβ species have been seen to influence various cellular and molecular processes in neuronal cells in AD. However, the influence of these Aβ species on active synapses is poorly understood. It has been indicated that the interaction of lipids with these Aβ species could be a possible underlying effect of early synaptic dysfunction, which leads to cognitive impairment in AD. In another study, we could provide a better understanding of the influence of these Aβ species on active synapse loss and lipid alterations *in vitro*. However, the exact time-dependent effect of lipid alterations caused by these Aβ species on neuronal cells remains unknown. Therefore, we conducted an investigation using hippocampal neurones and glial cells after either 3 hours or 12 hours of treatment with $Aβ_{(1–40)}$ and $Aβ_{(1–42)}$. We found that lipid alterations occur before the loss of active synapses. Additionally, we discovered that lipid profiles of sphingolipid and glycerophospholipid classes in these brain

cells are altered depending on the variation in Aβ species and duration of treatment. Furthermore, our findings indicate that the loss of active synapses is not dependent on the specific Aβ species.

This exploration into the mechanisms of neurodegeneration and the impact of Aβ species on synaptic function and lipid metabolism in AD naturally leads us to consider the potential therapeutic interventions currently under investigation. Therapeutic intervention for AD currently focuses on delaying disease progression and managing the deterioration symptoms of cognitive impairment. Despite decade-long research, efforts to find drugs to prevent or even reverse AD pathology have been challenging. Therefore, the use of tryptamine derivatives might show a new promising role in addressing the behavioural and psychological symptoms of dementia (BPSD) associated with AD. In addition, these tryptamine derivatives are anti-inflammatory and neuroprotective in neurological disorders. Recent *in vitro* and *in vivo* studies have demonstrated that N,N-dimethyltryptamine (DMT) and its derivatives might have an anti-neuroinflammatory and neuroprotective role in AD. The potential impact of N,N-diethyltryptamine (DET), which shares structural similarities to DMT, remains to be elucidated.

Due to promising results with these previous tryptamine derivatives in Dr. Ana Perez Castillo's laboratory affiliated with CIBERNED and CSIC-UAM in Madrid (Spain), they showed a reduced neuroinflammatory response and improved adult neurogenesis *in vitro* and *in vivo*. Therefore, we tried to examine the role of DET in AD models. We performed both magnetic resonance imaging (MRI) and magnetic resonance spectroscopy (MRS) to elucidate the effect of DET in the AD rodent brain. Unfortunately, our data revealed no significant effect on the structural integrity, Aβ accumulation and metabolic spectrums after DET treatment. However, some macromolecules and lipid resonance spectra were indicated to be important for further research clarification.

To conclude, our results indicate a potential role of lipids as an early diagnostic biomarker and a conceivable effect of DET for further in-depth investigation as a novel therapeutic agent in amyloidosis-related disorders. We also saw that time and Aβ species are crucial factors in lipid alterations. Further, no specific Aβ species-dependent alterations are seen in the loss of active synapses. Despite this, we saw changes in neuroplasticity and neuroinflammation during this preliminary observation; however, this needs to be further elucidated.

Zusammenfassung

Das Altern und die damit verbundenen Erkrankungen wie die Alzheimer-Erkrankung stellen eine zunehmende Belastung für die heutige Gesellschaft dar. Beide sind durch einen Rückgang der kognitiven Fähigkeiten gekennzeichnet. Die erste Auswirkung des physiologischen und pathologischen Alterns ist jedoch eine Veränderung der Neuroplastizität im erwachsenen Gehirn. Diese Veränderungen sind auf neuroinflammatorische Auslöser wie die abnormale Aggregation von Amyloid-beta (Aβ)-Spezies und metabolische Faktoren sowohl in der extrazellulären als auch in der intrazellulären Umgebung der Gehirnzellen zurückzuführen.

An der Enstehung der Alzheimer-Erkrankung sind primäre zwei Aβ-Spezies, $Aβ_{(1-40)}$ und $Aβ_{(1-42),}$ beteiligt. Wobei $Aβ_{(1-42)}$ die toxischere der beiden Aβ-Spezies. Es wurde berichtet, dass diese Aβ-Spezies Synapsen angreifen und dort bevorzugt aggregieren. Reelin (RELN), ein großes extrazelluläres Matrixglykoprotein, das für die Neurogenese im Hippocampus und die synaptische Plastizität wichtig ist, scheint neuroprotektiv gegen Aβ-induzierte Toxizität zu sein. RELN ist im Zusammenhang mit Alzheimer-Erkrankung untersucht worden. Der spezifische Zusammenhang zwischen RELN und Neuroinflammation wurde jedoch noch nicht in einer Längsschnittstudie an Alzheimer-Erkrankung-Nagetieren untersucht. Deshalb haben wir bestimmte Regionen in Gehirnschnitten und Neurosphärenkulturen mit Hilfe von Immunfluoreszenzaufnahmen untersucht. In einer Längsschnittstudie mit einem Alzheimer-Erkrankung-Mausmodell im Alter von 2-12 Monaten versuchten wir, Mikrogliose und RELN zu beobachten. Außerdem untersuchten wir die adulte Neurogenese in Neurosphären aus einer Gruppe von ca. 16 Monate alten Wildtyp- und transgenen Mäusen. Wir beobachteten eine Dysregulation von RELN in alten und transgenen Tieren sowie eine Beeinträchtigung der adulten Neurogenese. Das Verständnis der Rolle von RELN bei der Bereitstellung von Neuroprotektion gegen Aβ-induzierte Toxizität bei Alzheimer-Erkrankung wirft nicht nur ein Licht auf die Mechanismen der Neurodegeneration, sondern schlägt auch eine Brücke zur Erforschung, wie Aβ-Spezies die synaptische Funktion und den Lipidstoffwechsel in neuronalen Zellen beeinflussen.

Es wurde festgestellt, dass Aβ-Spezies bei der Alzheimer-Erkrankung verschiedene zelluläre und molekulare Prozesse in neuronalen Zellen beeinflussen. Allerdings ist der Einfluss dieser Aβ-Spezies auf aktive Synapsen nur unzureichend verstanden. Es wurde angedeutet, dass die Interaktion von Lipiden mit diesen Aβ-Spezies eine mögliche

Auswirkung der frühen synaptischen Dysfunktion sein könnte, die zu kognitiven Beeinträchtigungen auf Grund der Alzheimer-Erkrankung führt. Unsere Studie könnte ein besseres Verständnis des Einflusses dieser Aβ-Spezies auf den aktiven Synapsenverlust und die Lipidveränderungen *in vitro* ermöglichen. Die genaue zeitabhängige Wirkung der durch diese Aβ-Spezies verursachten Lipidveränderungen auf neuronale Zellen ist jedoch noch nicht bekannt. Deshalb untersuchten wir Hippocampus-Neuronen und Gliazellen entweder nach 3 Stunden oder nach 12 Stunden Behandlung mit $A\beta_{(1-40)}$ und $A\beta_{(1-42)}$. Wir fanden heraus, dass die Lipidveränderungen vor dem Verlust der aktiven Synapsen auftreten. Außerdem entdeckten wir, dass die Lipidprofile der Sphingolipid- und Glycerophospholipidklassen in diesen Gehirnzellen in Abhängigkeit von der Variation der Aβ-Spezies und dem Zeitintervall der Behandlung verändert sind. Wir fanden auch heraus, dass der Verlust aktiver Synapsen unabhängig von der Aβ-Spezies ist.

Die Erforschung der Mechanismen der Neurodegeneration und der Auswirkungen von Aβ-Spezies auf die synaptische Funktion und den Lipidstoffwechsel bei Alzheimer-Erkrankung führt uns natürlich zu den potenziellen therapeutischen Interventionen, die derzeit untersucht werden. Die derzeitige therapeutische Intervention bei Alzheimer-Erkrankung besteht darin, das Fortschreiten der Krankheit zu verzögern und die Symptome der Verschlechterung der kognitiven Fähigkeiten zu behandeln. Trotz jahrzehntelanger Forschung konnte noch keine Therapie zur Vorbeugung der Alzheimer-Erkrankung gefunden werden. Der Einsatz von Tryptaminderivaten könnte dazu beitragen, die bei Alzheimer-Erkrankung auftretenden verhaltensbezogenen und psychologischen Symptome der Demenz (BPSD) zu überwinden. Diese Tryptaminderivate haben sich bei neurologischen Störungen als entzündungshemmend und neuroprotektiv erwiesen. Jüngste In-vitro- und In-vivo-Studien haben gezeigt, dass N,N-Dimethyltryptamin (DMT) und seine Derivate eine entzündungshemmende und neuroprotektive Wirkung bei Alzheimer-Erkrankung haben könnten. Die Wirkung von N,N-Diethyltryptamin (DET), das dem DMT strukturell ähnlich ist, ist noch nicht bekannt.

Aufgrund der vielversprechenden Ergebnisse mit diesen früheren Tryptaminderivaten im Labor von Dr. Ana Perez Castillo, die dem CIBERNED und dem CSIC-UAM in Madrid (Spanien) angegliedert ist, wo sie eine verringerte neuroinflammatorische Reaktion und eine verbesserte adulte Neurogenese *in vitro* und *in vivo* zeigten. Deshalb haben wir versucht, die Rolle von DET in Alzheimer-Erkrankung-Modellen zu untersuchen. Wir führten sowohl Magnetresonanztomographie (MRT) als auch Magnetresonanzspektroskopie (MRS) durch,

um die Wirkung von DET im Gehirn von Alzheimer-Erkrankung-Nagern zu untersuchen. Leider zeigten unsere Daten keine signifikanten Auswirkungen auf die strukturelle Integrität, die Aβ-Akkumulation und die Stoffwechselspektren nach der DET-Behandlung. Allerdings wurden einige Makromoleküle und Lipidresonanzspektren als wichtig für die weitere Forschung identifiziert.

Zusammenfassend lässt sich sagen, dass unsere Ergebnisse auf eine potenzielle Rolle der Lipide als frühzeitiger diagnostischer Biomarker hinweisen und dass die Wirkung von DET als neuartiges therapeutisches Mittel bei mit Amyloidose zusammenhängenden Erkrankungen eingehender untersucht werden sollte. Wir haben auch gesehen, dass Zeit und Aβ-Spezies entscheidende Faktoren für Lipidveränderungen sind. Außerdem wurden keine spezifischen, von der Aβ-Spezies abhängigen Veränderungen beim Verlust aktiver Synapsen festgestellt. Trotzdem haben wir während dieser vorläufigen Beobachtung Veränderungen in der Neuroplastizität und der Neuroinflammation gesehen, was jedoch noch weiter aufgeklärt werden muss.

1. Introduction

Alzheimer's disease (AD) is a multifactorial disorder and the most prevalent dementia in the elderly. According to the World Health Organization, in 2023, the estimated cases of dementia will impact over 50 million individuals globally and are predicted to double by 2050 (Nichols et al., 2022). In addition, behavioural and psychological symptoms of dementia (BPSD), such as major depressive disorders (MDD), have a multifaceted, interconnected relationship with AD. Growing evidence indicates shared genetic factors, neurobiological mechanisms, and pathophysiological pathways linking these two disorders (Botto et al., 2022; Cassano et al., 2019; Chakraborty et al., 2019).

AD is generally described as a complex neurological disorder, pathological characterised by the accumulation of amyloid-beta (Aβ) plaques and neurofibrillary tangles. The neurofibrillary tangles consist of Tau protein. These pathological features lead to progressive neurodegeneration and cognitive decline. There is a growing understanding of the bidirectional link between AD and MDD, with MDD being considered both a risk factor and a symptom of AD. In addition, early-stage MDD, especially when accompanied by amyloid pathology, is associated with an increased risk of developing AD later in life (Cassano et al., 2019). However, the precise nature of the relationship between MDD and AD, and whether MDD is a prodromal symptom or an independent risk factor for AD, remains unclear.

AD and MDD have been linked to a range of neurobiological mechanisms, such as neuroinflammation, increased amyloid deposition, neurodegeneration, and deficiencies in neuroplasticity processes like neurogenesis and synaptic plasticity. The impact of impairment of adult hippocampal neurogenesis and disrupted synaptic plasticity have been observed in the pathophysiology of both AD and MDD (Morales-Garcia et al., 2020; Pilozzi et al., 2023).

The alterations in lipid metabolism, particularly in glycerophospholipids and sphingolipids, have been investigated in these disorders. Disruption of these lipid classes has been demonstrated to contribute to neuroinflammation, oxidative stress, and impaired neuronal membrane integrity, all of which are key pathological features of AD and MDD (Kao et al., 2020). Furthermore, lipid metabolism has been found to play a vital role in neurogenesis and synaptic plasticity, suggesting a potential link between lipid dysregulation and the observed impairments in neuroplasticity in both pathological conditions (Alaamery et al., 2021; Farooqui et al., 2000b; Kao et al., 2020).

There are several therapeutic interventions available to alleviate the symptomatic patterns of depressive-like systems in AD. Commonly prescribed antidepressants such as selective serotonin reuptake inhibitors, serotonin-norepinephrine reuptake inhibitors and monoamine inhibitors (MAOI) have been utilised in the treatment of MDD in AD patients. However, their effectiveness remains a topic of debate (Cassano et al., 2019). Therefore, emerging research has indicated that N,N-tryptamine-based compounds, capable of modulating serotonin and other neurotransmitter systems, may offer potential benefits for both MDD and AD. These benefits are attributed to the pathways that promote neurogenesis and neuroplasticity while reducing neuroinflammation (Cassano et al., 2019; Morales-Garcia et al., 2020).

1.1. The amyloid cascade hypothesis and neuroinflammatory processes

Genetically AD can be divided into early onset, known as “Familial AD”, affecting patients under 65 years old (approximately 5%), and late-onset or “Idiopathic AD”, affecting patients 65 years and older (approximately 95%). In Idiopathic AD, the presence of apolipoprotein-E-ε4 (ApoE-ε4) allele isoforms has been linked to a higher risk of developing the disease at a younger age (Holtzman et al., 2011; Reitz & Mayeux, 2014). Conversely, Familial AD is attributed to autosomal mutations in genes, including amyloid precursor protein (APP) on chromosome 21q, presenilin-1 (PSEN-1) on chromosome 14 and presenilin-2 (PSEN-2) on chromosome 1 (Benilova et al., 2012; van der Flier et al., 2011; Zhang et al., 2013).

In the early stages of AD, extracellular Aβ deposits stimulate an inflammatory response by microglia and immune cells, leading to pathological changes such as Tau pathology, synaptic dysfunction, and neurodegeneration. However, mitochondrial dysfunction, characterised by oxidative stress, has been identified as the primary cause of neuroinflammation in AD. Studies have shown that PSEN-1 and PSEN-2 proteins are located on the endoplasmic reticulum (ER) and mitochondrial-associated membranes. Mutations in PSEN-1 and PSEN-2 lead to increased cytosolic Ca^{2+} in mitochondrial-associated membranes, which in turn triggers an increase in reactive oxygen species (ROS) (Kim et al., 2015).

Here, we will only focus on the amyloid cascade hypothesis and the involvement of Aβ in neuroinflammation. In addition, genome-wide studies have pinpointed several genetic risk factors, such as ATP-binding cassette subfamily A, bridging integrator 1, clusterin, GRB-associated binding protein 2, galanin-like peptide, phosphatidylinositol binding clathrin

assembly protein and triggering receptors expressed on myeloid cells 2, which are involved in lipid metabolism and immunity processes. Also, risk factors such as MDD and stress can impact and modify AD pathology (Kepp et al., 2023).

The amyloid cascade hypothesis suggests that the amyloid precursor protein (APP) plays a crucial role in both non-amyloidogenic and amyloidogenic pathways. In the amyloidogenic pathway, which primarily occurs in endosomal compartments, the cleavage of APP results in Aβ, leading to the formation of senile plaques (Rajendran & Annaert, 2012) (Figure 1).

The non-amyloidogenic pathway (Figure 1), primarily located at the plasma membrane, involves the cleavage of APP by α-secretase, which belongs to ADAM (a disintegrin and metalloprotease) family (Rajendran & Annaert, 2012). Among ADAM-9, ADAM-10, and ADAM-17, ADAM-10 appears to be the main α-secretase, responsible for generating a significant amount of soluble APPα (sAPPα) and α-cleaved C-terminal fragment (CTF-α), as well as an 83 amino acid fragment (C83) (De Strooper, 2010; Kuhn et al., 2010; Nhan et al., 2015). The α-CTF, when cleaved by γ-secretase (which contains the catalytic subunit of presenilin), releases p3 peptide and intracellular APP domain (AICD), neither of which contributes to Aβ formation or promotes the activity of the ADAM-10 (De Strooper, 2010).

The amyloidogenic pathway (Figure 1) involves the proteolytic cleavage of APP by β-secretase (BACE-1), resulting in the production of soluble APPβ (sAPPβ) and CTF-β (C99). CTF-β serves as a substrate for γ-secretase, leading to the generation of Aβ and AICD (De Strooper et al., 2010). It has been noted that Aβ can be eliminated from the brain through enzymatic (e.g., Aβ-degrading enzymes such as neprilysin (NEP) and matrix metalloproteinases (MMP)) or non-enzymatic mechanisms (e.g., interstitial fluid, uptake by microglial phagocytosis and transport across the blood-brain barrier (BBB)) (Ries & Sastre, 2016; Żukowska et al., 2024). NEP is primarily located in the axons and synapses of neurones, while MMP (e.g., MMP-2 and MMP-9) is predominantly expressed in astrocytes and microglia. These enzymes are upregulated in response to $A\beta_{(1-40)}$ and $A\beta_{(1-42)}$ peptides and inflammatory processes. This upregulation enhances the breakdown of toxic Aβ oligomers by altering the permeability of the BBB (Yan et al., 2006; Yin et al., 2006). However, NEP has also been seen in activated astrocytes and microglia. NEP levels decrease with age in various brain regions, such as the cortex and hippocampus, which are crucial for early Aβ accumulation. MMP and NEP are overexpressed in astrocytes within amyloid plaques. In both early- and late-onset AD, impaired Aβ clearance is linked to NEP

deficiency (Hatami et al., 2017; Iwata et al., 2001; Mawuenyega et al., 2010; Yan et al., 2006; Yin et al., 2006).

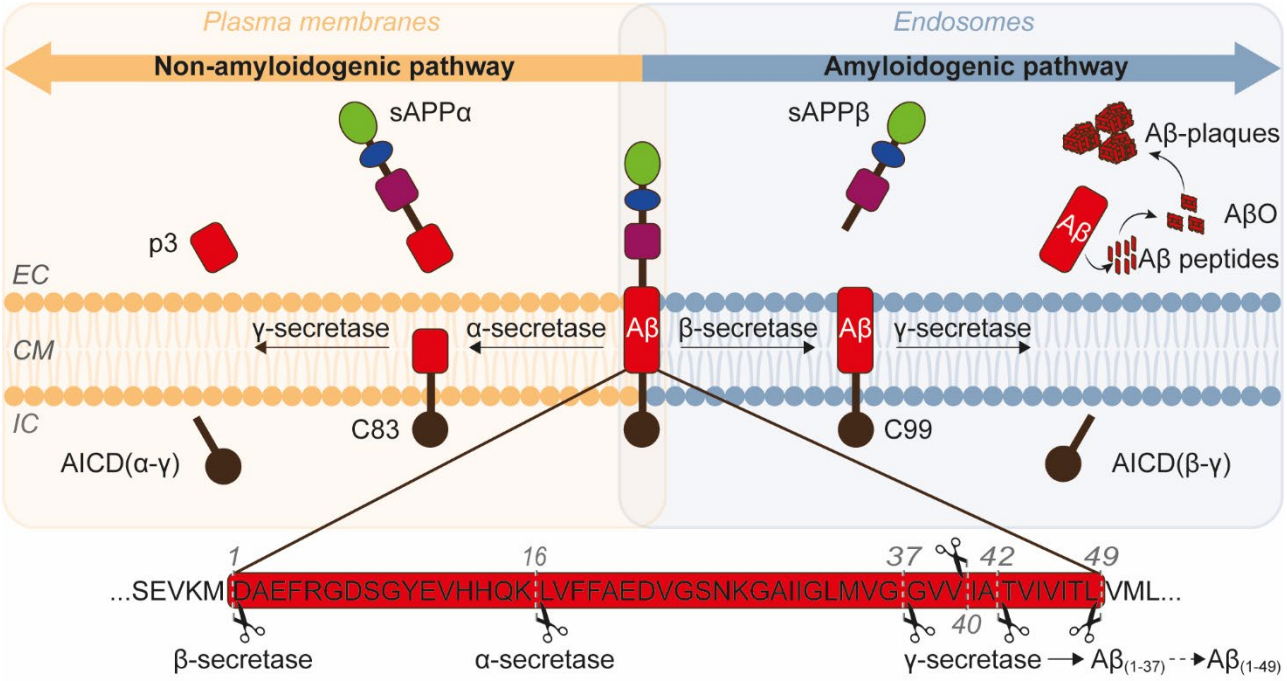

Figure 1: *APP cleavage pathways*

In the non-amyloidogenic pathway, α-secretase cleavage at plasma membranes results in the production of soluble APPα (sAPPα) fragments and 83 amino acid fragments (C83), which are further cleaved in p3 peptide and C-terminal intracellular domain (AICD) by γ-secretase. In the amyloidogenic pathway, cleavage by β-secretase at the endosomal location leads to the production of soluble APPβ (sAPPβ) fragment and a 99 amino acid fragment (C99), which is then cleaved by γ-secretase, resulting in different extracellular Aβ-peptides and AICD. The Aβ section (red) is in the transmembrane. In the amyloidogenic pathways, cleavage γ-secretase contributes to the production of Aβ peptides with varying amino acid lengths ($Aβ_{(1-37)}$ → $Aβ_{(1-49)}$). These Aβ peptides can aggregate into soluble amyloid fibrils and fibrillar oligomers (AβO). Furthermore, these AβO can accumulate and lead to the formation of insoluble Aβ plaques. Other abbreviations: EC, extracellular compartment; IC, intracellular compartment; CM, cell membrane. The illustration was created using Adobe Illustrator CC 2024.

Neuroinflammatory processes play a significant role in AD, with glial cells such as astrocytes and microglia recognised as major contributors. These cells are crucial due to their immune functions, which become dysregulated in AD. In physiological conditions, their immune responses are under tight control. However, in pathophysiological states, such as neuronal death, these immune responses become exacerbated over time. In AD, a self-perpetuating positive feedback loop between neuronal death and neuroinflammation arises due to the Aβ accumulation. Each of these processes fuels and exacerbates the other. The activation of astrocytes and microglia, triggered by the binding of misfolded Aβ proteins to the toll-like

receptors and nod-like receptor protein-3 on these glial cells, stands out as the critical cause for AD neuroinflammation (Guo et al., 2020).

In addition, the damage-associated molecular patterns found in AD activate other pattern recognition receptors on glial cells, contributing to their activation (Amor et al., 2014). The prolonged exposure of glial cells to Aβ and damage signals in this progressive disorder leads to exacerbated immune responses. These immune responses trigger the production of various substances such as free radicals, caspases, prostanoids, neuroprotectin D1, pro-inflammatory cytokines (IL-6, IL-1β and TNF-α) and chemokines (CXCL1, CCL2, CCL4, and CCL11) by the activated glial cells. These inflammatory substances activate pathways leading to neuronal death and perpetuate the cycle by stimulating additional astrocytes and microglia cells, causing the amplification of the neuroinflammatory responses (Heneka et al., 2015). It has been demonstrated that glial cells play a crucial role in the clearance and breakdown of Aβ, an essential factor in Aβ-induced inflammatory processes. However, glial activation could protect against Aβ-induced neuronal toxicity (Ries & Sastre, 2016). Furthermore, we will explore the variation in Aβ peptides, their toxicity and their impact on synaptic aberration and neurodegeneration.

1.1.1. Amyloid-beta peptides: $A\beta_{(1-40)}$ and $A\beta_{(1-42)}$

The amyloidogenic pathway produces Aβ peptides, a significant factor in AD. Aβ peptide was first isolated and characterised as a protein with an approximate molecular weight of 4 kilodaltons in 1984 by Glenner and Wong (Glenner & Wong, 1984). The Aβ peptides can take on various structural forms, including soluble monomeric Aβ, dimers, and oligomers. The oligomers are small soluble clusters of several monomers. Aβ can also exist as protofibrils, soluble intermediates, representing a transitional phase towards more prominent and stable fibrillar structures. The stable oligomeric species, fibrillar structures, and insoluble deposits accumulate in amyloid plaques, which are unable to cross between the intra- and extracellular space of the cell (Gouras et al., 2010; Klementieva et al., 2017).

The soluble Aβ intermediate structures are identified as the most neurotoxic species, posing a greater threat to neuronal viability than insoluble Aβ fibrils. The cleavage location of the γ-secretase substrate complex determines the production of Aβ species with varying amino acid lengths ($A\beta_{(1-49)}$ → $A\beta_{(1-37)}$, as shown in Figure 1). $A\beta_{(1-40)}$ and $A\beta_{(1-42)}$ are the two major Aβ species in the brain, with soluble $A\beta_{(1-40)}$ being more prevalent than soluble $A\beta_{(1-42)}$ forms. However, longer Aβ peptides, such as $A\beta_{(1-42)}$, are more hydrophobic, neurotoxic and more

prone to aggregation than $A\beta_{(1-40)}$. $A\beta_{(1-42)}$ oligomers also exhibit greater stability compared to $A\beta_{(1-40)}$ (Coalier et al., 2013; Masters & Selkoe, 2012). The aggregation of these Aβ species in AD is highly regulated by time and their aggregation affinity (Gouras et al., 2010; Thal et al., 2000b).

Extensive *in vitro* and *in vivo* research demonstrated that the build-up of soluble Aβ species, particularly $A\beta_{(1-42)}$, tends to accumulate at synaptic sites, which are the specialised junctions facilitating communication between neurones (Gouras et al., 2010; Lacor et al., 2004). Experimental results have shown that other Aβ species, such as Aβ oligomers, especially low molecular weight types, might trigger synapse failure and memory impairment (Ferreira & Klein, 2011; Takahashi et al., 2004). Additionally, research studies using AD mouse models and human brains have demonstrated that the Aβ accumulation leads to a shift of intraneuronal $A\beta_{(1-42)}$ toward the extracellular Aβ pool (Gouras et al., 2010; Gouras et al., 2000). The interaction between intracellular and extracellular $A\beta_{(1-42)}$ could have a substantial effect on the progression of AD. These findings suggest that extracellular Aβ could enhance the intraneuronal $A\beta_{(1-42)}$, which is responsible for neurotoxicity induced by the intracellular Aβ pool (Oddo et al., 2006; Takahashi et al., 2002). Therefore, intracellular Aβ accumulation may initiate early synaptic alterations, while extracellular amyloid deposition represents a later stage in the progression of AD.

1.1.2. Aβ peptides in synaptic dysfunction and neurodegeneration

The accumulation of Aβ peptides at synapses has been shown to have detrimental effects on synaptic plasticity. Synaptic plasticity refers to the ability of synapses to undergo structural and functional changes in response to neuronal activity (Zhang et al., 2022b). The presence of Aβ at synaptic sites disrupts the processes involved in long-term potentiation (LTP), a crucial mechanism underlying learning and memory formation. By impairing this process, the accumulation of Aβ at synapses disrupts the ability to establish and maintain solid synaptic connections, ultimately leading to impairment in learning and memory processes (Zhang et al., 2022b).

Recent extensive research (notably reviewed in (Zhang et al., 2022b)), has demonstrated that Aβ species exert varying effects on both pre- and postsynaptic densities, influenced by several factors: Aβ concentration, Aβ chemical structure (α-helical or β-sheet), duration of Aβ exposure, and the aggregation state of Aβ (monomers, oligomers, or fibrils) (Almeida et al., 2005; Cai et al., 2023; Hu et al., 2009; Sokolow et al., 2012; Takahashi et al., 2003;

Takahashi et al., 2004). The interplay of these factors can determine the differential influences and the impacts of Aβ species on synaptic structures and their function. Synapses are critical mediators in this context, as Aβ accumulates and aggregates preferentially in synaptic terminals in AD, often occurring before the formation of plaques. Notably, studies have shown that oligomeric Aβ levels in the synaptosomes (isolated synaptic terminals) of neurones are elevated in the early stages of AD but not observed in the brains of cognitively normal individuals who are at risk of developing AD pathology (Bilousova et al., 2016; Lacor et al., 2004; Takahashi et al., 2004).

The discussion regarding the presumed neurotoxicity of various Aβ species in the brain is an ongoing debate. It is essential to clarify the exact physiological and pathological pathways involved in the cleavage of APP and its various Aβ products. This is especially important given the differing findings seen in human studies compared to animal studies (Brothers et al., 2018; Morley et al., 2010; Morley et al., 2019). It has been proposed that the levels of Aβ in the human brain and cerebrospinal fluid vary from the nanomolar to the picomolar scale, while pathological levels span from nanomolar to micromolar levels (Cai et al., 2023). Both low and high concentrations can negatively impact synaptic functions and inflammatory responses. Previous research indicates that Aβ species begin to aggregate from monomeric to oligomeric forms within approximately 1 to 3 hours, with continued aggregation occurring over time (Chemuru et al., 2016). Personal laboratory experience and insights from previous colleagues (Willén et al., 2017) in the field suggest that specific synthetic human Aβ species exhibit heterogenous binding and uptake in culture neurones.

Given the discrepancy in the literature concerning Aβ species ($Aβ_{(1-40)}$ and $Aβ_{(1-42)}$) and their concentrations associated with pathological features, we conducted experiments at two distinct time points using synthetic human $Aβ_{(1-40)}$ and $Aβ_{(1-42)}$. Our goal was to explore the effect of early and late Aβ aggregation on synaptic loss and the pathological impacts of these Aβ species.

1.2. Inflammatory signalling and serotonergic dysregulation: linking amyloid pathology and BPSD

Inflammation could be a possible connection between AD and MDD. The imbalance of cytokines resulting from inflammatory responses might influence the serotonin levels and the metabolism of Aβ in the brain. Therefore, it suggests that AD and MDD might share a common pathophysiological mechanism. A crucial link exists in the metabolism of

tryptophan (Trp) metabolism within the gut-brain axis, impacting both AD and neuropsychiatric disorders such as MDD (Cutuli et al., 2022). Herein, we will mainly focus on the Aβ-related dysregulation of serotonergic and neuroinflammatory pathways in both AD and MDD. Consequently, in the following sections, we will provide an overview of the Trp metabolism and its effect on the production and aggregation of Aβ.

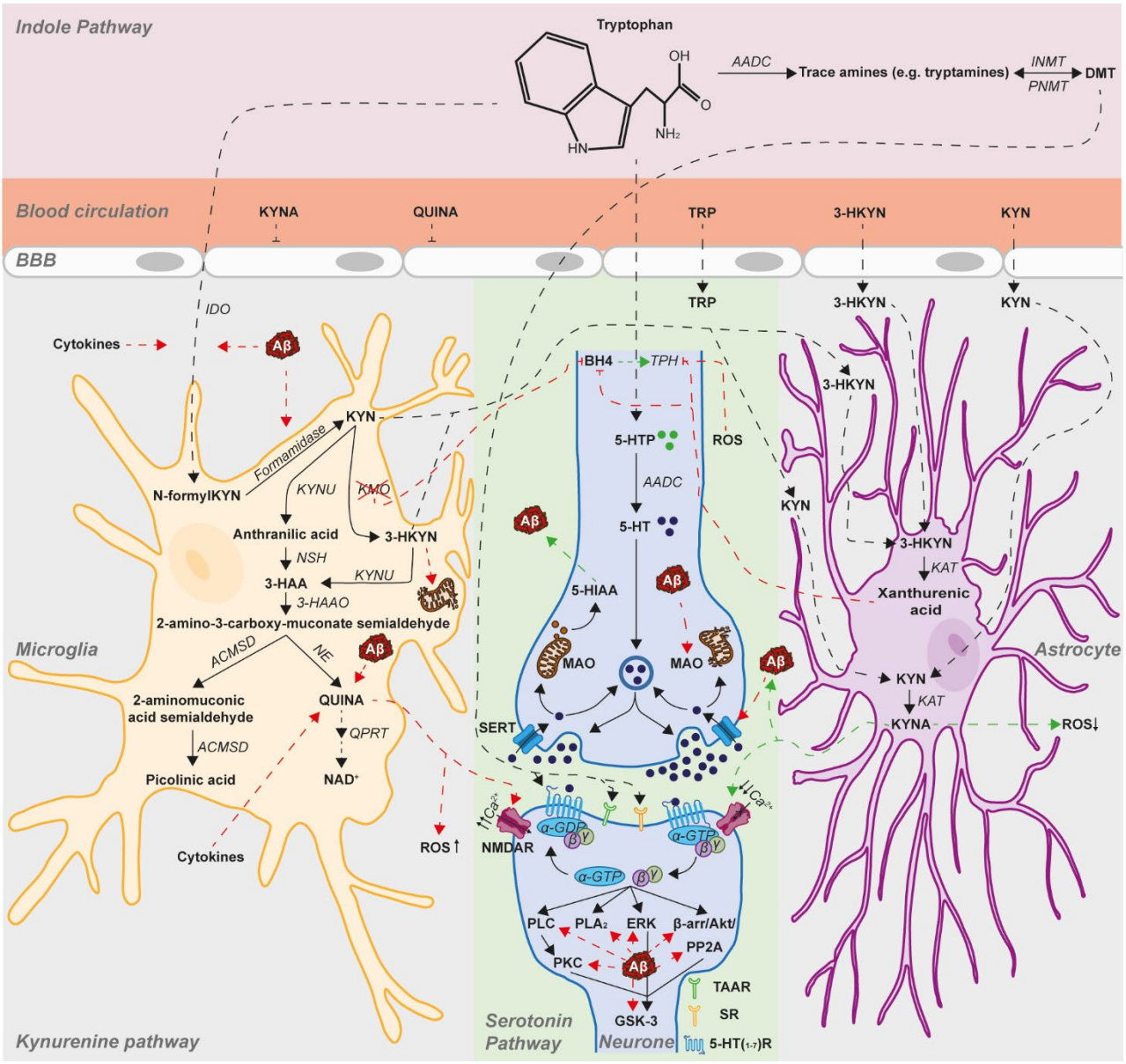

Figure 2: *Tryptophan metabolism in the brain and its dysregulation in AD*

Tryptophan (Trp) can be metabolised through the indole, kynurenine and serotonin pathways. Within the indole pathway, Trp can be converted by aromatic amino acid decarboxylase (AADC) into various trace amines, explicitly focussing on the tryptamines. N,N-dimethyltryptamine (DMT) can be synthesised through indolethylamine-N-methyltransferase or catabolised into other trace amines through phenylethanolamine N-methyltransferase (PNMT). DMT can cross the blood-brain barrier (BBB) and stimulate serotonin receptors (5-HTR), trace amine-associated receptors (TAAR) and sigma receptors (SR). In the kynurenine pathway, a variety of metabolites are produced, some of which are neurotoxic (e.g., quinolinic acid (QUINA), 3-

hydroxykynurenine (3-HKYN), 3-hydroxyanthranilic acid (3-HAA)) and others that are neuroprotective (e.g., kynurenic acid (KYNA), picolinic acid, nicotinamide adenine dinucleotide (NAD+)). While metabolites such as Trp, 3-HKYN and kynurenine (KYN) can cross the BBB, KYNA and QUINA need to be produced in microglial cells or astrocytes. KYNA generated in astrocytes through kynurenine aminotransferase (KAT) helps prevent the NMDA receptor excitotoxicity from abundant intracellular calcium (Ca^{2+}) influx (green dashed arrows). Additionally, KYNA enhances Aβ clearance and modulates reactive oxygen species (ROS) activity (green dashed arrows). A similar protective effect has been ascribed to 5-hydroxyindoleacetic acid (5-HIAA), formed by the breakdown of 5-HT through monoamine oxidase (MAO). 5-HIAA also alleviates neuroinflammatory responses by reducing ROS levels (green dashed arrows). Conversely, 3-HKYN can induce oxidative mitochondrial damage and increase the production of ROS (red dashed arrows). QUINA, produced in microglia, acts as an opposite stressor compared to KYNA. Additionally, QUINA has been shown to rise in response to Aβ toxicity (red dashed arrows). Inhibition of kynurenine monooxygenase (KMO) results in decreased levels of xanthurenic acid and elevated ROS activity, which can suppress the activity of Trp hydroxylase (TPH) and BH4 (cofactor of TPH). This suppression ultimately hinders the synthesis of the neurotransmitter serotonin (5-HT), leading to a reduction in downstream serotonin pathways (PLC, PLA2, ERK, β-arrestin/Akt/PP2A) through the inactivation of the intracellular G-coupled αβγ complex. In AD, neurotoxicity from Aβ disrupts these pathways, which promote the production and aggregation of Aβ peptides. Furthermore, the proinflammatory response by cytokines is amplified by Aβ synthesis and impaired Aβ clearance due to TDO modulation, resulting in an increase of 3-HKYN and QUINA and a decrease in KYNA. In addition, serotonin reuptake transporters (SERT) and mitochondrial dysfunction are negatively affected in AD due to Aβ toxicity. Other abbreviations: N-formylKYN, N-formylkynurenine; KYNU: kynureninase; NSH, non-specific hydroxylase; NE, non-enzymatic; 3-HAAO, 3-hydroxyanthranilate 3,4-dioxygenase; 5-HTP, 5-hydroxytryptamine; ACMSD, 2-amino-3-carboxymuconate semialdehyde decarboxylase; IDO, indoleamine 2,3-dioxygenase; NMDA, N-methyl-D-aspartate; QPRT, quinolinic acid phosphoribosyl transferase. The illustration was created using Adobe Illustrator CC 2024.

Trp is an essential amino acid involved in synthesising serotonin, as well as the indole pyruvate and kynurenic pathways. The indole pyruvate pathways contribute to the synthesis of various small biological active amino compounds, commonly referred to as trace amines (e.g., *β*-phenylethylamine, *p*-tyramine, tryptamine, *p*-octopamine) (Platten et al., 2019; Zucchi et al., 2006) (Figure 2). Herein, we will primarily focus on tryptamines, which are monoamine alkaloids containing an indole ring. These compounds are formed through the decarboxylation of Trp and are rapidly degraded by monoamine oxidase A or B (MAO-A or MAO-B). Additionally, tryptamine can be converted into dimethyltryptamine (DMT) through indole-N-methyltransferase. Although, DMT exists in very low concentrations (e.g., nanomolar (nM)) as an endogenous trace neurotransmitter in the brains of various animals (Saavedra & Axelrod, 1972; Zucchi et al., 2006) (Figure 2).

Tryptamines can cross the BBB and modulate the effects of classical monoamine neurotransmitters such as serotonin. They interact with trace amine-associated receptors (TAAR), serotonin receptors (5-HTR) and sigma receptors (SR), which can initiate downstream signalling cascades (Dhakal & Macreadie, 2021; Platten et al., 2019; Zucchi et al., 2006) (Figure 2).

1.2.1. Tryptamine pathway and their mediators in AD

Tryptamines and their derivatives might have a promising effect on regulating serotonergic and glutamatergic neurotransmitter systems in AD. Several tryptamine derivatives have shown promising results in cholinesterase inhibition, which could enhance the levels of neurotransmitter acetylcholine (Asghar et al., 2024; Bai et al., 2021). This enhancement could contribute to improvements in cognitive function and memory performance.

Moreover, tryptamine derivatives have been found to inhibit Aβ aggregation and MAO activity (Asghar et al., 2024; Bai et al., 2021). These derivatives also exhibit neuroprotective properties by ameliorating synaptic failure and neurotransmission deficiencies (Bai et al., 2021). Additionally, tryptamine derivatives have been linked to reductions in oxidative stress and anti-inflammatory responses (Asghar et al., 2024).

In addition, only about 5% of Trp is converted into serotonin (5-hydroxytryptamine, 5-HT), while over 95% follows the kynurenic pathway. Within the 5-HT pathway, Trp is hydroxylated to 5-hydroxytryptophan (5-HTP) and then decarboxylated to form 5-HT (Figure 2). Under healthy brain conditions, the kynurenine pathway metabolises Trp into both neuroprotective (such as kynurenic acid (KYNA), picolinic acid, nicotinamide adenine dinucleotide (NAD+)) and neurotoxic metabolites (including quinolinic acid (QUINA), 3-hydroxykynurenine (3-HKYN), 3-hydroxy anthranilic acid (3-HAA)). These metabolites are produced by enzymes located in astrocytes (kynurenine aminotransferases (KAT)) and microglial cells (indoleamine-2,3-dioxygenase (IDO), kynurenine 3-monooxygenase (KMO) and 3-hydroxyanthranilate 3,4-dioxygenase (3-HAAO)) (Platten et al., 2019) (Figure 2).

Research has shown that the kynurenic pathway enhances Trp metabolism throughout the pathophysiology of AD (Guillemin et al., 2005; Schwarcz et al., 2012; Widner et al., 2000). This enhancement is linked to the upregulation of Trp, which is thought to contribute to the oxidative stress and neuroinflammatory pathways underlying the symptoms of AD. QUINA depends on the IDO, both of which are stimulated by proinflammatory cytokines (e.g. IL-1β,

IL-2, IL-6, IFN-γ) (Connor et al., 2008; Guillemin et al., 2005). This process is exacerbated by abnormal synthesis and clearance of Aβ in AD and is further influenced by ROS and nitric acid (Bohár et al., 2015). Elevated levels of 3-HKYN and QUINA metabolites, along with a reduction in KYNA, have been associated with excitotoxicity in AD (Schwarcz et al., 2012) (Figure 2).

QUINA acts as an N-methyl-D-aspartic acid (NMDA) receptor agonist, leading to excitotoxic neurodegeneration. 3-HKYN can trigger neuronal apoptosis. Besides this, KYNA participates as an NMDA receptor antagonist and protects against excitotoxicity and apoptotic effects (Figure 2). It has been seen that Aβ and Tau in the AD brain co-localised with QUINA (Bonda et al., 2010; Parrott & O'Connor, 2015; Schwarcz et al., 2012; Wu et al., 2013). At the same time, inhibition of KMO will reduce neuronal/synaptic loss and memory impairment. This inhibition will lead to the inactivation of the 3-HKYN build-up in the brain. Furthermore, BH4, a cofactor for activating the Trp hydroxylase (TPH), is reduced by KMO inhibition, leading to the depletion of both 3-HKYN and xanthurenic acid (Haruki et al., 2016; Zwilling et al., 2011) (Figure 2).

In addition, TPH is closely linked to iron homeostasis and is dysregulated in AD due to elevated ROS activity (Klein et al., 2013; Klein et al., 2018; Liu et al., 2018; Maitre et al., 2020). 5-HT is a vital neurotransmitter that significantly influences cognition and memory, which are critical aspects of BPSD in AD (Nichols & Nichols, 2008). The majority of 5-HT neurones are found in the brainstem, especially in an area known as the raphe nuclei, which facilitate the distribution of serotonergic projections throughout the central nervous system (Vertes, 1991; Vertes et al., 1999).

1.2.2. 5-HT and receptors in AD

5-HT is synthesised in presynaptic terminals of 5-HT neurones and released into the synaptic cleft, where it can induce pharmacological activity across 14 receptor subtypes, categorised into seven classes (5-HT_1, 5-HT_2, 5-HT_3, 5-HT_4, 5-HT_5, 5-HT_6, 5-HT_7). Most of the 5-HTR are G-protein coupled receptors, while the 5-HT_3R is an ion channel (Hoyer et al., 1994; Nichols & Nichols, 2008). 5-HT regulates the activation or inhibition of various downstream mechanisms, such as adenylate cyclase, extracellular signal-regulated kinase (ERK), and phospholipase C (PLC) signalling, which in turn modulate the glycogen synthase kinase 3 (GSK-3). Following the excitatory transmission of 5-HT, the remaining 5-HT in the synaptic cleft is recycled by serotonin reuptake transporters (SERT) and degraded by MAO

in 5-hydroxyindole acetic acid (5-HIAA) (Figure 2 and Figure 3). Research has suggested that 5-HIAA and KYNA may modulate the NEP expression, which is critical in clearing toxic Aβ peptides (Klein et al., 2013; Klein et al., 2018) (Figure 3). The 5-HT_2R, 5-HT_4R, 5-HT_6R and 5-HT_7R (Lorke et al., 2006; Nitsch et al., 1996; Pimenova et al., 2014; Solas et al., 2021) exert direct effects, whereas 5-HT_1R and 5-HT_3R (Shinohara et al., 2019; Vidal et al., 2016; Watson et al., 1998) subtypes have indirect effects on influencing APP processing and Aβ toxicity (reviewed in (Joshi et al., 2020)). Furthermore, we will mainly focus on the role of 5-HT_2R concerning BPSD in AD.

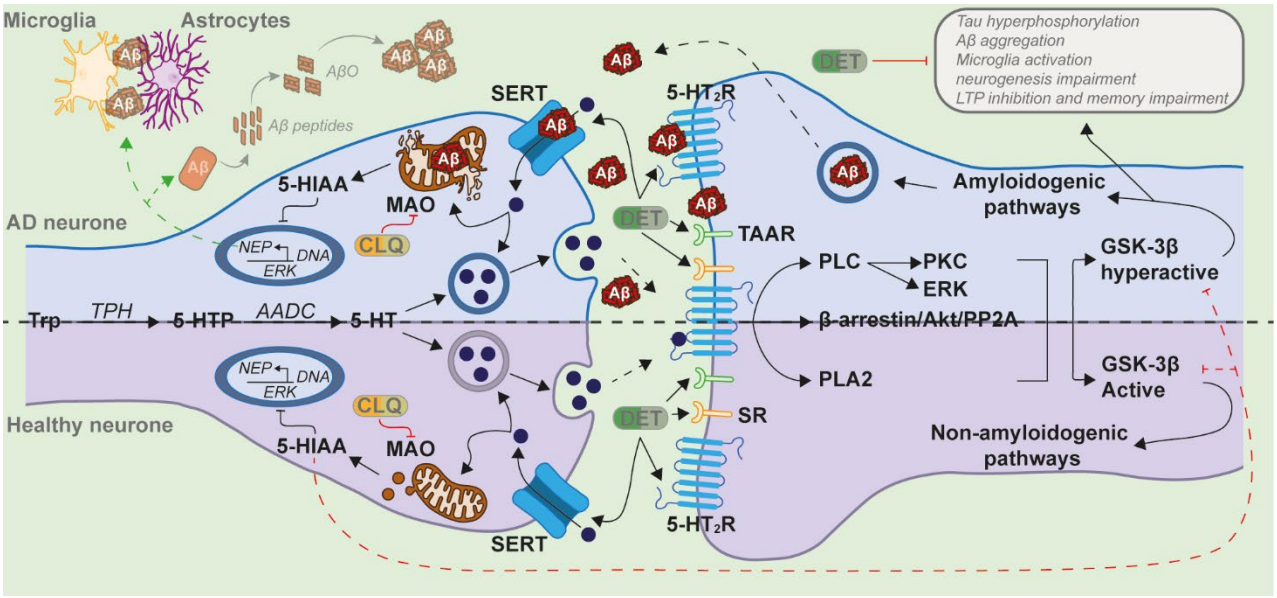

Figure 3: *Serotonin pathway and the involvement of a novel therapeutic drug interaction in AD. Serotonin (5-HT) is released into the synaptic cleft, where it binds to the 5-HT subtype 2 receptors (5-HT_2R). This interaction activates phospholipase C (PLC), phospholipase A2 (PLA2), and the β-arrestin/Akt/PP2A signalling pathways. Consequently, this leads to the activation of GSK-3β, which is known to be dysregulated in AD. Under normal physiological conditions, PLC stimulates the ERK pathway, and this further promotes the transcription of neprilysin (NEP). NEP is a protein that plays a vital role in the degradation and clearance of Aβ through phagocytosis by microglia and astrocytes (green dashed arrows). This regulatory action of PKC supports dendritic synaptic plasticity, while PLA2 initiate the release of arachidonic acid, a key component of phospholipids. In AD, GSK-3β mediates neuronal and synaptic dysfunction by promoting Tau hyperphosphorylation. Furthermore, GSK-3β regulates inflammatory responses through microglia activation and influences adult neurogenesis, synaptic plasticity, and cognitive abilities. Dysregulation, characterised by the overactivation of GSK-3β-kinase can contribute to the pathogenesis of AD. In contrast, the inhibition of GSK-3β can occur through the action of 5-hydroxyindoleacetic acid (5-HIAA), which is generated from the serotonin reuptake and subsequently metabolised in the mitochondria by monoamine oxidase (MAO) (red dashed lines). In addition, we highlight potential therapeutic compounds such as clorgyline hydrochloride (CLQ), a selective MAO inhibitor, and N,N-diethyltryptamine (DET), which may help regulate the serotonin pathway and their possible implications in AD. Other abbreviations: Trp, tryptophan; 5-HTP, 5-hydroxytryptamine; TPH, Trp hydroxylase; AADC, aromatic amino acid decarboxylase; TAAR, trace amine-*

associated receptors; SR, sigma receptors; SERT, serotonin reuptake transporters; DNA, deoxyribonucleic acid. This illustration was created using Adobe Illustrator CC 2024.

1.2.3. 5-HT$_2$R and their subtypes in AD with the link to inflammation

5-HT$_2$R consists of three subtypes: 5-HT$_{2A}$R, 5-HT$_{2B}$R, and 5-HT$_{2C}$R. All subtypes of 5-HT$_2$R are dysregulated in MDD and AD (Hannon & Hoyer, 2008). However, this dysregulation is complex and varies based on specific conditions, brain regions and the nature of the investigations conducted. Therefore, we will provide a general concept of how the 5-HT receptor can be modulated in relation to AD.

The receptor preferentially binds to intracellular GTPases, such as G$_{\alpha q}$-GDP, to form protein complexes. Upon the binding of ligands to 5-HT$_2$R, a conformational change occurs that replaces guanosine diphosphate (GDP) with guanosine triphosphate (GTP) (Hannon & Hoyer, 2008; Leysen, 2004). This exchange leads to the activation of the G$_{\alpha q}$ protein, which initiates the activation of PLC or PLA2 (Figure 2). The activation of PLC stimulates protein kinase C (PKC), while PLA2 facilitates the release of arachidonic acid (Figure 3). (Hannon & Hoyer, 2008; Leysen, 2004). Increased PLA2 activity has been observed in the hippocampus of both AD patients and AD mice (Sanchez-Mejia et al., 2008).

Moreover, the 5-HT$_2$R plays a vital role in activating β-arrestin, which mediates the Akt/PP2A signalling pathway. In AD, the dysregulation of β-arrestin contributes to the synthesis of Aβ through the γ-secretase pathway (Hamm, 1998; Hannon & Hoyer, 2008; Morel et al., 2013; Thathiah et al., 2013). The activation of PKC and Akt/PP2A pathways is essential for regulating the homeostasis of GSK-3 expression in the brain. GSK-3 comprises two distinct variants: GSK-3α and GSK-3β (Polter & Li, 2011). Research has linked GSK-3 to AD, indicating that inhibition of especially GSK-3β can diminish BACE-1-mediated APP cleavage. This inhibition also reduces hyperphosphorylated Tau, leading to decreased levels of Aβ, as well as a reduction in Tau oligomers and neurofibrillary tangles (Griebel et al., 2019; Lauretti et al., 2020; Ly et al., 2013) (Figure 2 and Figure 3).

Various 5-HT$_2$R subtypes regulate neuroinflammation and the processing of APP. Specifically, both 5-HT$_{2A}$R and 5-HT$_{2c}$R promote APP processing, while 5-HT$_{2c}$R also mediate the activity of enzymes that degrade Aβ, such as NEP (Tian et al., 2015) (Figure 3). Inhibiting the 5-HT$_{2B}$R has improved synaptic function and alleviated behavioural deficits associated with Aβ and Tau toxicity in AD (Acquarone et al., 2024; Meneses et al., 2018).

Neuroinflammation plays a pivotal role in the early stage of AD. Research suggests that activation of 5-HT_{2A}R can trigger an anti-inflammatory response by inhibiting tumour necrosis factor-α (TNF-α) (Nau et al., 2013). Furthermore, selective inhibition of 5-HT_{2A}R may mitigate AD pathology by promoting the microglial phagocytosis of Aβ (Lu et al., 2021). Moreover, 5-HT_{2B}R is upregulated in AD patients compared to controls. This upregulation, particularly near degenerating neurones, has been linked to microglial activation and explored in the context of ageing (Buga et al., 2016; Ries & Sastre, 2016). Targeting the activation or inhibition of 5-HT_2R subtypes may lead to new therapeutic approaches for treating AD and addressing the corresponding neuropsychological behaviours and symptoms of the disorder.

5-HTR has been shown to influence a broad spectrum of effects related to mood, cognition, behaviour, and physiological processes, as well as the regulation of various other neurotransmitters (e.g., glutamate, γ-aminobutyric acid (GABA) and acetylcholine), and hormones (e.g., cortisol and substance P) (Johansson et al., 2015; Kaur et al., 2019). Dysregulation in serotonergic innervation has been associated with several neuropsychiatric (e.g., MDD) and neurological disorders (e.g., AD) (Correia et al., 2021). Both human patients with AD and animal models bearing the APP/PSEN-1 mutation have demonstrated a reduction in serotonergic neurones projections (Hendricksen et al., 2004; Liu et al., 2008). The decrease in neuronal projections may disrupt the process of adult neurogenesis. We will explore the effects of this impaired neurogenesis in the context of AD more thoroughly in the next section.

1.3. Adult neurogenesis and impairment in AD

Neurogenic niches are essential environments of the adult brain, acting as reservoirs for the neural stem cells (NSC). Among these niches, the subgranular zone of the dentate gyrus in the hippocampus and the subventricular zone at the lateral ventricles are particularly abundant in NSC (Jurkowski et al., 2020). Additionally, other brain regions regulate NSC migration and maturation into new neuronal cells. Adult hippocampal neurogenesis plays a significant role in mood regulation and cognitive function, while neurogenesis in the subventricular zone forms olfactory circuits (Jurkowski et al., 2020).

Research into neurogenesis impairment has been conducted in AD and extensively reviewed for human and animal models (Babcock et al., 2021; Jurkowski et al., 2020; Seki, 2020). However, these results remain controversial. It has been indicated that neurogenesis

is adversely affected by the accumulation of Aβ peptides. Furthermore, Aβ oligomers have been demonstrated to enhance NSC dysfunction through GSK-3β pathways (Lee et al., 2013; Naumann et al., 2010).

Recent studies have shown how reduced NSC proliferation and neuronal maturation are linked to microgliosis, a condition often observed in the early stages of AD (Salta et al., 2023). Also, microglia are crucial in regulating synaptic pruning and refinement throughout brain development. Microglia can release several signalling molecules (e.g., IL-4, CX3CL1) linked to synaptic activity and neuroplasticity regulation. They play an essential role in maintaining synaptic homeostasis through phagocytosis of synapses, a process that becomes dysregulated in AD (Cornell et al., 2022; Gao et al., 2023; Salta et al., 2023).

In addition, the entorhinal cortex is essential for maintaining proper neuronal connectivity within the hippocampal regions. The entorhinal cortex consists of 6 layers, with the pyramidal neurones of layer II, being particularly significant and among the first to exhibit impairment in AD. Research shows that layer II neurones in the entorhinal cortex produce reelin and are highly sensitive to Aβ-induced toxicity in the early stages of AD (Chin et al., 2007; Ramos-Moreno et al., 2006; Yu et al., 2014).

1.3.1. Reelin: a neuromodulator in amyloid pathology and BPSD-associated neuroplasticity

Reelin (RELN), a large extracellular matrix glycoprotein, is crucial in regulating neurogenesis in the hippocampus and synaptic plasticity (Weeber et al., 2002). The processing of APP can be influenced by its interactions with various extracellular glycoproteins, including alcadein, F-spondin, reelin, low-density lipoprotein receptor-related protein-1, sortilin-related receptor-1, Nogo-66 receptor and Notch 2 (Müller & Zheng, 2012).

Furthermore, RELN is crucial in both embryonic and postnatal brain development, influencing neuronal cell migration, proper brain lamination, and the formation of dendrites and spines. In adult brains, RELN is essential for modulating synaptic function and plasticity (Folsom & Fatemi, 2013; Förster et al., 2006; Lane-Donovan et al., 2015). Dysregulation of the molecular mechanisms associated with RELN can lead to disruptions in cortical lamination, synaptic plasticity, and dendritic growth, which have been linked to various brain disorders, including AD (Campo et al., 2009; Katsuyama & Terashima, 2009; Sato et al., 2016). RELN has been shown to bind to apolipoprotein E receptor 2 and very low-density

lipoprotein receptor (Campo et al., 2009). ApoE-ε4 isoform, a significant genetic risk factor for idiopathic AD, appears to prevent the endosomal recycling of both the RELN and its associated receptors at the presynaptic and postsynaptic surfaces (Cuchillo-Ibáñez et al., 2013; Lane-Donovan et al., 2015; Xian et al., 2018).

Oligomeric Aβ species disrupt synaptic plasticity; however, RELN can prevent spine deterioration and synaptic dysfunction. Also, the presence of RELN within amyloid plaques plays a crucial role in regulating Tau hyperphosphorylation (Cuchillo-Ibáñez et al., 2013; Lane-Donovan et al., 2015; Pujadas et al., 2014). RELN induce phosphorylation of disabled-1, an adapter protein that regulates the intracellular transduction of RELN signalling. This activation leads to processes that regulate the trafficking and localization of postsynaptic proteins, such as NMDAR and PSD-95 (Durakoglugil et al., 2009; Hoe et al., 2009; Lacor et al., 2000; Lane-Donovan et al., 2015; Schmidt et al., 2014). Mutations or dysregulation of apolipoprotein E receptor 2 can prevent disabled-1 phosphorylation, leading to inhibition of the GSK-3β pathway. This inhibition, in turn, leads to reduced Ca^{2+} influx and a decrease in LTP, ultimately impairing synapse regulation, cognition and memory processing, as observed in AD (Durakoglugil et al., 2009; Folsom & Fatemi, 2013; Lacor et al., 2000; Lane-Donovan et al., 2015; Schmidt et al., 2014).

Inappropriate binding of RELN to its receptors can disrupt its three-dimensional structure of RELN. Alterations in the homo-dimerization of RELN due to Aβ binding can result in inactive complexes from impaired glycosylation, which diminishes effective binding to apolipoprotein E receptor 2 (Cuchillo-Ibáñez et al., 2013). Nevertheless, a deeper understanding of RELN could pave the way for novel therapeutic molecules to mitigate Aβ-mediated toxicity in AD.

1.3.2. Reelin and neuroinflammation

The connection between neuroinflammation and RELN in the context of AD requires further examination. A recent study utilising proteomic profiling of cerebrospinal fluid (CSF) identified novel proteins associated with AD pathology, most of which were synaptic proteins and those linked to RELN-positive cells (Dayon et al., 2018). Another study found that soluble ectodomain fragments of Apolipoprotein E receptor 2 in CSF correlated more strongly with RELN signalling in both sporadic and autosomal-dominant forms of AD (Lopez-Font et al., 2019). In a pivotal study conducted in 2000, researchers detected RELN concentrations in the blood of adult mice, rats and humans. It was noted that the circulating levels of RELN are significantly influenced by

organ-specific secretion of the protein and the mRNA expression of RELN in the bloodstream (Smalheiser et al., 2000).

Another study indicated that the interaction of RELN with liposomes containing phosphatidylserine (PS) or phosphatidylcholine (PC) along with blood cascade factors (thrombin and FXa), which are crucial for the restoration of impaired thrombin generation (Tseng et al., 2014). In various preclinical AD models, blood-related biomarkers have been thoroughly examined within the intrinsic blood coagulation pathway. A key player in triggering this pathway is plasma protein FXIIa, which activates plasma kallikrein to cleave high kininogen. This cleavage leads to the release of bradykinin. This blood cascade pathway promotes inflammatory processes, including increased BBB permeability, oedema, and cytokine expression. All these responses are implicated in both the early and late stages of AD (Heneka et al., 2015; Zamolodchikov et al., 2015). Consequently, we investigated the characterisation of neuroinflammation (i.e. microgliosis) and neurogenesis/neuroplasticity (i.e. RELN) across different ages of the AD mouse model, specifically in the brain of these mice.

1.4. Lipid homeostasis and their disruptions in AD

Neuronal cell membranes are vital for maintaining membrane fluidity and integrity, with their lipid composition categorised into sphingolipids, glycerophospholipids and cholesterol (Hussain et al., 2019). Sphingolipids play a pivotal role in cellular signalling pathways, influencing processes such as APP metabolism, apoptosis, calcium homeostasis, Tau phosphorylation and acetylcholine biosynthesis (Varma et al., 2018). Glycerophospholipid and cholesterol, the most abundant lipids in the cell membranes, are crucial for various intracellular signalling pathways and contribute to structural stability, fluidity, and permeability of the cell membranes (Farooqui et al., 2000b; Hussain et al., 2019). Dysregulation in these lipids affects brain lipid homeostasis and is linked to neurological disorders (Quinville et al., 2021; Tracey et al., 2018; Zhao et al., 2023). This section focuses on the metabolism of sphingolipids and glycerophospholipids, particularly their role in synaptogenesis and synaptic plasticity, and AD, especially concerning Aβ pathology.

1.4.1. Sphingolipids metabolism

Sphingolipids are categorised into two structural classes: sphingoid bases and derivatives (including sphingosines (So), sphinganines (Sa), sphingosine-1-phosphates (So1P), sphinganine-1-phosphates (Sa1P) and ceramides (Cer)), and complex sphingolipids (sphingosphopholipids and glycosphingolipids). Their biosynthesis occurs through three pathways: the biosynthesis pathway in ER, the salvage pathway in late endosomes or

lysosomes, and sphingomyelin synthesis primarily in the Golgi apparatus. Cer synthesis is a crucial link among these pathways (Quinville et al., 2021; Tracey et al., 2018) (Figure 4).

The biosynthesis pathway begins with the synthesis of Sa, which can be converted into Sa1P and dihydroceramide (DHCer) by sphingosine kinases (e.g., SphK 1 and SphK 2), DHCer synthase, or Sa hydroxylase. So is generated through ceramidase activation in the salvage pathway and can be phosphorylated to So1P by SphK. Sphingosine-1-phosphate lyase (SPL) can then break down So1P to So and convert Sa1P back to Sa. Cer is synthesised by ceramide synthase (CerS) from So and by DHCer desaturase (DEGS) from DHCer (Quinville et al., 2021). Ceramide kinase (CerK) produces ceramide-1-phosphates (C1P), while ceramide phosphate phosphatase (C1PP) reverses this reaction (Hait & Maiti, 2017).

Sphingomyelins (SM) are complex sphingolipids that can be converted to Cer by sphingomyelinase (SMase), with subtypes such as lysosomal acidic SMase, secreted acidic SMase and membrane-neutral SMase. SM is produced by sphingomyelin synthase (SMS) (Kilkus et al., 2008; Quinville et al., 2021). In addition, sphingosylphosphorylcholines (SPC), a bioactive metabolite from SM, is generated by SM deacylase (SMDase) (Nixon et al., 2008).

Glycosphingolipids are formed by combining a hydrophobic Cer base with a hydrophilic carbohydrate head group. In the Golgi apparatus, glucose or a galactosyl molecule is added to Cer by uridine diphosphate glucose ceramide glucosyltransferase (UGCG) or ceramide galactosyltransferase (CGT), producing galactosyl ceramides (GalCer) or glucosyl ceramides (GlcCer). GalCer can then be converted to Neu5Acα2-3GalβCer (GM4) by sialyl-transferase, such as ST3GalV), or to sulfo-galactolipids by cerebroside sulfotransferase (D'Angelo et al., 2013; Quinville et al., 2021; Tracey et al., 2018).

GlcCer is further converted to lactosylceramides (LacCer) by LacCer synthase (β4-galactosyltransferases V and VI). LacCer acts as a critical branching for various substrates, producing precursors such as GA2, GM3, Gb3 and Lc3). These precursors are essential for synthesising the seven complex glycosphingolipids series, including asialo, ganglio, globo/iso-globo and lacto/neo-lacto series. The most prominent in vertebrates are ganglio-, globo-, and neolacto-series (D'Angelo et al., 2013; Quinville et al., 2021).

The breakdown of complex glycosphingolipids into Cer is regulated by glycosyl hydrolases, such as β-galactosidase, β-hexosaminidase, and sialidase, along with lysosomal binding proteins. This process leads to the generation of simpler glycosphingolipids, such as GlcCer and GalCer. The lysosomal binding proteins include the GM2 activator protein and four saponin subtypes A-D (Darmoise et al., 2010; Quinville et al., 2021). GlcCer produced from LacCer hydrolysis can be converted to Cer by glucosylceramide-β-glucosidase and saponin C. Sulfo-galactolipids are transformed into GalCer through arylsulfatase A with saponin B, while GalCer is degraded to Cer with the help of galactosyl ceramide-β-galactosidase and saponin A (Quinville et al., 2021; Yu et al., 2011; Zschoche et al., 1994).

1.4.2. Glycerophospholipids metabolism

Glycerophospholipid synthesis starts from glycerol-3-phosphate (G3P), producing precursor lipid mediators like phosphatidic acid (PA), diacylglycerol (DAG), and cytidine diphosphate-DAG (CDP-DAG). These precursors are essential for forming various glycerophospholipids, including PC, phosphatidylethanolamines (PE), phosphatidylglycerols (PG), PS, phosphatidylinositols (PI), platelet-activating factor (PAF) (Tracey et al., 2018). PC and PS can be synthesised by either phosphatidylethanolamine N-methyltransferase (PE-NMT) or PS-decarboxylase (Tan et al., 2020) (Figure 4).

PLA can further metabolise many glycerophospholipids, mainly PLA 1 or 2, in the ER and mitochondrial-associated membranes (Hishikawa et al., 2014). Depending on the specific glycerophospholipid, five distinct subtypes of phospholipases (e.g., cPLA2, sPLA2, iPLA2, PAF acetylhydrolases and lysosomal PLA2) participate in synthesising various lysoglycerophospholipids such as lysophosphatidylcholines (LPC), lysophosphatidylethanolamines (LPE), lysophosphatidylglycerols (LPG), lysophosphatidylserines (LPS). These lysoglycerophospholipids act as precursors for lipid synthesis in the neuronal cells. The generation of lyso-platelet-activating factor (lyso-PAF) is mediated by PAF acyl hydrolase. (Tan et al., 2020). Remodelling pathways convert lysoglycerophospholipids back into glycerophospholipids through various lysoglycerophospholipid acyltransferases (LPLAT) (Hishikawa et al., 2014).

In addition, intracellular lysoglycerophospholipid concentrations are low due to widespread lysoacyltranferases expression compared to extracellular compartments (Harayama et al., 2014; Wang & Tontonoz, 2019). Therefore, alterations in the concentration of these lipids can be cytotoxic to cells. However, understanding these lipids is crucial to exploring their

production and secretion in specific neuronal cell types. Our study utilises glial cells and primary hippocampal neurones derived from mice to examine their role in synaptogenesis and Aβ-induced toxicity, both critical factors in AD pathology.

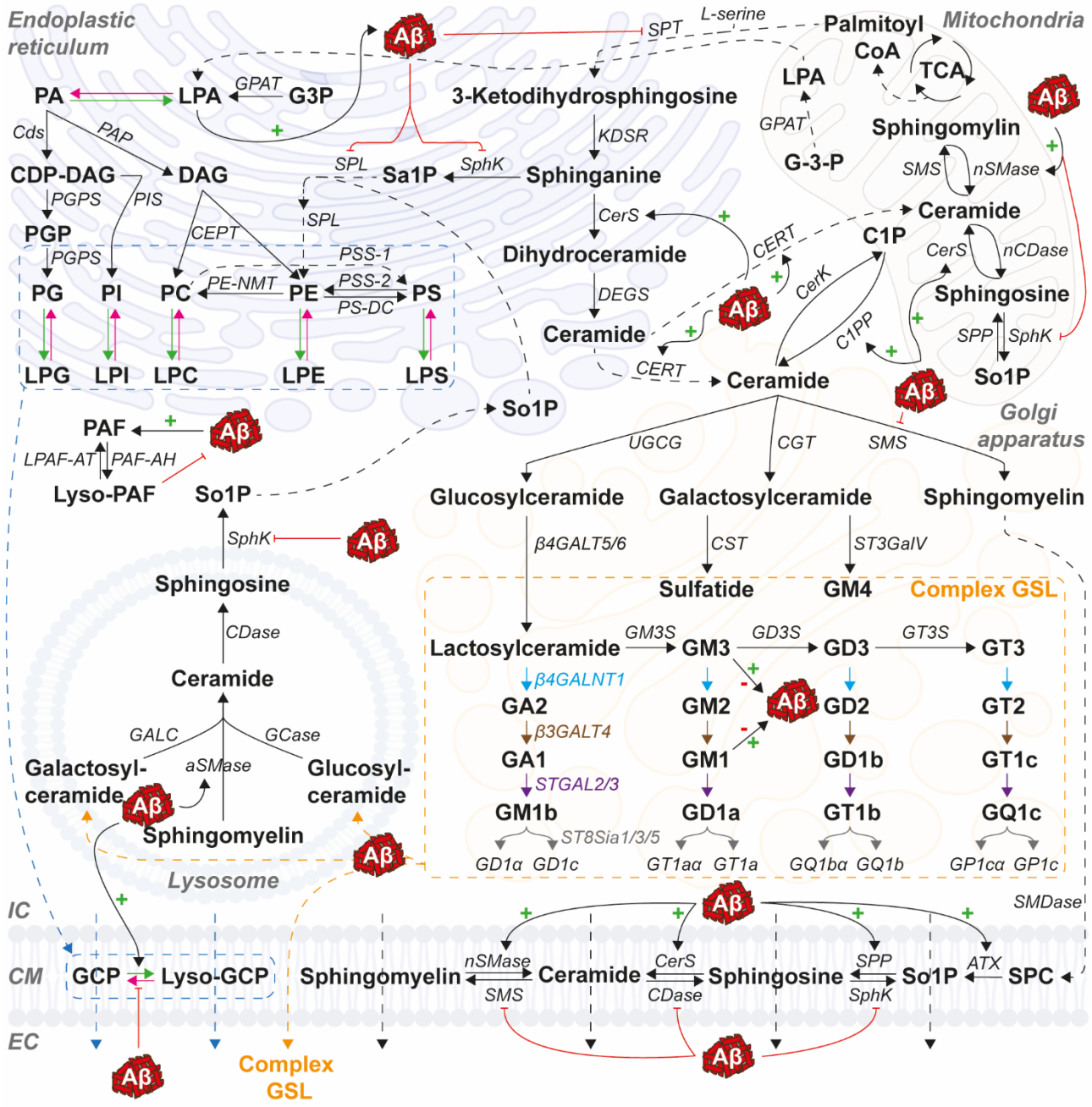

Figure 4: *Compartmentalization of sphingolipids and glycerophospholipids metabolism in relation to AD. This overview outlines the biosynthesis and salvage pathways of sphingolipids and glycerophospholipids. Both are synthesised in the endoplasmic reticulum, with degradation occurring in lysosomes. Lipid remodelling happens in various cellular regions, such as the Golgi apparatus, mitochondria, cell membrane (CM), intracellular compartments (IC) and extracellular compartments (EC). The glycerophospholipids (GCP) can be converted to lysoglycerophospholipids (lyso-GCP) by phospholipase (green arrows) and deacylated by specific acyltransferases (magenta arrows). The link between sphingolipid and glycerophospholipids involves the degradation of sphinganine-1-phosphate (Sa1P) and sphingosine-1-phosphate (So1P) by lyases into fatty*

acid aldehydes, which are then remodelled into palmitoyl-coenzyme A (palmitoyl-CoA). The figure does not depict the phosphorylation pathways of phosphatidylinositols (PI) or the degradation of complex glycosphingolipids (GSL). However, simpler GSL, such as galactosylceramide and glucosylceramide, are recycled into ceramides through glucocerebrosidase (GCase) and galactocerebrosidase (GALC). Here, we focus on four complex GSL: sulfo-galactoceramide (sulfatide), Neu5Acα2-3GalβCer (GM4)), and the asialo/gangliosides series (GA2, GM3 (a-series), GD3 (b-series) and GT3 (c-series)) which are vital for myelin integrity and neuronal phenotypes (orange box). These GSL are synthesised in the Golgi apparatus from galactosylceramide, involving enzymes like sialyltransferase (ST3GalV) and cerebroside sulfotransferase (CST). The asialo/gangliosides series is produced stepwise from lactosylceramide through lactosylceramide α-2,3-sialyltransferases (GM3S, GD3S and GT3S), β-1,4-N-acetyl-galactosaminyl transferases 1 (β4GALNT1, blue arrows), β-1,3-galactosyltransferases 4 (β3GALT4, brown arrows), ST3 β-galactoside alpha-2,3-sialyltransferases 2 or 3 (ST3GAL2/3, purple arrows) and ST8 α-N-acetyl-neuraminide-α-2,8-sialyltransferases 1, 3 or 5 (ST8Sia 1/3/5, grey arrows). In addition, Aβ pathology significantly impacts ceramide production and remodelling of (lyso-) glycerophospholipid, either stimulating (+) or inhibiting (red arrows) key enzymes (e.g., sphingomyelin synthase (SMS), neutral and acidic sphingomyelinase (nSMase and aSMase), ceramide synthase (CerS), (sphingosine/sphinganine kinase (SphK), sphingomyelin synthase (SMS), sphingosine/sphinganine-1-Phosphate lyase (SPL), ceramide-1-phosphate phosphatases (C1PP), sphingosine-1-phosphate phosphatase (SPP), autotaxin (ATX) and ceramidase (CDase)) and transporters (ceramide transfer protein (CERT)), which can lead to lysosomal and mitochondrial dysfunction. Further, gangliosides and LPA can influence the Aβ aggregation positively (+) or negatively (-), while lyso-PAF inhibits and PAF enhances the neuroinflammatory Aβ toxicity. Other abbreviations: CerK, ceramide kinase; CDP-DAG, cytidine diphosphate diacylglycerol; CDS, cytidine diphosphate diacylglycerol synthase; CEPT, choline/ethanolamine phosphotransferase; DAG, diacylglycerol; DEGS, dihydroceramide desaturase; β4GALT5/6, β-1,4-galactosyltransferase 5 or 6; CGT, ceramide galactosyltransferase; G3P, glycerol-3-phosphate; GPAT, glycerol-3-phosphate acyltransferase; KDSR, 3-ketodihydrosphingosine reductase; PA, phosphatidic acid; LPA, lysophosphatidic acid; PAF, platelet-activating factor; lyso-PAF, lyso-platelet-activating factor; PAF-AH, PAF-acetyl hydrolase; LPAF-AT, lyso-PAF-acyltransferase; PAP, phosphatidic acid phosphatase; PC, phosphatidylcholine; LPC, lysophosphatidylcholine; PE, phosphatidylethanolamine; LPE, lysophosphatidylethanolamine; PE-NMT, phosphatidylethanolamine N-methyltransferase; PG, phosphatidylglycerol; LPG, lysophosphatidylglycerol; PGP, phosphatidylglycerol phosphate; PGPS, phosphatidylglycerol phosphate synthase; PIS, phosphatidylinositol synthase; LPI, lysophosphatidylinositol; PS, phosphatidylserine; LPS, lysophosphatidylserine; PS-DC, phosphatidylserine decarboxylase; PSS-1, phosphatidylserine synthase 1; PSS-2, phosphatidylserine synthase 2; SMDase, sphingomyelin deacylase; SPT, serine palmitoyltransferase; TCA, Citric acid cycle; UGCG, glucosylceramide synthase. The illustration was created using Adobe Illustrator CC 2024.

1.4.3. Sphingolipids and (lyso-) glycerophospholipids in synaptogenesis

Synaptogenesis is vital for forming new synaptic connections in the central nervous system, and the loss of these connections is an early sign of AD (Lacor et al., 2007). Sphingolipids and glycerophospholipids are key building blocks of the neuronal membranes, crucial for maintaining synaptic function and plasticity. Sphingolipids specialise in neurogenesis and

synaptogenesis, while glycerophospholipids maintain membrane stability (Gulbins et al., 2015; Hussain et al., 2019; Sonnino & Prinetti, 2016). The specific role of (lyso-) glycerophospholipids, particularly PC and PE in dendritic growth and PA and PS in dendritic branching morphology, has been highlighted (Lee et al., 2011; Ziegler & Tavosanis, 2019). Additionally, phospholipases like PLA2 and PLD1 convert glycerophospholipids to lysoglycerophospholipids, supporting neurite outgrowth and neuronal viability in AD (Cai et al., 2006; Forlenza et al., 2007; Sanchez-Mejia et al., 2008).

The sphingolipids, particularly the variation in ganglioside profiles, undergo significant changes during early embryogenesis, transitioning from simpler isoforms (such as GM3 and GD3) to more complex forms (including GM1, GD1a, GD1b and GT1b) in later stages of development. Other sphingolipids, such as SM, GalCer, Sulfo-galactolipids and GM4, are crucial for axonal and dendritic arborisation in synaptogenesis and myelination. After birth, ganglioside profiles shift in the opposite direction (Olsen & Faergeman, 2017). SM and Cer depletion can impair axon sprouting, dendritic branching and degradation of more complex GlcCer in hippocampal neurones (Schwarz et al., 1995).

Sphingolipids are essential in modulating the pre- and postsynaptic terminals. S1P influences presynaptic localisation while it also enhances hippocampal glutamate transmission. Activation of neutral sphingomyelinase (nSMase) by TNF-α, which leads to hydrolyses of SM into Cer, which is also crucial for NMDA receptor clustering and synaptic plasticity in the hippocampus (Riganti et al., 2016; Wheeler et al., 2009). The balance between SM and Cer is vital for neuronal plasticity, and in MDD, increased Cer levels are noted. Knockdown of acidic sphingomyelinase (aSMase) or antidepressants that inhibit aSMase can reduce Cer levels and enhance hippocampal neurogenesis (Gulbins et al., 2013; Gulbins et al., 2015).

1.4.4. Sphingolipids and glycerophospholipids in neuroinflammation

Lipid homeostasis is essential, and dysregulation recruits glial cells in neuroinflammatory processes related to neurodegenerative diseases. For example, LacCer activates astrocytes through various pathways, such as Ras-ERK and NF-κB signalling. Pro-inflammatory factors and toxins can increase LacCer levels, leading to astrocyte proliferation and neuronal apoptosis (Chao et al., 2019; Mayo et al., 2014; Pannu et al., 2005).

Furthermore, oxidative stress and neuroinflammation are associated with Cer accumulation (Hait & Maiti, 2017).

Lysoglycerophospholipid play a significant role in neuroinflammation. Increased levels of LPC are linked to pro-inflammatory and demyelination (Plemel et al., 2018). LPC species are vital for brain development through neuronal membrane synthesis and myelination. The neuroinflammatory effect of LPC is influenced by its biochemical structure (saturated or unsaturated LPC species) and its concentration. The expression of LPC in brain endothelial cells is significantly reliant on a protein known as the major facilitator superfamily domain-containing protein 2A, with deficiencies leading to increased plasma LPC levels (Tan et al., 2020). The role of LPE and LPG in neuroinflammation remains largely unknown. LPS can act as an immunomodulator through G-protein coupled receptors on microglial cells (Sayo et al., 2019; Sugo et al., 2006). Lyso-PAF is recognised as an anti-inflammatory agent towards PAF activity (Shindou et al., 2007). However, the precise mechanism through which lysoglycerophospholipid affect neuroinflammation and their potential for neurodegenerative diseases, such as AD, remains poorly understood. Possible mechanisms are illustrated in Figure 5.

1.4.5. Impact of AD on lipid metabolism alterations and membrane integrity

Emerging research indicates that genetic risk factors for AD may play a vital role in the disruption of lipid homeostasis. A notable example is the ApoE-ε4 isoform, which plays a role in enhancing the synthesis of arachidonic acid. This increase may lead to the activation of cPLA-2, potentially initiating inflammatory responses. Other late-onset AD genetic risk factors, such as triggering receptors expressed on myeloid cells 2, clusterin, phosphatidylinositol binding clathrin assembly protein, sterol regulatory-element binding protein, ATP-binding cassette subfamily A member 1 and 7, may influence Aβ aggregation and Aβ clearance, could be involved in modulation of lipid metabolism (Yin, 2023). Herein, we will focus on how APP and its major Aβ peptides ($A\beta_{(1-40)}$ and $A\beta_{(1-42)}$) affect lipid homeostasis. Figure 5 illustrates the key sphingolipids and glycerophospholipids involved in these processes.

APP and cleavage peptides $A\beta_{(1-40)}$ and $A\beta_{(1-42)}$ significantly influence lipid homeostasis (Grimm et al., 2005). In this context, Aβ plays a crucial role in modulating the neuronal membranes through the cholesterol and sphingolipid metabolic pathways. Notably, 3-Hydroxy-3-methylglutaryl-coenzyme A (HMG-CoA) reductase and nSMase are vital

molecular targets for Aβ (Grimm et al., 2005). Research has shown that $A\beta_{(1-40)}$ inhibits the activity of HMG-CoA reductase, while $A\beta_{(1-42)}$ activates nSMase. This dynamic leads to a decrease in both cholesterol and SM levels. The reduction in these lipids, associated with Aβ aggregation, can be mitigated by restoring the lysosomal biogenesis through inhibiting aSMase (Grimm et al., 2005; Lee et al., 2014). Furthermore, elevated levels of cholesterol have been observed following the inhibition of the HMG-CoA reductase, which results in decreased cellular and extracellular $A\beta_{(1-40)}$ and $A\beta_{(1-42)}$ peptides (Kim et al., 2016).

SM, essential components of lipid rafts, diminish γ-secretase activity, leading to reduced levels of $A\beta_{(1-40)}$ or $A\beta_{(1-42)}$ in the amyloidogenic pathway (Grimm et al., 2005; He et al., 2010; Kim et al., 2016) (Figure 5). Lipid rafts are complex, dynamic structures composed of a mix of sphingolipids, cholesterol, and fatty acids found within cell membranes. They play a significant role in lipid and protein sorting, cell adhesion and signal transduction. Notably, APP, BACE-1, γ-secretase and NEP have all been identified within lipid rafts. The composition of these lipid rafts is vital for regulating Aβ production and aggregation (Kao et al., 2020; Kawarabayashi et al., 2004).

Mitochondrial-associated membranes shares structural similarities with lipid rafts and consists of SM, cholesterol and proteins, which are essential for lipid synthesis and trafficking (Vance, 2014). It plays a role in Aβ synthesis due to its enriched membrane environment that contains BACE-1, γ-secretase, and C99 fragments (Area-Gomez et al., 2009; Pera et al., 2017). This mechanism is associated with a decline in mitochondrial function. C99 and Aβ peptides enhance the Cer cascade by increasing the SMase of SM (Area-Gomez et al., 2018; Pera et al., 2017) (Figure 5).

Furthermore, Aβ aggregation in the entorhinal cortex of AD is linked to increased SPL and decreased SphK 1, while SphK 2 is upregulated in the AD brain. (Ceccom et al., 2014). Cer promotes Aβ formation by interfering with the BACE-1 activity of APP, whereas So1P plays a protective role in neuronal cells (Figure 5). Inhibition of SPL leads to an intracellular accumulation of So1P, which impairs the degradation of APP and its CTF in lysosomes. In addition, a reduction in γ-secretase activity has been observed, resulting in decreased Aβ production (Karaca et al., 2014). The So1P transporter exacerbates inflammation and cognitive impairment caused by $A\beta_{(1-42)}$. Furthermore, So1P regulates anti-apoptosis by inhibiting caspase 3 activity through its receptor (Rutherford et al., 2013; Zhong et al., 2019).

Additionally, Cer plays a role in regulating and influencing various cellular processes, with one of its functions promoting Aβ production through the cleavage of APP by BACE-1. Studies indicate that fibrillar $A\beta_{(1-42)}$ peptides enhance the SMase activity indirectly through the action of ROS or directly by cPLA2 and arachidonic acid (Han et al., 2002; Jana & Pahan, 2004; Jazvinšćak Jembrek et al., 2015). Treatment with $A\beta_{(1-42)}$ can modulate the cPLA-2 activity and arachidonic acid synthesis in a dose- and time-dependent manner in neuronal cultures (Figure 5). Inhibiting cPLA-2 has alleviated $A\beta_{(1-42)}$-induced neurotoxicity and improved memory deficits in AD mouse models (Sanchez-Mejia et al., 2008). This inhibition promotes the hydrolysis of SM, leading to the production of Cer, which may contribute to Aβ-induced apoptosis. Notably, the concentration of Cer decreases with the progression of AD, with the highest levels observed in the early stages of AD (Han et al., 2002; Jana & Pahan, 2004; Jazvinšćak Jembrek et al., 2015).

The more complex glycosphingolipids, particularly gangliosides, are abundant in lipid rafts and exhibit a high affinity for soluble Aβ oligomers (Hong et al., 2014; Matsuzaki, 2020). Gangliosides such as GM1 and GM3 are strongly associated with AD (Figure 5). Research indicates that both GM1 and GM3 levels are elevated in the brains of AD patients and AD animal models (Dodge et al., 2022; Shin et al., 2019; Yanagisawa et al., 1995; Zha et al., 2004). These gangliosides facilitate the conformational change of α-helical Aβ into more toxic β-sheet Aβ structures, such as Aβ oligomers and fibrils, leading to synaptotoxicity and memory impairment. Nevertheless, several studies have shown that GM1 and GM3 can reduce Aβ production and neurotoxicity, contributing to improvements in cognitive decline (Dodge et al., 2022; Matsuzaki, 2020; Shin et al., 2019).

In AD, glycerophospholipids, such as PE, PC and PI, are reduced in neuronal membranes (reviewed in (Frisardi et al., 2011; Kao et al., 2020)). Briefly, research indicates that Aβ-induced excitotoxicity may enhance the activity of PLA2, leading to lower levels of glycerophospholipids (Figure 5). Both plasma and CSF levels of PLA2 are elevated in AD (Chalbot et al., 2009; Doody et al., 2015; Sanchez-Mejia et al., 2008). Additionally, plasma concentrations of PC and lyso-PAF are significantly reduced in normal ageing and AD, while PC in CSF samples of AD patients are increased (Dorninger et al., 2018). Despite this, there has been limited focus on lysoglycerophospholipid in AD. It has been noted that lysoglycerophospholipids are well-determined in interstitial fluids and plasma from both human and animal samples (Tan et al., 2020). However, the mechanisms through which

these lysoglycerophospholipids are produced or secreted in response to external neurotoxic stimuli such as Aβ peptides require further investigation.

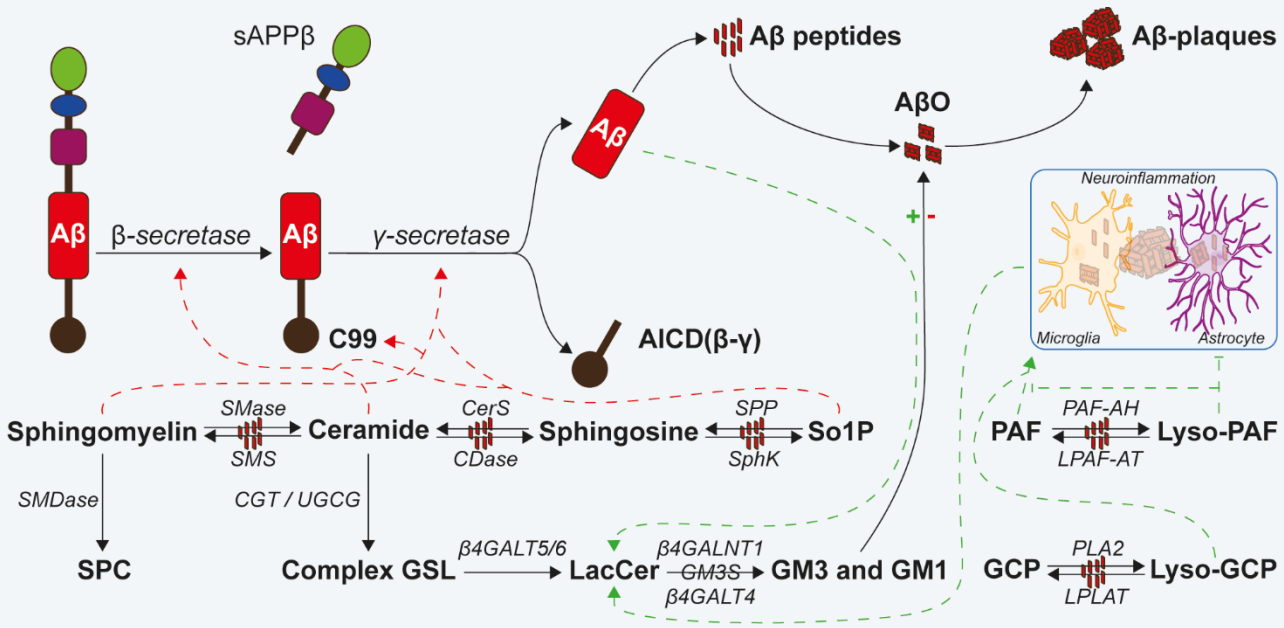

Figure 5: *Involvement of lipid homeostasis on APP cleavage and Aβ-induced neuroinflammation in AD. This schematic provides an overview of the interaction between sphingolipids and glycerophospholipids (GCP) concerning the cleavage of APP and neuroinflammation induced by Aβ toxicity. Sphingomyelin inhibits β-secretase and γ-secretase (red arrows), while sphingosine-1-phosphate (So1P) regulates γ-secretase and C-terminal fragments (C99). Ceramide promotes β-secretase cleavage of APP (red arrows), and Aβ-peptides affect lipid enzymes such as sphingosine-1-phosphate phosphatase (SPP), sphingomyelinase (SMase), ceramide synthase (CerS), which increasing ceramide production. Aβ-induced toxicity, alongside the inflammatory response to Aβ synthesis, can result in the upregulation of LacCer (green arrows). Further gangliosides (GM1 and GM3) exhibit both negative (-) and positive (+) effects on the accumulation of toxic Aβ peptides (green arrows). Lysoglycerophospholipids (lyso-GCP) and platelet-activating factor (PAF) enhance neuroinflammation, exacerbated by Aβ-peptides toxicity on phospholipases (e.g. PLA2) and PAF-acyl acetylhydrolase but countered by lyso-PAF. Other abbreviations: CDase, ceramidase; CGT, ceramide galactosyltransferase; GM3S, lactosylceramide α-2,3-sialyltransferase; β4GALNT1, β-1,4-N-acetyl-galactosaminyl transferase 1; β3GALT4, β-1,3-galactosyltransferases 4; β4GALT5/6, β-1,4-galactosyltransferase 5 or 6; AICD (β-γ), intracellular APP domain after β-secretase and γ-secretase; LPAF-AT, lyso-PAF-acyltransferase; LPLAT, lysophospholipid acyltransferase; SphK, sphingosine kinase; SMS, sphingomyelin synthase; SMDase, sphingomyelin deacylase; UGCG, glucosylceramide synthase. The illustration was created using Adobe Illustrator CC 2024.*

Furthermore, Aβ binding and aggregation significantly impact the composition of glycerophospholipids within neuronal membranes, affecting the fluidity, thickness and charge of these membranes (Niu et al., 2018; Williams & Serpell, 2011). Research has demonstrated that PC can modify $Aβ_{(1-40)}$ mediated aggregation based on the thickness of

the lipid membrane (Korshavn et al., 2017). While charged phospholipid bilayers composed of PC and PG can facilitate the production of $A\beta_{(1-40)}$ fibrils (Niu et al., 2014). The curvature of these lipid membranes is crucial, and this process is affected by Aβ aggregation. Additionally, PE has demonstrated a reduction in $A\beta_{(1-42)}$ binding and toxicity, which leads to alteration in curvature and influences the overall membrane structure (Cazzaniga et al., 2011). In neuronal cells, glycerophospholipids are present at low concentrations and engage interactively with lipid and protein functions (Farooqui et al., 2000a; Kern et al., 2001).

Despite extensive research on sphingolipids and glycerophospholipids in the context of health and diseases, there is still a limited understanding of the specific neurotoxic and neuroprotective effects of different Aβ species on these lipid classes in neuronal cells. To address this gap, we explored the impact of two major Aβ species ($A\beta_{(1-40)}$ and $A\beta_{(1-42)}$) on their lipid profiles in glial cells and hippocampal neurones using high-throughput methods.

1.5. Novel therapeutic interventions and approaches

Only 10 FDA-approved drugs to treat AD are currently available on the market (Therapeutics Search | ALZFORUM). These drugs can help slow the disease progression (e.g., anti-Aβ antibodies), address cognitive symptoms such as memory and thinking issues (e.g., acetylcholinesterase inhibitors and NMDA receptor antagonists), and manage non-cognitive symptoms such as behavioural and psychological symptoms (e.g., Brexpiprazole and Suvorexant) (Varadharajan et al., 2023).

MDD is highly associated with AD. Therefore, classical antidepressant drugs, such as tricyclic antidepressants and selective serotonin reuptake inhibitors, which primarily target the inhibition of the SERT, are mainly prescribed (Aaldijk & Vermeiren, 2022). Research has shown that various AD mouse models exhibit reduced levels of Aβ and plaques across several brain regions after the administration of selective serotonin reuptake inhibitors. Also, an improvement in cognitive function was observed (Aaldijk & Vermeiren, 2022). In addition, microgliosis and mitochondrial deficits have been repaired after selective serotonin reuptake inhibitors administration (Reddy et al., 2021; Zhang, Q. et al., 2018). Besides this, young adults and AD animals exhibited a reduction in Aβ in CSF. While selective serotonin reuptake inhibitors are commonly prescribed and considered safe for treating depression, it is essential to note that long-term use may lead to side effects (Cirrito et al., 2011; Sheline et al., 2014).

Treatment with selective serotonin reuptake inhibitors is not specific to 5-HTR. They function by prolonging the presence of 5-HT in the synaptic cleft by inhibiting SERT at the presynaptic terminal of serotonergic neurones (Hamon & Blier, 2013). There is growing interest in compounds that can modulate the serotonergic system in AD. In the next section, we will provide a short overview of potential 5-HT_2R subtype modulators, including both psychedelics and antipsychotics, that may influence AD pathology (Table 1).

1.5.1. Psychedelics and antipsychotics on 5-HT_2R subtypes

There are various agonists and antagonists that modulate 5-HT_{2A}R activity, which can lead to a potential therapeutic application in the treatment of neurological and psychiatric disorders. TCB-2, a potent and selective agonist of the 5-HT_{2a}R, can reduce the Aβ plaques load and diminish the neuroinflammatory response. It ameliorates cognitive impairment by increasing the brain-derived neurotrophic factor (BDNF) and lowering hippocampal neuronal loss (Afshar et al., 2019; Afshar et al., 2018). Desloratadine, an antagonist of the 5-HT_{2A}R, shows a similar effect by blocking the 5-HT_{2A}R (Lu et al., 2021).

Other 5-HT_{2A}R antagonists (EMD281014 and M100907) have shown a reduction in Aβ peptides across various brain regions and in CSF. These antagonists also improved memory (Terry et al., 2005; Yuede et al., 2021). The regulation of APP can be modified by both 5-HT_{2A}R and 5-HT_{2C}R antagonists (such as ketanserin, mianserin and ritanserin), thereby alleviating symptoms of delirium in AD. Ketanserin and ritaserin have been found to moderate Tau hyperphosphorylation in the hippocampus (Busceti et al., 2015; Ikeguchi & Kuroda, 1995; Nitsch et al., 1996). Inhibition of Tau hyperphosphorylation, as well as repair in LTP and memory deficiency, was seen by treatment with a 5-HT_{2C}R antagonist (RS102,221) (Busceti et al., 2015). In addition, 5-HT_{2C}R agonist (dexfenfluramine) has a beneficiary effect on the APP metabolism by reducing the $Aβ_{(1-42)}$ levels and increasing the soluble APP metabolites in CSF (Arjona et al., 2002; Nitsch et al., 1996). 5-HT_{2C}R agonist (RO-60-0175) and 5-HT_{2C}R antagonist SB242084) contribute positively to the clearance of Aβ toxicity (Tian et al., 2015).

Table 1: *Summary of possible compounds that stimulate the 5-HT_2R subtypes with a direct positive impact on the AD pathology.*

This table presents both pre-clinical and clinical psychedelics and antipsychotics concerning AD pathology or depressive systems associated with AD. Our focus is briefly overviewing how various 5-HT2R subtypes (5-HT_{2A}R, 5-HT_{2B}R and 5-HT_{2c}R) influence AD pathology. (7R)-3-bromo-2,5-dimethoxy-bicyclo[4.2.0]octa-1,3,5-

trien-7-yl] methanamine (TCB-2); hippocampus (HC); bone-derived neurotrophic factor (BDNF); long term potential (LTP); neprilysin (NEP); Cerebrospinal fluid (CSF); soluble APP (sAPP); cornu ammonis (CA 1).

5-HT$_2$R subtypes	**Receptor (ant-) agonist**	**Compounds**	**Effects**	**Source**
5-HT$_{2A}$R	Agonist	TCB-2	↓ Aβ plaques, ↓ HC neuronal loss, ↑ HC BDNF levels, ↓ Oxidative stress, Improvement in cognitive impairment	(Afshar et al., 2019; Afshar et al., 2018)
	Inverse agonist	Pimavanserin	↓ Aβ peptides in cortex, HC and CSF	(Yuede et al., 2021)
	Antagonist	EMD281014	Improvement in memory	(Terry et al., 2005)
		M100907	↓ Aβ peptides in cortex, HC and CSF	(Yuede et al., 2021)
		Desloratadine	↓ Aβ plaques in CA1 of HC, ↓ Neuroinflammation, Improvement in LTP and cognitive functions, ↑ microglial Aβ phagocytosis and degradation	(Lu et al., 2021)
		Ketanserin / Ritaserin	Regulate the APP turnover, Preventing Tau hyperphosphorylation in CA 1	(Busceti et al., 2015; Ikeguchi & Kuroda, 1995)
5-HT$_{2B}$R	Antagonist	MW071	Rescued synaptic plasticity and memory induced by Aβ- and Tau-oligomers	(Acquarone et al., 2024)
5-HT$_{2C}$R	Agonist	Dexnorfenfluramine	↑ sAPP levels in CSF, ↓ $A\beta_{(1-42)}$ levels in CSF	(Arjona et al., 2002; Nitsch et al., 1996)
		RO-60-0175	↑ NEP	(Tian et al., 2015)
	Antagonist	SB242084	↓ NEP	(Tian et al., 2015)
		RS-102,221	Preventing Tau hyperphosphorylation Repair in hippocampal LTP and memory deficiency	(Busceti et al., 2015)
		Vortioxetine	Improvement in depressive symptoms and cognitive functions	(Christensen et al., 2023; Cumbo et al., 2022; Cumbo et al., 2019)

5-HT$_{2A}$R/ 5-HT$_{2C}$R	Antagonist	Mirtazapine	↓ Depressive systems, ↓ Aβ induced neurite atrophy, Rescuing Aβ induced dendritic Golgi vesicle trafficking	(Correia & Vale, 2021; Fabbretti et al., 2021)
		Mianserin	Improvement in AD delirium, Regulate the APP turnover	(Ikeguchi & Kuroda, 1995; Nitsch et al., 1996)

Recently, the selective inverse agonist pimavanserin, which inhibits the intrinsic activity of the 5-HT$_{2A}$R, has been investigated in APP/PSEN-1 mouse model. It has been shown to reduce the Aβ$_{(1-40)}$ and Aβ$_{(1-42)}$ peptide levels and aggregation in the cortex, hippocampus and CSF (Yuede et al., 2021). 5-HT$_{2B}$R antagonist, MW071, showed neuroprotective effects on synaptic plasticity and ameliorated memory deficits induced by Aβ- and Tau-oligomers toxicity in rodents (Acquarone et al., 2024). The antagonist of both 5-HT$_{2A}$R and 5-HT$_{2C}$R, such as mirtazapine, diminished the depressive symptoms and cognitive impairments. Vortioxetine, a 5-HT$_{2C}$R antagonist, induce a similar effect. Mirtazapine can also improve brain atrophy and restore vesicle trafficking in neurones impacted by Aβ toxicity (Christensen et al., 2023; Correia & Vale, 2021; Cumbo et al., 2022; Cumbo et al., 2019; Fabbretti et al., 2021).

1.5.2. N,N-tryptamines: new class of psychedelics in AD

The classic psychedelics are categorised into ergolines and tryptamines. Herein, we will focus on the tryptamine derivatives structurally related to the neurotransmitter serotonin. The tryptamines consist of a benzene and a pyrrole ring (indole ring structure) combined with an amino group and two carbon side chains. Various structural and chemical modifications are possible on the indole ring to make more complex tryptamine derivatives. These structural changes can significantly impact the pharmacological, behavioural effects, neuroprotective, neuro-regenerative and anti-inflammatory properties of these tryptamines (Araújo et al., 2015; Kozlowska et al., 2022).

Overall, the characteristics and impacts of tryptamines derivatives from both natural (e.g. DMT, 5-methoxy-N,N-dimethyltryptamines (5-MeO-DMT)) and synthetic (N,N-diethyltryptamines (DET) and N,N-dipropyltryptamines (DPT)) origin have been studied before (Tittarelli et al., 2015). DMT and 5-MeO-DMT are the most well-known psychedelics investigated for their profound effect on anti-inflammatory and neurogenic effects in neurological disorders. (Morales-Garcia et al., 2020; Tittarelli et al., 2015).

In addition, DET has structural similarities with DMT. Little is known about DET functionality in adult neurogenesis and AD pathology in the literature. There is an essential need for an update on the potential hazard of synthetic tryptamines based on their pharmacological and toxicological properties in animal and human studies (Araújo et al., 2015). Therefore, more research is needed to elucidate the effect of DET as a potential drug candidate in neurological disorders (Figure 3). However, alternative administration routes and drug doses need to be further elucidated in AD.

The primary advantage of DET lies in its ability to be administered orally without undergoing degradation by MAO. In contrast, DMT is pharmacologically inactive when absorbed through the oral route. 5-MeO-DMT can be administered through several routes, including inhalation, intravenous injection, sublingual or intranasal insufflation, and orally using in combination with a MAOI (Tittarelli et al., 2015). DET exhibits pharmacological efficacy that extends beyond DMT, suggesting that it shares similar agonist activity for 5HTR (Figure 3). DMT is characterised by considerable binding affinity as an agonist, primarily targeting the 5-HT_{2A}R (Böszörményi et al., 1959; Cohen & Vogel, 1972; Tittarelli et al., 2015). In addition, studies indicated that the binding affinities of DMT and its derivatives are also notable for other receptors, such as TAAR and SR1, which are widely distributed throughout the brain (Fontanilla et al., 2009; Rickli et al., 2016).

Furthermore, human cerebral organoids have revealed the involvement of various receptors (such as SR1, 5-HT_{2A}R and 5-HT_{2C}R) compared to traditionally used human neural progenitor cell cultures. The latter did not exhibit 5-HT_{2A}R and 5-HT_{2C}R activity and failed to increase dendritic branch density after 5-MeO-DMT treatment (Dakic et al., 2017). Consequently, we explored the neurogenic role of DET in preliminary experiments using three-dimensional cellular AD models and *in vivo* experiments in the APP/PSEN-1 mouse model.

1.5.3. N,N-tryptamine derivatives: potential neuroprotective properties

In vitro and *in vivo* models have shown that psychedelics can elevate neuronal plasticity through the activation of 5-HT_{2A}R (Olson, 2022). These substances can promote spine density, morphology, and synaptic plasticity. Increased spine plasticity results from 5-HT_{2A}R stimulation, which activates Ras-related C3 botulinum toxin substrate 1 (RAC1). Psychedelics can regulate synaptic plasticity by further enhancing BDNF/Trk and mTOR

signalling. The pathways involving Rac1, BDNF/Trk, and mTOR signalling have been implicated in AD (Ly et al., 2018; Mi et al., 2017; Wu et al., 2019; Zhang et al., 2022a).

In vitro, DMT has been shown to promote adult neurogenesis by inducing the proliferation and migration of NSC progenitors, as well as increasing differentiation into various neuronal phenotypes such as astrocytes, oligodendrocytes and neurones (Morales-Garcia et al., 2020). Further, DMT induces NSC proliferation and supports adult hippocampal neurogenesis *in vivo*. It has also been seen to improve learning and memory performance in animal models. Research conducted by Dr. Ana Perez Castillo's laboratory and others found that hippocampal neurogenesis was also mediated through the SR1. Similar outcomes were observed for 5-MeO-DMT. (Fukunaga & Moriguchi, 2017; Morales-Garcia et al., 2020). However, a single intracerebroventricular injection of 5-MeO-DMT resulted in enhanced complexity of dendritic branching of neurones (Lima da Cruz et al., 2018).

Human cerebral organoids have shown alterations in their proteome following treatment with 5-MeO-DMT. Research has shown an increase in the formation of dendritic spine and cellular protrusion, and enhancement in microtubule and cytoskeletal organisation after this treatment (Dakic et al., 2017). Predictions suggest biological functions linked to neurodegeneration and neuroinflammation. Furthermore, proteomic investigations following 5-MeO-DMT treatment have identified proteins that may play a role in regulating the LTP (Dakic et al., 2017).

DMT and 5-MeO-DMT have been shown to promote dendritic and spine neurogenesis by activating 5-HT_{2A}R in cortical neurones. The membrane permeability of these psychedelics influences enhanced neurogenesis (Vargas et al., 2023). Compounds featuring N-methylation, such as N,N dimethyl derivatives, have been shown to promote neuronal growth by increasing the dendritic spine density. Additionally, membrane-permeable intracellular 5-HT_{2A}R agonists have been associated with increased spine formation (Vargas et al., 2023). Endogenous DMT and 5-MeO-DMT exist in humans but are rapidly degraded (Barker et al., 2012). As a result, studying their roles in health and disease processes is significantly challenging, even with advanced technology. Besides this, using N,N-ethylated synthetic compounds, such as DET, similar in structural and functionality to DMT, could present a promising new therapeutic approach in neurological disorders.

1.5.4. Targeting neuroinflammation and serotonergic pathways: implications for Alzheimer's disease and amyloid-associated depressive disorder

Astrocytes and microglia have been reported to exert neuroprotective effects through the activation of 5-HTR, S1R and TAAR (Barnes et al., 2021; Borbély et al., 2022; Nardai et al., 2020; Polini et al., 2023; Schipke et al., 2011). These receptors on these glial cells can trigger a neuroinflammatory response. Research indicates that DMT and 5-MeO-DMT reduce both mRNA and protein levels of pro-inflammatory markers (IL- 1β, IL- 6, TNF- α, IL-8 and APAF-1) while simultaneously enhancing the regulation of anti-inflammatory responses (IL-10) and increasing BDNF levels (Nardai et al., 2020; Szabo et al., 2014).

5-MeO-DMT treatment in human cerebral organoids has been demonstrated to elicit an anti-inflammatory response through the NF-κB signalling pathway (Dakic et al., 2017). Additionally, the S1R agonist DMT mitigated the effect of induced hypoxia in human-induced pluripotent stem cell-derived cortical neurones (Szabo et al., 2016). NF-κB is a crucial transcription factor that plays a pivotal role in the production of Aβ by regulating pro-inflammatory and anti-inflammatory responses in AD (Faria et al., 2014; Gao et al., 2022; Ly et al., 2013).

Immune regulation through the inhibition of IDO has been observed in AD (Yu et al., 2015). DMT and its precursor tryptamines can inhibit IDO, which plays a crucial role in the downstream regulation of the kynurenic pathways (Tourino et al., 2013). Oral administration of coptisine, an IDO inhibitor, has been shown to reduce microgliosis and astrogliosis in the APP/PSEN-1 mouse model, subsequently decreasing neuronal loss and the formation of Aβ plaques (Tourino et al., 2013; Yu et al., 2015). Furthermore, DMT can inhibit the SERT and vesicle monoamine transporter 2, leading to enhanced serotonin levels in the brain (Cozzi et al., 2009; Nagai et al., 2007). Harmala alkaloids influence the prolonged physiological effects of DMT and serotonin in the brain. Harmala alkaloids are found in ayahuasca brew and act as a MAOI, stimulating adult neurogenesis *in vitro* (Cameron et al., 2018; Morales-García et al., 2017; Riba et al., 2003).

Recent study have demonstrated that DMT modulates the Aβ accumulation in the hippocampus and prefrontal cortex of a triple AD transgenic mouse model (Cheng et al., 2024). It has also been shown that DMT reduces astrogliosis and slightly affects microgliosis after $A\beta_{(1-42)}$ induced toxicity *in vivo* (Borbély et al., 2022). Additionally, DMT has been found to increase S1R activity *in vitro* and *in vivo*. Furthermore, DMT has been investigated to

restore mitochondrial dysfunction caused by Aβ toxicity in hippocampal neurones (Cheng et al., 2024).

In summary, the bidirectional relationship between AD and MDD has shared pathological mechanisms. These mechanisms include amyloid pathology, neuroinflammation, impairments in neuroplasticity processes such as neurogenesis, synaptic plasticity, and alterations in lipid metabolism. Using tryptamine derivatives to influence these mechanisms may provide new and promising ways to treat both conditions.

1.6. Understanding the impact and relevance of AD models in current research

Experiments on AD models are designed to improve our comprehension of the onset and progression of the pathophysiological features of AD while also working towards developing novel diagnostic and treatment approaches (Centeno et al., 2018; Drummond & Wisniewski, 2017; Ranjan et al., 2018). None of the current models have fully captured human AD in its pathological, biochemical, and behavioural aspects. As there are no animals that naturally develop both key features of AD (Aβ buildup and Tau hyperphosphorylation), the most widely utilised models for studying this condition are *in vitro* two-dimensional and three-dimensional cell cultures, along with in vivo transgenic animal models (Drummond & Wisniewski, 2017; Sreenivasamurthy et al., 2023; Yokoyama et al., 2022). Two-dimensional and three-dimensional cultures consist of brain cells or stem cells (either embryonic or induced pluripotent cells) obtained from animals and patients, which will eventually differentiate into various somatic cells found in the brain (e.g., neurones, astrocytes, microglia). These cells are cultivated to replicate specific inherent characteristics of the native human brain (Cenini et al., 2021; Drummond & Wisniewski, 2017). These models encounter several limitations, including inadequate tissue availability from AD patients and variations in epigenetics and/or phenotypes within cell lines derived from donors (Drummond & Wisniewski, 2017; Ranjan et al., 2018; Velasco et al., 2019). Furthermore, long-term cultures can be both labour-intensive and costly, and there is currently a lack of standardised procedures necessary to replicate the ageing brain conditions associated with neurodegenerative diseases (Cenini et al., 2021; Drummond & Wisniewski, 2017; Liu et al., 2012; Papaspyropoulos et al., 2020; Ranjan et al., 2018; Sreenivasamurthy et al., 2023; Velasco et al., 2019). Additionally, challenges arise in recreating the most affected brain regions, such as the hippocampus and specific cortical layers, and in conducting imaging studies (D'Avanzo et al., 2015; Papaspyropoulos et al., 2020; Ranjan et al., 2018). These models also fall short of accurately representing the complex environment of the human

brain, which should encompass a broader range of essential brain cell types, intricate interactions among neurones throughout the brain, and systems related to vascular and drainage functions (Cenini et al., 2021; Drummond & Wisniewski, 2017; Papaspyropoulos et al., 2020; Sreenivasamurthy et al., 2023).

In conclusion, a significant challenge contemporary drug development models face is their ability to evaluate behavioural outcomes effectively. This limitation significantly restricts their applicability during the initial phases of the drug development process (Centeno et al., 2018; Choi et al., 2016). Although progress has been made by advancing from two-dimensional to more sophisticated three-dimensional cultures, numerous issues remain unaddressed. Therefore, it is imperative to integrate three-dimensional cultures with *in vivo* transgenic models to elucidate the specific effects of pharmacological compounds. These *in vivo* transgenic models consist of living organisms wherein specific genes, identified through human gene linkage studies pertinent to AD, have been modified or introduced into the animal genome. This genetic manipulation creates models that closely mirror human pathophysiology, reducing the need to use non-human primates or human subjects (Harvey et al., 2011; Vandamme, 2014).

The utility of these models offers valuable insights into the biological effects of AD due to their high physiological relevance and their similarity to the structural and biochemical aspects of brain ageing (Ranjan et al., 2018; Sreenivasamurthy et al., 2023; Vandamme, 2014). Moreover, they are pivotal in drug development and therapeutic assessment during preclinical testing (Ranjan et al., 2018; Yokoyama et al., 2022). The selection of mice as the animal model provides several advantages, including (1) their small size and genetic similarity to humans, coupled with low-cost maintenance for housing and feeding, which facilitates large-scale and high-throughput studies (Vandamme, 2014; Yokoyama et al., 2022); (2) their relatively short lifespan, which permits manageable long-term studies focussing on ageing and neurodegenerative diseases (Ranjan et al., 2018; Yokoyama et al., 2022); and (3) the availability of an established framework for genetic manipulation, complemented by a wide array of research tools, such as antibodies (Lecanu & Papadopoulos, 2013; Yokoyama et al., 2022).

1.6.1. Exploring the APP/PSEN-1 mouse model: a critical tool for understanding AD pathogenesis

Since the late 1980s, more than 200 mutations associated with AD have been identified, leading to the development of numerous transgenic mouse models that have substantially advanced the field (Alzheimer's Disease Research Models | ALZFORUM; Myers & McGonigle, 2019). These models exhibit distinct pathological and behavioural effects depending on the mutations expressed. The pursuit of expanding these effects has resulted in the creation of increasingly sophisticated transgenic models, including multi-transgenic variants (Myers & McGonigle, 2019; Sanchez-Varo et al., 2022). This section will primarily focus on transgenic models that harbour specific mutations in both APP and PSEN genes.

These models are based on the transgenic overexpression of human APP, incorporating various familial AD-associated mutations in the APP gene. These APP mutations lead to the production of different Aβ peptides that are more prone to aggregate. The decision to overexpress APP was made to mimic the β-amyloidosis typically observed in the brains of individuals with AD, resulting in increased levels of Aβ and APP fragments (such as sAPP, CTF-α, CTF-β, and AICD) (Kitazawa et al., 2012; Nilsson et al., 2014; Sasaguri et al., 2017). Furthermore, in these models, the PSEN genes are also linked to several familial mutations associated with AD. These genes encode proteins that are vital components of the γ-secretase complex, which is involved in the cleavage of APP and among many other cellular functions (Hernández-Sapiéns et al., 2022; Kitazawa et al., 2012; Nilsson et al., 2014; Sasaguri et al., 2017). Mutations in PSEN genes typically alter secretase cleavage, leading to an increased production of the amyloidogenic Aβ. These PSEN gene mutations can speed up the Aβ accumulation, which in turn causes more neuronal damage and cognitive decline (Hernández-Sapiéns et al., 2022; Kitazawa et al., 2012; Sasaguri et al., 2017). To study this further, researchers have developed various AD models featuring different combinations of mutations in both the APP and PSEN genes. Each of these models uses specific promoters and individually shows different characteristics of AD as well as different timelines when the symptoms appear in AD (Myers & McGonigle, 2019; Research Models Search | ALZFORUM)

Furthermore, a widely used and well-characterised model for AD that incorporates both APP and PSEN-1 mutations is the APP/PSEN-1 (Tg) mice model. This mouse model carries two transgenes with AD-linked mutations: the human APP gene featuring the Swedish mutation (KM670/671NL) and the modified human PSEN-1 gene, which lacks exon 9 due to a

nonsense mutation at the splice acceptor site (guanine changing to thymine). This alteration prevents the translation of exon 9, which was identified in the mid-1990s (Jankowsky et al., 2004; Jankowsky et al., 2001; Perez-Tur et al., 1995). The deletion of exon 9 corresponds to a form of early-onset AD. Both transgenes are controlled by the mouse prion protein promoter element, which directs transgene expression predominantly to neurones of the central nervous system (Jankowsky et al., 2004; Jankowsky et al., 2001).

The neuropathological characterisation of the Tg mice model starts at approximately 4-6 months with the accumulation of Aβ plaques in both the cortical and hippocampal regions. The accumulation of Aβ plaques increases in size and number with ageing (Garcia-Alloza et al., 2006; Izco et al., 2014; Jackson et al., 2013; Jankowsky et al., 2004; Kamphuis et al., 2012; Minkeviciene et al., 2008; Ruan et al., 2009). Alongside plaque formation, these mice exhibit a decline in synaptic function, neuronal loss, and reactive gliosis, characterised by the presence of astrocytes and activated microglia surrounding the Aβ plaques in the cortex and hippocampus (Bai et al., 2017; Hong et al., 2016; Jackson et al., 2013; Kamphuis et al., 2012; Malm et al., 2007; Minkeviciene et al., 2008; Ruan et al., 2009; Toledo & Inestrosa, 2010). Behaviourally, Tg mice show impairments in learning and memory, particularly difficulties in spatial memory and cognitive flexibility, starting between 6-10 months (Hulshof et al., 2022; Izco et al., 2014; Lalonde et al., 2005; Minkeviciene et al., 2008).

Furthermore, transcriptomics studies have revealed that differences between Tg and wild-type (WT) mice can be detected as early as 2 months of age (Chintapaludi et al., 2020). Variations in gene expression associated with the transgenes have been documented for genes related to protein translation, oxidative phosphorylation, hormonal signalling, proteolysis, and myeloid-cell activity, as well as among other factors (Chintapaludi et al., 2020; Jackson et al., 2013; Onos et al., 2019). Additionally, WT and Tg mice display age-related changes in their brain transcriptomes; genes exhibiting differential expression at 4 and 6 months, regardless of genotype, are linked to mRNA processing, protein translation, and oxidative phosphorylation (Jackson et al., 2013).

Studying these models, which incorporate mutations of APP and PSEN genes, gives us a valuable opportunity to deepen our understanding of Aβ pathology, neuroinflammation, and impaired neurogenesis in the context of ageing and AD. These models could also help discover new treatments to improve these conditions and slow their progression in ageing and AD.

2. Research aims and framework of this dissertation

2.1. Objectives

The research endeavours of this work are to reveal the pathological impact of human $A\beta_{(1-40)}$ and $A\beta_{(1-42)}$ species on early pathological effects in AD as well as the impact of neurogenic novel therapeutic agents (such as N,N-diethyltryptamine (DET) on pathological symptoms in AD models. Increasing evidence supports that Aβ pathology might affect synapses, lipids, neuroinflammation and neurogenesis in AD. The research challenges addressed here are presented as follows:

1. <u>How do adult neurogenesis and neuroinflammation manifest and interact in the APP/PSEN-1 (Tg) mouse model?</u>
   - *What might be the relation between RELN and microgliosis in various AD mice brain regions during ageing?*

RELN is expressed in layer II entorhinal cortical neurones and plays a crucial role in neuroplasticity, which is initially affected in AD. Additionally, neuroinflammation is an early symptom of AD. However, the relation between RELN and microgliosis in a longitudinal study involving 2-12-months-old brain slices from both hippocampal and entorhinal areas of Tg and WT mice has not been reported yet. Here, we will conduct primary research on the expression of RELN and microglial marker through immunohistochemistry in the hippocampal and entorhinal areas of 2-12-month-old WT and Tg mice. Our approach could contribute to a deeper understanding of the early stages of AD.

- *Can we develop an ageing-related AD in vitro model from Tg and WT mice for investigating the effect of Aβ pathology?*

Previous research has shown that neurospheres can be cultivated from both young and old animals. However, the exploration of adult neurogenesis and the impact of Aβ toxicity in neurospheres from WT and Tg mice, particularly those around 16 months old, has not yet been elucidated. Our objective was to cultivate neurospheres from WT and Tg mice at this age and investigate the implication of adult neurogenesis during the early stage of AD.

2. <u>What is the pathological effect of various Aβ species on synaptic and lipid homeostasis in various brain cells?</u>

Synaptic dysfunction is an early event in the pathology of AD. Research has demonstrated that various Aβ species exert differing effects on the synaptic

pathology in AD, with $A\beta_{(1-40)}$ being less toxic than $A\beta_{(1-42)}$. Furthermore, studies indicated that Aβ species might have a neurotrophic effect. Therefore, the aims of this study are divided into four parts:

- *Does synaptic loss occur before lipid alterations after Aβ-induced toxicity?*
- *Are there Aβ species-dependent alterations in synaptic loss and lipid changes?*
- *Does Aβ species have a neurotoxic or neurotrophic effect on synapses and lipids?*
- *Do extracellular lipid profiles differ from cellular lipid profiles after Aβ-induced toxicity?*

To investigate this effect, we utilised primary hippocampal neurones and glial cells from mice. These brain cells were treated for 3 or 12 hours with human $A\beta_{(1-40)}$ or $A\beta_{(1-42)}$ species. The synaptic analysis involved labelling both pre- and postsynaptic markers to evaluate the loss of active synapses resulting from Aβ species exposure and time-dependent toxicity. Specific regions were selected to count the loss of active synapses. In addition, we examined lipid profiles using high-performance thin-layer chromatography and tandem mass spectrometry on the same brain cells during the Aβ-induced treatment intervals.

3. <u>What is the therapeutic effect of N,N-diethyltryptamine on AD pathology?</u>

Previous research in Dr. Ana Perez Castillo's laboratory, affiliated with CIBERNED and CSIC-UAM in Madrid, demonstrated that N,N-diethyltryptamine (DET) exhibits neuroprotective and anti-inflammatory properties. Consequently, our objective is to investigate the effect of DET on AD pathology. Therefore, we are analysing both magnetic resonance images (MRI) and magnetic resonance spectroscopy (MRS) of WT and Tg mice following DET treatment. MRI will enhance our understanding of the neuroprotective implications of DET regarding Aβ accumulation and the structural integrity of the brain, including axonal and myelin integrity. Meanwhile, MRS might reveal the neuroprotective and anti-inflammatory effect of DET on key metabolites, macromolecules, and lipid resonance that are dysregulated in AD.

In conclusion, we propose an innovative approach to investigate adult neurogenesis *in vitro* and *in vivo*, particularly about amyloidosis-related pathologies, focussing on AD pathology. The study aims to characterise Aβ species, particularly $A\beta_{(1-40)}$ and $A\beta_{(1-42)}$, alongside examining neuroinflammatory processes and the neuroplasticity protein RELN in our Tg

mouse model of AD. Furthermore, we intend to explore an alternative treatment approach for AD involving compounds capable of modulating the serotonin pathway *in vitro* and *in vivo*. Our research will also assess how these Aβ species impact active synapses and cellular and extracellular lipid profiles. Thus, our approach could lead to a better understanding of the early stages associated with Aβ-induced toxicity in AD. This research might also contribute to developing new target-based molecules and innovative therapeutic tools for diagnosing, preventing, and treating this devastating disorder.

2.2. Framework of this dissertation

The framework of this monograph dissertation comprises two research chapters (Chapters 3 and 4). The dissertation outlines the research conducted at the laboratory of Dr. Ana Perez Castillo (CIBERNED) in Madrid, Spain (Chapter 3) and the research conducted at the research unit of Anatomy at the Carl von Ossietzky Universität Oldenburg, Germany (Chapter 4). The work in both chapters was part of a Marie Skłodowska-Curie Innovative Training Network project. The research work in Chapter 3 will not be published in a peer-reviewed journal. The work in Chapter 4 consists of an article in a peer-reviewed journal (Van Bulck et al., 2022) and unpublished data. Both published and unpublished data were incorporated into Chapter 4 of the dissertation to allow a comprehensive synthesis of the entire body of doctoral work. However, slight modifications were made to the layout of the published data figures, tables, and text without changing their initial published content. Herein, we briefly outline both chapters.

- **Chapter 3: Investigation of Aβ species, neuroinflammation, adult neurogenesis and therapeutic intervention in the AD mouse model**

  Here, we mainly focussed on characterising neuroinflammation, Aβ peptide aggregation, neuroplasticity/neurogenesis, and novel DET treatment in our Tg AD mouse model. Furthermore, we preliminarily explored adult neurogenesis and the impact of Aβ toxicity or DET treatment on neurospheres from aged WT and Tg mice.

- **Chapter 4: The impact of Aβ species on synaptic plasticity and lipid profiling: insights from *in vitro* physiological models**

  The outline of this chapter is based on the publication: “Aβ-induced alterations in membrane lipids occur before synaptic loss appears”, which shows the synaptic loss of hippocampal neurones and lipid profiles of hippocampal neurones and glial cells after Aβ species stimulation. Further, it also consists of supplementary material of unpublished lipid data from conditioned media of hippocampal neurones and glial cells.

Furthermore, the beginning of each chapter highlights a short overview of the provided data, contributions, and possible drawbacks.

3. Investigation of Aβ species, neuroinflammation, adult neurogenesis and therapeutic intervention in the AD mouse model

The results of this chapter, which will not be published, focus on the effect of various Aβ species ($A\beta_{(1-40)}$ and $A\beta_{(1-42)}$) and their relation to adult neurogenesis and neuroplasticity in WT and Tg mice. The data provides immunofluorescence imaging of Aβ species, neuroinflammation, and RELN in different developmental phases of WT and Tg mice. Also, these Aβ species were investigated on a three-dimensional model (neurospheres) obtained from the subventricular zone of old WT and Tg mice. Furthermore, a new potential tryptamine derivative was tested on these neurospheres and *in vivo*. In vivo magnetic resonance imaging (MRI) and magnetic resonance spectroscopy (MRS) were performed for this.

Contributions:

All *in vitro* and *in vivo* experiments were performed by Michiel Van Bulck (M.V.B.). M.V.B., Dr. José Angel Morales Garcia and Dr. Ana Pérez Castillo designed the study. M.V.B. did fluorescent imaging and data processing. The MRI, MRS, and raw data collection were performed by the Biomedical NMR Facility Sebastián Cerdán in the Instituto de Investigaciones Biomédicas (CSIC-UAM). M.V.B. did further data analysis of the data collected from the NMR facility. PD Dr. Peter Sörös and Prof. Dr. Anja U. Bräuer helped with the MRI data analysis.

Drawbacks:

Due to problems in the animal cohort, animal facility, and COVID-19 crisis, as well as diverse research interests in Dr. Ana Perez Castillo's laboratory, the pilot study with neurospheres and therapeutic compounds that M.V.B. started could not have been extended for a longer period. Therefore, there are some discrepancies and inconsistencies in the data sets.

Hereby, I confirm that Michiel Van Bulck contributed to the investigation as stated above.

(Place, Date) (Prof. Dr. Anja U. Bräuer)

Oldenburg, 27.06.2025 Prof. Dr. Anja Bräuer

3.1. Introduction

AD is a multifactorial neurodegenerative disorder characterised by the pathological accumulation of Aβ peptide species and neurofibrillary tangles within the brain (De Strooper, 2010; Haass et al., 2012). Increasing evidence indicates that neuroinflammation and impaired neuroplasticity may serve as early signs of this disorder, underlying the necessity for additional research into the intricate relationship between neuroinflammation and neuroplasticity in the context of AD pathology (Amor et al., 2014; Heneka et al., 2015; Sung et al., 2020). Recent investigations have revealed a correlation between diminished NSC proliferation and neuronal maturation, which can occur with microgliosis. These effects are frequently observed in the early stages of AD (Salta et al., 2023). Furthermore, microglia are vital in regulating synaptic pruning and refinement throughout neural development within the brain. They can release numerous signalling molecules associated with synaptic activity and the regulation of neuroplasticity. Their role in maintaining synaptic homeostasis is achieved through the phagocytosis of synapses, a process that can become dysregulated in AD due to Aβ-induced toxicity (Cornell et al., 2022; Gao et al., 2023; Salta et al., 2023).

Moreover, advancements in proteomic analyses have enriched our comprehension of AD by identifying novel proteins, primarily focussing on synaptic proteins associated with RELN-positive cells (Dayon et al., 2018). RELN itself is a vital glycoprotein located in the extracellular matrix of layer II neurones in the entorhinal cortex and is essential for neurogenesis in the hippocampus and in promoting synaptic plasticity (Kobro-Flatmoen et al., 2016; Krstic et al., 2012; Lane-Donovan et al., 2015; Weeber et al., 2002). The processing of APP can be modulated by its interactions with various extracellular glycoproteins, including RELN (Cuchillo-Ibañez et al., 2016). Besides its critical roles in embryonic brain development, RELN is integral to neuronal migration, proper cortical layering, and the maturation of dendrites and spines. In the adult brain, RELN regulates synaptic function and plasticity (Folsom & Fatemi, 2013; Förster et al., 2006; Lane-Donovan et al., 2015). Disruptions in RELN-mediated molecular mechanisms may result in significant impairments in cortical layering, synaptic plasticity, and dendritic growth, all of which are linked to various neurological disorders, including AD (Campo et al., 2009; Katsuyama & Terashima, 2009; Sato et al., 2016).

The current pharmacological options for treating AD are relatively limited, focussing primarily on a few available medications that aim to mitigate the progression of the disease. These treatments primarily address cognitive symptoms, such as impairments in memory and

cognition, while also attempting to manage non-cognitive symptoms, including behavioural and psychological issues (Varadharajan et al., 2023). However, the limitations of these treatments underline the need for novel drug approaches. Psychedelics, including N,N-tryptamines, are increasingly being considered as potential options to alleviate the behavioural symptoms associated with AD, offering a promising avenue for further research and development (Borbély et al., 2022; Garcia-Romeu et al., 2022; Johnson et al., 2019; Sinha et al., 2024).

In this framework, Dr. Ana Perez Castillo's laboratory and colleagues have conducted research into a novel class of psychedelics known as N,N-tryptamines (Araújo et al., 2015; Kozlowska et al., 2022; Morales-Garcia et al., 2020). Prior investigations have elucidated the attributes and effects of tryptamine derivatives derived from natural sources (e.g., DMT, 5-MeO-DMT) and synthetic compounds (such as DET and DPT). DMT and 5-MeO-DMT have garnered considerable attention for their significant anti-inflammatory and neurogenic properties relevant to neurological disorders (Morales-Garcia et al., 2020; Tittarelli et al., 2015).

Moreover, research led by Dr. Ana Perez Castillo and other investigators has examined various psychedelic N,N-tryptamines, including DMT, DET (Perez Castillo et al., 2018 (Patent No. US11723894B2)), DPT, and 5-MeO-DMT (Fontanilla et al., 2009; Lima da Cruz et al., 2018; Morales-Garcia et al., 2020; Szabo et al., 2014; Szabo et al., 2016; Winter, 1969). These studies highlight the ability of DET to modulate neuroinflammatory responses and promote adult neurogenesis in the context of neurological disorders (Fontanilla et al., 2009; Lima da Cruz et al., 2018; Morales-Garcia et al., 2020; Szabo et al., 2014; Szabo et al., 2016; Winter, 1969). Furthermore, preliminary findings from Dr. Ana Perez Castillo's laboratory indicate that DET may be a promising candidate for *in vivo* studies focussed on AD, based on experiments utilising neuroblastoma cell lines with either WT or Swedish APP mutations (unpublished data). Nonetheless, additional research is essential to comprehensively evaluate the potential of DET *in vivo* for addressing the complexities associated with AD. Our findings provide, for the first time, insight into the impact of DET on the pathology of AD through both *in vitro* and *in vivo* methodologies utilising a combination of qualitative and quantitative approaches. Using a descriptive qualitative approach, we aim to elucidate the potential interplay between neuroplasticity, human-specific Aβ aggregates, and neuroinflammation within our Tg AD model.

3.2. Descriptive analysis of AD neuropathology in diverse regions of the murine brain

3.2.1. Neuropathological characterisation of human-specific Aβ aggregates across various brain regions in a murine model of AD

The characterisation of amyloid plaques in the brains of Tg mice compared to WT littermates is essential for understanding the pathological mechanisms underlying AD. This study investigates human-specific Aβ aggregates in the cortex, entorhinal cortex, and hippocampus of 4- to 12-month-old WT and Tg mice. To achieve this, we utilised various specific Aβ antibodies, such as H31L21, 6E10 and OC, each designed to target distinct epitopes of the amyloid formation products (Table 2). Our findings reveal that Tg mice exhibit specific $A\beta_{(1-42)}$ aggregates, first appearing in the cortex at 4 months and in the hippocampus at 9 months (Figure 6 and Figure S1). Additionally, the entorhinal cortex exhibits human-specific $A\beta_{(1-42)}$ aggregates starting from 9 months of age (Figure 7). However, large specific $A\beta_{(1-42)}$ plaques begin to accumulate in the brains of Tg mice at 9 months compared to their WT littermates. No human-specific $A\beta_{(1-42)}$ aggregates were detected in the cortex, hippocampus, or entorhinal cortex of WT mice aged 4 to 12 months (Figure 6, Figure 7 and Figure S1). Beginning at 9 months, Aβ load is noticeably present in the cortex and hippocampus. Furthermore, the size of human-specific $A\beta_{(1-42)}$ plaques appears to increase at least twofold in the hilus between 9 and 12 months in Tg mice. Additionally, $A\beta_{(1-42)}$ aggregates show signs of extensive diffusion into destructed nuclei, starting at 9 months and increasing by 12 months in Tg mice's cortical and hippocampal regions (Figure 6 and Figure 7). The detection of Aβ aggregates becomes prominent in the cortex and hippocampus of 9-month-old Tg mice. Therefore, we aim to characterise various Aβ species in brain slices from 9- and 12-month-old Tg and WT mice. Our observations reveal that amyloid fibrils and specific oligomers are more widely dispersed in 9- and 12-month-old Tg mice than their WT counterparts (Figure S2). In addition, 9- and 12-month-old Tg mice exhibit significant scattering of specific Aβ, C99, APP, sAPPα, and C-terminus $A\beta_{(1-42)}$ within the cortex and hippocampus. However, no such findings were observed in the cortex and hippocampus of WT brain slices (Figure S2).

3.2.2. Neuropathological characterisation of human Aβ aggregates and neuroinflammation across various brain regions in a murine model of AD

We labelled 4- to 12-month-old Tg and WT brain slices to examine the presence of plaque-associated astrogliosis and microgliosis in the cortical and hippocampal regions. Our observations identify specific human $A\beta_{(1-42)}$-associated astrogliosis in the cortex of 4-month

Tg mice compared to WT mice. However, no notable human $A\beta_{(1-42)}$-associated astrogliosis is detected in the hippocampus of the 4-month-old Tg or WT mice (Figure S4). In contrast, the hippocampal region exhibits changes in human plaque-associated microgliosis staining in 4-month-old Tg mice compared to WT mice (Figure S3). Furthermore, 9- and 12-month Tg mice show alteration in human plaque-associated microgliosis staining compared to their matched WT counterparts (Figure S5).

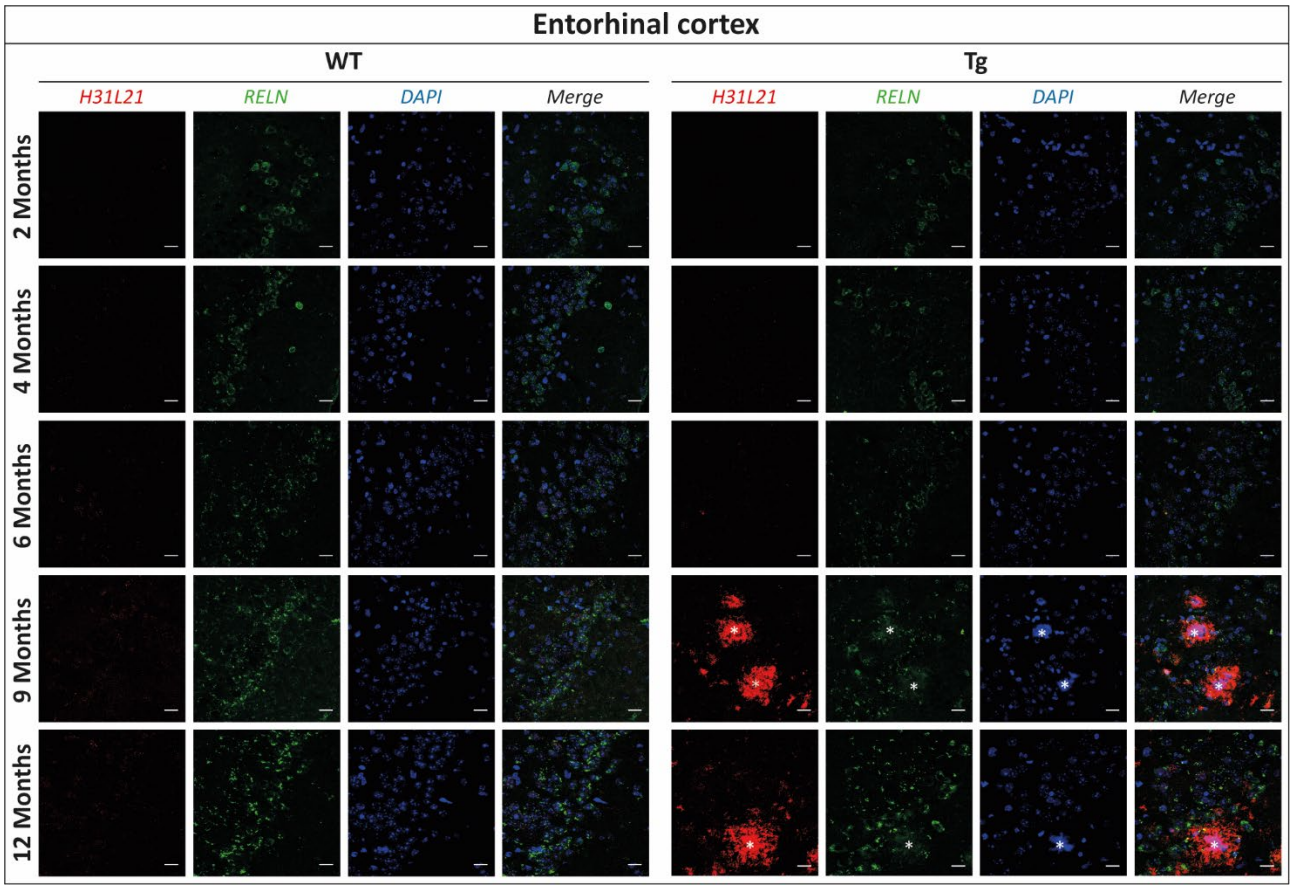

Figure 6: *Reelin-positive cells in the entorhinal cortex from 2-12 months old WT and Tg mice. Representative immunohistochemistry (IHC) fluorescence images depict human-specific $A\beta_{(1-42)}$ (H31L21, red) and reelin-positive cells (RELN, green) in layer II of the entorhinal cortex from WT and Tg mice aged 2 to 12 months. Here, we show the aggregation of human $A\beta_{(1-42)}$ in the entorhinal cortex of WT and Tg mice over the specified age range. Notably, RELN-positive cells show fluorescent alterations as early as 2 months in Tg compared to WT, with increases observed during normal ageing and AD. The area of human-specific $A\beta_{(1-42)}$ aggregation (white Asterix *) in 9-month-old Tg mice indicates a considerable destruction to the nuclei staining (DAPI, blue) of RELN-positive cells when compared to WT. The scale bar represents 20 µm.*

3.2.3. Neuropathological examination of adult neurogenesis and neuroplasticity across various brain regions in a murine model of AD

In this study, we conduct a descriptive observation of adult neurogenesis and neuroplasticity across various brain regions in WT and Tg animals aged 2 to 12 months. We focus on

microscopic analysis of RELN labelling concerning Aβ, microgliosis, and adult neurogenesis in mice's cortical and hippocampal areas of 2-12 months. Our preliminary data might indicate that fluorescent staining of RELN-positive cells (Figure 6 and Figure 7) is reduced in $A\beta_{(1-42)}$-affected hippocampal area and entorhinal cortex of 9-month-old Tg compared to their WT littermates. Notably, a decrease in RELN-positive cells appears to begin as early as 4 months in Tg mice compared to WT littermates, suggesting an increase during normal ageing and AD pathology (Figure 6 and Figure 7). Additionally, in 9-month-old Tg mice, the area of human-specific $A\beta_{(1-42)}$ aggregates is associated with enormous destruction of nuclei staining in RELN-positive cells compared to WT littermates in both the hippocampal area and the entorhinal cortex (Figure 6 and Figure 7). Furthermore, our initial assessment might indicate that reactive microglia are dysregulated around RELN-positive cells in 2-month-old WT and Tg mice.

A preliminary observation from the entorhinal cortex might indicate that microglia activation increases between 2 and 6 months and decreases from 9 months in WT and Tg mice (Figure 8). From an exploratory perspective, it appears that RELN-positive cells lack stem cell-based proliferating capacity in the cortical and hippocampal regions of 2- to 6-month-old WT and Tg mice (Figure S7). Consistent with findings from other studies and reviewed in different *in vitro* and *in vivo* AD models (da Silva Siqueira et al., 2021; Hanspal & Gillotin, 2022), our data suggest that neurogenesis is impaired at 6 months. These 6-month-old Tg mice might exhibit a decrease in neuronal progenitor and proliferating cells in the subventricular and subgranular zones compared to their WT littermates (Figure S6).

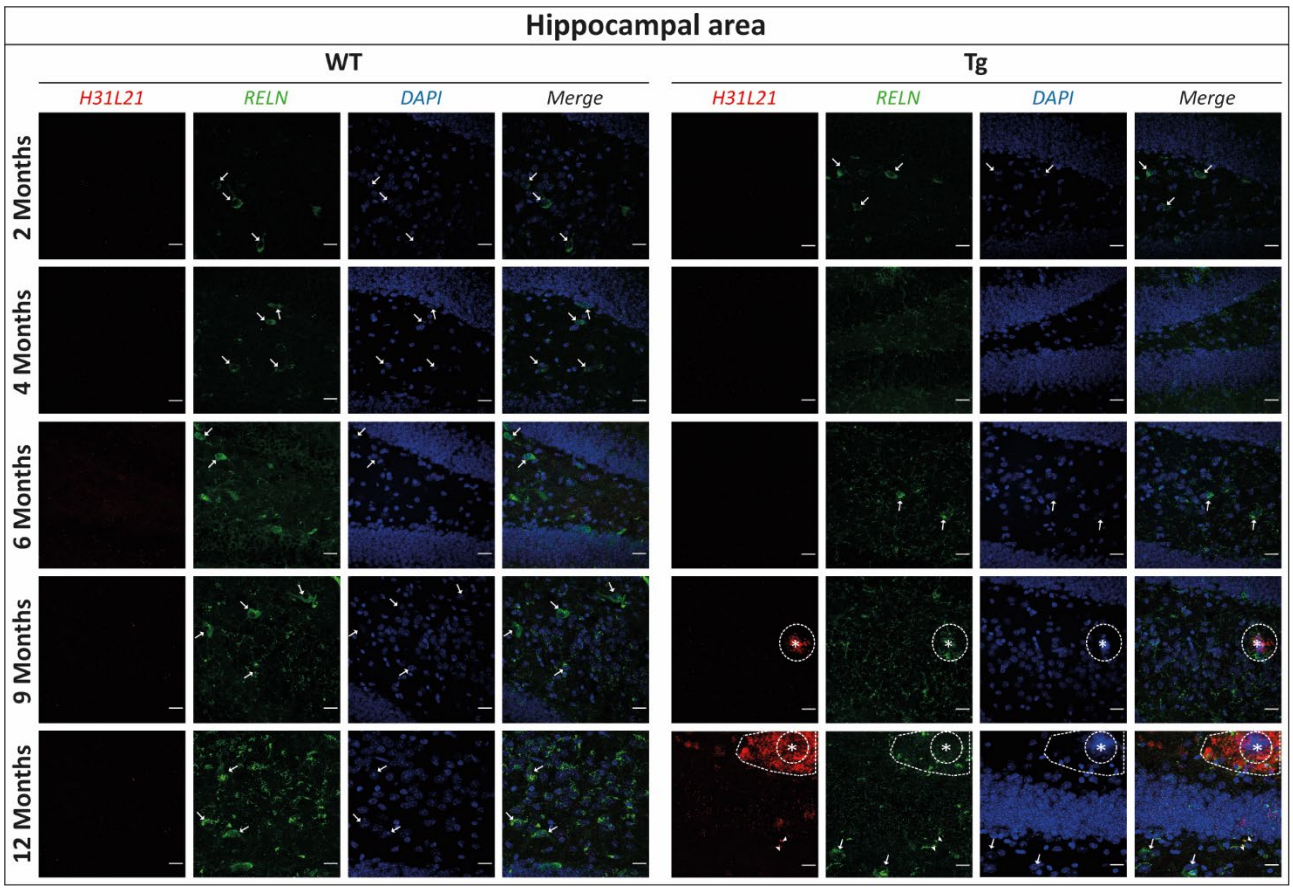

Figure 7: *Co-occurrence of adult neurogenesis and human-specific Aβ(1-42) plaques formation in the hilus of the hippocampus of WT and Tg mice.*

*Reelin-positive cells (RELN, green, white arrows) in the hippocampal area (hilus) are impacted by normal ageing and AD pathology in WT and Tg mice. In Tg mice, human-specific Aβ(1-42) plaques (H31L21, red, white dashed lines) begin to appear at 9 months, in contrast to WT. These human Aβ(1-42) (white dashed lines) aggregates are detrimental to the integrity of destroying RELN-positive cells. There is a noticeable alteration in the fluorescent signal of RELN-positive cells in the 4-month-old Tg mice compared to their WT littermates. Additionally, the size of the human Aβ(1-42) plaques (white dashed lines) in the hilus increases by at least twofold in Tg mice from 9 to 12 months. The aggregated area of Aβ(1-42) reveals enormous diffusion of damaged nuclei (DAPI, blue, white asterisk *), starting at 9 months and continuing to increase by 12 months in Tg mice. The scale bar represents 30 µm.*

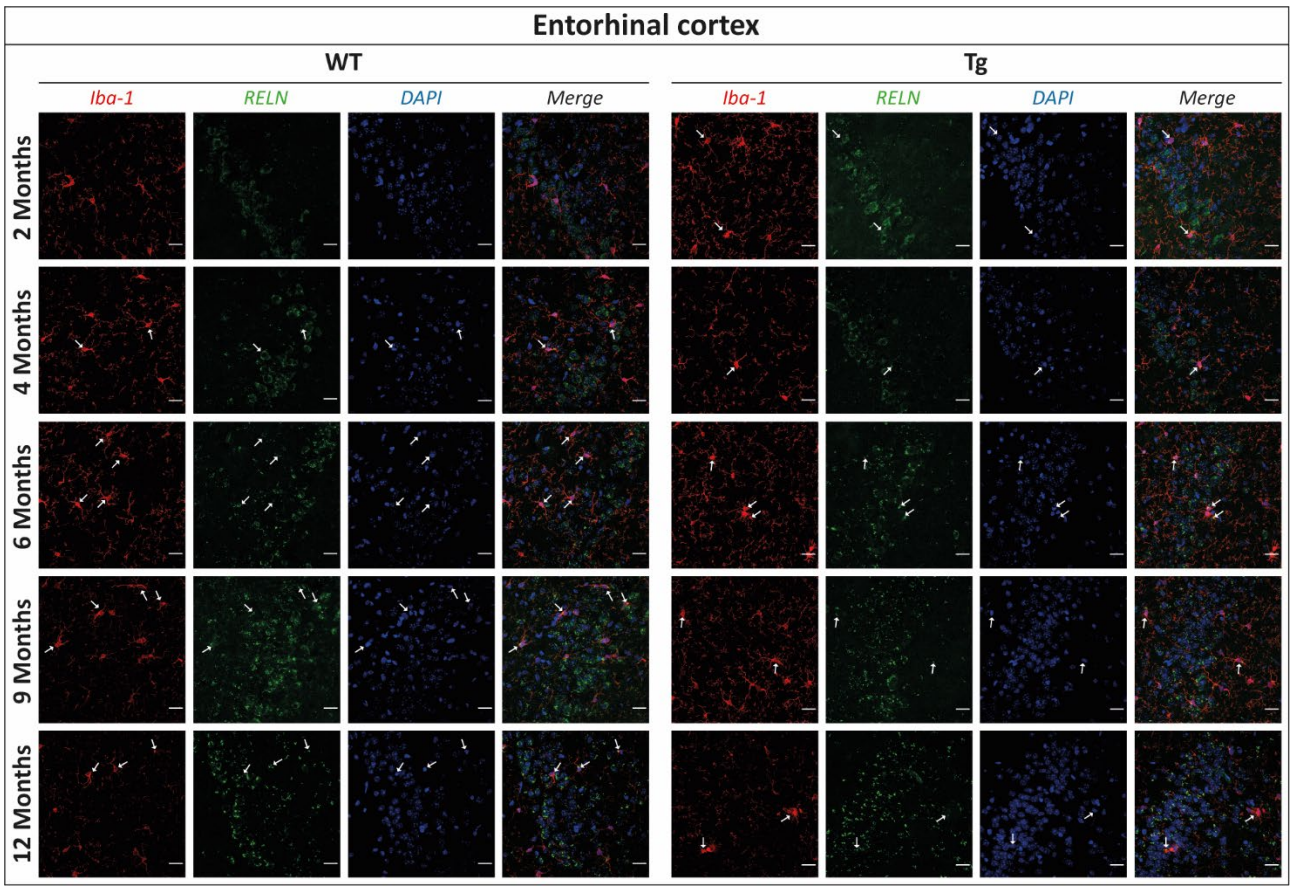

Figure 8: *Co-occurrence of inflammatory response and impairment of adult neurogenesis/neuroplasticity in the entorhinal cortex of 2-12 months old WT and Tg mice.*

Representative images from IHC reveal dysregulation in the fluorescent signal of Reelin-positive cells (RELN, green) in response to microglia (Iba-1, red) recruitment in 2-month-old Tg mice compared to WT. There might be an increase in fluorescent staining of microglia activation during normal ageing and AD. White arrows might indicate the uptake of extracellular RELN by reactive microglia. DAPI (blue) was utilised for nuclear staining. The scale bar represents 20 µm.

3.2.4. Descriptive analysis of N,N-diethyltryptamine and human-specific Aβ species treatment on neurospheres derived from adult murine model

To assess whether Aβ species and DET can promote the NSC differentiation within neurospheres, we collected samples from the subventricular zone of WT and Tg mice, approximately 16 months old. These neurospheres were then placed in conditions conducive to differentiation. Preliminary data exploration might indicate that the distal part of the Tg neurospheres exhibits altered populations of mature neurones (Figure 9, (MAP-2, red)) and immature neuronal cells (Figure 9, β-III-Tubulin (Tuj-1 clone), green) compared to WT neurospheres (Figure 9). Additionally, the central part of the WT neurospheres appears to demonstrate differences in the fluorescent signal of Tuj-1 positive cells and MAP-2 positive cells when compared to Tg neurospheres. Overall, NSC differentiation into mature

neurones might exhibit altered fluorescent expression patterns in Tg neurospheres compared to WT (Figure 9, white arrows).

We also investigated the impact of Aβ species on WT and Tg neurospheres at approximately 16 months old. This study treated the neurospheres for 30 minutes (min) with or without $Aβ_{(1-40)}$ or $Aβ_{(1-42)}$ during their proliferation and differentiation stages. Our preliminary results might indicate an increase in $Aβ_{(1-42)}$-treated WT neurospheres and a decrease in the differentiation of immature neurones compared to $Aβ_{(1-40)}$- and $Aβ_{(1-42)}$-treated Tg at the distal part and central part of the neurospheres (Figure 9, (Tuj-1, green)). Notably, $Aβ_{(1-42)}$-treated Tg neurospheres seem to exhibit prominent holes in the outer central part (outer white circle) compared to $Aβ_{(1-42)}$-treated WT (Figure 9). From an exploratory perspective, it appears that differentiation of NSC into mature neurones (white arrows) shows a decrease in fluorescent staining of Tg neurospheres treated with $Aβ_{(1-40)}$ and $Aβ_{(1-42)}$ when compared to those treated with the same Aβ species in WT neurospheres (Figure 9, (MAP-2, red)).

Additionally, $Aβ_{(1-40)}$-treated neurospheres seem to show a reduction in fluorescent signalling of mature neurones, particularly in the distal part of the Tg neurospheres compared to WT (Figure 9, (MAP-2, red)). Both $Aβ_{(1-42)}$ WT and Tg neurospheres might exhibit alterations in the fluorescent signal related to NSC differentiation into mature neurones when compared to control groups (non-treated WT and Tg) and $Aβ_{(1-40)}$-treated WT and Tg neurospheres (Figure 9, white arrows).

An initial evaluation of combined treatment ($Aβ_{(1-42)}$ + DET) in both central and distal parts of Tg neurospheres did not reveal any changes in fluorescent signalling of immature or mature neurones compared to $Aβ_{(1-42)}$-treated Tg neurospheres (Figure S9). Moreover, the distal and central part of WT neurospheres treated with DET exhibit no fluorescence alteration in MAP-2 and Tuj-1 positive cells compared to non-treated WT neurospheres. The differentiation of NSC into mature neurones is likely to show a modest increase in fluorescence staining in DET-treated WT neurospheres compared to non-treated WT (Figure S9, white arrows). Upon initial examination of the data, it became apparent that combined treatment ($Aβ_{(1-40)}$ + DET) in the central part of both WT and Tg neurospheres does not indicate any alteration in fluorescent signalling of immature or mature neurones when compared to the effects observed with $Aβ_{(1-40)}$ or $Aβ_{(1-42)}$ treatment in WT and Tg neurospheres, as well as control groups (Figure 9 and Figure S9).

Finally, we aimed to investigate the NSC identity of both WT and Tg neurospheres after $A\beta_{(1-40)}$ treatment. Preliminary analysis of the data might indicate that $A\beta_{(1-40)}$ treatment led to a reduction in the fluorescent signal of NSC in both the WT and Tg treated neurospheres, compared to non-treated WT and Tg neurospheres (Figure S8, (Nestin, red)). Interestingly, $A\beta_{(1-40)}$-treated WT neurospheres might show an increase in fluorescent signalling in $A\beta_{(1-40)}$ load compared to control groups (WT and Tg neurospheres) and $A\beta_{(1-40)}$-treated Tg neurospheres. In contrast, control groups might exhibit a modest increase in fluorescent signal of differentiating Nestin-positive cells compared to the $A\beta_{(1-40)}$-treated WT and Tg neurospheres (Figure S8).

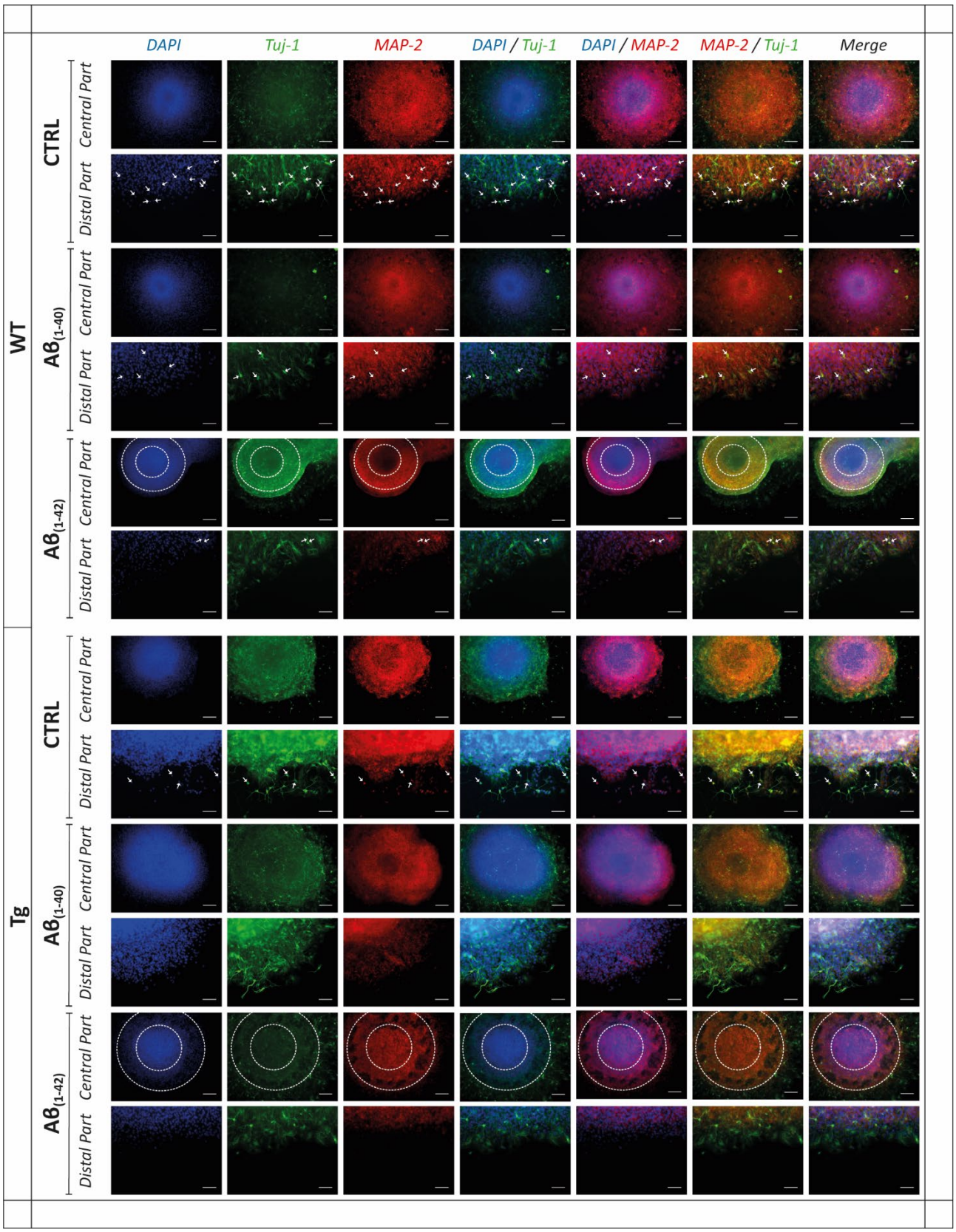

Figure 9: *Phenotypical characterisation of neuronal stem cell differentiation into mature neurones from WT and TG neurospheres with and without $A\beta_{(1-40)}$ and $A\beta_{(1-42)}$ treatment for 30 minutes.*

The differentiation of NSC into mature neurones, derived from the subventricular zone of WT and Tg neurospheres from mice aged 15.5 to 16.5 months, is presented (all groups from 1 independent culture (N = 1) with two technical replicates, n=2). The neurospheres were treated with $A\beta_{(1-40)}$ (0.5 µM) and $A\beta_{(1-42)}$ (0.5 µM). Observations reveal that the distal part of Tg neurospheres exhibits altered differentiation of mature

neurones (MAP-2, red) and immature neuronal cells (β-III-Tubulin (Tuj-1 clone), green) compared to WT. Conversely, the central part of WT neurospheres displays possible changes in the fluorescent signal of immature neuronal cells and mature neurones differentiation compared to TG. $A\beta_{(1-40)}$ treatment in WT neurospheres might slightly alter the fluorescent differentiation signal of immature neurones (Tuj-1 clone) at the distal part compared to Tg neurospheres. Mature neurones (MAP-2) in the distal part of Tg neurospheres might show a reduction in fluorescent signal compared to WT. In contrast, $A\beta_{(1-42)}$ treatment in WT neurospheres might lead to an increase in differentiation of immature neurones (Tuj-1 clone) compared to $A\beta_{(1-42)}$-treated Tg neurospheres, observed in both the distal and central parts. Notably, $A\beta_{(1-42)}$-treated Tg neurospheres display large holes in the outer central part (outer white circle) when compared to $A\beta_{(1-42)}$-treated WT. Both WT and TG neurospheres subjected to $A\beta_{(1-42)}$ treatment might exhibit altered fluorescent signal of NSC differentiation into mature neurones (white arrows) compared to control groups (non-treated WT and Tg neurospheres) and $A\beta_{(1-40)}$-treated WT and TG neurospheres. Nuclei staining (DAPI, blue); scale bars represent 100 µm (central part) and 50 µm (distal part).

3.3. In vivo evaluation of N,N-diethyltryptamine in WT and Tg mice

Dr. Ana Perez Castillo's laboratory has investigated clorgyline hydrochloride (CLQ) and DMT derivatives *in vitro* and *in vivo*, focussing on promoting adult neurogenesis (Morales-Garcia et al., 2020). Additionally, CLQ has been explored in the context of neurodegenerative disease (Garcia-Miralles et al., 2016; Kitaichi et al., 2012; Zhong et al., 2023). In Dr. Ana Perez Castillo's laboratory, various tryptamine derivatives have been examined (Morales-Garcia et al., 2020; Morales-García et al., 2017). Building on these findings and unpublished data from Dr. Ana Perez Castillo's laboratory, DET has emerged as a promising drug candidate for further *in vivo* examination. This pilot study assesses whether treatment with a control vehicle (CLQ) and a combined treatment (CLQ + DET) in both WT and Tg mice influences improvements in axonal damage, demyelination, and neurogenesis. Furthermore, we investigate whether this treatment potentially reduces Aβ aggregates accumulation *in vivo* and explore metabolites in the hippocampus of these WT and Tg mice.

The Biomedical NMR Facility Sebastián Cerdán in the Instituto de Investigaciones Biomédicas (CSIC-UAM) has developed an *in vivo* imaging and spectroscopic technique for an AD mice model featuring a double mutation in APP and human PSEN-1 (Esteras et al., 2012). Our pilot study utilised the same methodology described in that research; however, we expanded our investigation to include a broader range of brain regions, additional metabolites, and a more detailed examination of various tissue microstructures. As this was a preliminary study, we focussed solely on the effects observed in vehicle-treated control groups (WT (CLQ) and Tg (CLQ)) and DET-treated groups (WT (CLQ+DET) and Tg (CLQ

+ DET)). Unfortunately, our study faced several limitations due to issues with the animal cohort and a conflict of interest in Dr Ana Perez Castillo's laboratory. Consequently, this study did not implement non-treated WT and Tg, along with DET-treated WT and Tg mice.

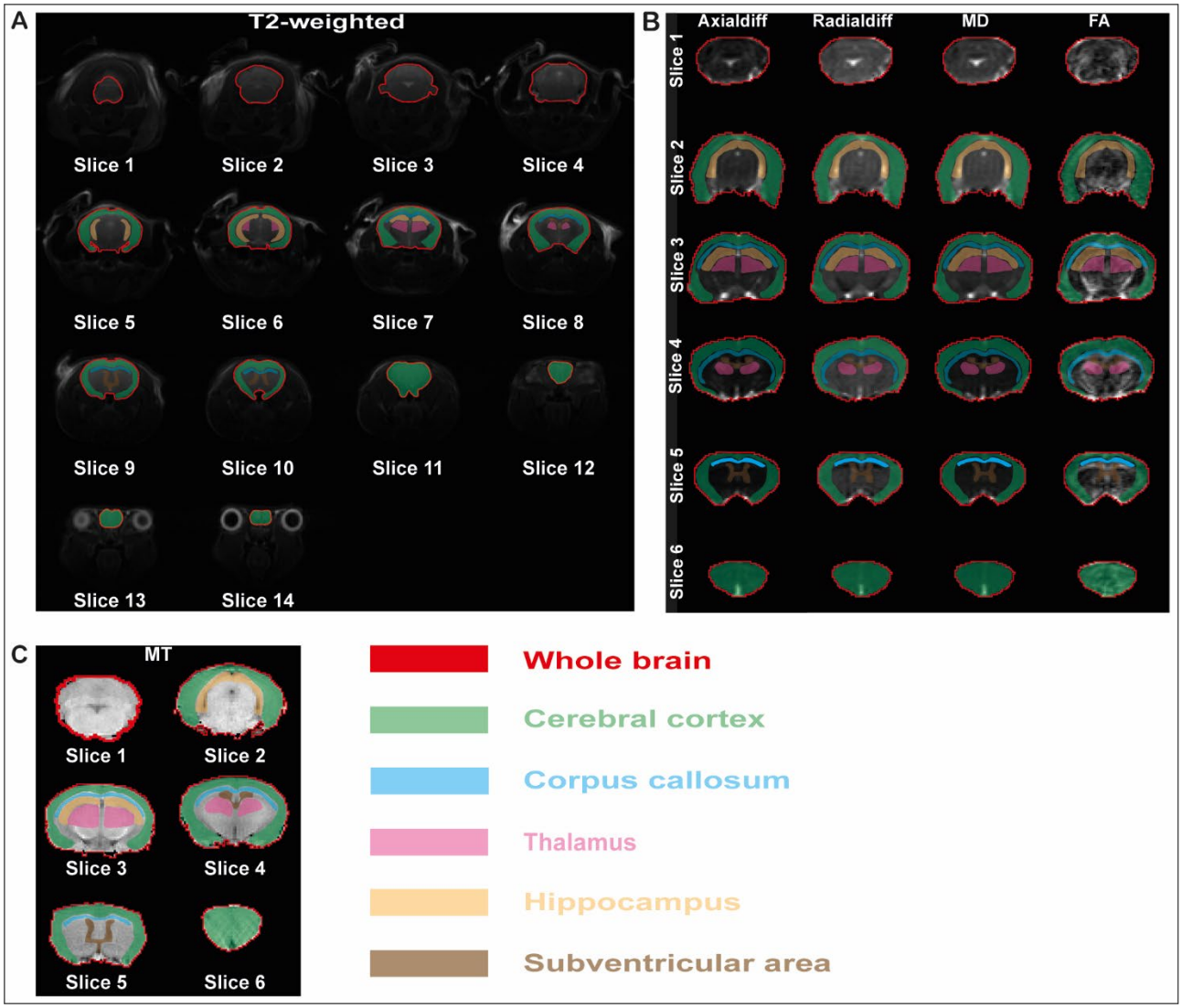

Figure 10: *Example of the brain regions selected from the analysed slices of T2-weighted, DTI and MT images. (**A**) Coronal T2-weighted images (slices 1-14) of the mice brain are presented. (**B**) Diffusion tensor images (DTI) images (slices 1-6) illustrate axial diffusion (axialdiff), radial diffusion (radialdiff), mean diffusion (MD) and fractional anisotropy (FA). (**C**) Also, MT images (slices 1-6) are shown. The whole brain (**A**, slices 1-14; **B-C**, slices 1-6) is outlined in red. The cerebral cortex is highlighted in green (**A**, slices 5-14; **B-C**, slices 2-6). The hippocampus is depicted in orange (**A**, slices 5-7; **B-C**, slices 2-3). The thalamus is represented in purple colour (**A**, slices 6-8; **B-C**, slices 3-4). The corpus callosum is illustrated in blue colour (**A**, slices 7-10; **B-C**, slices 3-5), and the subventricular area is shown in brown (**A**, slices 8-10; **B-C**, slices 4-5).*

3.3.1. T2-weighted imaging

We conducted volumetric studies to assess brain atrophy following administration with and without DET by analysing the T2-weighted images (Figure 11). A detailed explanation of

selecting the region of interest (ROI) is provided above (Figure 10). Briefly, we identified six brain regions, namely the whole brain, cerebral cortex, hippocampus, thalamus, corpus callosum, and subventricular area, based on the 14 anatomical selected slices from the MRI scans. Figure 11 presents the volumetric voxel analysis of the T2-weighted images from slices 1-14 through the brain of WT and Tg mice with the vehicle-treated control groups (CLQ) or DET-treated groups (CLQ + DET). Volumes in all brain slices and the sum of the volumes of all slices for each brain region show no significant difference between vehicle-treated and DET-treated in WT and Tg mice (Table S1). However, we observed a tendency towards an increase in the volume of the subventricular area in DET-treated groups compared to the vehicle-treated control groups across each brain slice and the total volume (Figure 11). Table S1 shows this trend indicated by the p-values, which reflect no statistically significant differences between the groups' volumetric analysis of the subventricular area. To explore whether the increase in the ventricular volume of DET-treated groups might indicate oedema in the cerebral parenchyma, we further analysed the impact of DET treatment on magnetisation transfer (MT) resonance and diffusion tensor imaging (DTI) maps.

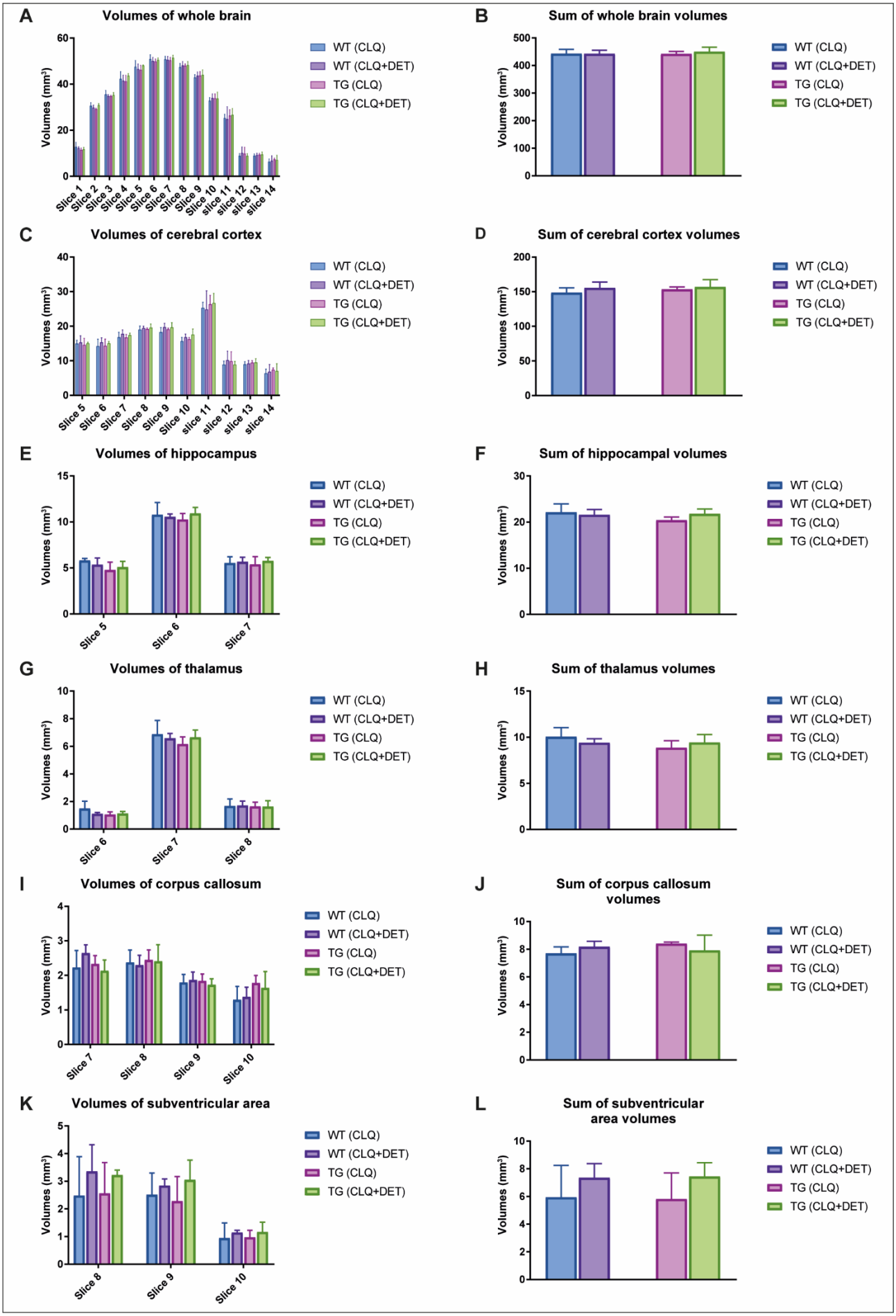

Figure 11: *Quantification of T2-weighted imaging from vehicle-treated control and DET-treated mice.*

*Volumetric voxel analysis and the sum of volumetric voxel analysis of specific ROI ((**A-B**) whole brain, (**C-D**) cerebral cortex, (**E-F**) hippocampus, (**G-H**) thalamus, (**I-J**) corpus callosum and (**K-L**) subventricular area) is quantified as previously described (**Figure 10**). (**A-B**) The volume of the whole brain is assessed using slices 1-14, while (**B-C**) the cerebral cortex is evaluated using slices 5-14. Furthermore, (**C-D**) The hippocampus (slices 5-7), (**G-H**) thalamus (slices 6-8), (**I-J**) corpus callosum (slices 7-10), and (**K-L**) subventricular area (slices 8-10) are included in the analysis. All data are computed from vehicle-treated control groups (WT (CLQ, N = 4) and Tg (ClQ, N = 3)) or DET-treated groups (WT (CLQ + DET; N = 4) and Tg (CLQ + DET; N = 4). The volumes (mm^3) of each slice within the ROI across vehicle-treated control and DET-treated groups are analysed using ANOVA. Additionally, the total volumes of ROI across all groups are evaluated with ANOVA. The statistically significant difference is indicated when the p-value threshold is $p < 0.05$ (* $p < 0.05$). Although, all comparisons show no significant difference between all groups. Specific p-values are provided in supplementary materials (Table S1).*

3.3.2. Magnetisation transfer imaging

Figure 12 and Figure 13 present MT maps from six brain regions (whole brain, cerebral cortex, hippocampus, thalamus, corpus callosum and subventricular area) from vehicle-treated and DET-treated groups. DET-treated Tg mice tend to decrease the percentual value in the accumulation of macromolecules in all slices (1-6) of the six brain regions compared to vehicle-treated counterparts. However, no significant differences are observed between DET-treated Tg and vehicle-treated Tg in all slices (1-6) from the whole brain, cerebral cortex, hippocampus, thalamus, corpus callosum and subventricular area (Table S2).

In contrast, all DET-treated WT mice demonstrate a slight increase of aggregated molecules in slices (1-3 and 5-6) across the six brain regions compared to vehicle-treated WT mice. Despite this increase, no significant differences are noted in these slices within all six brain regions (Table S2). Notably, slice 4 in all six brain regions of DET-treated WT shows a slight decrease in accumulated molecules compared to vehicle-treated WT. Nevertheless, this reduction in slice 4 in all six brain regions between DET-treated WT and vehicle-treated WT does not reach statistical significance (Table S2).

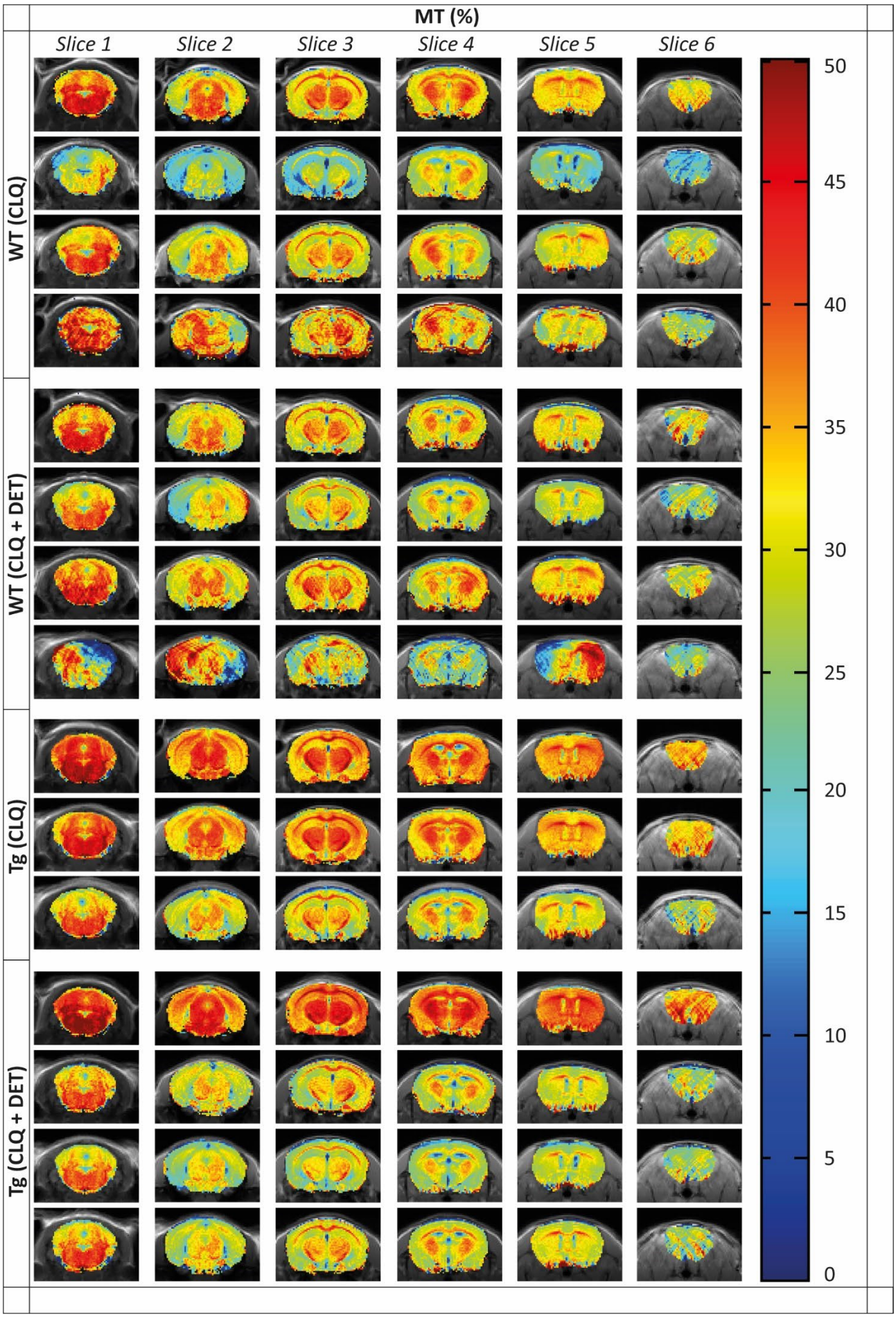

Figure 12: *Magnetisation transfer maps of vehicle-treated control and DET-treated mice.*

Representative MT images from vehicle-treated control groups (WT (CLQ, N = 4) and Tg (ClQ, N = 3)) or DET-treated groups (WT (CLQ + DET; N = 4) and Tg (CLQ + DET; N = 4) are shown. The colour scale bar represents the percentage (0-50 %) of changes observed in the accumulation of macromolecules (e.g. Aβ) between the vehicle-treated and DET-treated groups.

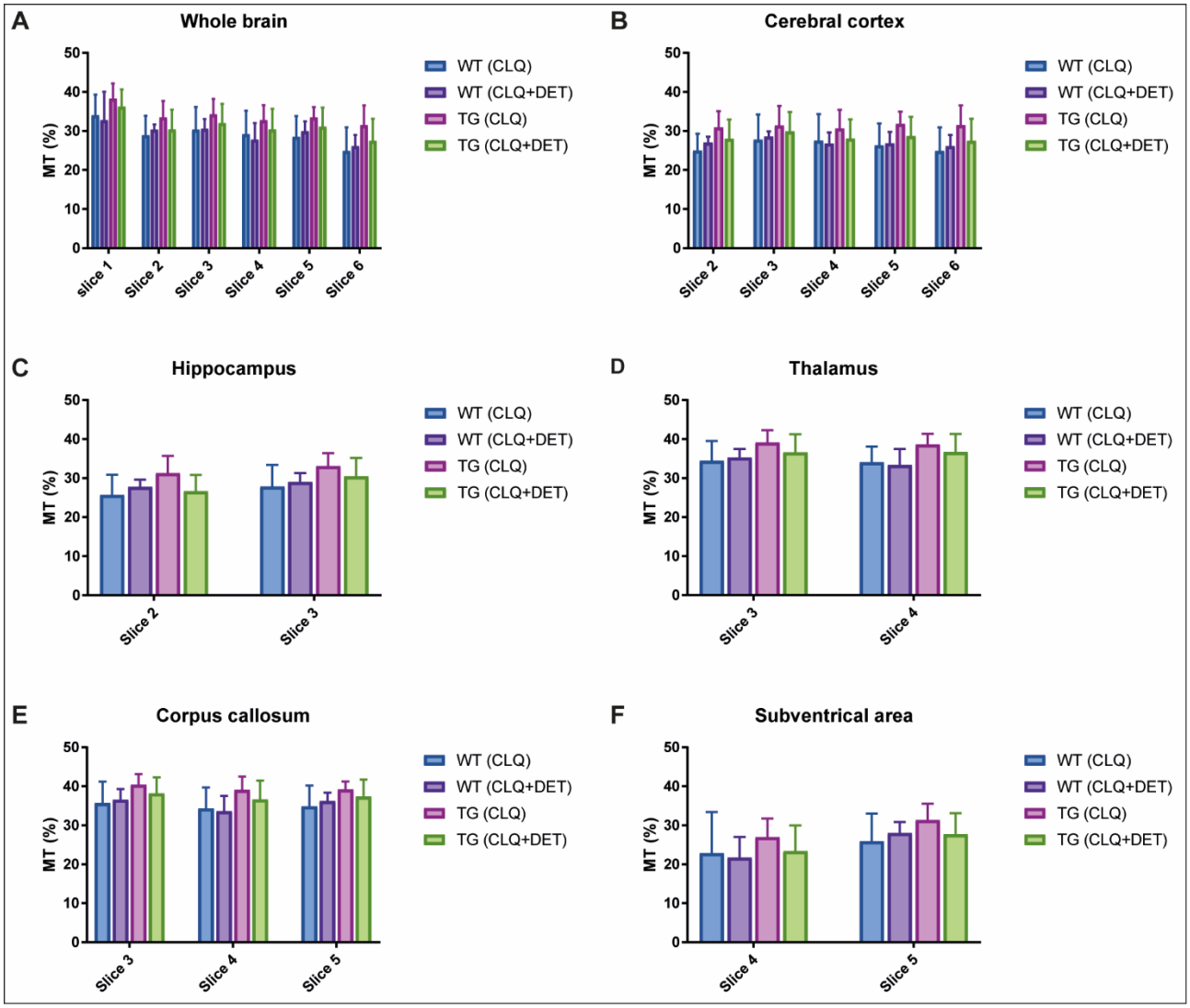

Figure 13: *Quantification of magnetisation transfer imaging from vehicle-treated control and DET-treated mice. (**A-F**) illustrates the quantification of MT images from vehicle-treated control groups (WT (CLQ, N = 4) and Tg (ClQ, N = 3)) as well as DET-treated groups (WT (CLQ + DET; N = 4) and Tg (CLQ + DET; N = 4) derived from specific ROI including the whole brain (slices 1-6), cerebral cortex (slices 2-6), hippocampus (slices 2-3), Thalamus (slices 3-4), corpus callosum (slices 3-5) and subventricular area (slices 4-5). All MT data is expressed in percentages (%), reflecting changes in the accumulation of macromolecules (e.g., Aβ) between vehicle-treated and DET-treated groups. A slight increase is observed in the DET-treated WT group (WT (CLQ + DET)) compared to the vehicle-treated WT group (WT (CLQ), while a decrease is noted in the DET-treated Tg group (Tg (CLQ + DET)) compared to the vehicle-treated Tg group (Tg CLQ)). The accumulation of macromolecules (e.g., Aβ) in each slice within the ROI across vehicle-treated control and DET-treated groups is analysed using ANOVA. The statistically significant difference is indicated when the p-value threshold is $p < 0.05$ (* $p < 0.05$). Although, all comparisons show no significant difference between all groups. Specific p-values are provided in supplementary materials (Table S2).*

3.3.3. Diffusion tensor imaging

We examined the DTI maps from the same slices (1-6) of vehicle- and DET-treated WT and Tg mice to validate our hypothesis. This analysis provided a deeper understanding of the brain tissue microstructure alterations based on water molecules' directional preferences and their overall diffusivity characteristics. DTI maps, which include axial diffusion (axialdiff), radial diffusion (radialdiff), fractional diffusion (FA) and mean diffusion (MD), revealed changes in the diffusion properties related to the white matter integrity. These alterations have been studied in age-related patterns and AD neurological disorders in animals and humans (Gold et al., 2012; Madden et al., 2009; Ni, 2021; Shu et al., 2013).

3.3.3.1. Axial diffusion

Axialdiff is derived from the largest eigenvalue of the diffusion tensor, which quantifies the diffusion rate in the fastest diffusion direction. It reflects the diffusion along the primary preferred direction, corresponding to the axonal fibres' length (Figley et al., 2021; Soares et al., 2013). In our study, no significant increase or decrease in axonal integrity was observed across all slices from the whole brain, cerebral cortex, thalamus, corpus callosum, and subventricular area in both vehicle- and DET-treated WT and Tg animals (Figure 14, Figure 15 and Table S3).

Nonetheless, DET-treated WT exhibited a trend towards increased axonal integrity in slice 4 of the thalamus, slices 3 and 5 of the corpus callosum, slice 4 of the subventricular area, and slices 3 to 6 of the cerebral cortex, as well as in the whole brain. Despite this observed trend, no statistically significant differences were noted in these slices of the ROI. Additionally, we found that slice 2 of vehicle-treated Tg animals showed a significant decrease in axonal integrity in the hippocampus compared to vehicle-treated WT animals ($p = 0.0491$) (Figure 15 and Table S3). Notably, no significant differences were observed among the groups in slice 3 of the hippocampus (Figure 15 and Table S3).

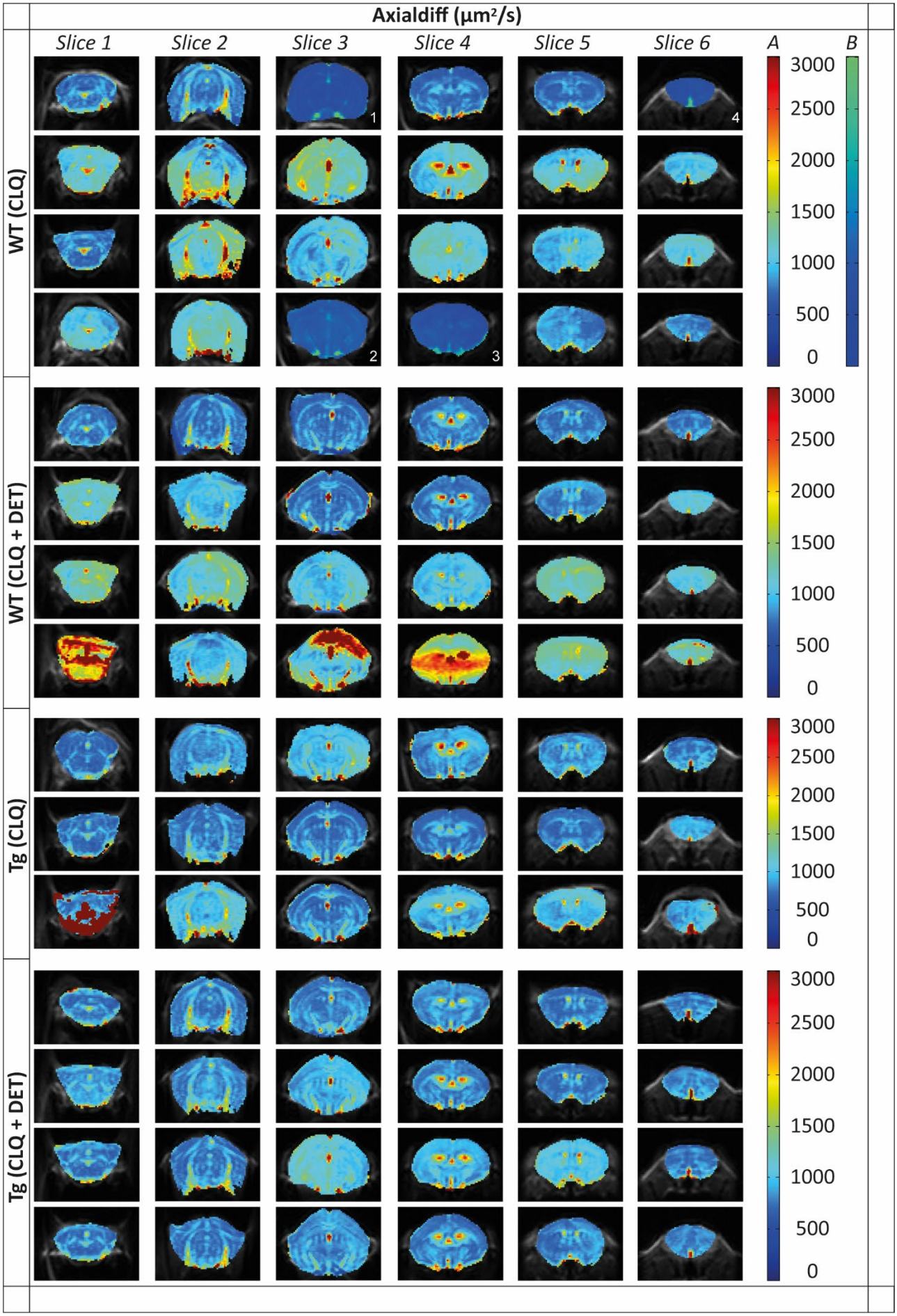

Figure 14: *Axial diffusivity maps of vehicle-treated control and DET-treated mice.*

Representative images of axial diffusivity (axialdiff) from vehicle-treated control groups, including WT (CLQ, N = 4) and Tg (ClQ, N = 3), as well as DET-treated groups, comprising WT (CLQ + DET; N = 4) and Tg (CLQ + DET; N = 4). The scale bars A and B range from (0-3000 μm²/s). In WT (CLQ), slice 3 (1 and 2), slice 4 (3) and slice 6 (4) feature images with scale bar colour code B. All other WT and TG mice slices have scale bar colour code A.

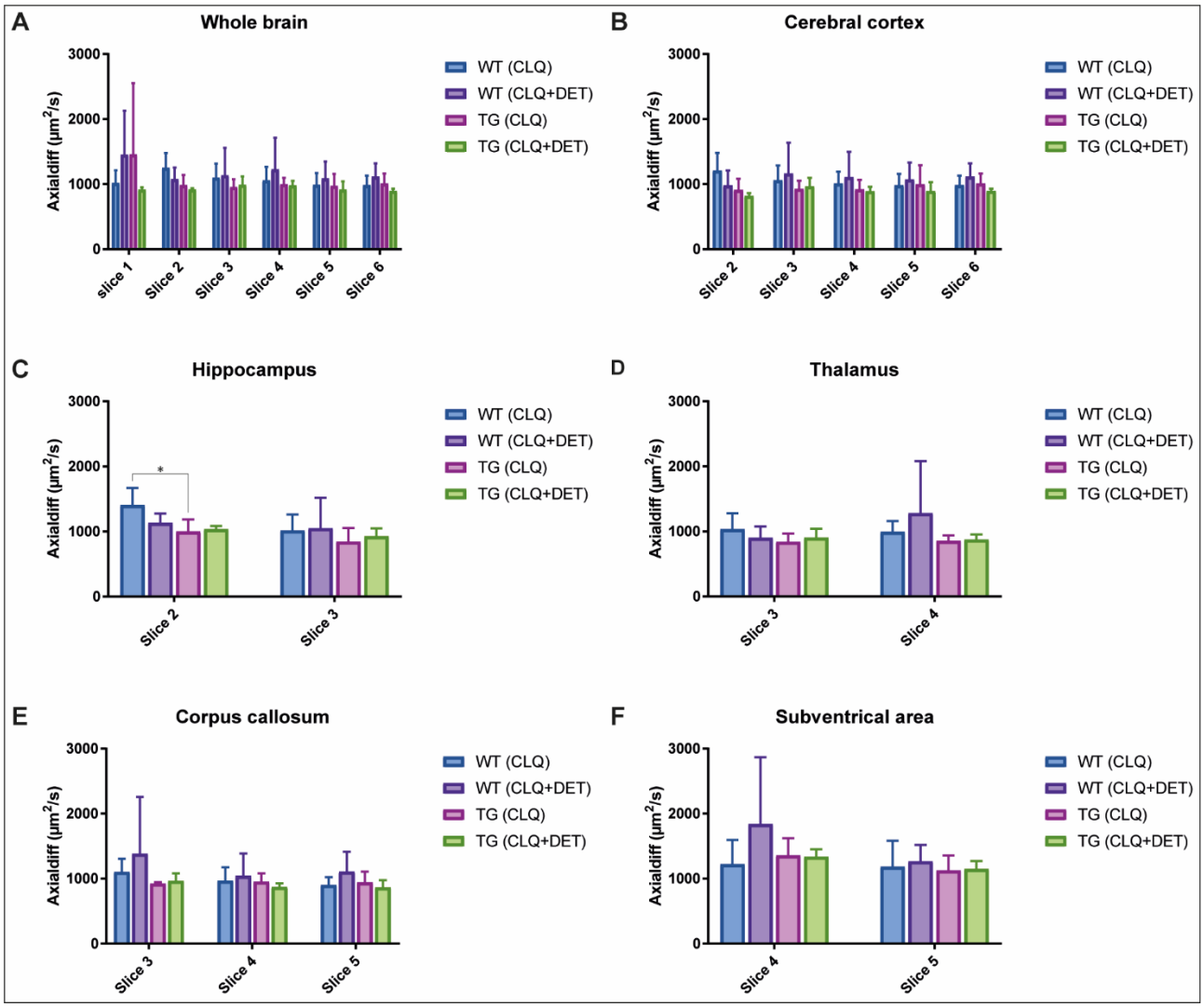

Figure 15: *Quantification of axial diffusivity images from vehicle-treated control and DET-treated mice. (**A-F**) Represent the quantification of axial diffusivity (axialdiff) images from vehicle-treated control groups (WT (CLQ, N = 4) and Tg (ClQ, N = 3)) as well as DET-treated groups (WT (CLQ + DET; N = 4) and Tg (CLQ + DET; N = 4) derived from specific ROI including the whole brain (slices 1-6), cerebral cortex (slices 2-6), hippocampus (slices 2-3), thalamus (slices 3-4), corpus callosum (slices 3-5) and subventricular area (slices 4-5). The change of axonal integrity in each slice within the ROI across vehicle-treated control and DET-treated groups is analysed using ANOVA. The statistically significant difference is indicated when the p-value threshold is $p < 0.05$ ($* p < 0.05$). (**A**) The whole brain, (**B**) the cerebral cortex, (**D**) the thalamus, (**E**) the corpus callosum, and (**F**) the subventricular area show no significant difference in all slices. (**C**) The hippocampus (slice 2) showed a significant reduction in axonal damage of WT (CLQ, N = 4) compared to Tg (ClQ = 3) ($p = 0.0491$). All comparisons in slice 3 of the hippocampus did not show a significant difference. Axialdiff is expressed in μm²/s. Specific p-values are provided in supplementary materials (Table S3).*

3.3.3.2. Radial diffusion

Radialdiff is derived from the second and third eigenvalues of the diffusion tensor, measuring diffusion in the transverse direction. It provides insight into diffusion perpendicular to the main axonal pathways, specifically across axonal fibres, and indicates myelin integrity (Figley et al., 2021; Soares et al., 2013). In our study, we observed no significant differences in the alterations associated with demyelination across slices 1 to 6 from the whole brain, cerebral cortex, hippocampus, thalamus, corpus callosum, and subventricular area, between vehicle-treated and DET-treated WT and Tg animals (Figure 16, Figure 17 and Table S3).

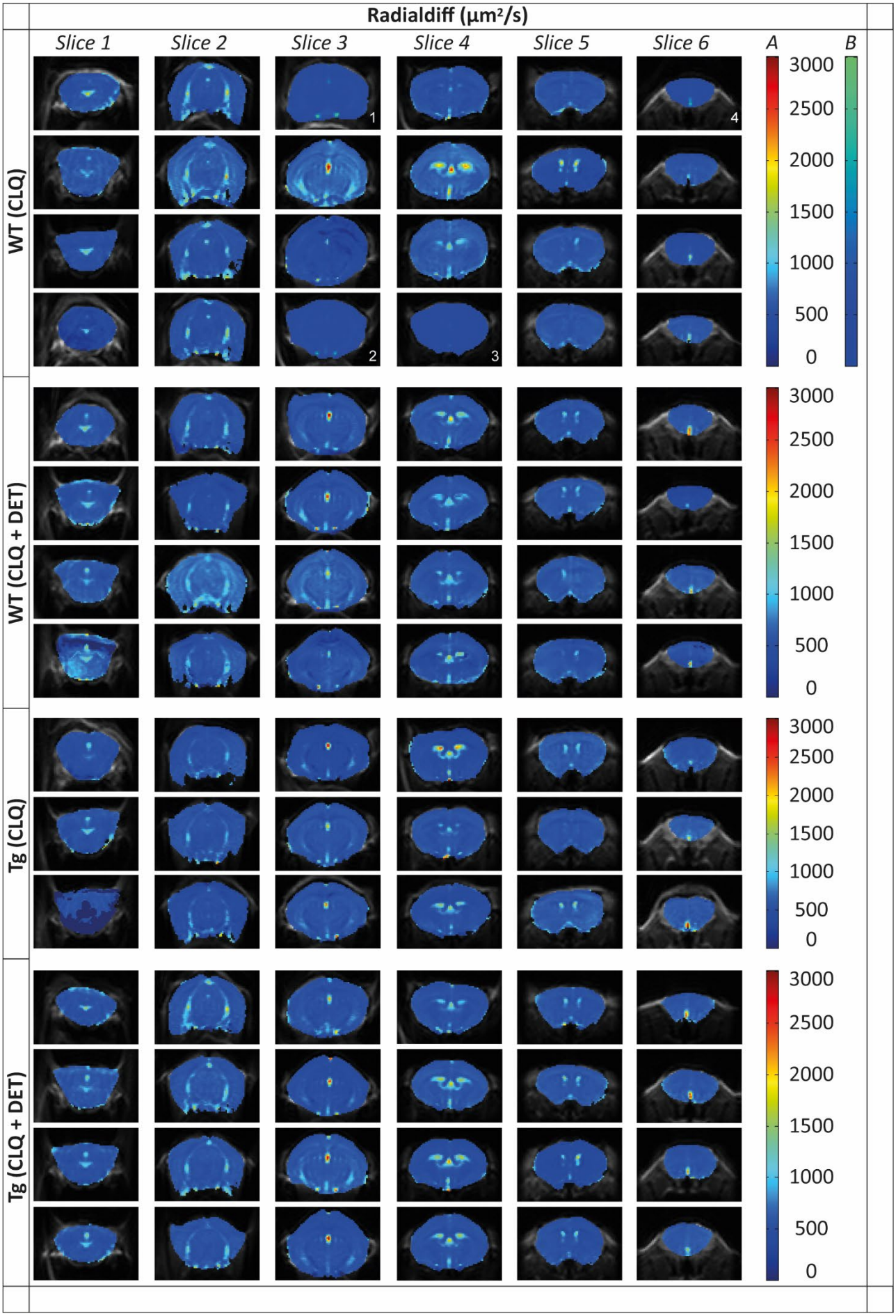

Figure 16: *Radial diffusivity maps of vehicle-treated control and DET-treated mice.*

Representative radial diffusivity (radialdiff) images from vehicle-treated control groups (WT (CLQ, N = 4) and Tg (ClQ, N = 3)) or DET-treated groups (WT (CLQ + DET; N = 4) and Tg (CLQ + DET; N = 4). Scale bars A and B range from 0-3000 μm²/s. In WT (CLQ), slice 3 (1 and 2), slice 4 (3) and slice 6 (4) are images with scale bar colour code B. All the other slices in WT and TG mice have scale bar colour code A.

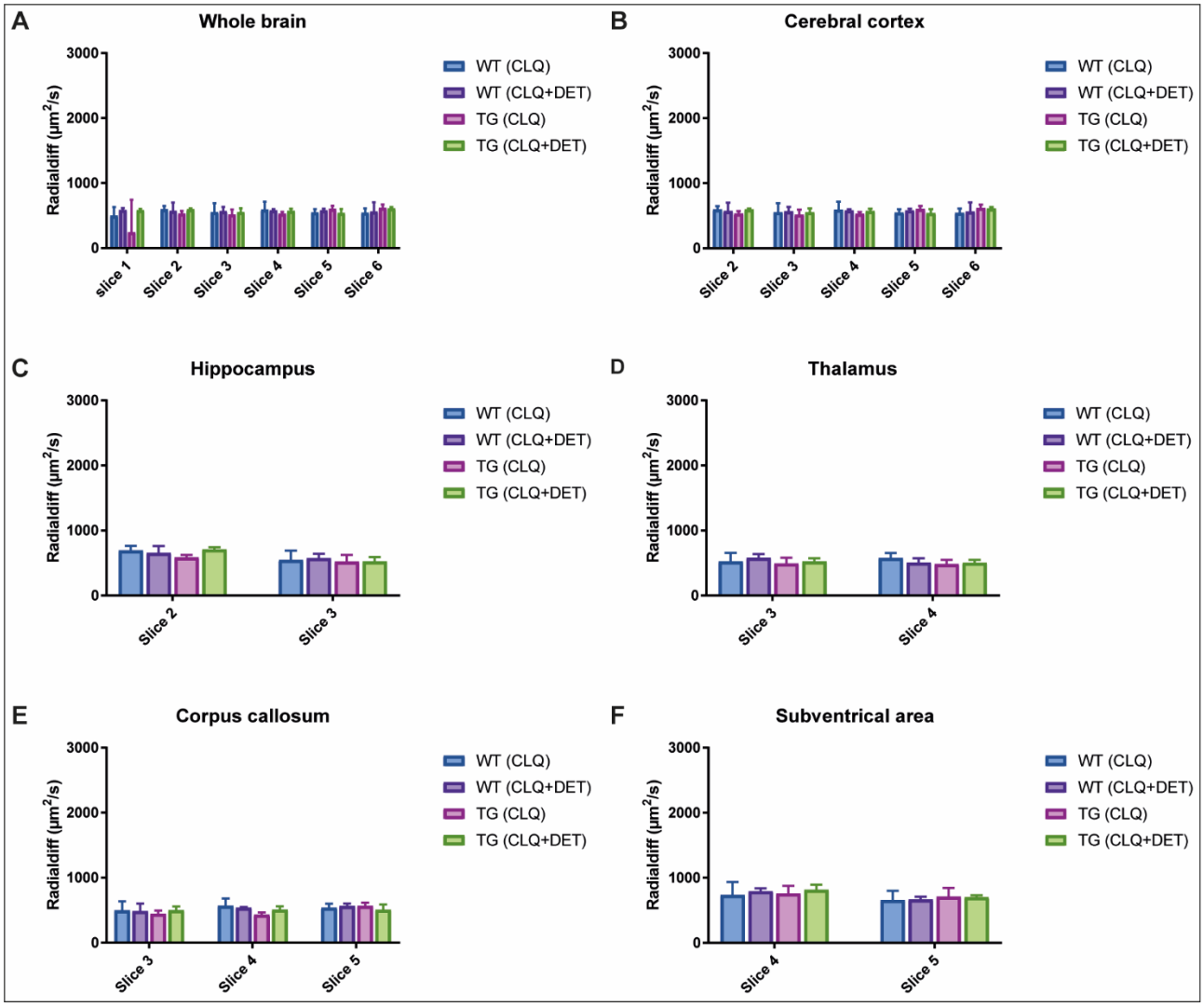

Figure 17: *Quantification of radial diffusivity images from vehicle-treated control and DET-treated mice. (**A-F**) Show the quantification of radial diffusivity (radialdiff) images from vehicle-treated control groups (WT (CLQ, N = 4) and Tg (ClQ, N = 3)) as well as DET-treated groups (WT (CLQ + DET; N = 4) and Tg (CLQ + DET; N = 4)) derived from specific ROI including the whole brain (slices 1-6), cerebral cortex (slices 2-6), hippocampus (slices 2-3), thalamus (slices 3-4), corpus callosum (slices 3-5) and subventricular area (slices 4-5). Changes in myeline integrity in each slice within the ROI across vehicle-treated control and DET-treated groups are analysed using ANOVA. The statistically significant difference is noted if the p-value threshold of p < 0.05 (* p < 0.05). (**A**) The whole brain, (**B**) cerebral cortex, (**C**) hippocampus, (**D**) thalamus, (**E**) corpus callosum, and (**F**) subventricular area reveals no significant differences within all slices. Radialdiff is expressed in μm²/s, and specific p-values can be found in the supplementary materials (Table S3).*

3.3.3.3. Fractional anisotropy diffusion

FA quantifies the degree to which isotropic or anisotropy water molecules preferentially diffuse along a specific direction. It is determined based on the eigenvalues of the diffusion tensor (Figley et al., 2021). Low FA values indicate isotropy, meaning that water molecules diffuse equally in all directions, reflecting no preferred motion of water molecules (e.g., in the ventricles). Conversely, high FA values signify anisotropy, indicating that water molecules preferentially diffuse in a specific direction, for example, observed in the corpus callosum (Figley et al., 2021).

Analysis revealed no significant differences across slices 1 to 6 in the whole brain, cerebral cortex, hippocampus, thalamus, corpus callosum, and the subventricular area between vehicle-treated and DET-treated WT and Tg animals (Figure 18, Figure 19 and Table S4). Notably, even the corpus callosum did not exhibit significant differences in the directional movement of water molecules, despite the formation of fibres in this region (Table S4). Additionally, the subventricular area exhibited no significant differences in water molecules diffusion (Table S4).

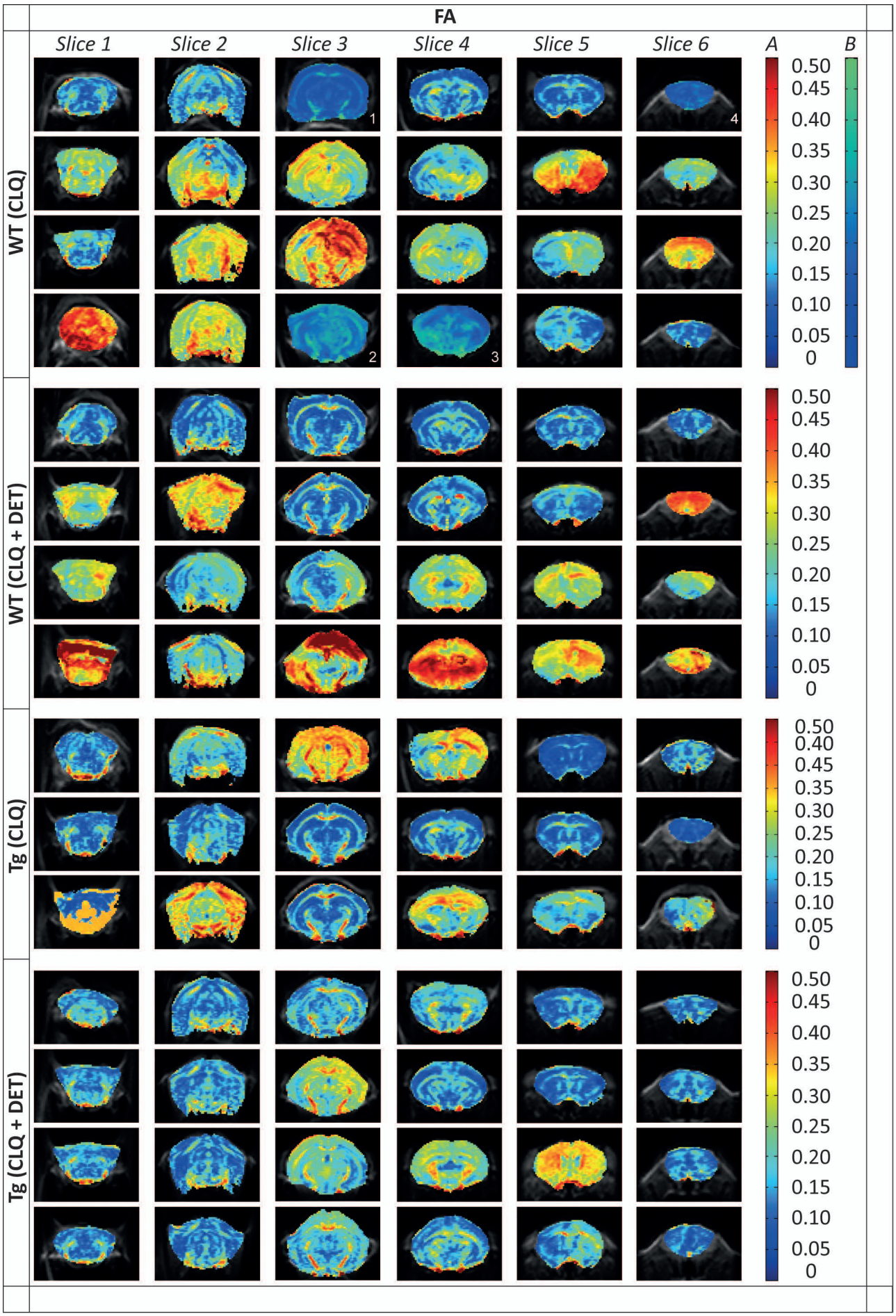

Figure 18: *Fractional anisotropy diffusivity maps of vehicle-treated control and DET-treated mice.*

Representative fractional anisotropy diffusivity (FA) images from vehicle-treated control groups (WT (CLQ, N = 4) and Tg (ClQ, N = 3)) or DET-treated groups (WT (CLQ + DET; N = 4) and Tg (CLQ + DET; N = 4). Scale bars A and B range from (0-0.5). In WT (CLQ), slice 3 (1 and 2), slice 4 (3) and slice 6 (4) are images with scale bare colour code B. All the other slices in WT and TG mice have scale bar colour code A.

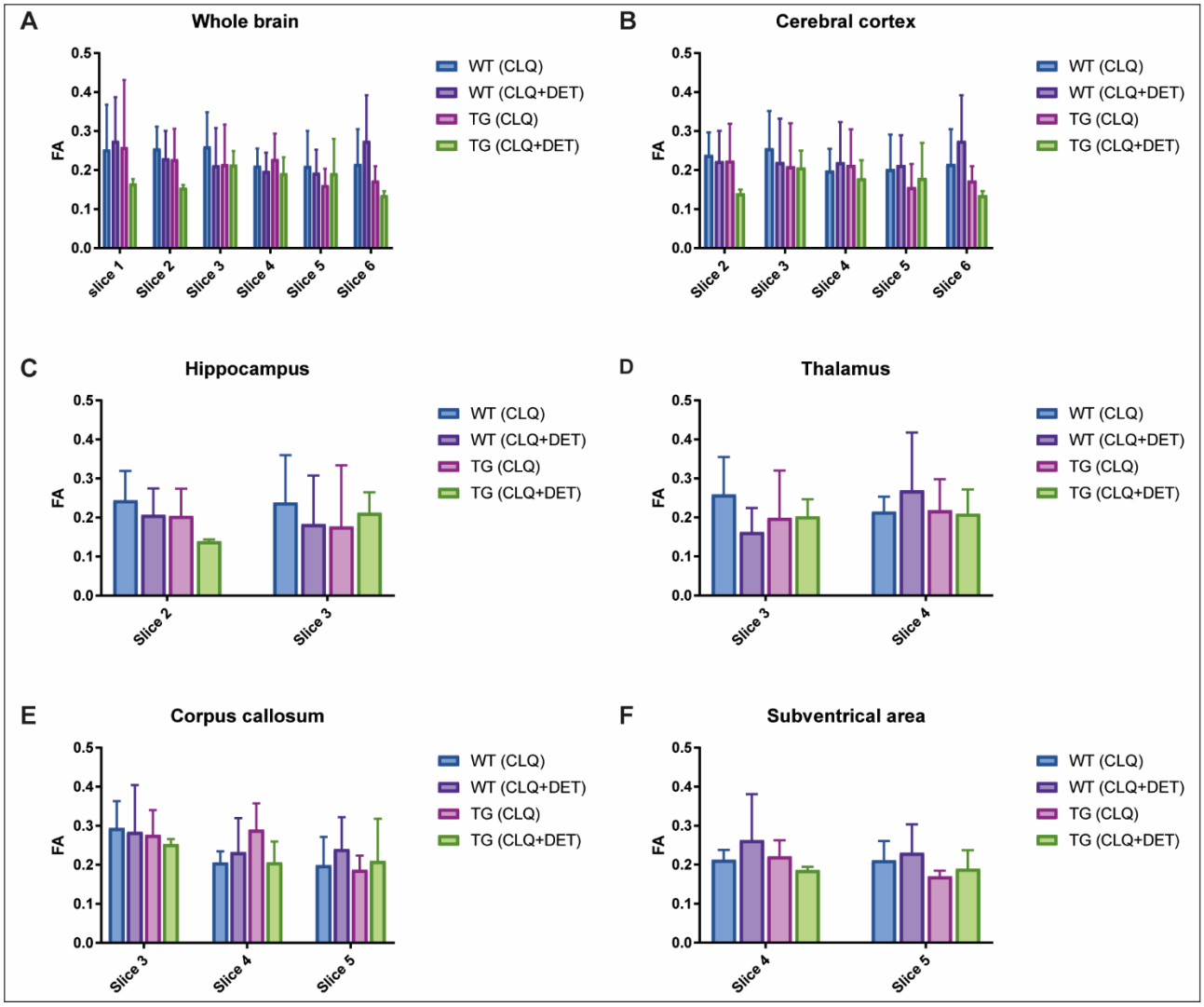

Figure 19: *Quantification of fractional anisotropy diffusivity images from vehicle-treated control and DET-treated mice.*

*(**A-F**) Show the quantification of fractional anisotropy diffusivity (FA) images from vehicle-treated control groups (WT (CLQ, N = 4) and Tg (ClQ, N = 3)) as well as DET-treated groups (WT (CLQ + DET; N = 4) and Tg (CLQ + DET; N = 4) derived from specific ROI including the whole brain (slices 1-6), cerebral cortex (slices 2-6), hippocampus (slices 2-3), thalamus (slices 3-4), corpus callosum (slices 3-5) and subventricular area (slices 4-5). The alterations in the diffusion of water molecules within each slice of the ROI between vehicle-treated control and DET-treated groups were analysed using ANOVA. The statistically significant difference is indicated by a p-value threshold of $p < 0.05$ (* $p < 0.05$). Results showed no significant differences across all slices in any of the ROI: (**A**) whole brain, (**B**) cerebral cortex, (**C**) hippocampus, (**D**) thalamus, (**E**) corpus callosum, and (**F**) subventricular area. The FA values, which range from 0 to 1, denote the movement of water molecules; low values indicate isotropy (0, representing no preferred direction in water molecules movement),*

while higher values indicate anisotropy (1, signifying a preferred direction of diffusion of water molecules). Detailed p-values are provided in the supplementary materials (Table S4).

3.3.3.4. Mean diffusion

MD represents the average magnitude of diffusion of water molecules within a voxel, indicating the degree to which water molecules can move freely. In certain pathological conditions, such as AD, the diffusion of water molecules is restricted due to interactions with macromolecules (e.g., Aβ), leading to a decrease in this parameter. This value is calculated by averaging the three eigenvalues (Figley et al., 2021). Overall, the mean diffusion of water molecules did not show significant differences between vehicle-treated and DET-treated WT and Tg mice across the whole brain (slices 1-6), cerebral cortex (slices 2-6), thalamus (slices 3-4), corpus callosum (slices 3-5) and subventricular area (slices 4-5). However, slice 2 of vehicle-treated Tg mice exhibited a significant reduction, indicating an average obstruction to water movement in the hippocampus compared to their vehicle-treated WT ($p = 0.0128$) (Figure 20, Figure 21 and Table S4). Notably, no significant differences were observed among the groups in slice 3 of the hippocampus (Figure 20, Figure 21 and Table S4).

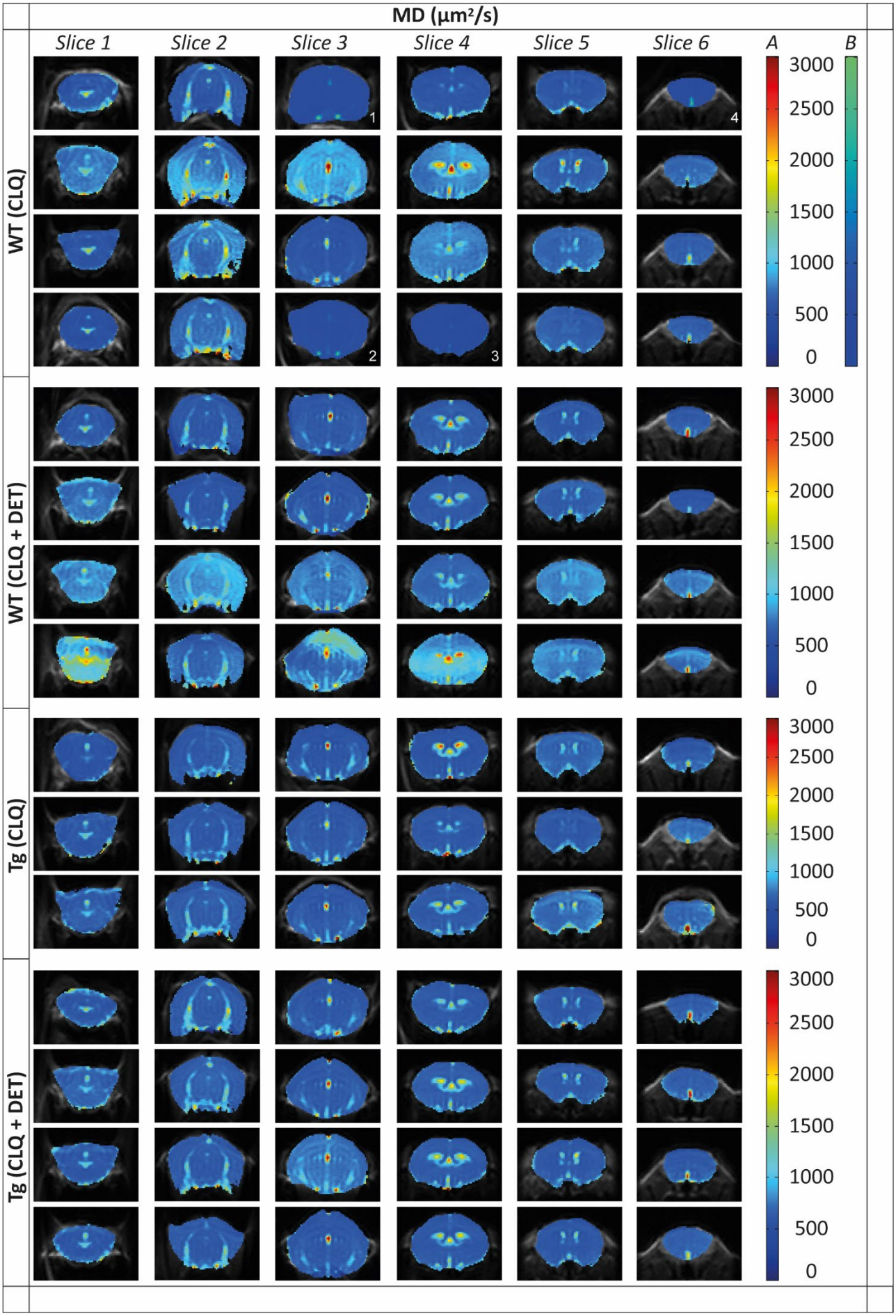

Figure 20: *Mean diffusivity maps of vehicle-treated control and DET-treated mice.*

Representative mean diffusivity (MD) images from vehicle-treated control groups (WT (CLQ, N = 4) and Tg (ClQ, N = 3)) or DET-treated groups (WT (CLQ + DET; N = 4) and Tg (CLQ + DET; N = 4). Scale bars A and B range from 0-3000 μm²/s. In WT (CLQ), slice 3 (1 and 2), slice 4 (3) and slice 6 (4) are images with scale bare colour code B. All the other slices in WT and TG mice have scale bar colour code A.

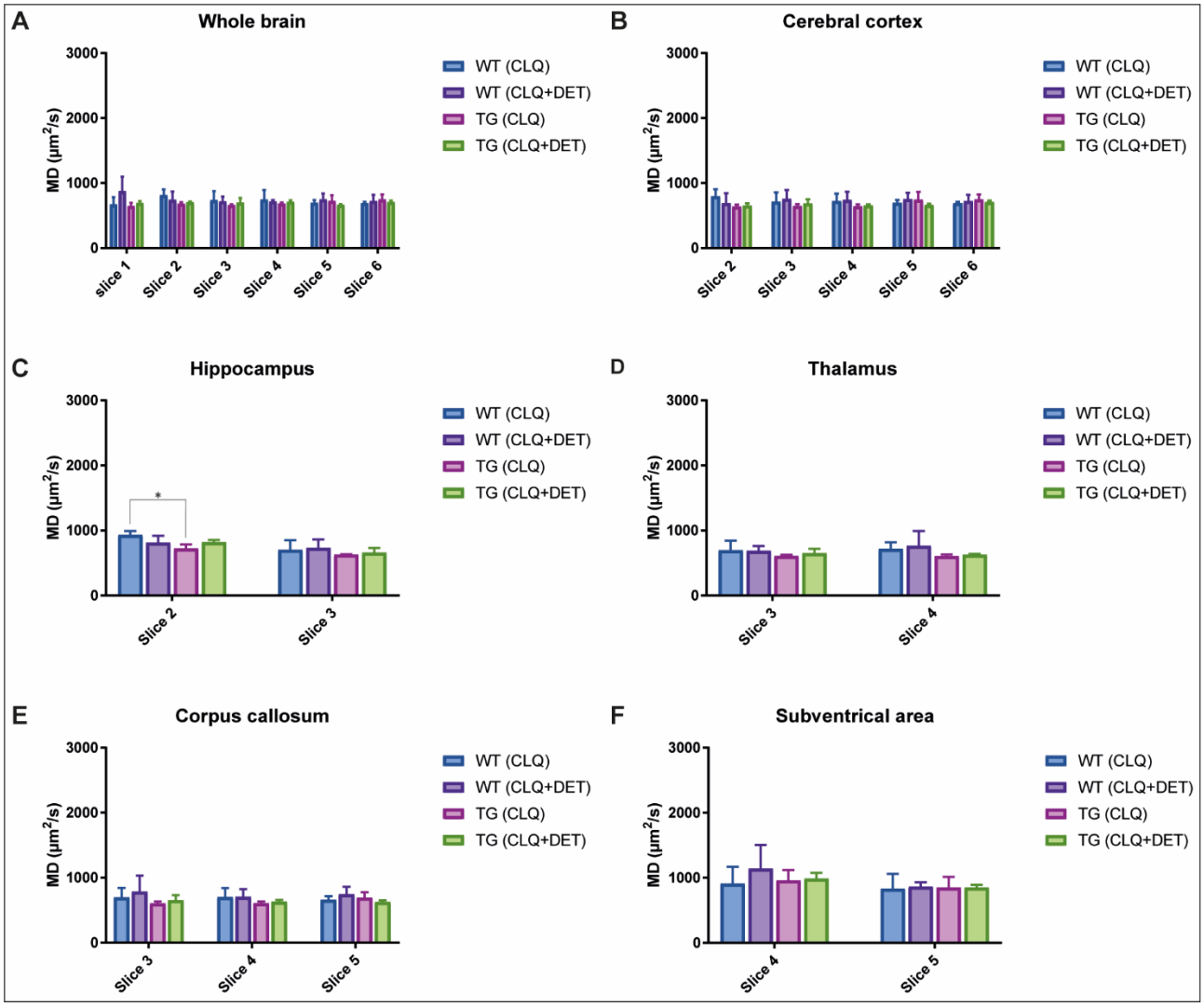

Figure 21: *Quantification of mean diffusivity images from vehicle-treated control and DET-treated mice. (**A-F**) Show the quantification of mean diffusivity (MD) images from vehicle-treated control groups, including WT (CLQ, N = 4) and Tg (ClQ, N = 3), as well as DET-treated groups, comprising WT (CLQ + DET; N = 4) and Tg (CLQ + DET; N = 4). This analysis focussed on specific ROI, including the whole brain (slices 1-6), cerebral cortex (slices 2-6), hippocampus (slices 2-3), thalamus (slices 3-4), corpus callosum (slices 3-5) and subventricular area (slices 4-5). The obstruction of water diffusion within each slice of the ROI between vehicle-treated control and DET-treated groups is analysed using ANOVA. Statistically significant differences are determined by a p-value threshold of $p < 0.05$ ($* p < 0.05$). Results exhibit no significant differences across all slices in any of the ROI: (**A**) whole brain, (**B**) cerebral cortex, (**D**) thalamus, (**E**) corpus callosum, and (**F**) subventricular area. Notably, (**C**) the hippocampus (slice 2) shows a significant reduction in WT (CLQ; N = 4) compared to Tg (ClQ; N = 3) ($p = 0.0128$). In contrast, no significant differences are observed in slice 3 of the hippocampus between the groups. MD is expressed in μm²/s. Detailed p-values are provided in the supplementary materials (Table S4).*

3.3.4. 1H-spectroscopy

We aimed to investigate the alterations in metabolites, lipids and macromolecules *in vivo*. To achieve this, we examined both WT and Tg mice following the administration with and without DET treatment, utilising MRS. This method describes *in vivo* levels of metabolites, lipids, or macromolecules in the brains of living mice. However, our study results could not be directly compared with the existing literature due to a lack of information on similar conditions, specifically concerning animal age groups, the genetic background of the mouse strains, and the selected brain region for analysis (Cudalbu et al., 2021; Esteras et al., 2012; Marjanska et al., 2005; Marjańska et al., 2014; Pardon et al., 2016; Shen et al., 2018). As a result, we focussed solely on comparing the effects between vehicle-treated and DET-treated WT and Tg mice. Of the 27 individual metabolites, lipids, and macromolecules analysed, only 7 yielded values below the threshold of the LCModel. Notably, one inositol metabolite value exceeded the threshold (22%) and was included in further analysis. This value originated from the vehicle-treated WT group and showed no discrepancy compared to the other inositol values within the same group. Therefore, it was included in the analysis.

The DET-treated WT mice showed no significant changes in the three metabolites evaluated individually, nor in the three metabolite/lipid complexes (NAA + N-acetyl-aspartyl-glutamate (NAAG) (NAA + NAAG), glycerophosphocholine + phosphocholine (GPC + PCh) and glutamate + glutamine (Glu + Gln)) when compared to the vehicle-treated groups and DET-treated Tg mice (Table S5). Nonetheless, DET-treated WT and TG tended to increase lipid/macromolecule resonance complex (MM09 + Lip09) compared to their vehicle-treated WT and Tg groups (Figure 22). However, no statistically significant differences between groups were noted for this lipid/macromolecule resonance complex (MM09 + Lip09) (Table S5).

Additionally, inositol and the (Glu + Gln) complex levels appeared higher in DET-treated Tg mice than in the vehicle-treated Tg mice. However, no significant differences were found for inositol ($p = 0.4208$) or (Glu + Gln) complex ($p = 0.8687$) within these Tg mice groups (Table S5). The (NAA + NAAG) complex and NAA resonance spectroscopy tended to be lower in DET-treated Tg mice compared to vehicle-treated Tg mice (Figure 22). Furthermore, DET-treated Tg displayed decreased levels for both (NAA+NAAG) complex and NAA resonance spectroscopy compared to vehicle-treated and DET-treated WT mice. All comparisons did not reveal significant differences between groups, as shown in Figure 22 and Table S5.

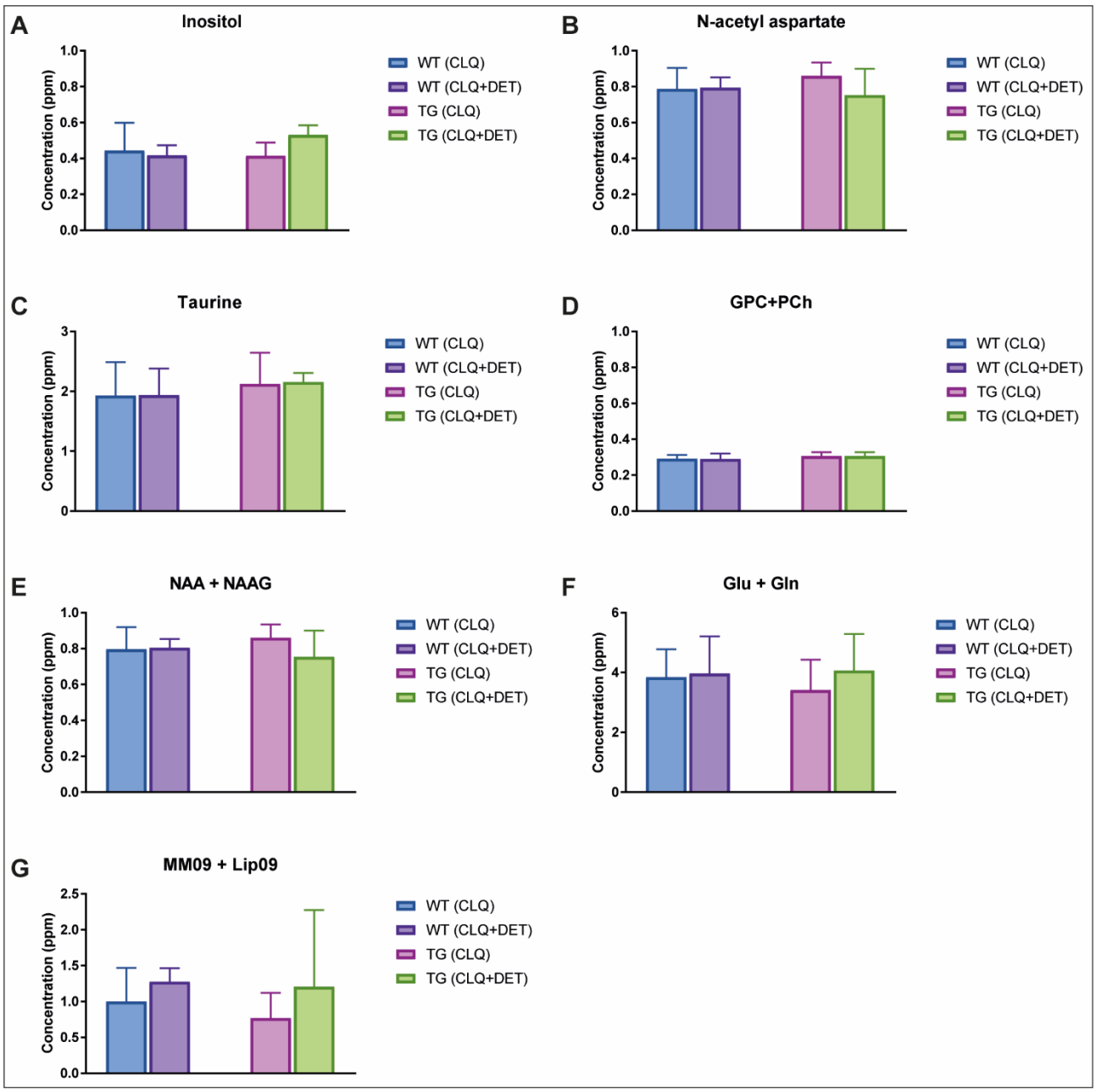

Figure 22: *Quantification of metabolites, macromolecules and lipids using 1H-spectroscopy imaging. Here, we present the concentrations of (**A-C** and **E-F**) metabolites, (**G**) macromolecules and (**D**) lipids quantified after 1H-spectroscopy imaging from vehicle-treated control groups (WT (CLQ, N = 4) and Tg (ClQ, N = 3)) as well as DET-treated groups (WT (CLQ + DET; N = 4) and Tg (CLQ + DET; N = 4)). The concentrations of these metabolites, macromolecules, and lipids between the vehicle-treated control and DET-treated groups are analysed using ANOVA. Statistically significant differences are determined with a p-value threshold of $p < 0.05$ ($* p < 0.05$). The results indicated no significant differences in the concentration of specific metabolites, macromolecules, and lipids among all groups. Concentrations of metabolites, macromolecules and lipids are expressed in parts per million (ppm), with detailed p-values available in the supplementary materials (Table S5).*

3.4. Discussion

3.4.1. Implications of Aβ pathology on neurogenesis: insights from AD models

APP proteins play a crucial role in neuronal processes such as neurite growth and synapse formation, significantly influencing the pathology of AD (Baumkötter et al., 2014; Müller & Zheng, 2012; Price et al., 1998). The use of antibodies that recognize APP epitopes and their cleavage fragments is invaluable for investigating Aβ pathology in genetically modified AD transgenic models (Gouras et al., 2015; Gouras et al., 2010; Gouras et al., 2000; Klementieva et al., 2017; Roos et al., 2021; Takahashi et al., 2004; Takahashi et al., 2013; Tampellini et al., 2007; Willén et al., 2017). Our research on Tg mice revealed distinctive $Aβ_{(1–42)}$ aggregates as early as 4 months, aligning with earlier studies (Jackson et al., 2013; Minkeviciene et al., 2008; Ordóñez-Gutiérrez et al., 2015). However, these studies reported disparities in Aβ burden across various brain regions and the ages at which it manifests in the specific AD transgenic models, as well as the different methodologies used for the analysis of Aβ aggregates (Hanspal & Gillotin, 2022; Minkeviciene et al., 2009). Additionally, consistent with our observations regarding plaque-related gliosis in the cortex and hippocampus of young Tg mice suggest a link between Aβ accumulation and neuroinflammation, underlining the complex and intriguing dynamics of Aβ aggregation and its effects on AD progression (Chen et al., 2017; Jackson et al., 2013; LaRocca et al., 2021; Malm et al., 2007; Minkeviciene et al., 2008).

Moreover, changes in adult neurogenesis manifest early in AD, beginning as early as two months in Tg mice (Demars et al., 2010). By six months, there is a notable decrease in progenitor cell proliferation (Faure et al., 2011), which aligns with our findings on possible reduced neurogenesis. Our research explicitly examines RELN expression concerning $Aβ_{(1–42)}$ and microglia-positive cells in the entorhinal cortex and hippocampus of ageing Tg mice, highlighting the potential decline in RELN levels and neuroinflammation associated with AD (Botella-López et al., 2010; Cuchillo-Ibáñez et al., 2013; Cuchillo-Ibañez et al., 2016; Kocherhans et al., 2010).

Furthermore, we present for the first time a potential application of neurospheres from aged WT and Tg mice, which serve as an ideal three-dimensional *in vitro* model for studying adult neurogenesis in AD (Ghate et al., 2014). Our findings indicate that $Aβ_{(1–40)}$ and $Aβ_{(1–42)}$ may influence adult neurogenesis and the differentiation of NSC. The limited research on neurospheres containing a similar APP/PSEN-1 mutation in Tg mice underlines the potential implications of our work and the significance of Aβ in neurogenesis (Esteve et al., 2022;

Ghate et al., 2014). Our results might suggest a possible neurotrophic effect of $A\beta_{(1–40)}$ on Tg neurospheres, which warrants further investigation.

3.4.2. Innovative approaches to AD treatment: an in vivo exploration of a novel drug compound

AD remains a devastating disorder, with currently available medications primarily serving to slow the progression of the disease (Varadharajan et al., 2023). Consequently, exploring alternative drug compounds that could mitigate Aβ-induced toxicity, neuroinflammation, and promote neurogenesis (Morales-Garcia et al., 2020; Van Bulck et al., 2019) may advance our efforts towards preventing this disorder. Previous studies, including research conducted in Dr. Ana Perez Castillo's laboratory, have demonstrated that psychedelic N,N-tryptamines, such as DET, can decrease neuroinflammation and enhance adult neurogenesis in various neurological conditions (Perez Castillo et al., 2018 (Patent No. US11723894B2)) (Fontanilla et al., 2009; Lima da Cruz et al., 2018; Morales-Garcia et al., 2020; Szabo et al., 2014; Szabo et al., 2016; Winter, 1969). Furthermore, preliminary tests using neuroblastoma cell lines in Dr. Ana Perez Castillo's laboratory (unpublished data) indicate that DET may be a promising candidate for further investigation in our Tg mice model, potentially leading to a significant breakthrough in AD research.

In this research, we integrate MRI analysis with MRS for the first time to investigate the effects of DET administration on the metabolic and biochemical changes in the brains of WT and Tg mice. Our findings indicate that DET does not influence axonal injury, demyelination, or the accumulation of macromolecules such as Aβ plaques, nor does it appear to affect adult neurogenesis *in vivo*. The absence of significant effects may be related to the age of the mice and the dosage of DET administered. However, cognitive decline is observed in these Tg mice between 6 and 10 months of age (Minkeviciene et al., 2008), which highlights the necessity for further studies involving younger mice and varying DET dosages.

Voxel-based morphometry analysis, utilising T2-weighted imaging and MT analysis, showed no significant changes in atrophy or Aβ accumulation when comparing DET-treated mice to those receiving vehicle treatment. While prior studies suggested that MT values might reflect histopathological changes associated with AD (Delatour et al., 2006; Esteras et al., 2012; Huang et al., 2016; Liang et al., 2017), our results indicate no structural correlations with Aβ buildup, which may be attributed to the age of the mice and the duration of treatment (Lau et al., 2008).

Furthermore, although some research has reported hippocampal atrophy and neuronal loss in AD models (Heneka et al., 2015; Huang et al., 2016; Ries & Sastre, 2016), our study did not identify significant volumetric structural changes. This is consistent with other studies that noted inconsistencies in neuronal density and glial activation without observable atrophy (Kuhla et al., 2017; Manaye et al., 2007).

Additionally, DTI scans are valuable for assessing white matter integrity by analysing water diffusivity, which aids in detecting anatomical changes before they become apparent in structural MRI (Shu et al., 2013; Zerbi et al., 2013). Our study found no effects of DET on white matter integrity; however, the hippocampus displayed significant reductions in axialdiff and MD, indicating increased axonal injury without signs of demyelination. In comparison, other research reported increases in axialdiff and FA in specific brain regions (Qin et al., 2013). However, contradictory findings have been observed, such as declines in all DTI metrics in the corpus callosum but an increase in MD and radialdiff in the hippocampus (Zerbi et al., 2013). Therefore, it is important to be cautious when interpreting DTI measurements, as relying exclusively on them without integrating them with additional MRI and MRS analysis could restrict comprehension of how DET influences white matter integrity.

We presented metabolic profiles for 7 of the 27 molecules identified in the hippocampus, highlighting 3 distinct metabolites, 2 complexes of metabolites, and 2 complexes of lipids/macromolecules in both WT and Tg mice. Minor alterations were observed in inositol, NAA, NAA + NAAG, Glu + Gln, and MM09 + Lip09 following DET treatment; however, the metabolic profiles noted no significant differences. Previous studies have demonstrated that MRS can distinguish metabolic profiles between WT and Tg mice, revealing decreased levels of NAA and Glu in Tg mice (Chen et al., 2012; Esteras et al., 2012; Kuhla et al., 2017; Liang et al., 2017; Marjanska et al., 2005; Marjańska et al., 2014; Shen et al., 2018; Westman et al., 2009).

Inositol, a key player in regulating biochemical pathways in the brain (López-Gambero et al., 2020), holds promise in mitigating toxic Aβ aggregation in AD. This potential is underlined by its ability to enhance cognitive functions (Aytan et al., 2013; Dorr et al., 2012; McLaurin et al., 2006; Morrone et al., 2020). Our research indicates that DET could function as a neuromodulator, reducing neuronal damage and glial activity in neurodegenerative conditions like Parkinson's disease (Perez Castillo et al., 2018 (Patent No.

US11723894B2)). However, our preliminary study is the first to report that DET does not affect AD pathology. This emphasises the need for in-depth analysis to clarify whether DET impacts the condition by improving neuroinflammation and neuronal damage. Additionally, NAA levels typically decrease in specific mouse models (Jansen et al., 2013; Kuhla et al., 2017), including our DET-treated Tg mice, which seems to suggest inhibition of protein aggregation (e.g. Aβ) in Tg mice (Moffett et al., 2007).

Taurine, a key player involved in the differentiation of neurones and the formation of synapses, has been the subject of studies that suggest its potential to influence neuronal plasticity and enhance cognitive function in AD models (Hernández-Benítez et al., 2013; Jang et al., 2017; Song et al., 2024). Our findings, which revealed no significant changes in taurine levels after DET treatment, suggest that it may not directly impact cognitive abilities. In contrast, Glx, a marker of glutamatergic activity (Senaratne et al., 2009), showed a slight reduction in vehicle-treated Tg mice compared to WT but returned to WT levels after DET treatment. Previous research has also observed declines in neuronal activity in Tg mice (Chen et al., 2012; Liang et al., 2017; Marjanska et al., 2005; Shen et al., 2018), while an increase was noted after donepezil treatment (Westman et al., 2009).

GPC and PCh, critical membrane density and integrity indicators, are closely linked to phospholipid synthesis and breakdown (Senaratne et al., 2009; Westman et al., 2009). Choline, an essential component for producing phosphatidylcholine in cellular membranes, may be affected by fluctuations in acetylcholine production, particularly in neurological conditions (Marjańska et al., 2014; Mohan et al., 2010; Wurtman et al., 1985). In contrast, research has reported varying levels of choline in Tg mice (Esteras et al., 2012; Marjanska et al., 2005; Westman et al., 2009), and notably, our study found no significant alteration in choline levels after DET treatment in our Tg model.

Furthermore, our MRS analysis effectively quantified Lip09 and MM09. However, the biological significance of the peaks identified in their spectra remains uncertain. Thymosin β4, which is implicated in neuroprotective responses, may be connected to these spectral peaks (Kauppinen et al., 1992a; Kauppinen et al., 1992b). Therefore, our elevated levels of Lip09 and MM09 in both WT and TG mice following DET treatment might suggest a potential neurotrophic effect. The discrepancy reported in the literature may be linked to factors such as the analysed brain regions, the age of the animals, and their genetic backgrounds (Doetschman, 2009; Pardon et al., 2016). This highlights the necessity for further studies

with diverse controls, a more comprehensive exploration of DET's metabolic pathways, and alternative methodology approaches.

3.5. Materials and methods

3.5.1. Experimental animals

We utilised the double transgenic mouse strain (B6.Cg-Tg (APPswe, PSEN1dE9)85Dbo/Mmjax, Lab Stock# 005864). These mice express a chimeric mouse/human APP featuring the Swedish mutation ($_{Mo/Hu}$APP695swe) and an exon-9 deletion in human presenilin-1 (PSEN1dE9) (Jankowsky et al., 2004). Corresponding WT littermates with identical backgrounds, carrying mouse APP and PSEN-1, were also utilised. We included WT and Tg mice aged 2 to 16.5 months for the experimental design. Genotyping was performed using a polymerase chain reaction of DNA extracted from tail biopsies (Jankowsky et al., 2001). All animal experiments received explicit approval from the "Ethics Committee for Animal Experimentation" of the Instituto de Investigaciones Biomédicas (CSIC-UAM) and were conducted in compliance with the European Communities Council Directive (2010/63/EEC) and National regulations (Normative 53/2013). We took special care to minimise the pain and discomfort experienced by the animals (Sethi et al., 2020).

3.5.2. Tissue preparation

Mice were intraperitoneally injected with 5-bromo-2-deoxyuridine (BrdU; 50 mg/kg) 24 hours (h) before being sacrificed to label short-term cell proliferation. The brain slices were collected as previously described (Morales-Garcia et al., 2011). In short, animals were anaesthetised and transcardially perfused using 4% paraformaldehyde (PFA; Merck, Spain). The brains were post-fixed in the same concentration of PFA overnight at 4°C. Before the brains were frozen down on dry ice, they were placed in a 4% PFA solution containing 30% sucrose (Sigma-Aldrich, Spain). 30 µm coronal sections were obtained in a cryostat (Cryocut 1900, Leica Biosystems, Barcelona, Spain, CM1900).

3.5.3. Isolation and culture of neurospheres

NSC were isolated from the subventricular zone using previously described methods (Ferrón et al., 2007; Morales-Garcia et al., 2012). We harvested and cultivated NSC from WT and Tg mice aged between 15.5 and 16.5 months, ensuring a sample size of at least seven from each group, as an alternative investigation model for AD. In brief, mice were cervical dislocated, their brains were extracted, and the subventricular zones were dissected as described following procedures outlined by Dr. Ana Perez Castillo's laboratory (Morales-Garcia et al., 2017; Morales-Garcia et al., 2011). The subventricular zones were dissociated in Dubecco's modified Eagle's medium (DMEM, Invitrogen, Spain), supplemented with 2%

glutamine and 0.1% gentamicin, and then filtered using a 40 µm cell strainer (Falcon cat. 352340). The tissue was digested with a mixture of trypsin-EDTA (1X), 0.4% hyaluronidase (200 mg/mL), and 0.1% DNase) for 15 min at 37°C (Morales-Garcia et al., 2015; Morales-Garcia et al., 2020). Following digestion, the cell suspension underwent two centrifuge steps: 10 min at 3000 rpm and 5 min at 1500 rpm. After centrifugation, the resuspended cells were filtered again using a 40 µm cell strainer. The cells were subsequently plated in 6-well plates and cultured in DMEM/F12 (1:1, Invitrogen) containing 10 ng/mL epidermal growth factor (Cat.100-15, Peprotech, London, UK), 10 ng/mL fibroblast growth factor (Cat. 100-18D, Peprotech), B27 medium (Gibco), and supplemented with 1% glutamine and 0.05% gentamicin (Morales-Garcia et al., 2020). The addition of growth factors (epidermal growth factor and fibroblast growth factor) was repeated every two days.

3.5.4. Differentiation of neurospheres culture

After 10 to 14 days *in vitro* (DIV), the maturation of neural progenitor-enriched growing spheres occurs, initiating differentiation into what are known as neurospheres. The differentiation process has been previously described by Dr. Ana Perez Castillo's laboratory (Morales-Garcia et al., 2017). Briefly, coverslips were coated with poly-L-lysine (PLL, Sigma, P2636, Spain) at a final concentration of 20 mg/mL in autoclaved milli-Q water. A single neurosphere was then carefully placed in the centre of the coated coverslip, which was subsequently immersed in differentiation media consisting of a 1:1 mixture of DMEM and F12 (Invitrogen), supplemented with B27 medium (Gibco), along with 1% glutamine, 0.05% gentamicin, and 10.4% foetal bovine serum (FBS) devoid of exogenous growth factors. The neurospheres were incubated for 24 to 48 hours without disturbance at 37°C in an atmosphere of 5% CO_2.

3.5.5. Amyloid beta and N,N-diethyltryptamine treatment

Prior to the differentiation of the neurospheres, they were subjected to treatment with low concentrations of human synthetic $A\beta_{(1-40)}$ ((0.5 µM), Tocris Bioscience, Cat. No 1428, Spain) and human synthetic $A\beta_{(1-42)}$ ((0.5 µM), Tocris Bioscience Cat. No. 1191, Spain) for 30 min. $A\beta_{(1-40)}$ (0.5 µM) and $A\beta_{(1-42)}$ (0.5 µM) were reconstituted in N,N-dimethylsulfoxide (DMSO, Sigma-Aldrich) to create a stock concentration of 250 µM, followed by sonication for 10 min and centrifugation at 13,523× g at 16 °C (Willén et al., 2017). During the proliferation and differentiation phases, the neurospheres were treated daily with DET (100 µM; CAS No. 61-51-8, Perez Castillo et al., 2018, Patent No. US11723894B2). The ability of DET to promote the differentiation of neuronal progenitor stem cells into neurones was

assessed by placing neurospheres from 10–14-day-old cultures onto coverslips pre-coated with PLL and culturing them in the presence of DET. After 72 h, the differentiated neurospheres were again exposed to $A\beta_{(1-40)}$ (0.5 µM) and $A\beta_{(1-42)}$ (0.5µM) for 30 min.

3.5.6. Clorgyline hydrochloride and N,N-diethyltryptamine administration in vivo

Mice (n=26, ages 10.5 to 12.5 months) were categorised based on the treatment administration (Figure 23). The classification of our mice groups was chosen based on previous findings obtained in Dr. Ana Perez Castillo's laboratory (Morales-Garcia et al., 2020) and unpublished data from neuroblastoma cell lines which featured the wild-type APP or Swedish APP mutation. The control groups included WT (n=6) and Tg (n=7), both of which received an intraperitoneal injection of CLQ treatment (1 mg/kg; CAS No. 17780-75-5). The DET-treated groups comprised WT (n=6) and Tg (n=7), who were administered with both CLQ and DET (1 nmol/gram). DET was delivered through subcutaneous injection. WT and Tg mice received intraperitoneal injections of CLQ alone or in combination with subcutaneous injections of DET every other day for 18 consecutive days. On day 1, all mice were given an intraperitoneal injection of BrdU (50 mg/kg) to label proliferating cells for long-term studies on their survival and differentiation between vehicle-treated control and DET-treated groups. Further investigations were carried out using MRI, as outlined below. After the completion of the study, all mice were sacrificed, and their brains were collected for further examination (Unfortunately, data is unavailable).

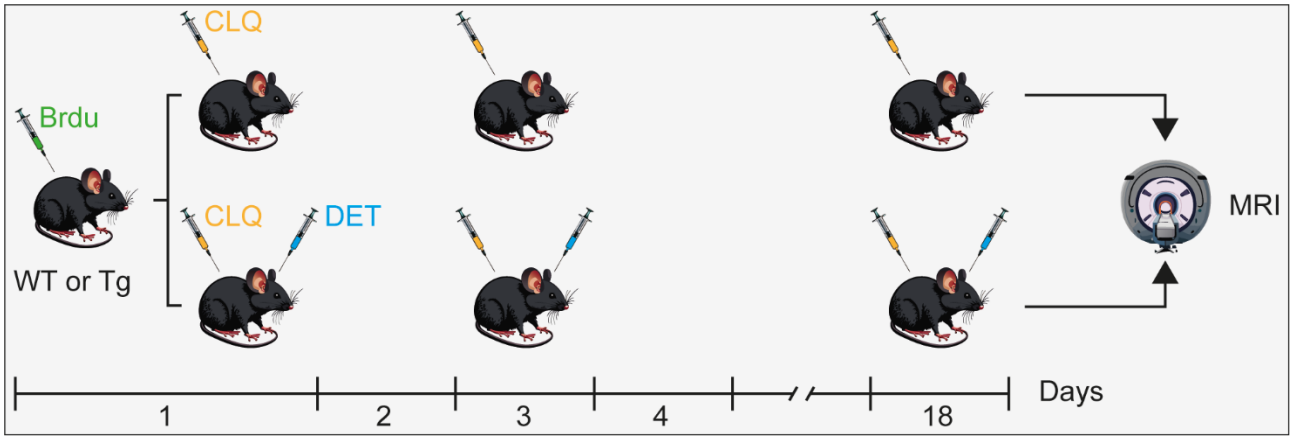

Figure 23: *Schematic overview of drugs administration and experimental setup.*
The illustration was created using Adobe Illustrator CC 2024.

3.5.7. Immunocytochemistry (ICC)

Neurospheres were cultured and treated as mentioned above. The neurospheres were fixed with 4% PFA on ice for 20 min after treatment. They were then permeabilised using 0.1 M Phosphate buffer (PB) containing 0.1% Triton X-100 (Sigma-Aldrich, Spain) and 5% normal goat serum (NGS; Vector Laboratories, Spain) for 30 min at 37°C. Subsequently, the neurospheres were incubated with primary antibodies (Table 2) diluted in a mixture of 0.1 M PB, 0.1% Triton X-100, and 1% NGS for 1 h at 37°C. After carefully washing with 0.1 M PB, the neurospheres were incubated with secondary antibodies (Alexa Fluor 488 (1:400) and Alexa Fluor 546 (1:400); Thermo Fisher Scientific, Madrid, Spain) along with 4',6-diamino-2-phenylindole (DAPI (1:400)); Calbiochem, Merck Life Science, Madrid, Spain 268298) for 1 h at 37°C. DAPI was utilised for nuclear staining, and both DAPI and the secondary antibodies were diluted in a mixture of 0.1 M PB, 0.1% Triton X-100, and 1% NGS. Following three washes with 0.1 M PB, the neurospheres were washed with autoclaved milli-Q water and 100% ethanol before mounting with Vectashield H-1200 (Vector Laboratories, Spain).

Table 2: *List of primary antibodies with their used application and dilution factor.*

Application	Antibody	Dilution	Source
Aβ, C99, APP and sAPPα	anti-$Aβ_{(1-16)}$ (clone 6E10)	IHC (1/1000)	Biolegend (SIG 39320
C-terminus $Aβ_{(1-42)}$	anti-Aβ (clone H31L21)	IHC (1/200)	Thermo Fisher Scientific 700254
C-terminus $Aβ_{(1-40)}$	anti-$Aβ_{(1-40)}$ (clone 11A50-B10)	ICC (1/200)	Biolegend (SIG 39140)
Amyloid fibrils and fibrillar oligomers	anti-Amyloid Fibrils (OC)	IHC (1/1000)	Sigma Aldrich (AB2286)
Astrogliosis	Glial fibrillary acidic protein (GFAP)	IHC (1/400)	Sigma (G3893)
Microgliosis	Ionized calcium-binding adaptor molecule 1 (Iba-1)	IHC (1/1500)	Wako, Japan
Neurogenesis/ neuroplasticity	Reelin (RELN, clone G10)	IHC (1/1000)	Abcam (ab78540)
Progenitor stem cells	Type VI intermediate filament protein (Nestin)	IHC (1/100), ICC (1/100)	Abcam (ab7659), Abcam (ab6142)
Proliferating cells	Bromodeoxyuridine (Brdu)	IHC (1/200)	DAKO (M0744) Abcam (ab6326)
Immature neurons	β-III-Tubulin (Tuj-1 clone)	IHC (1/400), ICC (1/400)	Abcam (68193)
Mature neurons	Microtubule Associated Protein2 (MAP-2)	ICC (1/200)	Sigma Aldrich (M4403)

3.5.8. Immunohistochemistry (IHC)

Immunofluorescence analysis was conducted on specific brain regions, including the hippocampus, subventricular zone, cortex, and entorhinal cortex, utilising 30 µm coronal sections as previously described (Alarcon-Gil et al., 2022; Sethi et al., 2020). Briefly, free-floating sections were blocked for 1 h at room temperature in phosphate buffer saline (PBS 1X) supplemented with 0.1% Triton X-100 and 3% NGS. For detection of BrdU, the samples were treated with 2 M HCl (Sigma-Aldrich, Spain) for 30 min at 37°C, followed by neutralisation with Borax (Sigma-Aldrich, Spain) performed twice (once for 1 minute and again for 15 min) at room temperature. After neutralisation, the sections were blocked for another hour in PBS containing 5% NGS and 0.1% Triton X-100, as previously described (Morales-Garcia et al., 2017). Subsequently, the brain sections were incubated overnight at 4°C on a shaker with the primary antibodies (Table 2), diluted in PBS with 0.1% Triton X-100 and 1% NGS. Following incubation, the sections were washed three times with PBS and then incubated to the corresponding secondary antibodies (Alexa Fluor 488 (1:400) and Alexa Fluor 546 (1:400)), along with DAPI (1:500)), all diluted in the blocking solution (PBS (1X) + 0.1% Triton X-100 + 3% NGS). The sections were rinsed once with 0.1M PB and mounted using Vectashield H-1200.

3.5.9. In vivo imaging

Mice that received injections of CLQ, either alone or in combination with DET, underwent brain scans using MRI. The MRI experiments were conducted on a Bruker Pharmascan Biospect system (Bruker Medical GmbH, Ettlingen, Germany) utilising a 7.0-T horizontal-bore superconducting magnet. This system was equipped with a 1H receive-only mouse brain surface coil, a volume transmission coil, and a Bruker gradient insert with a diameter of 90 mm (maximum intensity 36 G/cm). The surface coil was directly mounted on the mouse cradle and positioned over the animal's brain. The mouse was placed in the magnet while continuously inhaling anaesthesia delivered through a nose cone. A respiratory sensor connected to a monitoring system (SA Instruments, Stony Brook, NY) was positioned under the abdomen to track the rate and depth of respiration. The animals were anaesthetised with a 2% isoflurane-oxygen mixture in an induction chamber, and the flow of anaesthetic gas was constantly regulated to maintain a breathing rate of 60 ± 40 cycles per minute. All data were acquired using a Hewlett-Packard console equipped with Paravision 5.1 software (Bruker Medical GmbH), which operated on a Linux platform.

T2-weighted spin-echo anatomical images were acquired using a rapid acquisition with relaxation enhancement (RARE) sequence in an axial orientation. The parameters employed were as follows: repetition time (TR) of 3000 ms, time to echo (TE) of 44 ms, RARE factor of 8, an average of 4 acquisitions, a field of view (FOV) of 2.3 cm, an acquisition matrix of 256 × 256, corresponding to an in-plane resolution of 136 × 136 μm^2. The slice thickness set at 1 mm comprised a total of 14 slices.

Diffusion-weighted images were acquired using a spin-echo single-shot echo planar imaging (EPI) pulse sequence with the following parameters: TR/TE of 3500/40 ms, an average of 4 acquisitions, a diffusion gradient duration of 4 ms, a diffusion gradient separation of 20 ms, gradient directions of 7, two B-values (300 s/mm^2 and 1400 s/mm^2), and slices thickness of 1.5 mm without a gap. The acquisition matrix size was 128x128, which provided an in-plane resolution of 273x273 μm^2.

MT maps required acquiring two sets of magnetisation transfer contrast imaging: one with and the other without the off-resonance RF pulse. Both sets utilise a spin-echo sequence with the following parameters: TR/TE of 2500/9.85 ms, a matrix size of 128x128, FOV of 2.3 cm, a total number of six slices, a slice thickness of 1.5 mm, and the number of averages was 1. The RF saturation pulse was applied at a 1,5 kHz offset (downfield from the water signal) as a series of 50 Gaussian pulses, each lasting 5 ms. The pulse power was set at 5.5 μT, with a pulse bandwidth of 548 Hz and a total irradiation time of 266.3 ms.

Fractional anisotropy, mean diffusivity, trace, eigenvalues and eigenvector maps, as well as axial and radial diffusivity and MT maps, were computed with a custom-made software application written in Matlab (R2007a, Biomedical NMR Facility Sebastián Cerdán, Madrid, Spain). ROI analysis was performed with Image J (https://imagej.net/ij/).

The 1H-spectroscopy study was performed in the hippocampus. The *in vivo* spectroscopy protocol used a point-resolved spatially spectroscopy (PRESS) combined with VAPOR water suppression and has the following required parameters: TR of 3000 ms, TE of 35 ms, an average of 128 acquisitions, and a voxel volume of 3 mm^3. First- and Second-order shims were automatically adjusted utilising the FASTMAP application in a large voxel of 4 mm^3. All 1H-spectra were analysed automatically with LCModel version 6.2-OR (Stephen Provencher, Oakville, ON; Canada). The analysis included observed spectral data from 27 metabolites: alanine, aspartate, Creatine (Cr), phosphocreatine (PCr), γ-aminobutyric acid

(GABA), glucose, glutamine (Gln), glutamate (Glu), glycerophosphocholine (GPC), phosphocholine (PCh), inositol, lactate, N-acetyl aspartate (NAA) and N-acetyl-aspartyl-glutamate (NAAG), scyllo-inositol, taurine, creatine methylene, guanosine), various lipids (Lip09, Lip13a, Lip13b and Lip20), and macromolecules (MM09, MM12, MM14, MM17 and MM20).

3.5.10. Data analysis

All images obtained from IHC and ICC were captured using a Nikon Eclipse 90I microscope, equipped with Plan APO objectives of 4x, 10x, and 20x, along with Nikon DS-Fi1 digital camera connected to Nis-elements software (Nikon Instruments Inc, Nikon Europe B.V., Madrid, Spain) or with an invert confocal microscope LSM 710 (Carl Zeiss Inc, Carl Zeiss Iberia, S.L-Division Microscopy, Madrid, Spain). IHC was performed on three brain slices from three different mice in each group (WT and TG), while ICC was performed once with two technical replicates. Only the highest quality IHC and ICC samples were acquired for imaging, reducing imaging costs for Dr. Ana Perez Castillo's laboratory. Further image processing was carried out using Image J software, and all illustrated figures were created using Adobe Illustrator (version 2024).

In this study, *in vivo* images were acquired for treated WT mice (CLQ, N = 4; CLQ + DET, N = 4) and Tg mice (CLQ, N = 3; CLQ + DET, N = 4). Statistical analyses were conducted using GraphPad Prism 7 (GraphPad Software, San Diego, CA, USA). ROI values were calculated from the whole brain, cerebral cortex, corpus callosum, thalamus, hippocampus, and subventricular area across the scanned slices from T2-weighted, DTI and MT images (Figure 10) utilising ImageJ software. The ROI was delineated using the freehand selection tool in ImageJ. For T2-weighted images, values were determined based on the area represented by counted voxels within the ROI. The total volume of the ROI was calculated by summing the area from the different slices. For the DTI and MT images, the mean was used for further statistical analysis.

Additionally, the 1H-spectroscopy values utilised only the percentage (%) standard deviation. The processing software uses this parameter for the peak detection of a metabolite. If this value is below 20%, the program successfully identifies the peak, allowing for reliable metabolite analysis. However, if the value exceeds 20%, the program may mistakenly attribute the peak to noise detection. Therefore, avoiding working with metabolites that exhibit high standard deviation values is advisable. The relative

concentrations of the metabolites are expressed and plotted against the total creatine (tCr = Cr + PCr) concentration, which remains unchanged in both healthy and pathological conditions (Eisele et al., 2020). Therefore, tCr concentration serves as a suitable reference metabolite. Based on the threshold value related to the tCr signal, 7 metabolite levels (inositol, NAA, NAA + NAAG, taurine, GPC + PCh, Glu + Gln, and MM09 + Lip09) were selected for further analytical analysis.

The following statistical analyses were performed on the *in vivo* data. The Shapiro-Wilk test was performed to determine whether the values were normally distributed for each slice within the ROI. For normally distributed data, we conducted an ordinary one-way ANOVA followed by Tukey's post hoc multiple comparison test. In cases where the data did not follow a normal distribution, a Kruskal-Wallis test was carried out, accompanied by Dunn's multiple comparisons as a post hoc test. All data are presented as mean ± standard deviation (SD) and are considered statistically significant if $p < 0.05$ (* $p < 0.05$) (Table S1-Table S5).

3.6. Supplementary materials

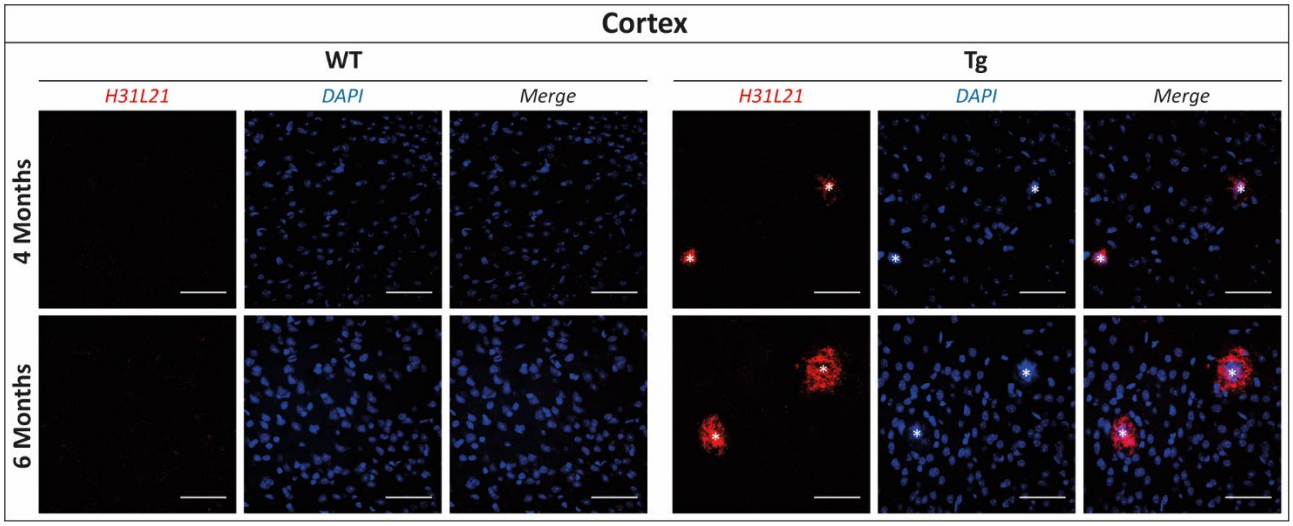

Figure S1: *Characterisation of human-specific Aβ(1-42)-aggregates in cortex from WT and Tg mice.*
*Fluorescence staining for human-specific Aβ(1-42) (H31L21, red) aggregates begins at 4 months in the cortex of Tg mice compared to their WT littermates. The volume of Aβ(1-42) plaques in the cortex of Tg mice tends to increase from 4 to 6 months Tg mice. The aggregated area of Aβ(1-42) (white asterisk *) reveals destructed nuclei staining (DAPI, blue) in the cortex of 4- to 6-month-old Tg mice compared to WT mice. The scale bar represents 50 µm.*

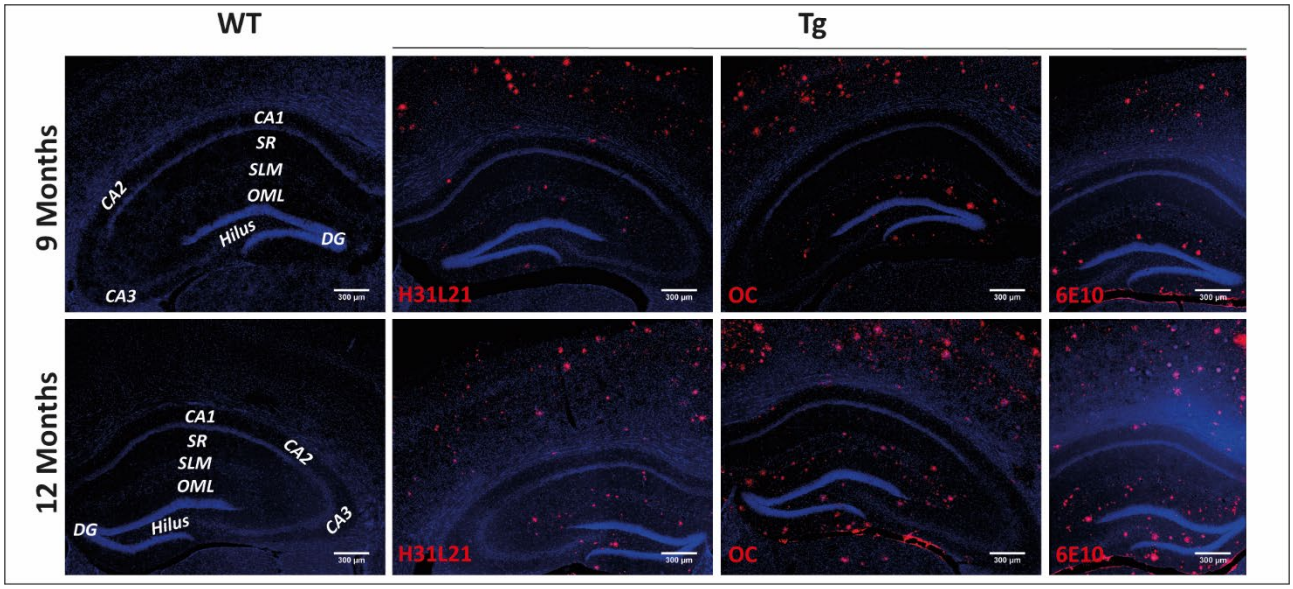

Figure S2: *Various isoforms of human Aβ-aggregates and oligomeric forms within the cortical and hippocampal brain regions of WT and Tg mice aged 9 to 12 months.*
Different isoforms of human Aβ aggregates in the cortex and hippocampus of 9–12 months WT and Tg mice are presented. Immunofluorescence analysis reveals the presence of human-specific Aβ(1-42) (H31L21), amyloid fibrils and fibrillary oligomers (OC), and with human Aβ(1-40)/Aβ(1-42) (6E10) plaques in the frontal cortex and hippocampal regions. Notably, these aggregates are primarily found in the stratum radiatum (SR), stratum lacunosum moleculare (SLM), the outer portion of the molecular layer of the dentate gyrus (OML), and the hilus of the dentate gyrus (DG) in 9-to 12-month-old mice. The cornu ammonis, which includes the CA1, CA2, CA3, and hilus (CA4) subfields, is a specific hippocampus area. DAPI (blue) is utilised for nuclear staining.

This image complements the data previously published by Sethi et al. (2020) (Sethi et al., 2020). The scale bar is 300 µm.

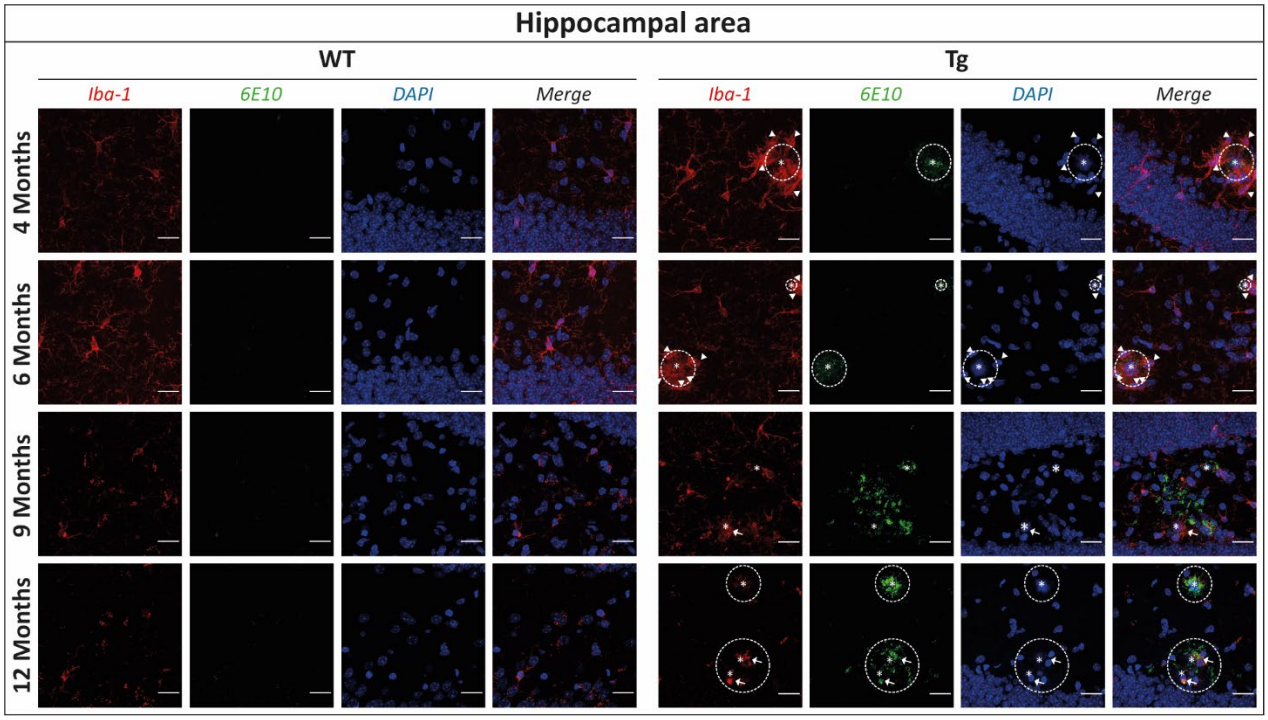

Figure S3: *Human Aβ-associated microgliosis in the hippocampus of WT and Tg mice aged 4 to 12 months. Representative immunofluorescence images depict microglial activation surrounding human Aβ aggregates in the hilus of the hippocampus of Tg mice aged 4 to 12 months, compared to WT. Activation and recruitment of reactive microglia (Iba-1, red, white arrowheads) to human Aβ aggregates (6E10, green) begin at 4 months in Tg mice. The human Aβ-associated microgliosis tends to increase with age, peaking at 9 months in Tg mice. Between 9 and 12 months, Tg mice display dying reactive microglia (white arrows) due to the abundance of human Aβ plaques, in contrast to their WT littermates. In WT mice, a notable decrease in microglia activation is observed in immunofluorescence starting at 9 months. Additionally, diffusible human Aβ aggregates (indicated by dashed white circles) are associated with destructed nuclei (DAPI, blue, marked with an asterisk *) that emerge at 4 months and tend to increase with age in Tg mice compared to WT littermates. The scale bar represents 20 µm.*

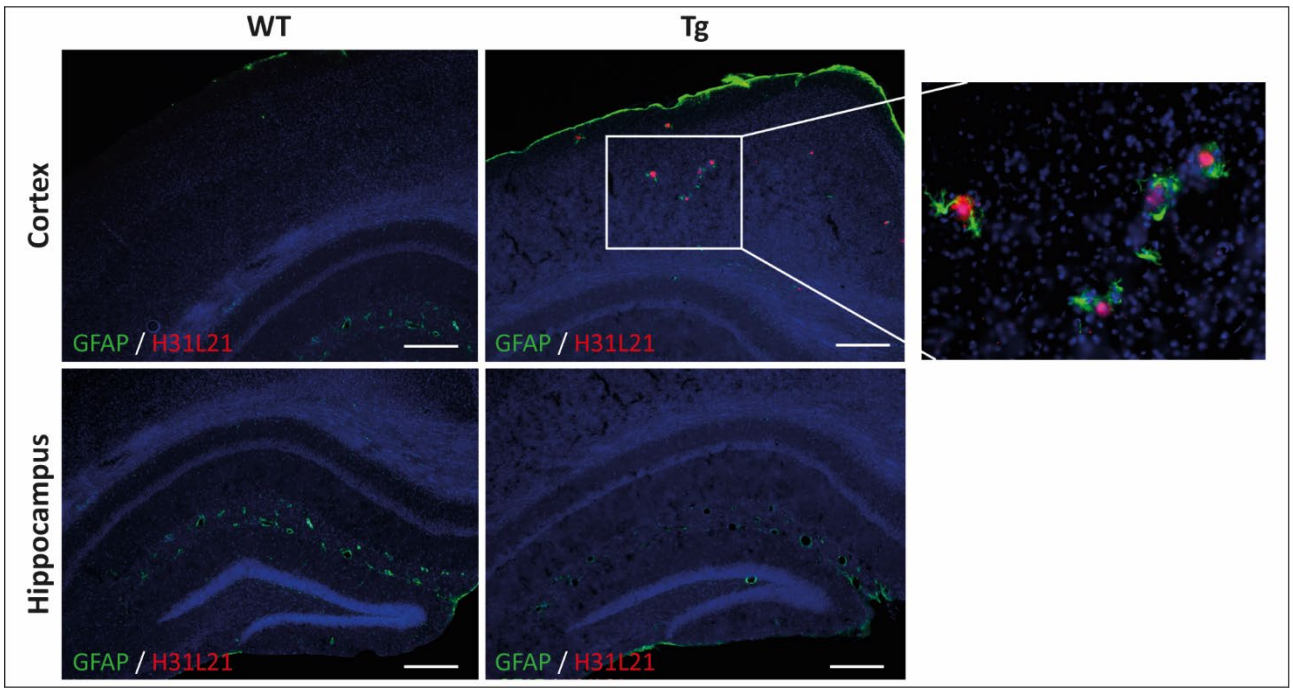

Figure S4: *Human-specific Aβ(1-42)-associated astrogliosis within the cortex and hippocampus of 4-month-old WT and Tg mice.*

Here, we show that astrocytes (GFAP, green) surround human Aβ(1-42) (H31L21, red) aggregates in the cortex and hippocampus of 4-month-old WT and Tg mice. Notably, no Aβ(1-42) induced astrogliosis is seen in the hippocampus of 4-month-old Tg and WT mice. In contrast, the cortex of Tg mice displays Aβ(1-42) aggregates surrounded by astrocytes (white box). DAPI (blue) is used for nuclear staining. The scale bar is 350 µm.

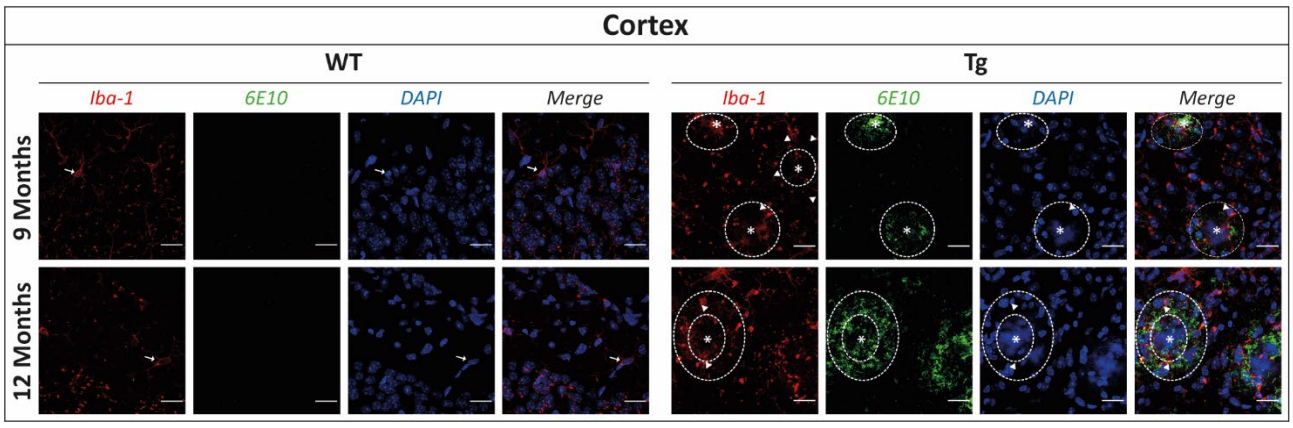

Figure S5: *The alteration in microgliosis activation surrounding human Aβ(1-40)/Aβ(1-42)-aggregates within the cortical region of WT and Tg mice aged between 9 to 12 months.*

We observe the co-occurrence of Aβ(1-40)/Aβ(1-42)-aggregates (6E10, green) and microglia (Iba-1, red) within the cortex of 9-12-month-old WT and Tg mice. The Tg mice exhibit an increase in fluorescent staining in Aβ(1-40)/Aβ(1-42)-aggregates compared to the WT mice. Altered activation of microglia is evidenced by the fluorescent signals surrounding these aggregates (white arrowheads). Notably, the 12-month Tg mice demonstrate a twofold increase in Aβ aggregates (outer white circle) compared to the 9-month WT mice (inner white circle). Non-reactive microglia are observed in the WT mice (white arrows), while reactive and dying microglial-positive cells surround Aβ plaques (white arrowheads). Significant diffusion of destructed nuclei (DAPI, blue, white

*asterisk *) is observed in the microglial surrounding the Aβ plaques from 9- to 12-month-old Tg mice. The scale bar represents 20 µm.*

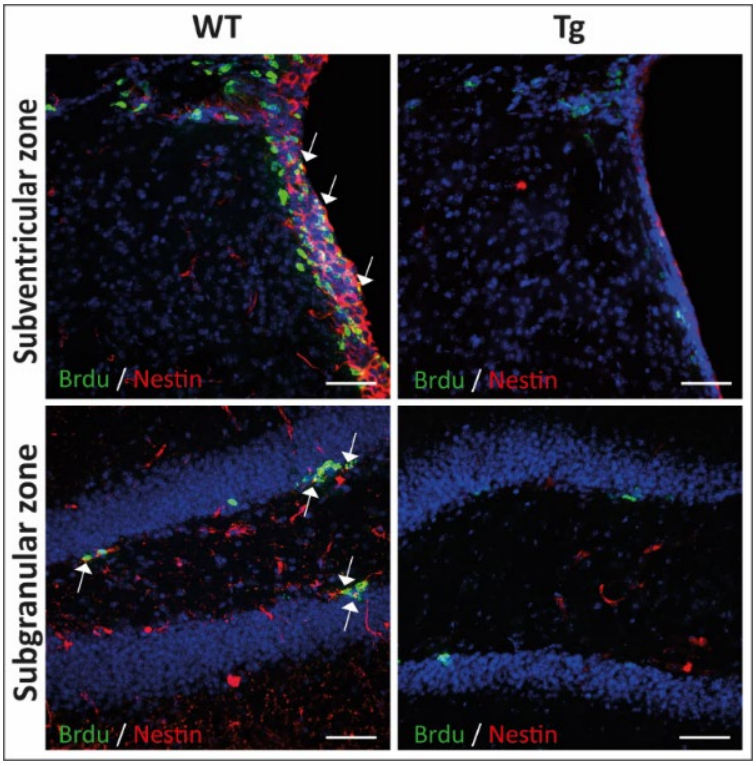

Figure S6: *The impact of adult neurogenesis in the subventricular and subgranular zones of 6-month-old WT and Tg mice.*

Immunofluorescence images illustrate the alteration in adult neurogenesis within the subventricular and subgranular zones of 6-month-old WT and Tg mice. Notably, decreases in the fluorescent signal of progenitor cells (Nestin, red) and proliferating cells (Brdu, green) are observed in Tg mice compared to their WT littermates. Additionally, a reduction in fluorescent staining of colocalization of newly formed neuronal cells during proliferation of neuronal stem cells is evident in the subventricular zone and subgranular zone of Tg compared to WT (white arrow). DAPI (in blue) is used for nuclear staining. The scale bar is 50 µm.

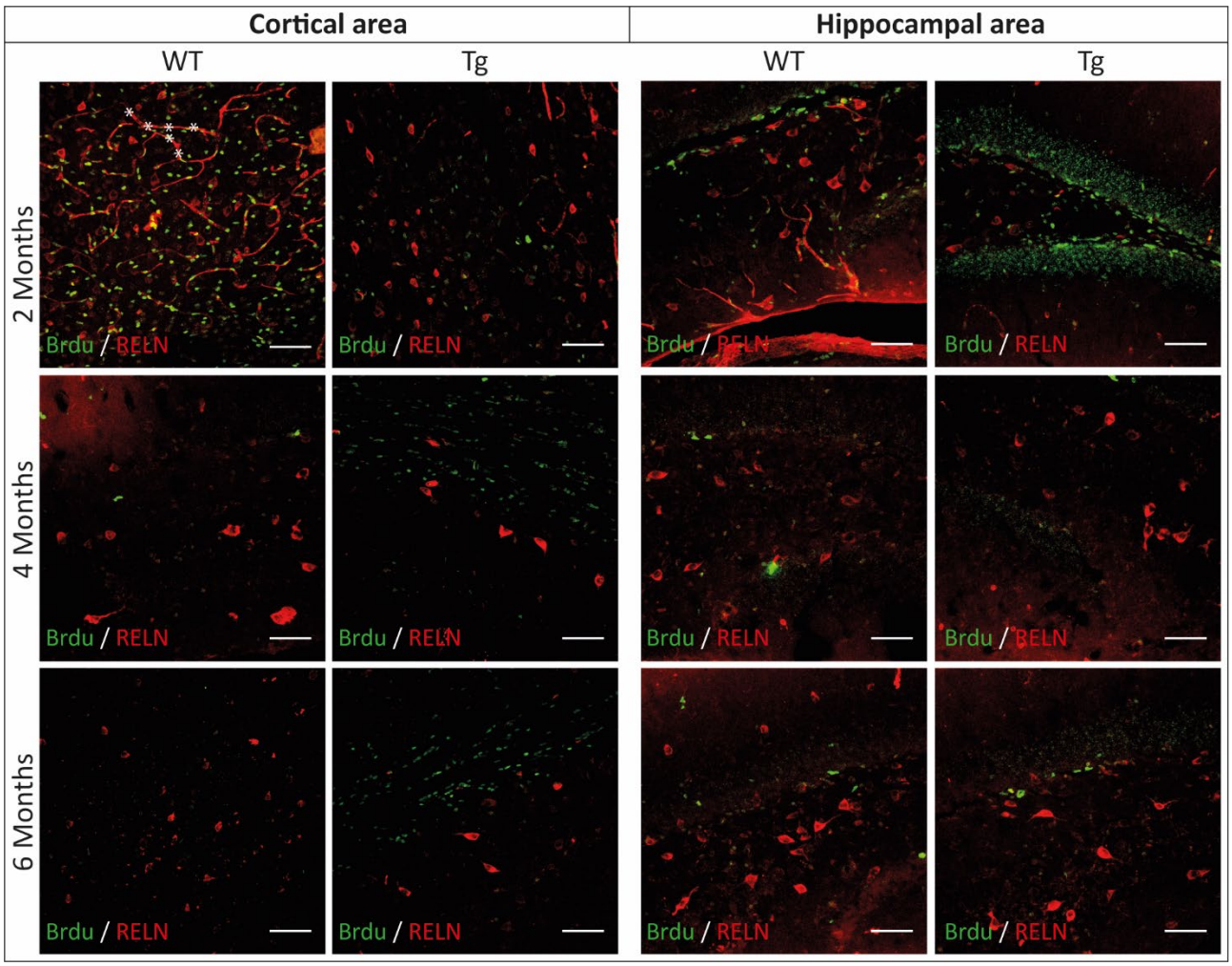

Figure S7: *Adult neurogenesis and neuroplasticity are unaffected in the cortex and hippocampus of WT and Tg mice aged 2 to 6 months.*

Immunofluorescence images show the localisation of proliferating cells (Brdu, green) and Reelin-positive cells (RELN, red) in specific brain regions, including the frontal cortex and the hilus of the hippocampus, from WT and Tg mice aged 2 to 6 months. The white asterisk (*) indicates artefacts and not RELN-positive cells. The data reveal that the fluorescent signal of RELN-positive cells is altered with age in both the cortical and hippocampal areas of WT and Tg mice. The scale bar represents 50 µm.

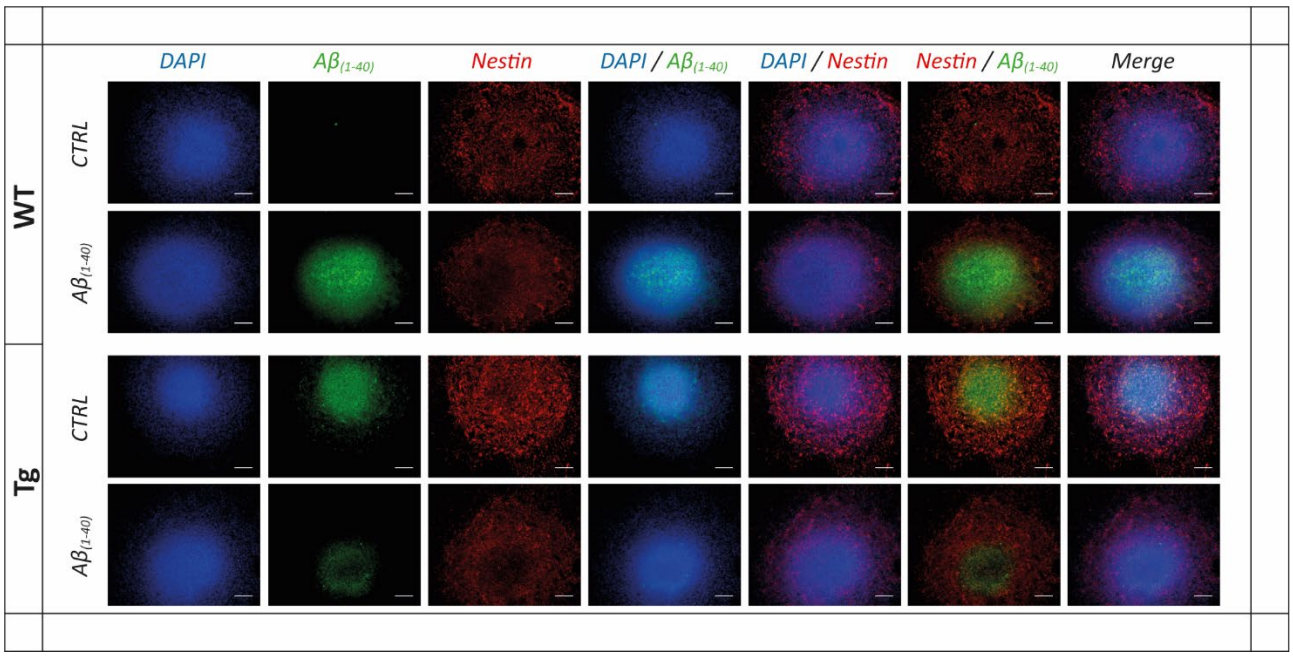

Figure S8: *Effect of adult neurogenesis in WT and Tg neurospheres following treatment with* $A\beta_{(1\text{-}40)}$.
The WT and TG neurospheres are derived from the subventricular zone of animals approximately 16 months old. These neurospheres are treated with and without $A\beta_{(1\text{-}40)}$ *(0.5 µM), representing data from one independent culture (N = 1) with two technical replicates (n=2). In* $A\beta_{(1\text{-}40)}$*-treated WT and TG neurospheres, there is a noticeable reduction in the fluorescent signal of progenitor cells (Nestin, red) compared to the non-treated WT and Tg controls (CTRL). The* $A\beta_{(1\text{-}40)}$*-treated WT exhibit an increase in fluorescent signal of* $A\beta_{(1\text{-}40)}$ *(11A50-B10, green) load compared to the control groups and* $A\beta_{(1\text{-}40)}$*-treated Tg neurospheres. Control groups show a slight increase in fluorescent signal of differentiating progenitor cells (Nestin, red) compared to* $A\beta_{(1\text{-}40)}$*-treated groups. Additionally, Tg neurospheres show a slight fluorescent alteration in the differentiating effect of Nestin-positive cells (red) compared to WT neurospheres. Nuclei are stained with DAPI (blue), and the scale bar is 100 µm.*

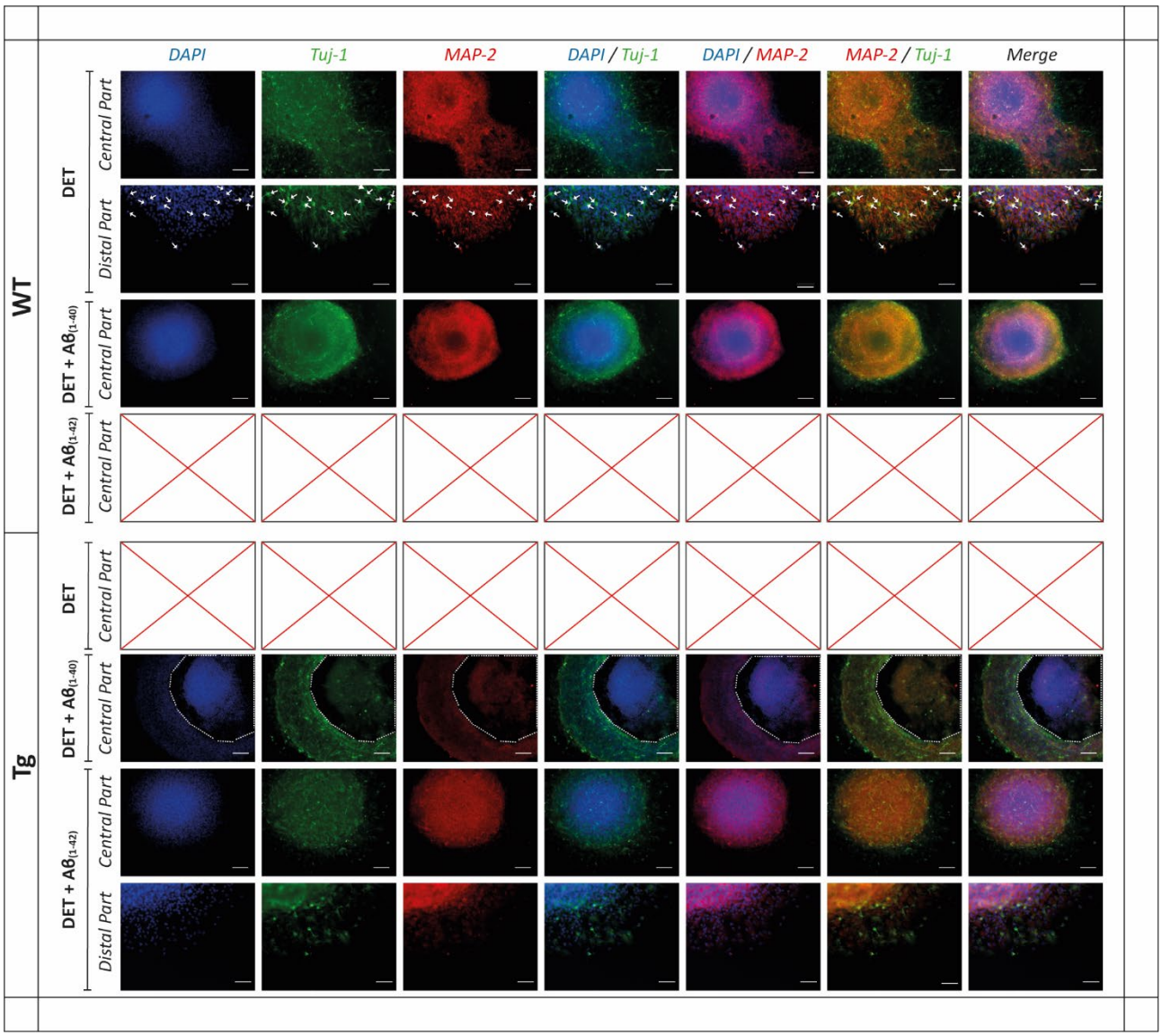

Figure S9: *DET promotes the differentiation of neuronal stem cells into mature neurons derived from WT neurospheres.*

The differentiation of NSC into mature neurones from the subventricular zone of WT neurospheres, obtained from approximately 16-month-old mice, is presented with and without DET stimulation (analysed from one independent culture (N = 1) with two technical replicates, n=2). The distal part of DET-treated WT neurospheres exhibits differentiation into mature neurones (MAP-2, red) and immature neuronal cells (β-III-Tubulin (Tuj-1 clone), green). The differentiation of NSC into mature neurones is highlighted in DET-treated WT neurospheres (white arrows). Additionally, we illustrate WT and Tg neurospheres stimulated with DET (100 µM) alongside 30 min treatment of either $A\beta_{(1-40)}$ (0.5 µM) or $A\beta_{(1-42)}$ (0.5 µM). The combined treatment (DET + Aβ) of Tg neurospheres shows no prominent reduction in the fluorescent differentiation signal of mature neurones (Map-2) when compared to DET-treated WT. An artefact (white stripes) is observed due to the disruption of the neurospheres during the mounting process. Unfortunately, extra technical replicates could not be obtained from Tg neurospheres treated with DET in combination with $A\beta_{(1-40)}$ or WT neurospheres treated with $A\beta_{(1-42)}$. Nuclei staining is DAPI (blue). The scale bars represent 100 µm (central part) and 50 µm (distal part).

Table S1: *List of statistically adjusted p-values from volumetric analysis of T2-weighted imaging.*

We present statistically adjusted p-values derived from the volumetric changes observed in various slices of distinct brain regions of interest (ROI), as well as the sum of volumetric changes of different ROI between different vehicle-treated control groups (WT (CLQ) and Tg (ClQ)) and DET-treated groups (WT (CLQ+DET) and Tg (CLQ+DET)) as illustrated in Figure 11. The adjusted p-values are reported for the following ROI: whole brain (slices 1-14), cerebral cortex (slices 5-14), hippocampus (slices 5-7), thalamus (slices 6-8), corpus callosum (slices 7-10), and subventricular area (slices 8-10) in both WT and Tg brains from the vehicle-treated control groups and DET-treated groups. To be considered significant, p-values must be less than 0.05 ($p < 0.05$). None of the datasets demonstrated significant differences. The adjusted p-value for the sum of volumetric data from a specific brain ROI is calculated from all volumetric data values across the various slices.*

ROI	Slices	Adjusted p-values from different groups					
		WT (CLQ) vs. WT (CLQ+DET)	**WT (CLQ) vs. TG (CLQ)**	**WT (CLQ) vs. TG (CLQ+DET)**	**WT (CLQ+DET) vs. TG (CLQ)**	**WT (CLQ+DET) vs. TG (CLQ+DET)**	**TG (CLQ) vs. TG (CLQ+DET)**
		Sum	*Sum*	*Sum*	*Sum*	*Sum*	*Sum*
Whole brain		*> 0.9999*	*> 0.9999*	*> 0.9999*	*> 0.9999*	*> 0.9999*	*> 0.9999*
	Slice 1	> 0.9999	> 0.9999	> 0.9999	> 0.9999	> 0.9999	> 0.9999
	Slice 2	0.6896	0.2980	0.9811	0.8388	0.4762	0.1807
	Slice 3	0.7931	0.8379	0.9742	>0.9999	0.9561	0.9691
	Slice 4	0.9619	0.9340	0.8587	0.9989	0.6002	0.5724
	Slice 5	> 0.9999	> 0.9999	> 0.9999	> 0.9999	0.9284	> 0.9999
	Slice 6	0.8739	0.7837	0.9917	0.9945	0.9642	0.9024
	Slice 7	0.9975	0.9772	0.8732	0.9956	0.7842	0.6980
	Slice 8	0.9130	0.9456	0.8496	>0.9999	0.9985	0.9969
	Slice 9	0.9239	0.9230	0.7486	>0.9999	0.9791	0.9890
	Slice 10	0.8316	0.8917	0.8864	0.9998	0.9993	>0.9999
	Slice 11	> 0.9999	> 0.9999	> 0.9999	> 0.9999	> 0.9999	> 0.9999
	Slice 12	> 0.9999	> 0.9999	> 0.9999	> 0.9999	> 0.9999	> 0.9999
	Slice 13	> 0.9999	> 0.9999	0.7350	> 0.9999	> 0.9999	> 0.9999
	Slice 14	> 0.9999	> 0.9999	0.9284	> 0.9999	> 0.9999	> 0.9999

			0.7985		*> 0.9999*		*0.4141*		*> 0.9999*		*> 0.9999*		*> 0.9999*
Cerebral cortex	**Slice 5**	0.9878		0.9857		> 0.9999		0.9172		0.9934		0.9777	
	Slice 6	0.7469		> 0.9999		0.8866		0.8177		0.9911		0.9277	
	Slice 7	0.4919		> 0.9999		> 0.9999		0.8594		> 0.9999		> 0.9999	
	Slice 8	> 0.9999		> 0.9999		> 0.9999		> 0.9999		> 0.9999		> 0.9999	
	Slice 9	0.9284		> 0.9999		0.4919		> 0.9999		> 0.9999		> 0.9999	
	Slice 10	0.5165		0.8951		0.1349		0.9268		0.7612		0.4584	
	Slice 11	> 0.9999		> 0.9999		> 0.9999		> 0.9999		> 0.9999		> 0.9999	
	Slice 12	> 0.9999		> 0.9999		> 0.9999		> 0.9999		> 0.9999		> 0.9999	
	Slice 13	> 0.9999		> 0.9999		0.7350		> 0.9999		> 0.9999		> 0.9999	
	Slice 14	> 0.9999		> 0.9999		0.9284		> 0.9999		> 0.9999		> 0.9999	
			0.9295		*0.3507*		*0.9815*		*0.6498*		*0.9955*		*0.5278*
Hippocampus	**Slice 5**	0.7269		0.1871		0.3952		0.6300		0.9306		0.9089	
	Slice 6	0.9797		0.8524		0.9933		0.9692		0.9145		0.7283	
	Slice 7	0.9853		0.9885		0.9440		0.9190		0.9966		0.8407	
			0.6596		*0.2607*		*0.6843*		*0.8155*		*> 0.9999*		*0.7955*
Thalamus	**Slice 6**	0.3144		0.2840		0.3698		0.9965		0.9993		0.9875	
	Slice 7	0.9183		0.5096		0.9640		0.8354		0.9983		0.7574	
	Slice 8	0.9996		0.9996		0.9982		0.9969		0.9923		> 0.9999	
			0.7332		*0.5286*		*0.9673*		*0.9713*		*0.9358*		*0.7678*
Corpus callosum	**Slice 7**	0.7943		> 0.9999		> 0.9999		0.8353		0.3440		> 0.9999	
	Slice 8	0.9882		0.9939		0.9993		0.9449		0.9700		0.9990	
	Slice 9	0.9639		0.9898		0.9690		0.9991		0.7964		0.8887	
	Slice 10	> 0.9999		0.7240		> 0.9999		0.7781		> 0.9999		> 0.9999	

Subventricular area		*0.6264*	*0.9996*	*0.5810*	*0.6206*	*0.9998*	*0.5786*
	Slice 8	0.6266	0.9995	0.7345	0.7389	0.9975	0.8298
	Slice 9	0.9017	0.9681	0.6915	0.7067	0.9726	0.4814
	Slice 10	0.8542	0.9996	0.8169	0.9175	0.9998	0.8906

Table S2: *List of statistically adjusted p-values from magnetisation transfer imaging*

This table presents the statistically adjusted p-values across various brain regions of interest (ROI) for different vehicle-treated control groups (WT (CLQ) and Tg (ClQ)) compared to DET-treated groups (WT (CLQ+DET) and Tg (CLQ+DET)), as illustrated in Figure 13. The adjusted p-values are detailed for the whole brain (slices 1-6), cerebral cortex (slices 2-6), hippocampus (slices 2-3), thalamus (slices 3-4), corpus callosum (slices 3-5), and subventricular area (slices 4-5) for both WT and Tg brains from the vehicle-treated control groups and DET-treated groups. Significant differences are indicated if $p < 0.05$ ($p < 0.05$). All comparisons did not show significant differences between groups.*

		Adjusted p-values from different groups					
ROI	**Slices**	**WT (CLQ) vs. WT (CLQ+DET)**	**WT (CLQ) vs. TG (CLQ)**	**WT (CLQ) vs. TG (CLQ+DET)**	**WT (CLQ+DET) vs. TG (CLQ)**	**WT (CLQ+DET) vs. TG (CLQ+DET)**	**TG (CLQ) vs. TG (CLQ+DET)**
Whole brain	**Slice 1**	> 0.9999	> 0.9999	> 0.9999	0.9860	> 0.9999	> 0.9999
	Slice 2	0.9620	0.5092	0.9579	0.7616	> 0.9999	0.7706
	Slice 3	> 0.9999	0.6789	0.9510	0.7125	0.9658	0.9153
	Slice 4	0.9756	0.7866	0.9861	0.5724	0.8761	0.9221
	Slice 5	0.9614	0.4336	0.8195	0.6846	0.9791	0.8698
	Slice 6	> 0.9999	0.6767	> 0.9999	> 0.9999	> 0.9999	> 0.9999
Cerebral cortex	**Slice 2**	> 0.9999	> 0.9999	> 0.9999	> 0.9999	> 0.9999	> 0.9999
	Slice 3	> 0.9999	> 0.9999	> 0.9999	> 0.9999	> 0.9999	> 0.9999
	Slice 4	> 0.9999	> 0.9999	> 0.9999	> 0.9999	> 0.9999	> 0.9999
	Slice 5	0.9981	0.3982	0.8692	0.4801	0.9322	0.7889
	Slice 6	> 0.9999	0.6767	> 0.9999	> 0.9999	> 0.9999	> 0.9999

Hippocampus	Slice 2	0.8912	0.3227	0.9875	0.6710	0.9797	0.4689
	Slice 3	0.9801	0.4078	0.8149	0.6014	0.9578	0.8512
Thalamus	Slice 3	> 0.9999	> 0.9999	> 0.9999	0.9423	> 0.9999	> 0.9999
	Slice 4	0.9947	0.4790	0.7939	0.3657	0.6604	0.9206
Corpus callosum	Slice 3	> 0.9999	> 0.9999	> 0.9999	> 0.9999	> 0.9999	> 0.9999
	Slice 4	0.9960	0.5373	0.8849	0.4273	0.7820	0.8927
	Slice 5	0.9575	0.4842	0.7987	0.7470	0.9751	0.9209
Subventricular area	Slice 4	> 0.9999	> 0.9999	> 0.9999	> 0.9999	> 0.9999	> 0.9999
	Slice 5	0.9391	0.5418	0.9615	0.8334	0.9997	0.7933

Table S3: *List of statistically adjusted p-values derived from axial and radial diffusivity imaging.*

This table presents the statistically adjusted p-values for various slices of different regions of interest (ROI) in the brain between the vehicle-treated control groups (WT (CLQ) and Tg (ClQ)) and DET-treated groups (WT (CLQ+DET) and Tg (CLQ+DET)), as illustrated in Figure 15 and Figure 17. The adjusted p-values are reported for the following ROI: whole brain (slices 1-6), cerebral cortex (slices 2-6), hippocampus (slices 2-3), thalamus (slices 3-4), corpus callosum (slices 3-5), and subventricular area (slices 4-5) in both WT and Tg brains from vehicle-treated control groups and DET-treated groups. A result is considered significant if $p < 0.05$ ($p < 0.05$). Notably, a significant difference is observed only in the axialdiff of the hippocampus (slice 2) between WT (CLQ) and Tg (CLQ) ($p = 0.0491$). All other datasets did not reach significance.*

ROI	Slices	Adjusted p-values from different groups											
		WT (CLQ) vs. WT (CLQ+DET)		**WT (CLQ) vs. TG (CLQ)**		**WT (CLQ) vs. TG (CLQ+DET)**		**WT (CLQ+DET) vs. TG (CLQ)**		**WT (CLQ+DET) vs. TG (CLQ+DET)**		**TG (CLQ) vs. TG (CLQ+DET)**	
		Axialdiff	*Radialdiff*	*Axialdiff*	*Radialdiff*	*Axialdiff*	*Radialdiff*	*Axialdiff*	*Radialdiff*	*Axialdiff*	*Radialdiff*	*Axialdiff*	*Radialdiff*
Whole brain	**Slice 1**	0.7337	0.9455	0.7688	0.4765	0.9944	0.9477	> 0.9999	0.2478	0.5923	> 0.9999	0.6402	0.2505
	Slice 2	0.4759	0.9668	0.2100	0.6557	0.0658	> 0.9999	0.8832	0.8754	0.5497	0.9622	0.9512	0.6440
	Slice 3	0.9979	0.9961	0.8827	0.9461	0.9294	> 0.9999	0.8074	0.8760	0.8622	0.9954	0.9980	0.9493
	Slice 4	> 0.9999	> 0.9999	> 0.9999	> 0.9999	> 0.9999	> 0.9999	> 0.9999	0.3422	> 0.9999	> 0.9999	> 0.9999	> 0.9999
	Slice 5	> 0.9999	0.7635	> 0.9999	0.4554	> 0.9999	0.9901	> 0.9999	0.9237	> 0.9999	0.5931	> 0.9999	0.3217
	Slice 6	0.6047	0.9284	0.9954	0.3618	0.8243	0.7985	0.7868	> 0.9999	0.2059	> 0.9999	0.7373	> 0.9999
Cerebral cortex	**Slice 2**	0.4015	0.7844	0.2593	0.4498	0.0741	0.9562	0.9681	0.9075	0.6743	0.9711	0.9286	0.7139
	Slice 3	0.9572	0.9978	0.9313	0.9527	0.9684	>0.9999	0.7199	0.9000	0.7794	0.9989	0.9978	0.9428
	Slice 4	0.9368	0.9425	0.9559	0.4007	0.8862	0.7694	0.7299	0.6869	0.5816	0.9754	0.9984	0.8804
	Slice 5	> 0.9999	0.6382	> 0.9999	0.3903	> 0.9999	0.9936	> 0.9999	0.9468	> 0.9999	0.4910	> 0.9999	0.2848
	Slice 6	0.6047	0.9910	0.9954	0.6085	0.8243	0.6456	0.7868	0.4579	0.2059	0.4807	0.7373	0.9987
Hippocampus	**Slice 2**	0.1860	> 0.9999	0.0491	0.5827	0.0530	> 0.9999	0.7560	> 0.9999	0.8597	> 0.9999	0.9930	0.1794
	Slice 3	> 0.9999	0.9815	> 0.9999	0.9878	> 0.9999	0.9893	> 0.9999	0.9074	> 0.9999	0.9026	> 0.9999	> 0.9999

Thalamus	**Slice 3**	0.7135	0.7985	0.5104	> 0.9999	0.7290	> 0.9999	0.9713	0.9423	> 0.9999	0.7985	0.9663	> 0.9999
	Slice 4	> 0.9999	0.4490	> 0.9999	0.2874	> 0.9999	0.4139	> 0.9999	0.9656	> 0.9999	0.9999	> 0.9999	0.9773
Corpus callosum	**Slice 3**	> 0.9999	0.9994	> 0.9999	0.9132	> 0.9999	> 0.9999	> 0.9999	0.9467	> 0.9999	0.9986	> 0.9999	0.9003
	Slice 4	0.9594	0.9132	0.9998	0.0847	0.9242	0.5976	0.9489	0.2164	0.6916	0.9231	0.9590	0.4633
	Slice 5	0.4745	0.9346	0.9921	0.9265	0.9934	0.8808	0.6952	0.9999	0.3446	0.5699	0.9527	0.5863
Subventricular area	**Slice 4**	> 0.9999	> 0.9999	> 0.9999	> 0.9999	> 0.9999	> 0.9999	> 0.9999	> 0.9999	> 0.9999	> 0.9999	> 0.9999	> 0.9999
	Slice 5	0.9713	> 0.9999	0.9930	> 0.9999	0.9983	> 0.9999	0.9067	> 0.9999	0.9302	> 0.9999	0.9994	> 0.9999

Table S4: *List of statistically adjusted p-values from fractional anisotropy and mean diffusivity imaging.*

The following statistically adjusted p-values were calculated for various brain regions of interest (ROI) across different vehicle-treated control groups (WT (CLQ) and Tg (ClQ)) and DET-treated groups (WT (CLQ+DET) and Tg (CLQ+DET)), as illustrated in Figure 19 and Figure 21. We present the adjusted p-values for the whole brain (slices 1-6), cerebral cortex (slices 2-6), hippocampus (slices 2-3), thalamus (slices 3-4), corpus callosum (slices 3-5), and subventricular area (slices 4-5) in the WT and Tg brains of both vehicle-treated control groups (CLQ) and DET-treated groups. Results are considered significant if $p < 0.05$ ($p < 0.05$). Significant difference is only observed in the MD of the hippocampus (slice 2) between WT (CLQ) and Tg (CLQ) ($p = 0.0128$). All other datasets did not reach significance.*

ROI	**Slices**	**Adjusted p-values from different groups**											
		WT (CLQ) vs. WT (CLQ+DET)		**WT (CLQ) vs. TG (CLQ)**		**WT (CLQ) vs. TG (CLQ+DET)**		**WT (CLQ+DET) vs. TG (CLQ)**		**WT (CLQ+DET) vs. TG (CLQ+DET)**		**TG (CLQ) vs. TG (CLQ+DET)**	
		FA	*MD*	*FA*	*MD*	*FA*	*MD*	*FA*	*MD*	*FA*	*MD*	*FA*	*MD*
Whole brain	**Slice 1**	0.9919	0.1886	0.9998	0.9948	0.6936	0.9946	0.9976	0.1673	0.5329	0.2688	0.6979	0.9648
	Slice 2	0.9294	> 0.9999	0.9236	0.4994	0.1219	> 0.9999	> 0.9999	> 0.9999	0.2981	> 0.9999	0.3876	> 0.9999
	Slice 3	0.8424	0.9939	0.8845	0.7235	0.8522	0.9359	> 0.9999	0.8453	> 0.9999	0.9874	> 0.9999	0.9537
	Slice 4	> 0.9999	> 0.9999	> 0.9999	> 0.9999	> 0.9999	> 0.9999	> 0.9999	> 0.9999	> 0.9999	> 0.9999	> 0.9999	> 0.9999

	Slice 5	0.9884	0.6509	0.8306	0.9145	0.9840	0.8885	0.9432	0.9691	> 0.9999	0.2839	0.9432	0.5756
	Slice 6	> 0.9999	0.8764	> 0.9999	0.6031	> 0.9999	0.9853	> 0.9999	0.9385	0.2874	0.9768	> 0.9999	0.7823
Cerebral cortex	**Slice 2**	0.9847	0.4637	0.9905	0.2241	0.1958	0.2342	> 0.9999	0.9083	0.3208	0.9521	0.3689	0.9978
	Slice 3	0.9471	> 0.9999	0.9120	> 0.9999	0.8761	> 0.9999	0.9986	> 0.9999	0.9967	> 0.9999	> 0.9999	> 0.9999
	Slice 4	> 0.9999	0.9930	> 0.9999	0.6675	> 0.9999	0.7230	> 0.9999	0.5256	> 0.9999	0.5697	> 0.9999	0.9980
	Slice 5	0.9977	0.7052	0.8770	0.8456	0.9778	0.9008	0.7980	0.9975	0.9363	0.3368	0.9807	0.4967
	Slice 6	> 0.9999	0.8764	> 0.9999	0.6031	> 0.9999	0.9853	> 0.9999	0.9385	0.2874	0.9768	> 0.9999	0.7823
Hippocampus	**Slice 2**	0.8213	0.1516	0.8211	0.0128	0.1264	0.1723	0.9999	0.3807	0.4317	0.9998	0.5298	0.3450
	Slice 3	0.9044	> 0.9999	0.8972	> 0.9999	0.9880	> 0.9999	0.9999	> 0.9999	0.9838	> 0.9999	0.9776	> 0.9999
Thalamus	**Slice 3**	0.3871	0.9988	0.7742	0.6264	0.7691	0.9020	0.9365	0.7044	0.8980	0.9486	> 0.9999	0.9326
	Slice 4	0.8383	> 0.9999	> 0.9999	0.2027	0.9998	> 0.9999	0.8865	0.0943	0.8010	0.6831	0.9994	> 0.9999
Corpus callosum	**Slice 3**	> 0.9999	0.8494	> 0.9999	0.8583	> 0.9999	0.9770	> 0.9999	0.4503	> 0.9999	0.6338	> 0.9999	0.9745
	Slice 4	0.9340	0.9998	0.3455	0.5798	> 0.9999	0.7204	0.6353	0.5410	0.9357	0.6788	0.3478	0.9877
	Slice 5	0.8886	0.4358	0.9972	0.9448	0.9979	0.9300	0.8255	0.8058	0.9478	0.1931	0.9831	0.6941
Subventricular area	**Slice 4**	> 0.9999	> 0.9999	> 0.9999	> 0.9999	> 0.9999	> 0.9999	> 0.9999	> 0.9999	0.9239	> 0.9999	> 0.9999	> 0.9999
	Slice 5	0.9536	0.9858	0.7364	0.9985	0.9352	0.9974	0.4659	0.9986	0.6977	0.9987	0.9597	> 0.9999

Table S5: *List of statistically adjusted p-values from 1H-spectroscopy.*

Statistically adjusted p-values are derived from molecules of interest comparing the different vehicle-treated control groups (WT (CLQ) and Tg (ClQ)) and DET-treated groups (WT (CLQ+DET) and Tg (CLQ+DET)) using 1H-spectroscopy data (refer to Figure 22). This analysis presents the adjusted p-values from metabolites (inositol, N-acetyl aspartate, taurine, NAA + NAAG and Glu + Gln), as well as macromolecules (MM09) and lipids (Lip09, GPC + PCh) identified through 1H-spectroscopy imaging. Results are considered significant if $p < 0.05$ ($* p < 0.05$).

Molecules of interest		Adjusted p-values from different groups					
		WT (CLQ) vs. WT (CLQ+DET)	**WT (CLQ) vs. TG (CLQ)**	**WT (CLQ) vs. TG (CLQ+DET)**	**WT (CLQ+DET) vs. TG (CLQ)**	**WT (CLQ+DET) vs. TG (CLQ+DET)**	**TG (CLQ) vs. TG (CLQ+DET)**
Metabolites	Inositol	0.9782	0.9783	0.5836	> 0.9999	0.3731	0.4208
	N-acetyl aspartate	0.9997	0.8090	0.9657	0.8486	0.9441	0.5697
	Taurine	> 0.9999	0.9371	0.8837	0.9440	0.8941	0.9996
	NAA + NAAG	0.9994	0.8601	0.9428	0.9044	0.9046	0.5818
	Glu + Gln	0.9987	0.9562	0.9919	0.9147	0.9992	0.8687
Macromolecules and lipids	MM09 + Lip09	0.9274	0.9623	0.9668	0.7299	0.9987	0.8043
	GPC + PCh	0.9997	0.8463	0.8342	0.8068	0.7902	> 0.9999

4. The impact of Aβ species on synaptic plasticity and lipid profiling: insights from *in vitro* physiological models

To broaden our research spectrum of $A\beta_{(1-40)}$ and $A\beta_{(1-42)}$ species, we conducted research to see the pathological effect of these Aβ species on an *in vitro* physiological model. We studied the synaptic loss and lipid alterations in neural cell types. Therefore, we used primary neurones and glial cultures to investigate the cellular responses to these Aβ species. Furthermore, we investigated the impact of the short and long influence of $A\beta_{(1-40)}$ and $A\beta_{(1-42)}$ species on synaptic loss and lipid alterations in these neural cell types. It reveals that these Aβ species might have a novel function in regulating the distribution of lipids in neural cell types. Also, it showed that synaptic dysregulation is a later pathological effect of AD.

This chapter's content is identical to the published article (Van Bulck et al., 2022). Although the lipid data from conditioned media of hippocampal neurones and glial cultures are unpublished, they are included in this chapter to give a comprehensive overview of the lipid profiling of both neuronal brain cells and their extracellular environment after Aβ species treatment.

Article:

Aβ-induced alterations in membrane lipids occur before synaptic loss appears

Michiel Van Bulck (M.V.B.), Nicola Brandt (N.B.), Ralf A. Claus (R.A.C.), Markus Gräler (M.G.), and Anja U. Bräuer (A.U.B.)

Published in: International Journal of Molecular Sciences (2022), 23 (4) 2300 (https://doi.org/10.3390/ijms23042300)

Contributions:

Conceptualization, A.U.B.; Data curation, M.V.B., R.A.C. and M.G.; Formal analysis, M.V.B., N.B., R.A.C. and M.G.; Investigation, A.U.B.; Methodology, M.V.B., N.B., R.A.C. and M.G.; Supervision, A.U.B.; Validation, N.B.; Visualization, M.V.B.; Writing—original draft, M.V.B. and A.U.B.; Writing—review & editing, M.V.B., N.B., R.A.C. and M.G. All authors have read and agreed to the published version of the manuscript.

Additional data:

Lipid profiles in conditioned media were implemented in this chapter of the dissertation. Data collection has been performed by R.A.C. and M.G. Further data quantification was performed by M.V.B.

Hereby, I confirm that Michiel Van Bulck contributed to the investigation as stated above.

(Place, Date) (Prof. Dr. Anja U. Bräuer)

Oldenburg, 27.06.2025 Prof. Dr. Anja Bräuer

Aβ-Induced Alterations in Membrane Lipids Occur before Synaptic Loss Appears

Michiel Van Bulck[1,2,*], Nicola Brandt[1], Ralf A. Claus[3], Markus Gräler[3,4] and Anja U. Bräuer[1,5,*]

[1] Research Group Anatomy, School for Medicine and Health Science, Carl von Ossietzky University Oldenburg, 26129 Oldenburg, Germany; nicola.brandt@uni-oldenburg.de

[2] Department of Experimental Models of Human Disease, Networked Center of Biomedical Research on Neurodegenerative Diseases (CIBERNED), Institute for Biomedical Research A. Sols (CSIC-UAM), 28029 Madrid, Spain

[3] Department of Anaesthesiology and Intensive Care Medicine Center for Molecular Biomedicine (CMB), Jena University Hospital, 07745 Jena, Germany; ralf.claus@med.uni-jena.de (R.A.C.); markus.graeler@med.uni-jena.de (M.G.)

[4] Centre for Sepsis Control and Care (CSCC), Jena University Hospital, 07745 Jena, Germany

[5] Research Centre for Neurosensory Science, Carl von Ossietzky University Oldenburg, 26129 Oldenburg, Germany

* Correspondence: michiel.van.bulck@uni-oldenburg.de (M.V.B.); anja.braeuer@uni-oldenburg.de (A.U.B.)

Abstract: Loss of active synapses and alterations in membrane lipids are crucial events in physiological ageing as well as in neurodegenerative disorders. Both are related to the abnormal aggregation of amyloid-beta (Aβ) species, generally known as amyloidosis. There are two major known human Aβ species: $A\beta_{(1–40)}$ and $A\beta_{(1–42)}$. However, which of these species have more influence on active synapses and membrane lipids is still poorly understood. Additionally, the time-dependent effect of Aβ species on alterations in membrane lipids of hippocampal neurones and glial cells remains unknown. Therefore, our study contributes to a better understanding of the role of Aβ species in the loss of active synapses and the dysregulation of membrane lipids *in vitro*. We showed that $A\beta_{(1–40)}$ or $A\beta_{(1–42)}$ treatment influences membrane lipids before synaptic loss appears and that the loss of active synapses is not dependent on the Aβ species. Our lipidomic data analysis showed early changes in specific lipid classes such as sphingolipid and glycerophospholipid neurones. Our results underscore the potential role of lipids as a possible early diagnostic biomarker in amyloidosis-related disorders.

Keywords: neurones; glia cells; synapses; Aβ species; membrane lipids; Alzheimer's disease; cell-communication

4.1. Introduction

Amyloidosis is used as an umbrella term for rare, serious diseases caused by the deposit of misfolded proteins. In brain tissue, it is characterised by the accumulation of amyloid-beta (Aβ), such as occurs in Alzheimer's disease (AD) (Brothers et al., 2018). Aβ species are products of a proteolytic cleavage, generated from amyloid precursor protein (APP) by α- or β-secretase and γ-secretase activity, and their characteristics have been extensively reviewed (Brothers et al., 2018; Kumar et al., 2015; Pearson & Peers, 2006). However, the presumed neurotoxic effects of the major Aβ species, $A\beta_{(1–40)}$ and $A\beta_{(1–42)}$, under pathological and physiological conditions remain unclear. So far, the molecular and cellular mechanism of Aβ species and their impact on the loss of synaptic sites, as well as on the changes of membrane lipids of brain cells, is poorly understood.

APP has been shown to play a pivotal role in synaptic and neural plasticity (Sosa et al., 2017). *In vitro* and *in vivo* studies have demonstrated that soluble Aβ species accumulate at the synaptic sites, resulting in disrupted synaptic plasticity and long-term potential (Lacor et al., 2004; Takahashi et al., 2002; Walsh et al., 2002; Walsh & Selkoe, 2004). However, $A\beta_{(1–42)}$ is thought to be more aggregation-prone compared to $A\beta_{(1–40)}$. The aggregation status of Aβ species in senile plaques in AD is strongly regulated by time and their aggregation affinity (Gouras et al., 2000; Thal et al., 2000b). Therefore, as has been demonstrated in vitro and *in vivo*, Aβ species have different influences on the pre- and postsynaptic densities dependent on the Aβ concentrations, the chemical structure of Aβ (α-helices or β-sheets), the time of Aβ treatment, and the Aβ aggregation status (Almeida et al., 2005; Chen et al., 2017; Gouras et al., 2015; Hayashi et al., 2009; Heras-Sandoval et al., 2012; Hu et al., 2009; Klementieva et al., 2017; Novo et al., 2018; Pearson & Peers, 2006; Sokolow et al., 2012; Takahashi et al., 2003; Takahashi et al., 2004). Previously, it was also shown that glial cells are involved in Aβ-induced inflammatory responses and play an important role in Aβ clearance and degradation (Ries & Sastre, 2016). In addition, glial activation itself could play a protective role against Aβ-induced toxicity on neurones (Ries & Sastre, 2016).

APP and the cleavage products $A\beta_{(1–40)}$ and $A\beta_{(1–42)}$ have different influences on lipid homeostasis (Grimm et al., 2005). Major molecular targets for Aβ in the cholesterol and sphingolipid metabolic pathways are 3-Hydroxy-3-methylglutaryl-coenzyme A (HMG-CoA) reductase and sphingomyelinases (nSMase) (Grimm et al., 2005). $A\beta_{(1–42)}$ activates nSMase, whereas $A\beta_{(1–40)}$ suppresses the activity of HMG-CoA reductase, resulting in decreased cholesterol levels. Sphingomyelins (SM) reduce γ-secretase activity, thus

reducing Aβ levels; cholesterol, on the contrary, induces γ-secretase activity and is responsible for elevated Aβ levels (Grimm et al., 2005; He et al., 2010). Inhibition of HMG-CoA reductase is responsible for a reduction of intracellular as well as extracellular $Aβ_{(1–40)}$ and $Aβ_{(1–42)}$ peptides, resulting in elevated levels of cholesterol (Kim et al., 2016). Sphingosine-1-phosphate (So1P) has been shown to be protective for neuronal cells, whereas ceramide promotes Aβ biogenesis by influencing the β-secretase of APP (Puglielli et al., 2003). Ceramides also interfere in the control of many cellular processes, influencing, e.g., Aβ aggregation in physiological and pathological ageing processes (Venkateswaran et al., 2000). Phosphatidylcholines can alter the $Aβ_{(1–40)}$ mediated aggregation, depending on the thickness of the lipid membrane (Korshavn et al., 2017). Charged phospholipid bilayers consisting of phosphatidylcholines and phosphoglycerol showed an increase in $Aβ_{(1–40)}$ fibril formation (Niu et al., 2014).

In this study, we investigated the direct effect and time-dependent influence of two major human Aβ species on primary hippocampal neurones and on glial cells. Hence, we examined whether the loss of active synapses in primary hippocampal neurones is Aβ-species- and time-dependent *in vitro*.

Our results show for the first time a detailed lipid profiling in two different types of brain cells, primary hippocampal neurones and glial cells, after 3 h (3 h) and 12 h (12 h) of $Aβ_{(1–40)}$ and $Aβ_{(1–42)}$ treatment. We established that both Aβ species cause changes in the membrane lipids of primary hippocampal neurones and glial cells after 3 h and 12 h of treatment. Interestingly, Aβ-induced alterations in membrane lipids occurred prior to the loss of active synapses.

4.2. Synaptic loss after $Aβ_{(1–40)}$ and $Aβ_{(1–42)}$ treatment

To examine whether Aβ species have a preferential early or late effect on the loss of active synapses, primary hippocampal neurones at 12 DIV were treated with (1 µM) $Aβ_{(1–40)}$ or (1 µM) $Aβ_{(1–42)}$ for 3 h and 12 h. Active synapses were analysed by colocalisation of fluorescent markers recognising vesicular glutamate transport 1 (Vglut-1) and postsynaptic density protein-95 (PSD-95) (Figure 24 A–C). We quantified three ROI (47 $µm^2$) on the dendritic tree of the hippocampal neurones by examining the colocalisation dots (Figure 24 A, white boxes) of a pre- and postsynaptic marker. No significant effect on active synapses was observed after 3 h treatment between our control groups (CTRL and DMSO) compared to Aβ-treated groups ($Aβ_{(1–40)}$ and $Aβ_{(1–42)}$). After 12 h, however, Aβ-treated groups showed a

significant reduction in active synapses as compared to the control groups (Figure 24 A and Table 3). Both 3 h and 12 h DMSO treatments showed a small decrease in active synapses compared to the CTRL, but this was not significant (Figure 24 B-C and Table 3). We observed no significant difference after 3 h and 12 h treatment between $A\beta_{(1–40)}$ and $A\beta_{(1–42)}$ treatments (Figure 24 B-C and Table 3). However, 3 h $A\beta_{(1–40)}$ and $A\beta_{(1–42)}$ treatment showed a slight decrease in active synapse numbers as compared to our control groups, but this was not significant (Figure 24 B-C and Table 3).

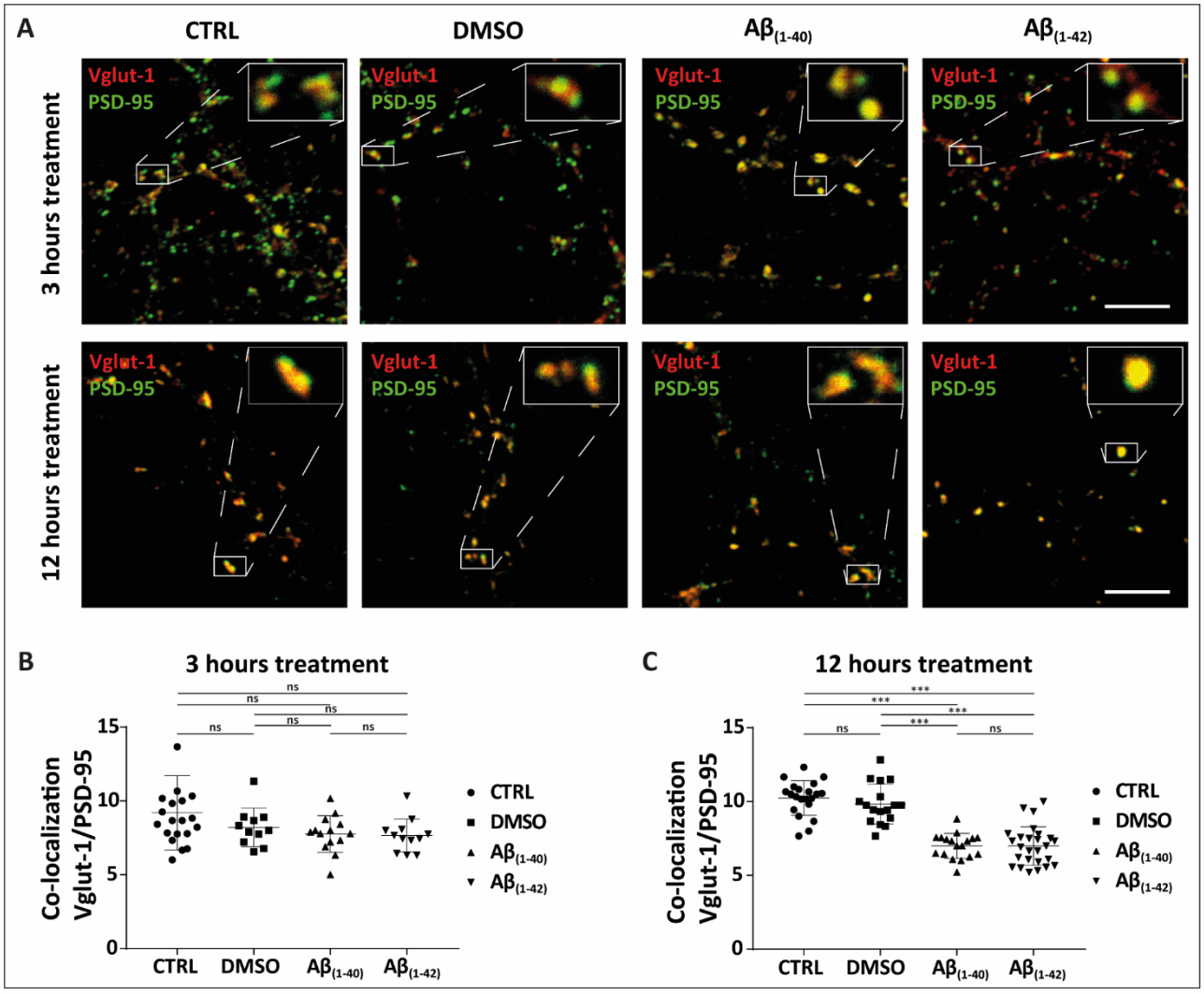

Figure 24: *Synaptic loss of active synapses of Aβ accumulation in hippocampal neurones.*
*(**A**–**C**) The synaptic study showed the colocalisation of presynaptic (Vglut-1) and postsynaptic (PSD-95) markers, which was defined as active synapses, in hippocampal neurones at DIV12 for both control groups (CTRL and DMSO) and Aβ-treated groups ((1 μM) $A\beta_{(1–40)}$ and (1 μM) $A\beta_{(1–42)}$) at different time points (3 h and 12 h) of treatment (all groups from four independent cultures (N = 4)). In the 3 h treatment, the following average number of neurones was counted in each group: CTRL (n = 12), DMSO (n = 9), $A\beta_{(1–40)}$ (n = 11) and $A\beta_{(1–42)}$ (n = 9). In the 12 h treatment, the following average number of neurones was counted in each group: CTRL (n = 14), DMSO (n = 13), $A\beta_{(1–40)}$ (n = 13), and $A\beta_{(1–42)}$ (n = 17). For both 3 h and 12 h treatments, 3 ROI from each neurone was counted. (**A**) Representative confocal images of control groups and Aβ-treated groups*

*of hippocampal neurones stained for both presynaptic (Vglut-1) and postsynaptic markers (PSD-95) are shown. There was a reduction in active synapses after 12 h of Aβ(1–40)- and Aβ(1–42)-treated neurones compared to control groups. White boxes show enlargements of an example of defined active synapses for both control groups and Aβ-treated groups (3 h and 12 h). (**B**-**C**) Quantification of active synapses from control- and Aβ-treated groups of hippocampal neurones. (**B**) No significant effect on active synapses was seen in Aβ-treated groups after 3 h (3 ROI of average counted cells; n = 10, from four independent cultures (n = 4)). (**C**) A significant reduction of active synapses was observed after 12 h of Aβ(1–40)- and Aβ(1–42)-treated neurones compared to control groups. No significance (ns) was seen between CTRL and DMSO, nor between Aβ(1–40)- and Aβ(1–42)-treated neurones (3 ROI of average counted cells; n = 14, from four independent cultures (n = 4)). *** p < 0.0001; scale bars represent 5 µm. The size of the ROI was 47 µm².*

***Table 3:** List of the statistically adjusted p-value (from Figure 24 B-C) between separate groups (CTRL, DMSO, Aβ(1–40) and Aβ(1–42)) after 3 h and 12 h of treatment conditions. A Kruskal–Wallis test was performed, followed by a Dunn's multiple comparison test.*

	3 h Treatment	**12 h Treatment**
Kruskal-Wallis test	0.0732	<0.0001
Dunn's multiple comparison test	*adjusted p-value*	*adjusted p-value*
CTRL vs DMSO	>0.9999	0.6106
CTRL vs Aβ(1-40)	0.3017	<0.0001
CTRL vs Aβ(1-42)	0.0867	<0.0001
DMSO vs Aβ(1-40)	>0.9999	<0.0001
DMSO vs Aβ(1-42)	>0.9999	<0.0001
Aβ(1-40) vs Aβ(1-42)	>0.9999	>0.9999

4.3. Alterations in cellular lipids of hippocampal neurones and glial cells after Aβ(1–40) and Aβ(1–42) treatment

4.3.1. Disruption in cellular lipids of hippocampal neurones and glial cells after Aβ(1–40) and Aβ(1–42) treatment using high-performance thin-layer chromatography (HPTLC)

Hippocampal neurones at 12 DIV and glial cells were treated with Aβ(1–40) and Aβ(1–42) for 3 h and 12 h to test whether Aβ species influence cellular lipids, whether that has a preference for a specific class of lipids, and to examine whether Aβ(1–40) and Aβ(1–42) have early effects on the lipid changes in these cells. Two different sets of analyses were performed: HPTLC and tandem MS. Lipids of hippocampal neurones and glial cells were extracted equally from our control groups (CTRL and DMSO) and Aβ-treated groups (Aβ(1–40) and Aβ(1–42)) after 3 h and 12 h of treatment. TopFluor lysophosphatidic acid (LPA) was used as the internal standard, to see whether the same amounts of lipids were extracted from each sample of control- and Aβ-treated groups (Figure S10 A-D). To analyse which different lipid classes (e.g., sphingolipids and glycerophospholipids) were dysregulated, we showed HPTLC-

derivatised copper (II)-sulphate images and their corresponding scanning profiles for hippocampal neurones and glial cells treated with $A\beta_{(1–40)}$ and $A\beta_{(1–42)}$ for 3 h and 12 h (Figure S11 A–D). These images and profiles revealed changes in different lipid classes (e.g., sphingolipids and glycerophospholipids), which were in accordance with the external standards used (Figure S11, purple arrows and boxes). Each numbered purple arrow and box refers to external standards that could be detected from hippocampal neurones and glial cells after 3 h and 12 h of $A\beta_{(1–40)}$ and $A\beta_{(1–42)}$ treatment. The copper (II)-sulphate scanning profiles are shown to facilitate examination of the changes between control groups and Aβ-treated groups. The represented retention factor (Rf, Table S6) and arbitrary unit (AU, Table S6) are both based on the peak's end in the copper (II)-sulphate scanning profiles. These show the changes in band intensity of the HPTLC copper (II)-sulphate images and correspond to the numbered labelled purple arrows and boxes (Figure S11). Our data showed small changes in sphingolipids and glycerophospholipids after 3 h $A\beta_{(1–40)}$ and $A\beta_{(1–42)}$ treatment for both neurones (Figure S11 A) and glial cells (Figure S11 C), and large changes after 12 h of $A\beta_{(1–40)}$ and $A\beta_{(1–42)}$ treatment (Figure S11 B,D).

4.3.2. Specific identification of various lipid isoforms after $A\beta_{(1–40)}$ and $A\beta_{(1–42)}$ treatment from hippocampal neurones and glial cells using tandem mass spectrometry analysis

To corroborate whether $A\beta_{(1–40)}$ and $A\beta_{(1–42)}$ preferentially influence specific sphingolipid or glycerophospholipids isoforms, we treated hippocampal neurones at DIV 12 and glial cells for 3 h and 12 h with $A\beta_{(1–40)}$ and $A\beta_{(1–42)}$ and subsequently analysed them by tandem MS. Here, the characterisation of altered lipid isoforms for hippocampal neurones and glial cells after 3 h and 12 h $A\beta_{(1–40)}$ and $A\beta_{(1–42)}$ treatment are shown, focussing on sphingolipids such as ceramides (Cer), dihydroceramides (DHCer), lactosylceramides (LacCer), monohexosylceramides (HexCer), sphingosine (So), sphinganine (Sa), sphingosine-1-phosphate (Sa1P), sphinganine-1-phosphate (So1P), sphingosylphosphorylcholine (SPC), sphingomylines (SM), dihydrosphingomylines (DHSM), and glycerophospholipids such as phosphatidylcholine (PC), lysophosphatidylcholine (LPC), lysophosphatidylethanolamine (LPE), lysophosphatidylglycerol (LPG), lysophosphatidylserine (LPS), Lyso-platelet-activating factor (Lyso-PAF) (Figure 25, Figure 26 and Figure 27). All results are presented as a $\log_{10}$ transformation and were performed in triplicate. Furthermore, ratios between the Aβ-treated groups and our negative control (DMSO) were calculated, setting the negative control (DMSO) to 0. After taking the ratios, the Z-score was taken for the total data set. Changes in lipid isoforms are shown as tendencies. This means that the red colours refer to

an increase of lipid quantities and the green colour indicates a reduction compared to our negative control (DMSO) which was set to 0 as baseline parameter (Figure 25, Figure 26 and Figure 27).

4.3.2.1. Ceramides (Cer)

Both hippocampal neurones and glial cells showed alterations in Cer isoforms after 3 h and 12 h $A\beta_{(1–40)}$ and $A\beta_{(1–42)}$ treatment (Figure 25). Neurones showed a reduction in C14 Cer after 3 h $A\beta_{(1–40)}$ treatment. An increase of C14 Cer was observed after 3 h and 12 h of $A\beta_{(1–40)}$ and $A\beta_{(1–42)}$ treatment. Other ceramide isoforms (C16 Cer, C18:0 Cer, C20 Cer, C22 Cer, C24:1 Cer) showed an increase in 3 h $A\beta_{(1–40)}$-and 12 h $A\beta_{(1–42)}$-treated neurons. Aβ-treated glial cells showed a strong increase after 3 h $A\beta_{(1–40)}$ and $A\beta_{(1–42)}$ treatment for C14 Cer. After 12 h, $A\beta_{(1–42)}$-treated glial cells showed a strong reduction compared to $A\beta_{(1–40)}$ for C14 Cer. A weak reduction in C18:1 Cer for 3 h $A\beta_{(1–42)}$ and 12 h $A\beta_{(1–40)}$ (Figure 25) was also observed. Other ceramide isoforms (C16 Cer, C18:0 Cer, C20 Cer, C22 Cer, C24:1 Cer) showed a weak increase after 12 h $A\beta_{(1–42)}$-treatment on glial cells. An increase was observed in C24 Cer after 3 h $A\beta_{(1–40)}$ as well as after 3 h and 12 h $A\beta_{(1–42)}$ in treated neurones. No changes were observed in C24 Cer of $A\beta_{(1–40)}$- and $A\beta_{(1–42)}$-treated glial cells (Figure 25).

4.3.2.2. Dihydroceramides (DHCer)

In $A\beta_{(1–42)}$-treated glial cells, C14 DHCer, C16 DHCer, and C18:0 DHCer decreased after 3 h and increased after 12 h treatment. However, in glial cells, C14 DHCer and C18:0 DHCer were increased after 3 h of $A\beta_{(1–40)}$ treatment. After 3 h $A\beta_{(1–40)}$- and $A\beta_{(1–42)}$- treatment on glial cells, a reduction in C20 DHCer and an increase in C22 DHCer was observed. After 12 h, there was a decrease in $A\beta_{(1–40)}$- and a slight increase in $A\beta_{(1–42)}$- treated glial cells. C24:1 DHCer showed a weak reduction after 3 h $A\beta_{(1–40)}$ and $A\beta_{(1–42)}$ treatment as well as an increase after 12 h $A\beta_{(1–42)}$ treatment in glial cells. After 3 h and 12 h Aβ treatment, glial cells showed a decrease in C24 DHCer (Figure 25). $A\beta_{(1–40)}$- and $A\beta_{(1–42)}$-treated hippocampal neurones showed a specific decrease in C20 DHCer after 3 h, and no changes after 12 h $A\beta_{(1–40)}$ and $A\beta_{(1–42)}$ treatment. C22 DHCer showed a decrease in 3 h $A\beta_{(1–40)}$- and 12 h $A\beta_{(1–42)}$-treated hippocampal neurones. An increase in C22 DHCer was seen in 3 h $A\beta_{(1–42)}$- and 12 h $A\beta_{(1–40)}$-treated hippocampal neurones (Figure 25). Other dihydroceramide isoforms (C14 DHCer, C16 DHCer, C24:1 DHCer, C24 DHCer) showed a weak increase in 3 h $A\beta_{(1–40)}$-treated neurons. However, 3 h $A\beta_{(1–42)}$ treatment showed a reduction in C14 DHCer, C16 DHCer, C24:1 DHCer, and increase in C24 DHCer (Figure 25).

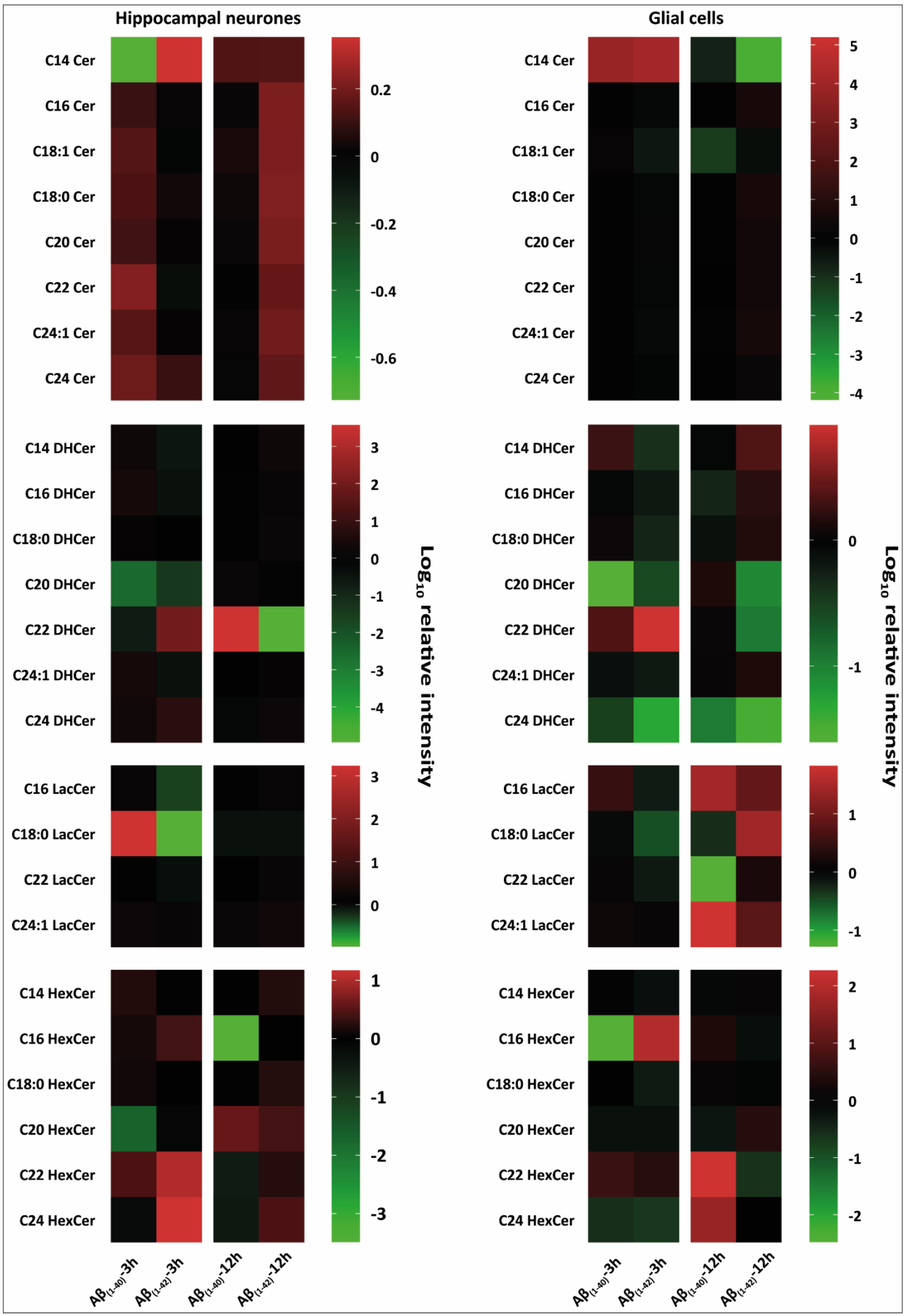
Hippocampal neurones
Glial cells
C14 Cer
C16 Cer
C18:1 Cer
C18:0 Cer
C20 Cer
C22 Cer
C24:1 Cer
C24 Cer
C14 DHCer
C16 DHCer
C18:0 DHCer
C20 DHCer
C22 DHCer
C24:1 DHCer
C24 DHCer
C16 LacCer
C18:0 LacCer
C22 LacCer
C24:1 LacCer
C14 HexCer
C16 HexCer
C18:0 HexCer
C20 HexCer
C22 HexCer
C24 HexCer
Log10 relative intensity
Aβ(1-40)-3h
Aβ(1-42)-3h
Aβ(1-40)-12h
Aβ(1-42)-12h

Figure 25: *Heat-map-based mass spectrometry analysis of sphingolipid classes from hippocampal neurones and glial cells after 3 h and 12 h Aβ treatment.*
Here, we examined different sphingolipid isoforms: ceramides (Cer), dihydroceramides (DHCer), lactosylceramides (LacCer), and monohexosylceramides (HexCer) after 3 h and 12 h treatment with (1 µM) $Aβ_{(1–40)}$ and (1 µM) $Aβ_{(1–42)}$ of hippocampal neurons at DIV 12 and glial cells (all groups, from three independent experiments (N = 3)). Changes of these lipid classes are shown as logarithmic (log_{10}) relative intensity (arbitrary unit); the green colour refers to a reduction, and the red colour refers to an increase of lipid levels compared to our negative control (DMSO), which was set to 0 as baseline. Both hippocampal neurones and glial cells showed an increased and reduced intensity of Cer, DHCer, LacCer, and HexCer isoforms after both 3 h and 12 h $Aβ_{(1–40)}$ and $Aβ_{(1–42)}$ treatment. Different changes in the lipid classes are shown between treated hippocampal neurones and glial cells. Aβ-treated hippocampal neurones showed prominent increases and decreases in Cer, LacCer and HexCer isoforms after 3 h and 12 h of $Aβ_{(1–40)}$ and $Aβ_{(1–42)}$ treatment. There was both a prominent intensity increase and a decrease of DHCer isoforms after 3 h and 12 h of $Aβ_{(1–40)}$ and $Aβ_{(1–42)}$ treatment. Glial cells showed prominent lipid changes of Cer, DHCer, LacCer, and HexCer isoforms after 3 h and 12 h of $Aβ_{(1–40)}$ or $Aβ_{(1–42)}$ treatment.

4.3.2.3. Lactosylceramides (LacCer)

Glial cells treated with $Aβ_{(1–40)}$ and $Aβ_{(1–42)}$ showed a reduction in all LacCer isoforms after 12 h. In 3 h $Aβ_{(1–42)}$-and 12 h $Aβ_{(1–40)}$-treated glial cells, decreases in C18:0 LacCer and C22 LacCer and an increase after 12 h $Aβ_{(1–42)}$ treatment were seen. In C16 LacCer and C24:1 LacCer an increase after 12 h $Aβ_{(1–40)}$ and $Aβ_{(1–42)}$ treatment on glial cells was seen. A reduction was observed in C16 LacCer after 3 h $Aβ_{(1–40)}$ and a decrease after 3 h $Aβ_{(1–42)}$ treatment on glial cells. After 3 h, $Aβ_{(1–40)}$-treated hippocampal neurones showed an increase in C18:0 LacCer. A decrease in C16 LacCer and C18 LacCer was seen in 3 h $Aβ_{(1–42)}$-treated hippocampal neurons (Figure 25). A slight decrease was observed in C18:0 LacCer after 12 h $Aβ_{(1–40)}$ and $Aβ_{(1–42)}$-treatment on neurones as well as in C22 LacCer after 3 h $Aβ_{(1–42)}$ treatment (Figure 25).

4.3.2.4. Monohexosylceramides (HexCer)

After $Aβ_{(1–40)}$ treatment, C16 HexCer showed a strong reduction in 12 h-treated hippocampal neurones and in 3 h-treated glial cells, whereas 3 h $Aβ_{(1–42)}$-treated glial cells and 3 h $Aβ_{(1–40)}$- and $Aβ_{(1–42)}$-treated hippocampal neurones showed an increase (Figure 25). C22 HexCer and C24 HexCer showed strong increases after 12 h $Aβ_{(1–40)}$ and decreases in 12 h $Aβ_{(1–42)}$ for glial cells and a slight reduction in 12 h $Aβ_{(1–40)}$- and a strong increase in 12 h $Aβ_{(1–42)}$-treated hippocampal neurones. After 3 h of $Aβ_{(1–40)}$- and $Aβ_{(1–42)}$-treated hippocampal neurons and glial cells, a strong increase was seen in C22 HexCer. C24 HexCer showed an increase in 3 h $Aβ_{(1–40)}$- and $Aβ_{(1–42)}$-treated glial cells as well as in 3 h $Aβ_{(1–42)}$-treated hippocampal neurons. Slight increases were observed in C14 HexCer,

C18:0 HexCer, and C20 HexCer after 3 h $A\beta_{(1–40)}$ treatment on hippocampal neurones. However, C14 HexCer showed a weak increase after 3 h $A\beta_{(1–40)}$ and 12 h $A\beta_{(1–42)}$ treatment on hippocampal neurones. A slight reduction was seen in C14 DHCer after 3 h $A\beta_{(1–42)}$ and 12 h $A\beta_{(1–40)}$ treatment on glial cells. C18:0 HexCer showed an increase after 3 h $A\beta_{(1–40)}$ and 12 h $A\beta_{(1–42)}$ on hippocampal neurones. A slight decrease in C18:0 HexCer was observed after 3 h $A\beta_{(1–42)}$ treatment (Figure 25).

4.3.2.5. Sphingosine (So) and sphingosine-1-phosphate (So1P)

Hippocampal neurones and glial cells showed weak changes of d18:1 So after both 3 h and 12 h $A\beta_{(1–40)}$ and $A\beta_{(1–42)}$ treatments (Figure 26). There was a decrease in d18:1 So1P after 3 h $A\beta_{(1–42)}$ treatment in hippocampal neurones and an increase after 12 h $A\beta_{(1–42)}$ treatment in glial cells. A reduction in d18:1 So1P was also observed after 3 h and 12 h $A\beta_{(1–40)}$ treatment of hippocampal neurones (Figure 26). An increase in d18:1 So1P for both 3 h $A\beta_{(1–40)}$-treated glial cells and 12 h $A\beta_{(1–42)}$-treated hippocampal neurones was observed (Figure 26).

4.3.2.6. Sphinganine (Sa) and sphinganine-1-phosphate (Sa1P)

A prominent reduction was seen in d18:0 Sa for glial cells after 3 h and 12 h $A\beta_{(1–40)}$ and $A\beta_{(1–42)}$ treatment (Figure 26). In hippocampal neurones d18:0 Sa was slightly increased after 3 h $A\beta_{(1–40)}$ treatment and slightly reduced after 12 h $A\beta_{(1–42)}$ treatment. A reduction was also observed in d18:0 Sa1P after 3 h $A\beta_{(1–40)}$- and $A\beta_{(1–42)}$-treated hippocampal neurones, as well as 3 h and 12 h $A\beta_{(1–40)}$-treated glial cells. No strong reduction was observed in d18:0 Sa1P after 12 h $A\beta_{(1–40)}$ and $A\beta_{(1–42)}$ treatment of hippocampal neurones as well as in 3 h $A\beta_{(1–42)}$-treated glial cells (Figure 26).

4.3.2.7. Sphingosylphosphorylcholine (SPC)

Both, hippocampal neurones and glial cells showed alterations in SPC 16:0 after 3 h $A\beta_{(1–40)}$ and $A\beta_{(1–42)}$ treatment. The most prominent decrease in SPC 16:0 was shown after 3 h of $A\beta_{(1–40)}$ and $A\beta_{(1–42)}$ treatment for both hippocampal neurones and glial cells. A decrease was also observed after 12 h of $A\beta_{(1–42)}$ treatment for both hippocampal neurones and glial cells (Figure 26).

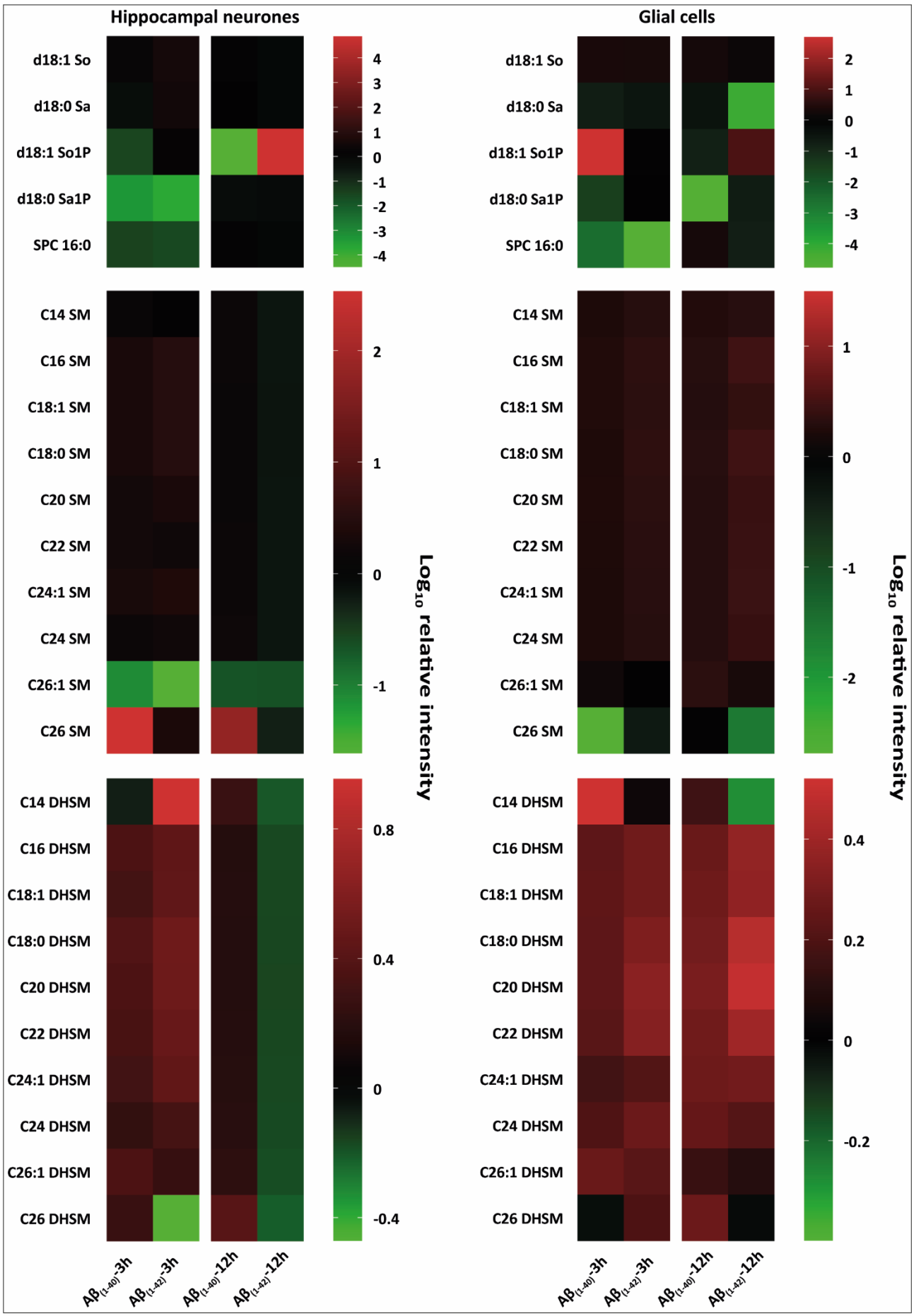
Hippocampal neurones
Glial cells
d18:1 So
d18:0 Sa
d18:1 So1P
d18:0 Sa1P
SPC 16:0
C14 SM
C16 SM
C18:1 SM
C18:0 SM
C20 SM
C22 SM
C24:1 SM
C24 SM
C26:1 SM
C26 SM
C14 DHSM
C16 DHSM
C18:1 DHSM
C18:0 DHSM
C20 DHSM
C22 DHSM
C24:1 DHSM
C24 DHSM
C26:1 DHSM
C26 DHSM
Aβ(1-40)-3h
Aβ(1-42)-3h
Aβ(1-40)-12h
Aβ(1-42)-12h
Log10 relative intensity

Figure 26: *Heat-map-based mass spectrometry analysis of sphingophospholipid classes from hippocampal neurones and glial cells after 3 h and 12 h Aβ treatment.*
Here, we examined different sphingophospholipid isoforms; sphingosine (d18:1 So), sphinganine (d18:0 Sa), sphingosine-1-phosphate (d18:1 So1P), sphinganine-1-phosphate (d18:1 Sa1P), sphingosylphosphoryl-choline (SPC (16:0)), sphingomyelines (SM) and dihydrosphingomyelines (DHSM) after 3 h and 12 h treatment with (1 µM) $Aβ_{(1–40)}$ and (1 µM) $Aβ_{(1–42)}$ hippocampal neurones at DIV 12 and glial cells (all groups, from three independent experiments (N = 3)). Changes of these lipid classes are shown as logarithmic (log_{10}) relative intensity (arbitrary unit); the green colour refers to a reduction and the red colour refers to an increase in lipid levels compared to our negative control (DMSO), which was set to 0 as baseline. Major intensity changes in lipid classes of d18:1 So, d18:0 Sa, d18:1 So1P, d18:1 Sa1P after 3 h and 12 h $Aβ_{(1–40)}$ and $Aβ_{(1–42)}$ treatment of hippocampal neurones and glial cells were observed. Specific lipid intensity changes after $Aβ_{(1–40)}$ and $Aβ_{(1–42)}$ treatment of hippocampal neurones of very long fatty acid SM compared to Aβ-treated glial cells were detected.

4.3.2.8. Sphingomyelines (SM)

All SM isoforms (C14 SM, C16 SM, C18:1 SM, C18:0 SM, C20 SM, C22 SM, C24:1 SM, C24 SM, C26:1 SM, and C26 SM) showed a slight increase after 3 h $Aβ_{(1–40)}$ and $Aβ_{(1–42)}$ treatment on hippocampal neurones, and glial cells after 3 h and 12 h $Aβ_{(1–40)}$ and $Aβ_{(1–42)}$ treatment (Figure 26). The most prominent reductions were observed in C26 SM for glial cells after 3 h $Aβ_{(1–40)}$ and 12 h $Aβ_{(1–42)}$ treatment and in C26:1 SM for hippocampal neurones after 3 h and 12 h $Aβ_{(1–40)}$ and $Aβ_{(1–42)}$ treatment. 3 h and 12 h $Aβ_{(1–40)}$-treated hippocampal neurones showed a strong increase in C26 SM (Figure 26).

4.3.2.9. Dihydrosphingomyelines (DHSM)

Almost all DHSM isoforms (C14 DHSM, C16 DHSM, C18:1 DHSM, C18:0 DHSM, C20 DHSM, C22 DHSM, C24:1 DHSM, C24 DHSM, C26:1 DHSM and C26 DHSM) showed an increase after 3 h $Aβ_{(1–40)}$ and $Aβ_{(1–42)}$ and 12 h $Aβ_{(1–40)}$ treatment, as well as a decrease after 12 h $Aβ_{(1–42)}$ treatment of hippocampal neurones. The most prominent reduction in DHSM for hippocampal neurones was observed after 3 h in C14 DHSM after $Aβ_{(1–40)}$ treatment and C26 DHSM after $Aβ_{(1–42)}$ treatment, and for all DHSM isoforms after 12 h $Aβ_{(1–42)}$ treatment (Figure 26). However, the most prominent increase in DHSM for hippocampal neurones was observed after 3 h in C14 DHSM after $Aβ_{(1–42)}$ treatment and C26 DHSM after $Aβ_{(1–40)}$ treatment, and for all DHSM isoforms after 12 h $Aβ_{(1–40)}$ treatment (Figure 26). Almost all DHSM isoforms (C14 DHSM, C16 DHSM, C18:1 DHSM, C18:0 DHSM, C20 DHSM, C22 DHSM, C24:1 DHSM, C24 DHSM, C26:1 DHSM, and C26 DHSM) from glial cells treated with Aβ were increased, whereas in glial cells, the most prominent increase are observed after 3 h $Aβ_{(1–40)}$ treatment for C14 DHSM and after 12 h $Aβ_{(1–42)}$ treatment for C18:0 DHSM,

C20 DHSM, and C22 DHSM. Additionally, glial cells showed a prominent decrease in C14 DHSM after 12 h $A\beta_{(1–42)}$ (Figure 26).

4.3.2.10. Phosphatidylcholines (PC) and lysophosphatidylcholines (LPC)

A prominent decrease in PC (38:0) in hippocampal neurones after 3 h $A\beta_{(1–40)}$ as well as 12 h $A\beta_{(1–40)}$ and $A\beta_{(1–42)}$ was observed, as well as a strong increase after 3 h $A\beta_{(1–42)}$ treatment. All other PC isoforms (PC (28:0), PC (30:0), PC (30:1), PC (32:0), PC (32:1), PC (34:1), PC (34:2), PC (36:1), PC (36:2), PC (36:2), PC (36:3), PC (38:0), PC (38:1), PC (38:2), PC (38:3), PC (38:4)) showed a decrease in 3 h $A\beta_{(1–40)}$- and 12 h $A\beta_{(1–40)}$-treated glial cells. Besides PC (28:0), a weak increase was observed after 12 h $A\beta_{(1–42)}$ treatment in glial cells. The following PC isoforms (PC (28:0), PC (30:1), PC (32:0), PC (32:1), PC (34:1), PC (36:1), PC (38:0), PC (38:1), PC (38:2), PC (38:3)) were reduced after 3 h $A\beta_{(1–40)}$ treatment of glial cells. Glial cells also showed a prominent increase in PC (36:0) after 3 h $A\beta_{(1–40)}$ and $A\beta_{(1–42)}$ treatment. No changes were observed in PC (38:0) after 12 h $A\beta_{(1–42)}$ treatment of glial cells. LPC (20:0) showed a strong increase after 3 h $A\beta_{(1–40)}$ treatment of hippocampal neurones and in 3 h $A\beta_{(1–42)}$- and 12 h $A\beta_{(1–40)}$-treated glial cells (Figure 27). A prominent decrease was observed in LPC (20:0) in 3 h $A\beta_{(1–40)}$ and 12 h $A\beta_{(1–42)}$ treated glial cells and a weak decrease in 12 h $A\beta_{(1–40)}$-treated hippocampal neurones (Figure 27).

4.3.2.11. Lysophosphatidylethanolamine (LPE)

A reduction in all LPE isoforms (LPE (16:0), LPE (16:1), LPE (18:0), LPE (18:1), LPE (18:2), and LPE (20:4)) was shown in 3 h $A\beta_{(1–40)}$- and $A\beta_{(1–42)}$-treated hippocampal neurones. A slight decrease in all LPE isoforms (LPE (16:0), LPE (16:1), LPE (18:0), LPE (18:1), LPE (18:2), and LPE (20:4)) was shown in 3 h $A\beta_{(1–42)}$-treated glial cells (Figure 27). An increase was observed in all LPE isoforms (LPE (16:0), LPE (16:1), LPE (18:0), LPE (18:1), LPE (18:2), and LPE (20:4)) in 12 h $A\beta_{(1–42)}$-treated glial cells (Figure 27). 12 h $A\beta_{(1–40)}$-treated hippocampal neurones showed an decrease in LPE (16:1), LPE (18:0), LPE (18:2), and LPE (20:4) as well as an increase in LPE (16:0), LPE (18:1) isoforms. An increase of LPE (16:0), LPE (18:1), and LPE (20:4)) was seen in 12 h $A\beta_{(1–42)}$-treated hippocampal neurones(Figure 27).

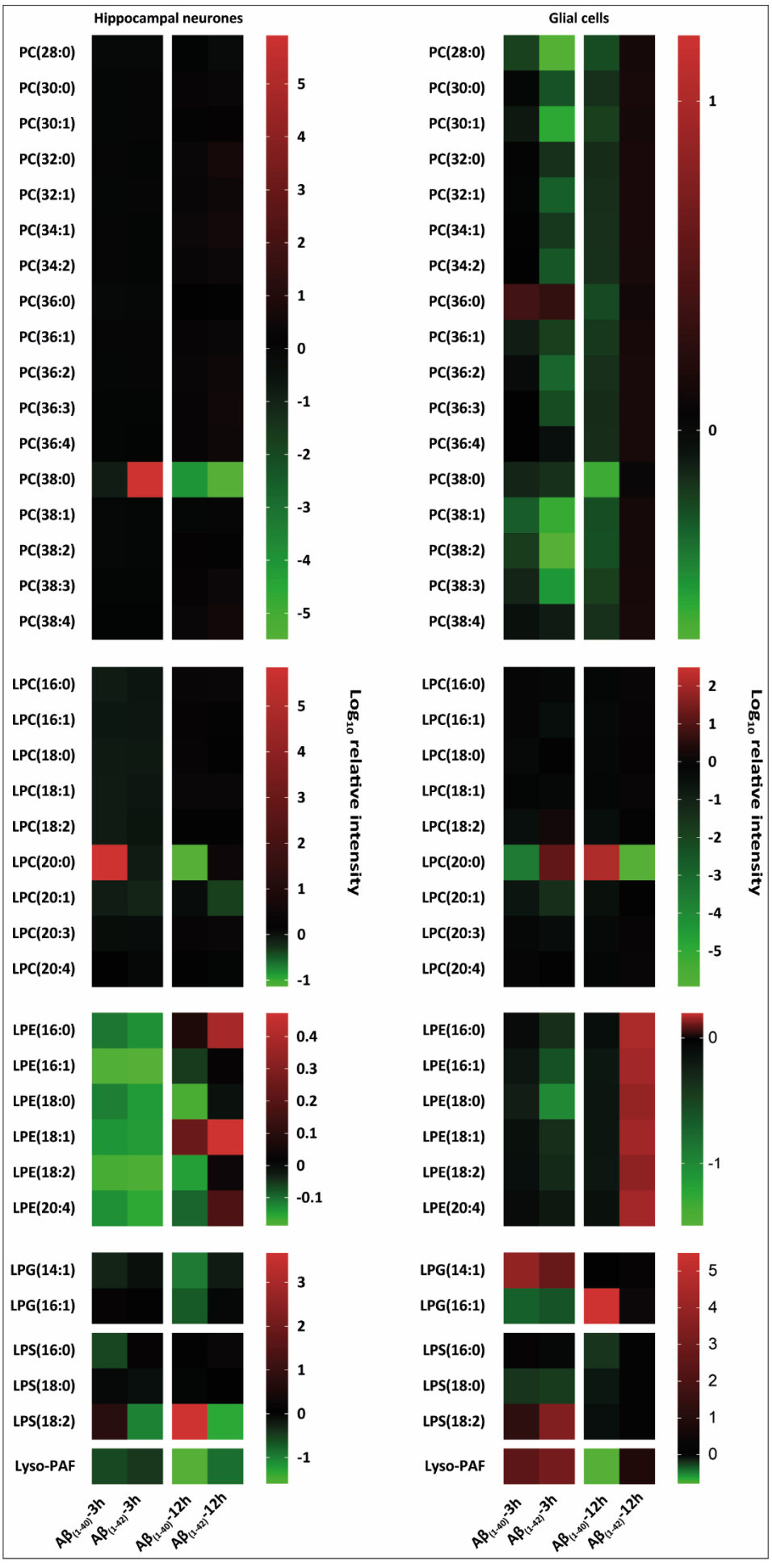
Hippocampal neurones
Glial cells
PC(28:0)
PC(30:0)
PC(30:1)
PC(32:0)
PC(32:1)
PC(34:1)
PC(34:2)
PC(36:0)
PC(36:1)
PC(36:2)
PC(36:3)
PC(36:4)
PC(38:0)
PC(38:1)
PC(38:2)
PC(38:3)
PC(38:4)
LPC(16:0)
LPC(16:1)
LPC(18:0)
LPC(18:1)
LPC(18:2)
LPC(20:0)
LPC(20:1)
LPC(20:3)
LPC(20:4)
LPE(16:0)
LPE(16:1)
LPE(18:0)
LPE(18:1)
LPE(18:2)
LPE(20:4)
LPG(14:1)
LPG(16:1)
LPS(16:0)
LPS(18:0)
LPS(18:2)
Lyso-PAF
Log10 relative intensity
Aβ(1-40)-3h
Aβ(1-42)-3h
Aβ(1-40)-12h
Aβ(1-42)-12h

Figure 27: *Heat map-based mass spectrometry analysis of glycerophospholipid classes from hippocampal neurones and glial cells after 3 h and 12 h Aβ treatment.*
Here, we examined different glycerophospholipids isoforms: phosphatidylcholine (PC), lysophosphatidylcholine (LPC), lysophosphatidylethanolamine (LPE), lysophosphatidylglycerol (LPG), lysophosphatidylserine (LPS), and lyso-platelet-activating factor (Lyso-PAF) after 3 h and 12 h treatment with (1 µM) $Aβ_{(1–40)}$ and (1 µM) $Aβ_{(1–42)}$ of hippocampal neurones at DIV 12 and glial cells (all groups, from three independent experiments (N = 3)). Changes in these lipid classes are shown as logarithmic (log_{10}) relative intensity (arbitrary unit); the green colour refers to a reduction and the red colour refers to an increase in lipid levels compared to our negative control (DMSO), which was set to 0 as baseline. Hippocampal neurones specifically showed PC (38:0) intensity changes after 3 h and 12 h $Aβ_{(1–40)}$ and $Aβ_{(1–42)}$ treatment compared to an overall reduction in PC for $Aβ_{(1–40)}$ and $Aβ_{(1–42)}$-treated glial cells. LPC, LPG, LPS, and Lyso-PAF showed specific changes after 3 h and 12 h $Aβ_{(1–40)}$ and $Aβ_{(1–42)}$ treatment in both hippocampal neurones and glial cells

4.3.2.12. Lysophosphatidylglycerol (LPG)

LPG (14:1) and LPG (16:1) showed a reduction in 12 h $Aβ_{(1–40)}$-treated hippocampal neurones. Glial cells showed a strong increase after 3 h $Aβ_{(1–40)}$ and $Aβ_{(1–42)}$ treatment in LPG (14:1) and after 12 h $Aβ_{(1–40)}$ treatment in LPG (16:1). In addition, LPG (16:1) showed a decrease after 3 h $Aβ_{(1–40)}$ and $Aβ_{(1–42)}$ treatment of glial cells (Figure 27).

4.3.2.13. Lysophosphatidylserine (LPS)

LPS (18:2) showed an increase in 3 h $Aβ_{(1–40)}$- and $Aβ_{(1–42)}$-treated glial cells as well as in 3 h and 12 h $Aβ_{(1–40)}$-treated hippocampal neurones. A reduction was observed in $Aβ_{(1–42)}$-treated hippocampal neurons after 3 h and 12 h (Figure 27). A decrease was observed in LPS (18:0) after 3 h $Aβ_{(1–40)}$- and $Aβ_{(1–42)}$-treated glial cells. LPS (16:0) was reduced in 3 h $Aβ_{(1–40)}$-treated hippocampal neurones, as well as in 12 h $Aβ_{(1–40)}$-treated glial cells (Figure 27).

4.3.2.14. Lyso-platelet-activating factor (Lyso-PAF)

Lyso-PAF showed a reduction in 12 h $Aβ_{(1–40)}$-treated glial cells, as well as in hippocampal neurones after 3 h and 12 h, for both $Aβ_{(1–40)}$ and $Aβ_{(1–42)}$ treatment. A prominent increase of lyso-PAF was observed in 3 h $Aβ_{(1–40)}$- and $Aβ_{(1–42)}$-treated glial cells (Figure 27).

4.4. Discussion

In this study, using different quantitative cellular techniques in different Aβ-treated primary brain cells, we showed for the first time that lipid profiles change after treatment and before synaptic loss was observed. We showed that human Aβ species exogenously applied to primary neurones and glial cells influence the numbers of active synapses and led to lipid alterations in a time-dependent manner. We also demonstrated that $Aβ_{(1–40)}$ and $Aβ_{(1–42)}$ treatment have a specific-species dependent influence on the integrity of cellular lipids in hippocampal neurones and glial cells.

4.4.1. $Aβ_{(1–40)}$ and $Aβ_{(1–42)}$ induces synaptic loss only after 12 h of treatment.

Synaptic dysfunctions due to Aβ accumulation are strongly associated with the cognitive disturbances of AD. The Aβ species $Aβ_{(1–40)}$ and $Aβ_{(1–42)}$ are the major forms of amyloid β peptides in the brain, whereby $Aβ_{(1–42)}$ seems to be more toxic than $Aβ_{(1–40)}$ (Bate & Williams, 2010; Fu et al., 2017; Willén et al., 2017). We found no selective influences of $Aβ_{(1–40)}$ or $Aβ_{(1–42)}$ on the loss of active synapses in cultured hippocampal neurones. Moreover, both Aβ species induced synaptic loss after a 12 h treatment, whereas a 3 h treatment did not show effects on synapses either with $Aβ_{(1–40)}$ or $Aβ_{(1–42)}$. Differences between these Aβ species on the synapse alterations are dependent on the concentration and aggregated forms of Aβ (Willén et al., 2017). Moreover, Fu et al. (2017) (Fu et al., 2017) showed that the $Aβ_{(1–42)}$ oligomers have a moderate but significantly higher level of neurotoxicity, whereas monomers have the weakest neurotoxic effect (~20%) on neuronal cells, without differences between $Aβ_{(1–40)}$ and $Aβ_{(1–42)}$. These results correspond to our findings on primary hippocampal neurones. $Aβ_{(1–40)}$ and $Aβ_{(1–42)}$ differently influence cellular lipids before synaptic loss appears.

Previous studies have shown changes in different lipid classes and a correlation to AD pathology. Although we do not fully understand the connection between AD and lipid metabolism, there is more and more evidence that lipids could be a useful blood biomarker in the diagnostics of AD, in addition to other risk factors (Agarwal & Khan, 2020; Ceccom et al., 2014). Nevertheless, it is poorly understood which lipid isoforms are dysregulated on a cellular level. We showed here that changes in lipid composition in hippocampal neurones and glial cells occur early, even before synaptic loss becomes evident, and independently of the Aβ species.

Our data indicate an increase of ceramides (especially C14 Cer) in glial cells and a reduction of these in hippocampal neurones. Both types of brain cells indicate an early reduction of

specific dihydroceramides (C20 DHCer and C22 DHCer). These different amounts of lipids caused by Aβ could be a result of activated apoptotic-survival pathways and inflammatory activity due to their response to oxidative stress (Jazvinšćak Jembrek et al., 2015).

Glycosylated ceramides exhibited a reduced (C16 HexCer; C20 HexCer) or an increased level (C16 HexCer, C22 HexCer, C24 HexCer, C16 LacCer, C18 LacCer, C24:1 LacCer) for either hippocampal neurones or glial cells. Sphingomyelin (C26 SM) was upregulated in hippocampal neurones and downregulated in glial cells. It has been suggested that $A\beta_{(1–40)}$, $A\beta_{(1–42)}$ and Aβ-islet amyloid polypeptide concentrations lead to nSMase-mediated induction of apoptosis, resulting in neuronal cell death and Aβ-induced oxidative stress. $A\beta_{(1–40)}$ and $A\beta_{(1–42)}$ species and their oligomeric isoforms modify ceramide levels, which could explain the elevated nSMase and reduced cellular sphingomyelin activity (Grimm et al., 2005; He et al., 2010; Malaplate-Armand et al., 2006; Qi et al., 2005; Zhang et al., 2009). In comparison with $A\beta_{(1–40)}$, it was shown that $A\beta_{(1–42)}$ directly activates nSMase by a γ-secretase-dependent mechanism, leading to increased ceramide levels (Michno et al., 2018).

Furthermore, we found an upregulation of d18:1 So1P in hippocampal neurones and glial cells after 3 h and 12 h treatment. An increase in So1P levels has been discussed in relation to Aβ-induced toxicity in hippocampal neurones and glial cells *in vitro* and *in vivo* (Czubowicz et al., 2015; Zhong et al., 2019). We also showed a reduction of SPC (16:0), Sa (d18:0 Sa), and Sa1P (d18:0 Sa1P) in hippocampal neurones and glial cells after $A\beta_{(1–40)}$ and $A\beta_{(1–42)}$ treatment. These reductions might be regulated by the increase of toxic Aβ species' aggregates by enhancing β-secretase mediated pathways and the anti-inflammatory response in neuronal cells (Park & Lee, 2019; Yi et al., 2011). Furthermore, after $A\beta_{(1–40)}$ and $A\beta_{(1–42)}$ treatment we showed an early increase in specific isoforms of phospholipids in hippocampal neurones and lyso-phospholipids in hippocampal neurones and glial cells. Additionally, we verified that Aβ-treated hippocampal neurones and glial cells showed a specific reduction in phospholipids (PC (38:0), LPC (20:0), all LPE, LPG, LPE (18:1), LPS (18:2) and Lyso-PAF) as well as a specific upregulation in phospholipids (PC (38:0), LPC (20:0), all LPE, LPG, LPE (18:1), LPS (18:2), and Lyso-PAF) after either 3 h or 12 h Aβ treatment. These glycerophospholipid alterations have been discussed in association with cytosolic phospholipase A2 hyperactivity in neuro-inflammatory responses and synapse-mediated Aβ toxicity (Moses et al., 2006; Sundaram et al., 2012).

In conclusion, we found that after $A\beta_{(1–40)}$ or $A\beta_{(1–42)}$ treatment, levels of specific sphingolipid and glycerophospholipid isoforms change before there is any detectable loss of active synapses. No significant differences were seen between the effects of $A\beta_{(1–40)}$ and $A\beta_{(1–42)}$ species in the loss of active synapses. Our data contributes to a better understanding of the cellular influences of Aβ species. It remains to be elucidated whether these influences of Aβ species on changes in membrane lipid profiles could be useful as an early diagnostic biomarker in amyloidosis-related disorders.

4.5. Materials and methods

4.5.1. Animals

For all experiments, timed-pregnant and postnatal mice were obtained from the central animal facility of the Carl von Ossietzky Universität Oldenburg. The primary hippocampal neurones were derived from C57 BL/6 mouse embryos at embryonic stage 18 (E18). These experiments were carried out in accordance with the institutional guidelines for animal welfare and approved by the “Niedersächsisches Landesamt für Verbraucherschutz und Lebensmittelsicherheit” (33.19-45502-04-18/2766). The glial cells were obtained from postnatal day 2 (P2) mouse pups in accordance with the institutional guidelines of German animal welfare (§4) for the use of laboratory animals at the Carl von Ossietzky Universität Oldenburg.

4.5.2. Primary hippocampal neurone cultures

Primary hippocampal neurones were prepared from E18 mouse embryos. The hippocampi were dissected and pooled in a 15 mL falcon tube with HBSS (1X, Phenol red, Thermo Fisher Scientific, Waltham, MA, USA) and stored on ice. Afterwards, they were washed twice in HBSS and incubated in 0.25% trypsin (Gibco, Thermo Fisher Scientific) for 15 min at 37 °C. The supernatant was then carefully removed and replaced by plating media, containing MEM (Gibco, Thermo Fisher Scientific), supplemented with 0.6% D-(+)- glucose (≥99.5, Sigma-Aldrich, Taufkirchen, Germany), 10% horse serum (HS, Gibco, Thermo Fisher Scientific) and 100 U/mL penicillin with 100 µg/mL streptomycin (Pan-Biotech, Aidenbach, Germany). They were subsequently triturated with a fire-polished glass pipette until neurones were dissociated. Before plating the cells, culture plates and glass coverslips (Marienfeld 12 mm, VWR, Darmstadt, Germany) were coated with 0.2 mg/mL poly-L-lysine (PLL, P2636-100MG, Sigma-Aldrich) in ortho-boric acid (VWR chemicals, Darmstadt, Germany) buffer (pH 8.5) overnight, followed by rinses with cell culture water (USP WFI, Lonza, Biozym, Germany). The dissociated neurones were filtered through a 40 µm cell strainer (Greiner Bio-one, Frickenhausen, Germany), and for immunofluorescence, ~3 × 10^4 neurones were plated into 24-well plates (TPP® Faust lab Science, Klettgau, Germany). For high-performance thin-layer chromatography (HPTLC) and tandem mass spectrometry (MS/MS) analysis, ~1 × 10^6 neurones were seeded into 60 mm-diameter petri dishes (NunclonTM Delta surface, Thermo Fisher Scientific) containing plating media. Three to four hours after plating, cells were washed twice with 1 x PBS (phosphate-buffered Saline, Thermo Fisher Scientific), incubated, and maintained in Neurobasal A media (Gibco, Thermo Fisher Scientific) supplemented with 0.25% L-glutamine (200 mM, Sigma Aldrich,

Omnilab, Bremen, Germany), 2% B27-supplement (50X, Thermo Fisher Scientific) and 100 U/mL penicillin with 100 µg/mL streptomycin (Pan-Biotech). Hippocampal neurones used for synaptic study and lipid analysis were maintained for 12 days *in vitro* (DIV) at 37 ◦C, 5% CO2.

4.5.3. Primary glial cell cultures

Glial cell cultures were prepared from cortical tissue of P2 mouse pups. The brains were dissected and washed twice in HBSS (1X, Phenol red, Thermo Fisher Scientific). After removing the meninges from the brains, cortical tissue was isolated, washed twice in HBSS and incubated with 0.05% trypsin-EDTA (Gibco, Thermo Fisher Scientific) for 12 min at 37 °C. The supernatant was then carefully removed and replaced by plating media, consisting of DMEM (high glucose with L-glutamine, 4500 mg/L D-glucose, 110 mg/L sodium pyruvate, Gibco, Thermo Fisher Scientific) supplemented with 10% FBS (Pan-Biotech), 10% HS (Pan-Biotech) and 100 U/mL penicillin with 100 µg/mL streptomycin (Pan-Biotech). Tissue was carefully triturated and centrifuged for 1 min at 20× g. Supernatant was cautiously transferred to a new falcon tube and centrifuged for 5 min at 300× g. The supernatant was discarded and the pellet resuspended in plating media. Before plating, the T75 flask (Sarstedt, Label A, The Netherlands), coated overnight with 0.1 mg/mL PLL (P2636-100MG, Sigma-Aldrich) in ortho-boric acid (VWR chemicals) buffer (pH 8.5), was rinsed three times in MilliQ water. The dissociated glial cells were filtered through a 70 µm cell strainer (Corning, VWR, Darmstadt, Germany) and plated into the T75 flasks. After 2–3 days, the culture medium was changed and further maintained in 37 °C at 5% CO2. After 10–12 DIV, microglia were separated from astrocytes by agitation (230 rpm) at 37 °C for 3–4 h for obtaining the microglia. Adherent astrocytes were harvested using 0.25% trypsin-EDTA for 5 min in an incubator. Astrocytes were collected and centrifuged at 473× g for 10 min. The cell pellet was resuspended in plating media consisting of 45.5% DMEM (high glucose with L-glutamine, 4500 mg/L D-glucose, 110 mg/L sodium pyruvate, Gibco, Thermo Fisher Scientific), 45.5% HAMS-F12 nutrient mix (Gibco, Thermo Fisher Scientific), 8% FBS (Pan-Biotech), 1% Pen/Strep (Pan-Biotech), and seeded into 60 mm-diameter Petri dishes (NunclonTM Delta surface, Thermo Fisher Scientific).

4.5.4. Aβ treatment

Human synthetic amyloid-beta 42 ($A\beta_{(1–42)}$, Tocris Cat. No. 1191, Bio-Techne GmbH, Wiesbaden, Germany) and human synthetic amyloid-beta 40 ($A\beta_{(1–40)}$, Tocris Cat. No 1428, Bio-Techne GmbH) were reconstituted in dimethylsulfoxide (DMSO, (≥99.5%, Carl Roth,

Karlsruhe, Germany)) to a 250 µM stock concentration, sonicated for 10 min, and centrifuged at 13523× g at 16 °C (Willén et al., 2017). Finally, the 12 DIV hippocampal primary neurones and glial cells were treated with or without 1 µM of $A\beta_{(1–40)}$ and $A\beta_{(1–42)}$ for 3 h and 12 h.

4.5.5. Synaptic study

4.5.5.1. Immunofluorescence

After 3 h and 12 h DMSO and Aβ treatment, the conditioned medium was removed and the cultured hippocampal neurones were washed once with warm phosphate buffer saline (PBS (1X), Gibco, Thermo Fisher Scientific), followed by fixation with 4% paraformaldehyde (PFA, Merck Millipore, Darmstadt, Germany) in PBS (1X) containing 15% D-(+)-saccharose (≥99.7%, Carl Roth) at 4 °C for 10 min. After fixation, the cells were washed three times with PBS (1X) before being permeabilised with 0.1% triton X-100 (Carl Roth) for three minutes at room temperature (RT). The neurones were then washed three times with PBS (1X) for 10 min while gently shaking on a shaker at RT. The neurones were blocked in PBS (1X) containing 10% foetal bovine serum (FBS, Pan Biotech) and 1% normal goat serum (NGS, Vector laboratories, Biozol, Germany) for 1 h on a shaker at RT. Afterward, they were incubated with two primary antibodies: guinea-pig anti-vesicular glutamate transporter-1 (VGlut-1 (1:200), Synaptic Systems, 135304, Göttingen, Germany) and mouse anti-postsynaptic density protein-95 (PSD-95 (1:1000), clone (7E3-1B8), Thermo Fisher Scientific, MA1-046) overnight on a shaker at 5 °C. After washing the neurones three times with PBS they were incubated with two secondary antibodies: goat anti-mouse Alexa Fluor 488 (1:1500, Molecular probes) and goat anti-guinea-pig cyanine fluorescent dye (Cy3) (1:1000, Jackson Immuno Research, Cambridgeshire, UK) on a shaker for 1.5 h at RT. Nuclear staining was performed using DAPI (1:2000). All primary and secondary antibodies, as well as DAPI (Carl Roth), were diluted in PBS (1X) containing 5% FBS and 1% NGS. The coverslips with neurones were mounted on glass slides (Duran 76 mm × 26 mm, Carl Roth) with Immu-mount® (Shandon, Thermo Fisher). Immunofluorescent images for quantification of synaptic profiling between pre-and postsynaptic markers were captured using an Olympus IX83 invert microscope with DP80 camera (Olympus, Shinjuku, Japan) using the UPlanSApo 100×/1.4 oil objective with the following filter modules: U-F39002 AT-FITC for Alexa Fluor 488, U-F39004 AT-CY3 for Cy3, and U-FF for DAPI. Background correction, adjustment of brightness and contrast, and selection of regions of interest (ROI) were performed by CellSense software (Olympus, Shinjuku, Japan). Fluorescent images (Figure 24 A) were captured with an inverted laser-scanning confocal microscope (SP8, Leica,

Wetzlar, Germany) with a 63×/1.4 oil objective (zoom 3) using the Leica software. Images were taken using 488 nm and 564 nm lasers. Background correction, brightness, and contrast were adjusted by ImageJ software (NIH, Bethesda, MD, USA). Further processing of the images was carried out using Adobe Illustrator CC 2020.

4.5.6. Lipidomic study

4.5.6.1. Samples collection for lipid analysis

Hippocampal primary neurones (12 DIV) and glial cells were harvested and collected in Eppendorf® LoBind micro-centrifuge tubes (Eppendorf, Omnilab) after 3 h and 12 h with and without $A\beta_{(1–40)}$ and $A\beta_{(1–42)}$ treatment. The supernatant was discarded. Dishes were washed once with cold PBS (1X), neurones and glial cells collected in LoBind tubes after 2 min' centrifugation (9391× g) at 4 °C, the supernatant was discarded, and the pellets were snap-frozen and stored at −80 °C.

4.5.6.2. Lipid extraction

Hippocampal primary neurone (12 DIV) and glial-cell pellets were transferred by glass pipettes into transparent glass centrifuge tubes (Corning) containing chloroform ($CHCl_3$, SupraSolv®, Merck, Darmstadt, Germany), methanol (LiChrosolv® HPLC gradient grade, Merck), and fuming hydrochloric acid 37% (Rotipuran®, p.a., ACS, ISO, Carl Roth) solutions supplemented with 1% butylhydroxytoluol (BHT, ≥99%, Carl Roth) and fractioned by pipetting up and down while the sample was on ice. Then, 1 µL TopFluor lysophosphatidic acid (LPA) (702.58 g/mol, Avanti 810280P-1MG), was added per 1 million cells. The TopFluor LPA was dissolved in 1 mL $CHCl_3$ (1 mg/mL). Then $CHCl_3$ and water (H_2O, Rotisolv® HPLC gradient grade, Carl Roth) were added, followed by vortexing and 30 min incubation in the dark at RT. Samples were centrifuged at 1260× g for 10 min at RT. Finally, the lipid phase was collected using a glass Pasteur pipette into a new glass vial (Thermo Fisher Scientific) and placed in a nitrogen chamber with 6% O_2 concentration, overnight in the dark. Until measurement, the samples were stored at −20 °C

4.5.6.3. High-performance thin layer chromatography

We used various external standards as references, such as 1,2-dioleoyl-sn-glycero-3-phosphocholine (18:1 (Δ9-Cis) PC (DOPC), Avanti 850375); 1,2-dioleoyl-sn-glycero-3-phosphoethanolamine (18:1 (Δ9-Cis) PE (DOPE), Avanti 850725); 1,2-dioleoyl-sn-glycero-3-phospho-L-serine (18:1 PS (DOPS), Avanti 840035) for lipid classes of glycerophospholipids, and N-nervonoyl-D-erythro-sphingosylphosphorylcholine (24:1 SM,

Avanti 860593) for lipid class of sphingolipids. Extracted lipid samples from the neuronal cell lysates were analysed by dilution in 12 µL $CHCl_3$ for 1 million cells, using a Hamilton® syringe. The samples and external standard were vortexed and transferred by a Hamilton® syringe to a glass vial with glass micro-insert (31 × 6 mm, Omnilab). The diluted samples and standards were sprayed band-shaped onto the silica gel plates (TLC silica gel $60F_{254}$ (20 × 10 cm plates), Merck) using the CAMAG automatic TLC sampler 4 (ATS 4). The sprayed bands were separated by capillary force, based on a polarity gradient in the mobile phase, using the CAMAG horizontal developing chamber. The mobile phase contained $CHCl_3$, methanol, H_2O, and ammonia (NH_3, 32% HiPerSolv® Chromanorm for HPLC, VWR). We performed visualisation (CAMAG TLC Visualizer 2) and scanning (CAMAG TLC Scanner 4) using the mercury lamp at a wavelength of 366 nm for the measurement of the fluorescent signal of the internal standard, Topfluor LPA, followed by a development step with a solution containing copper (II)-sulphate pentahydrate (≥99.5%, p.a., ACS, ISO, Carl Roth), H_2O, ortho-phosphoric acid (85%, Carl Roth), and methanol using the CAMAG Derivatizer. After derivatisation, the plate was placed for 1 h at 120 °C. Finally, the plates were visualised and scanned using a Tungsten lamp with a wavelength of 420 nm. All data were processed by the CAMAG VisionCATS software 2.4, Adobe Photoshop CC 2020, and Adobe Illustrator CC 2020.

4.5.6.4. Tandem mass spectrometry

Lipid analyses were performed using lipid chromatography coupled to tandem mass spectrometry (tandem MS). Lipids were extracted as previously described (Sundaram et al., 2012). Briefly, cells were resuspended in 1 mL H_2O and directly transferred into glass centrifuge tubes. After addition of 10 µL of the internal standard (30 µM of C17-lysophosphatidylcholine (C17-LPC), C15-ceramide (C15-Cer), C17-sphingosine (C17-So), C34:0 phosphatidylcholine (PC 17:0/17:0), C17-sphingomyelin (C17-SM), C34:0 phosphatidylserine (PS 17:0/17:0), C17-lysophosphatidylserine (C17-LPS), C17-lysophosphatidylethanolamine (C17-LPE), 10 µM C17-sphingosine 1-phosphate (C17-So1P), all from Avanti Polar Lipids, Alabaster, AL, USA, and 1 mM ergosterol from Merck), 200 µL 6 N HCl, 1 mL methanol and 2 mL $CHCl_3$ were also added. Samples were vigorously vortexed for 10 min. After centrifugation at 1900× g, the lower $CHCl_3$ phase was collected. Extraction was repeated with an additional 2 mL of $CHCl_3$, and the two $CHCl_3$ phases were combined and evaporated using the SpeedVac RVC 2–25 CDplus (Christ, Osterode, Germany). Samples were resuspended in 100 µL methanol: $CHCl_3$ (4:1 v/v) and analysed using the Prominence high-performance liquid chromatography (HPLC) system (Shimadzu,

Duisburg, Germany) with a 60 mm × 2 mm MultoHigh 100 RP 18 column with 3 µm particle size (CS-Chromatographie Service, Langerwehe, Germany), which was maintained at 50 °C. The mobile phase A consisted of 1% (v/v) formic acid in ddH_2O, and the mobile phase B of 100% methanol. The column was equilibrated in 10% B with a flow rate of 0.5 mL min^{-1}. The mobile phase switched to 100% B after sample injection. The flow rate increased linearly from 0.5 mL min^{-1} at 5 min to 1.0 mL min^{-1} at 7 min and remained constant until 10 min. Subsequently, the mobile phase changed to 10% B, and the flow rate decreased linearly from 1.0 mL min^{-1} at 10 min to 0.5 mL min^{-1} at 10.5 min and remained constant until the end of the program at 11.3 min. Detection took place between 2 and 10 min. The injection volume per sample was 10 µL, and samples were cooled to 4 °C. The HPLC system was coupled to the API 2000 triple-quadrupole mass spectrometer (Sciex, Foster City, CA, USA) equipped either with an ESI or an APCI source (Table S7), both operating in positive mode under the following source parameters: source temperature 450 °C, curtain gas 40, collision gas “low”, ion spray voltage 5500, ion source gas 1 60 (APCI: 30), ion source gas 2 30 (APCI: 60). The analytical results were quantified with Analyst 1.6.2 (AB Sciex, Forster City, CA, USA) based on internal standard samples and an external standard curve.

4.5.7. Data analysis

For quantification of our synaptic study, we counted active synapses on hippocampal neurones from 12 DIV. Synapses in hippocampal neurones were stained with antibodies specific for synaptic proteins (PSD-95, postsynaptic in green; Vglut-1, presynaptic in red). Only puncta with obvious PSD-95/Vglut-1 overlap (in yellow) were counted as active synapses (Verstraelen et al., 2020). We analysed three regions of interest (ROI = 47 $µm^2$) on each neurone for an average of ≥12 neurones from four different cultures (n = 4) after both 3 h and 12 h of Aβ treatment. In the 3 h treatment, the following average amount of neurones were counted in each group: CTRL (n = 12), DMSO (n = 9), $Aβ_{(1–40)}$ (n = 11) and $Aβ_{(1–42)}$ (n = 9). For the 12 h treatment, the following average amount of neurones were counted in each group: CTRL (n = 14), DMSO (n = 13), $Aβ_{(1–40)}$ (n = 13) and $Aβ_{(1–42)}$ (n = 17). Statistical analysis was performed using GraphPad Prism 7 (GraphPad Software, San Diego, CA, USA). Values were analysed for normal distribution using the Shapiro–Wilk test. As the data were not normally distributed, they were analysed by performing a Kruskal–Wallis test followed by a post hoc Dunn’s multiple comparison test. All data are presented as mean + standard deviation (SD) and considered to be significant if $p < 0.05$ (*** $p < 0.0001$). Tandem mass spectrometry data of three independent experiments (n = 3) from neurones and glial cells were further processed by GraphPad Prism 7, performing

logarithmic 10 transformation, and plotted to our negative control (DMSO). This was because the raw data showed that a low concentration of DMSO (final concentration 0.03%) showed an effect on both the lipid composition of glial cells and hippocampal primary neurones, as previously demonstrated (de Ménorval et al., 2012). Z-score transformation was performed, and data were plotted as heat maps for each lipid class.

Funding: This research was funded by H2020 MSCA-ITN-ETN BBDiag project under grant No. 721281.

Institutional Review Board Statement: These experiments were carried out in accordance with the institutional guidelines for animal welfare and approved by the “Niedersächsisches Landesamt für Verbraucherschutz und Lebensmittelsicherheit” (33.19-45502-04-18/2766).

Informed Consent Statement: Not applicable.

Acknowledgments: We acknowledge the financial support by H2020 MSCA-ITN-ETN BBDiag project under grant No. 721281 and Research Group Anatomy, School for Medicine and Health Science, Carl von Ossietzky University Oldenburg, Germany. In particular, Jennifer Sevecke-Rave and Isabel Groß are acknowledged for their excellent technical support in the laboratory. The authors also acknowledge the Fluorescence Microscopy Service Unit, Carl von Ossietzky University of Oldenburg, for the use of the imaging facilities.

Conflicts of Interest: The authors declare that they have no conflict of interest in the work performed. The sponsor had no role in design of the study, analysis, interpretation of data, in the writing of the manuscript, or in the decision to publish the results.

Abbreviations

POPC	1-Palmitoyl-2-oleoyl-sn-glycero-3-phosphocholine
DMPC	1,2-dimyristoyl-sn-glycero-3-phosphocholine
DMPG	1,2-Dimyristoyl-sn-glycero-3-phosphoglycerol
nSMase	Neutral isoform sphingomyelinase
aSMase	Acid sphingomyelinase

4.6. References

Agarwal, M., & Khan, S. (2020). Plasma Lipids as Biomarkers for Alzheimer's Disease: A Systematic Review. *Cureus*, *12*(12). https://doi.org/10.7759/cureus.12008

Almeida, C. G., Tampellini, D., Takahashi, R. H., Greengard, P., Lin, M. T., Snyder, E. M., & Gouras, G. K. (2005). Beta-amyloid accumulation in APP mutant neurons reduces PSD-95 and GluR1 in synapses. *Neurobiol Dis*, *20*(2), 187-198. https://doi.org/10.1016/j.nbd.2005.02.008

Bate, C., & Williams, A. (2010). Amyloid-β_{1-40} Inhibits Amyloid-β_{1-42} Induced Activation of Cytoplasmic Phospholipase A_2 and Synapse Degeneration. *J Alzheimers Dis*, *21*(3), 985-993. https://doi.org/10.3233/JAD-2010-100528

Brothers, H. M., Gosztyla, M. L., & Robinson, S. R. (2018). The Physiological Roles of Amyloid-β Peptide Hint at New Ways to Treat Alzheimer's Disease. *Front Aging Neurosci*, *10*, 118. https://doi.org/10.3389/fnagi.2018.00118

Ceccom, J., Loukh, N., Lauwers-Cances, V., Touriol, C., Nicaise, Y., Gentil, C., Uro-Coste, E., Pitson, S., Maurage, C. A., Duyckaerts, C., Cuvillier, O., & Delisle, M. B. (2014). Reduced sphingosine kinase-1 and enhanced sphingosine 1-phosphate lyase expression demonstrate deregulated sphingosine 1-phosphate signaling in Alzheimer's disease. *Acta Neuropathol Commun*, *2*, 12. https://doi.org/10.1186/2051-5960-2-12

Chen, G.-F., Xu, T.-H., Yan, Y., Zhou, Y.-R., Jiang, Y., Melcher, K., & Xu, H. E. (2017). Amyloid beta: structure, biology and structure-based therapeutic development. *Acta Pharmacol Sin*, *38*(9), 1205-1235. https://doi.org/10.1038/aps.2017.28

Czubowicz, K., Cieślik, M., Pyszko, J., Strosznajder, J. B., & Strosznajder, R. P. (2015). Sphingosine-1-Phosphate and Its Effect on Glucose Deprivation/Glucose Reload Stress: From Gene Expression to Neuronal Survival. *Mol Neurobiol*, *51*(3), 1300-1308. https://doi.org/10.1007/s12035-014-8807-5

de Ménorval, M. A., Mir, L. M., Fernández, M. L., & Reigada, R. (2012). Effects of Dimethyl Sulfoxide in Cholesterol-Containing Lipid Membranes: A Comparative Study of Experiments In Silico and with Cells. *PLoS ONE*, *7*(7), e41733. https://doi.org/10.1371/journal.pone.0041733

Fu, L., Sun, Y., Guo, Y., Chen, Y., Yu, B., Zhang, H., Wu, J., Yu, X., Kong, W., & Wu, H. (2017). Comparison of neurotoxicity of different aggregated forms of Aβ40, Aβ42 and Aβ43 in cell cultures. *J Pept Sci*, *23*(3), 245-251. https://doi.org/10.1002/psc.2975

Gouras, G. K., Olsson, T. T., & Hansson, O. (2015). β-amyloid Peptides and Amyloid Plaques in Alzheimer's Disease. *Neurotherapeutics*, *12*(1), 3-11. https://doi.org/10.1007/s13311-014-0313-y

Gouras, G. K., Tsai, J., Naslund, J., Vincent, B., Edgar, M., Checler, F., Greenfield, J. P., Haroutunian, V., Buxbaum, J. D., Xu, H., Greengard, P., & Relkin, N. R. (2000). Intraneuronal Aβ42 Accumulation in Human Brain. *Am J Pathol*, *156*(1), 15-20. https://doi.org/10.1016/s0002-9440(10)64700-1

Grimm, M. O. W., Grimm, H. S., Pätzold, A. J., Zinser, E. G., Halonen, R., Duering, M., Tschäpe, J.-A., De Strooper, B., Müller, U., Shen, J., & Hartmann, T. (2005). Regulation of cholesterol and sphingomyelin metabolism by amyloid-β and presenilin. *Nat Cell Biol*, *7*(11), 1118-1123. https://doi.org/10.1038/ncb1313

Hayashi, M. K., Tang, C., Verpelli, C., Narayanan, R., Stearns, M. H., Xu, R.-M., Li, H., Sala, C., & Hayashi, Y. (2009). The Postsynaptic Density Proteins Homer and Shank Form a Polymeric Network Structure. *Cell*, *137*(1), 159-171. https://doi.org/10.1016/j.cell.2009.01.050

He, X., Huang, Y., Li, B., Gong, C.-X., & Schuchman, E. H. (2010). Deregulation of sphingolipid metabolism in Alzheimer's disease. *Neurobiol Aging*, *31*(3), 398-408. https://doi.org/10.1016/j.neurobiolaging.2008.05.010

Heras-Sandoval, D., Ferrera, P., & Arias, C. (2012). Amyloid-β Protein Modulates Insulin Signaling in Presynaptic Terminals. *Neurochem Res*, *37*(9), 1879-1885. https://doi.org/10.1007/s11064-012-0800-7

Hu, X., Crick, S. L., Bu, G., Frieden, C., Pappu, R. V., & Lee, J. M. (2009). Amyloid seeds formed by cellular uptake, concentration, and aggregation of the amyloid-beta peptide. *Proc Natl Acad Sci U S A*, *106*(48), 20324-20329. https://doi.org/10.1073/pnas.0911281106

Jazvinšćak Jembrek, M., Hof, P. R., & Šimić, G. (2015). Ceramides in Alzheimer's Disease: Key Mediators of Neuronal Apoptosis Induced by Oxidative Stress and Aβ Accumulation. *Oxid Med Cell Longev*, *2015*, 346783. https://doi.org/10.1155/2015/346783

Kim, Y., Kim, C., Jang, H. Y., & Mook-Jung, I. (2016). Inhibition of Cholesterol Biosynthesis Reduces γ-Secretase Activity and Amyloid-β Generation. *J Alzheimers Dis*, *51*(4), 1057-1068. https://doi.org/10.3233/JAD-150982

Klementieva, O., Willén, K., Martinsson, I., Israelsson, B., Engdahl, A., Cladera, J., Uvdal, P., & Gouras, G. K. (2017). Pre-plaque conformational changes in Alzheimer's disease-linked Aβ and APP. *Nat Commun*, *8*, 14726. https://doi.org/10.1038/ncomms14726

Korshavn, K. J., Satriano, C., Lin, Y., Zhang, R., Dulchavsky, M., Bhunia, A., Ivanova, M. I., Lee, Y.-H., La Rosa, C., Lim, M. H., & Ramamoorthy, A. (2017). Reduced Lipid Bilayer Thickness Regulates the Aggregation and Cytotoxicity of Amyloid-β. *J Biol Chem*, *292*(11), 4638-4650. https://doi.org/10.1074/jbc.M116.764092

Kumar, A., Singh, A., & Ekavali. (2015). A review on Alzheimer's disease pathophysiology and its management: an update. *Pharmacol Rep*, *67*(2), 195-203. https://doi.org/10.1016/j.pharep.2014.09.004

Lacor, P. N., Buniel, M. C., Chang, L., Fernandez, S. J., Gong, Y., Viola, K. L., Lambert, M. P., Velasco, P. T., Bigio, E. H., Finch, C. E., Krafft, G. A., & Klein, W. L. (2004). Synaptic Targeting by Alzheimer's-Related Amyloid β Oligomers. *J Neurosci*, *24*(45), 10191-10200. https://doi.org/10.1523/JNEUROSCI.3432-04.2004

Malaplate-Armand, C., Florent-Béchard, S., Youssef, I., Koziel, V., Sponne, I., Kriem, B., Leininger-Muller, B., Olivier, J.-L., Oster, T., & Pillot, T. (2006). Soluble oligomers of amyloid-β peptide induce neuronal apoptosis by activating a cPLA$_2$-dependent sphingomyelinase-ceramide pathway. *Neurobiol Dis*, *23*(1), 178-189. https://doi.org/10.1016/j.nbd.2006.02.010

Michno, W., Kaya, I., Nyström, S., Guerard, L., Nilsson, K. P. R., Hammarström, P., Blennow, K., Zetterberg, H., & Hanrieder, J. (2018). Multimodal Chemical Imaging of Amyloid Plaque Polymorphism Reveals Aβ Aggregation Dependent Anionic Lipid Accumulations and Metabolism. *Anal Chem*, *90*(13), 8130-8138. https://doi.org/10.1021/acs.analchem.8b01361

Moses, G. S., Jensen, M. D., Lue, L.-F., Walker, D. G., Sun, A. Y., Simonyi, A., & Sun, G. Y. (2006). Secretory PLA2-IIA: a new inflammatory factor for Alzheimer's disease. *J Neuroinflammation*, *3*(1), 28. https://doi.org/10.1186/1742-2094-3-28

Niu, Z., Zhao, W., Zhang, Z., Xiao, F., Tang, X., & Yang, J. (2014). The Molecular Structure of Alzheimer β-Amyloid Fibrils Formed in the Presence of Phospholipid Vesicles. *Angew Chem Int Ed Engl*, *53*(35), 9294-9297. https://doi.org/10.1002/anie.201311106

Novo, M., Freire, S., & Al-Soufi, W. (2018). Critical aggregation concentration for the formation of early Amyloid-β (1–42) oligomers. *Sci Rep*, *8*(1), 1783. https://doi.org/10.1038/s41598-018-19961-3

Park, M. K., & Lee, C. H. (2019). Role of Sphingosylphosphorylcholine in Tumor and Tumor Microenvironment. *Cancers (Basel)*, *11*(11), 1696. https://doi.org/10.3390/cancers11111696

Pearson, H. A., & Peers, C. (2006). Physiological roles for amyloid β peptides. *J Physiol*, *575*(1), 5-10. https://doi.org/10.1113/jphysiol.2006.111203

Puglielli, L., Ellis, B. C., Saunders, A. J., & Kovacs, D. M. (2003). Ceramide Stabilizes β-Site Amyloid Precursor Protein-cleaving Enzyme 1 and Promotes Amyloid β-Peptide Biogenesis. *J Biol Chem*, *278*(22), 19777-19783. https://doi.org/10.1074/jbc.M300466200

Qi, X.-L., Xiu, J., Shan, K.-R., Xiao, Y., Gu, R., Liu, R.-Y., & Guan, Z.-Z. (2005). Oxidative stress induced by beta-amyloid peptide$_{1–42}$ is involved in the altered composition of cellular membrane lipids and the decreased expression of nicotinic receptors in human SH-SY5Y neuroblastoma cells. *Neurochem Int*, *46*(8), 613-621. https://doi.org/10.1016/j.neuint.2005.02.007

Ries, M., & Sastre, M. (2016). Mechanisms of Aβ Clearance and Degradation by Glial Cells. *Front Aging Neurosci*, *8*, 160. https://doi.org/10.3389/fnagi.2016.00160

Sokolow, S., Luu, S. H., Nandy, K., Miller, C. A., Vinters, H. V., Poon, W. W., & Gylys, K. H. (2012). Preferential accumulation of amyloid-beta in presynaptic glutamatergic terminals (VGluT1 and VGluT2) in Alzheimer's disease cortex. *Neurobiol Dis*, *45*(1), 381-387. https://doi.org/10.1016/j.nbd.2011.08.027

Sosa, L. J., Cáceres, A., Dupraz, S., Oksdath, M., Quiroga, S., & Lorenzo, A. (2017). The physiological role of the amyloid precursor protein as an adhesion molecule in the developing nervous system. *J Neurochem*, *143*(1), 11-29. https://doi.org/10.1111/jnc.14122

Sundaram, J. R., Chan, E. S., Poore, C. P., Pareek, T. K., Cheong, W. F., Shui, G., Tang, N., Low, C.-M., Wenk, M. R., & Kesavapany, S. (2012). Cdk5/p25-Induced Cytosolic PLA2-Mediated Lysophosphatidylcholine Production Regulates Neuroinflammation and Triggers Neurodegeneration. *J Neurosci*, *32*(3), 1020-1034. https://doi.org/10.1523/JNEUROSCI.5177-11.2012

Takahashi, H., Sekino, Y., Tanaka, S., Mizui, T., Kishi, S., & Shirao, T. (2003). Drebrin-Dependent Actin Clustering in Dendritic Filopodia Governs Synaptic Targeting of Postsynaptic Density-95 and Dendritic Spine Morphogenesis. *J Neurosci*, *23*(16), 6586-6595. https://doi.org/10.1523/JNEUROSCI.23-16-06586.2003

Takahashi, R. H., Almeida, C. G., Kearney, P. F., Yu, F., Lin, M. T., Milner, T. A., & Gouras, G. K. (2004). Oligomerization of Alzheimer's β-Amyloid within Processes and Synapses of Cultured Neurons and Brain. *J Neurosci*, *24*(14), 3592-3599. https://doi.org/10.1523/JNEUROSCI.5167-03.2004

Takahashi, R. H., Milner, T. A., Li, F., Nam, E. E., Edgar, M. A., Yamaguchi, H., Beal, M. F., Xu, H., Greengard, P., & Gouras, G. K. (2002). Intraneuronal Alzheimer Aβ42 Accumulates in Multivesicular Bodies and Is Associated with Synaptic Pathology. *Am J Pathol*, *161*(5), 1869-1879. https://doi.org/10.1016/s0002-9440(10)64463-x

Thal, D. R., Schultz, C., Dehghani, F., Yamaguchi, H., Braak, H., & Braak, E. (2000b). Amyloid β-protein (Aβ)-containing astrocytes are located preferentially near N-terminal-truncated Aβ deposits in the human entorhinal cortex. *Acta Neuropathol*, *100*(6), 608-617. https://doi.org/10.1007/s004010000242

Venkateswaran, A., Laffitte, B. A., Joseph, S. B., Mak, P. A., Wilpitz, D. C., Edwards, P. A., & Tontonoz, P. (2000). Control of cellular cholesterol efflux by the nuclear oxysterol receptor LXRα. *Proc Natl Acad Sci U S A*, *97*(22), 12097-12102. https://doi.org/10.1073/pnas.200367697

Verstraelen, P., Barriga, G. G.-D., Verschuuren, M., Asselbergh, B., Nuydens, R., Larsen, P. H., Timmermans, J. P., & De Vos, W. H. (2020). Systematic Quantification of Synapses in Primary Neuronal Culture. *Iscience*, *23*(9), 101542. https://doi.org/10.1016/j.isci.2020.101542

Walsh, D. M., Klyubin, I., Fadeeva, J. V., Cullen, W. K., Anwyl, R., Wolfe, M. S., Rowan, M. J., & Selkoe, D. J. (2002). Naturally secreted oligomers of amyloid β protein potently inhibit hippocampal long-term potentiation *in vivo*. *Nature*, *416*(6880), 535-539. https://doi.org/10.1038/416535a

Walsh, D. M., & Selkoe, D. J. (2004). Deciphering the Molecular Basis of Memory Failure in Alzheimer's Disease. *Neuron*, *44*(1), 181-193. https://doi.org/10.1016/j.neuron.2004.09.010

Willén, K., Sroka, A., Takahashi, R. H., & Gouras, G. K. (2017). Heterogeneous Association of Alzheimer's Disease-Linked Amyloid-β and Amyloid-β Protein Precursor with Synapses. *J Alzheimers Dis*, *60*(2), 511-524. https://doi.org/10.3233/JAD-170262

Yi, H., Lee, S. J., Lee, J., Myung, C.-S., Park, W.-K., Lim, H.-J., Lee, G. H., Kong, J. Y., & Cho, H. (2011). Sphingosylphosphorylcholine Attenuated β–Amyloid Production by Reducing BACE1 Expression and Catalysis in PC12 Cells. *Neurochem Res*, *36*(11), 2083-2090. https://doi.org/10.1007/s11064-011-0532-0

Zhang, Y., Ranta, F., Tang, C., Shumilina, E., Mahmud, H., Föller, M., Ullrich, S., Häring, H.-U., & Lang, F. (2009). Sphingomyelinase dependent apoptosis following treatment of pancreatic beta-cells with amyloid peptides Aß$_{1-42}$ or IAPP. *Apoptosis*, *14*(7), 878-889. https://doi.org/10.1007/s10495-009-0364-4

Zhong, L., Jiang, X., Zhu, Z., Qin, H., Dinkins, M. B., Kong, J.-N., Leanhart, S., Wang, R., Elsherbini, A., Bieberich, E., Zhao, Y., & Wang, G. (2019). Lipid transporter Spns2 promotes microglia pro-inflammatory activation in response to amyloid-beta peptide. *Glia*, *67*(3), 498-511. https://doi.org/10.1002/glia.23558

4.7. Supplementary materials and methods

From the published article:

Aβ-Induced Alterations in Membrane Lipids Occur before Synaptic Loss Appears

Michiel Van Bulck[1,2,*], Nicola Brandt[1], Ralf A. Claus[3], Markus Gräler[3,4] and Anja U. Bräuer[1,5,*]

[1] Research Group Anatomy, School for Medicine and Health Science, Carl von Ossietzky University Oldenburg, 26129 Oldenburg, Germany; nicola.brandt@uni-oldenburg.de

[2] Department of Experimental Models of Human Disease, Networked Center of Biomedical Research on Neurodegenerative Diseases (CIBERNED), Institute for Biomedical Research A. Sols (CSIC-UAM), 28029 Madrid, Spain

[3] Department of Anaesthesiology and Intensive Care Medicine Center for Molecular Biomedicine (CMB), Jena University Hospital, 07745 Jena, Germany; ralf.claus@med.uni-jena.de (R.A.C.); markus.graeler@med.uni-jena.de (M.G.)

[4] Centre for Sepsis Control and Care (CSCC), Jena University Hospital, 07745 Jena, Germany

[5] Research Centre for Neurosensory Science, Carl von Ossietzky University Oldenburg, 26129 Oldenburg, Germany

* Correspondence: michiel.van.bulck@uni-oldenburg.de (M.V.B.); anja.braeuer@uni-oldenburg.de (A.U.B.)

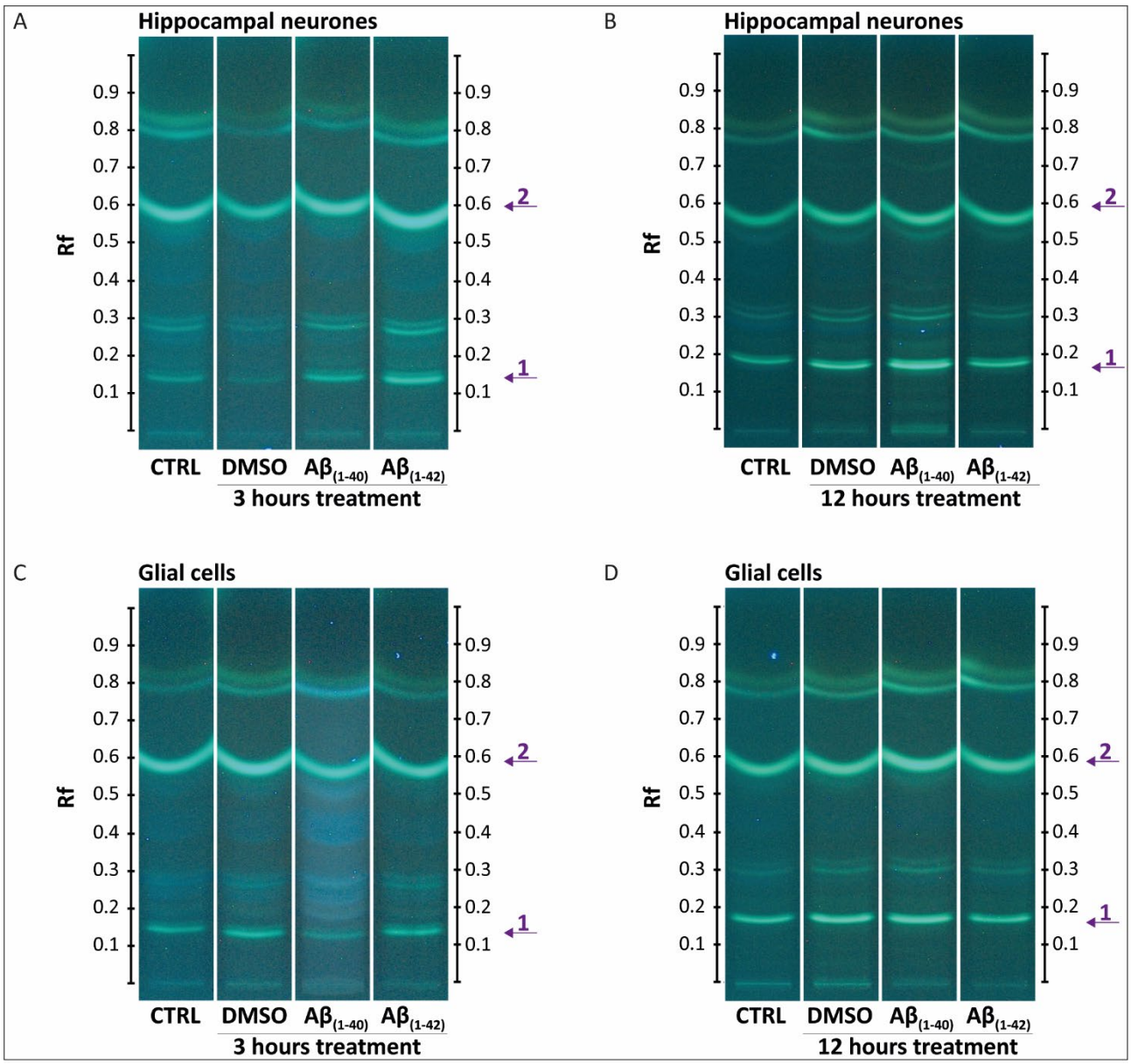

Figure S10: *HPTLC-analysis based TopFluor lysophosphatidic acid (LPA) images of hippocampal neurones at DIV 12 and glial cells after 3 h and 12 h Aβ(1–40) and Aβ(1–42) treatment.*

*LPA was used as an internal standard from control groups (CTRL and DMSO) and Aβ-treated groups (Aβ(1–40) and Aβ(1–42)) at various time points of treatment (3 h and 12 h) of hippocampal neurones and glial cells ((**A–D**), all groups, from three independent experiments (N = 3)). 1µL/1 million cells fluorescent internal standard TopFluor LPA was added to each sample and fluorescence was detected with the CAMAG TLC Visualizer 2 at 366 nm. TopFluor LPA bound to the silica HPTLC plates at retention factor (Rf) around Rf 0.13 and Rf 0.59 (purple arrow 1 and 2).*

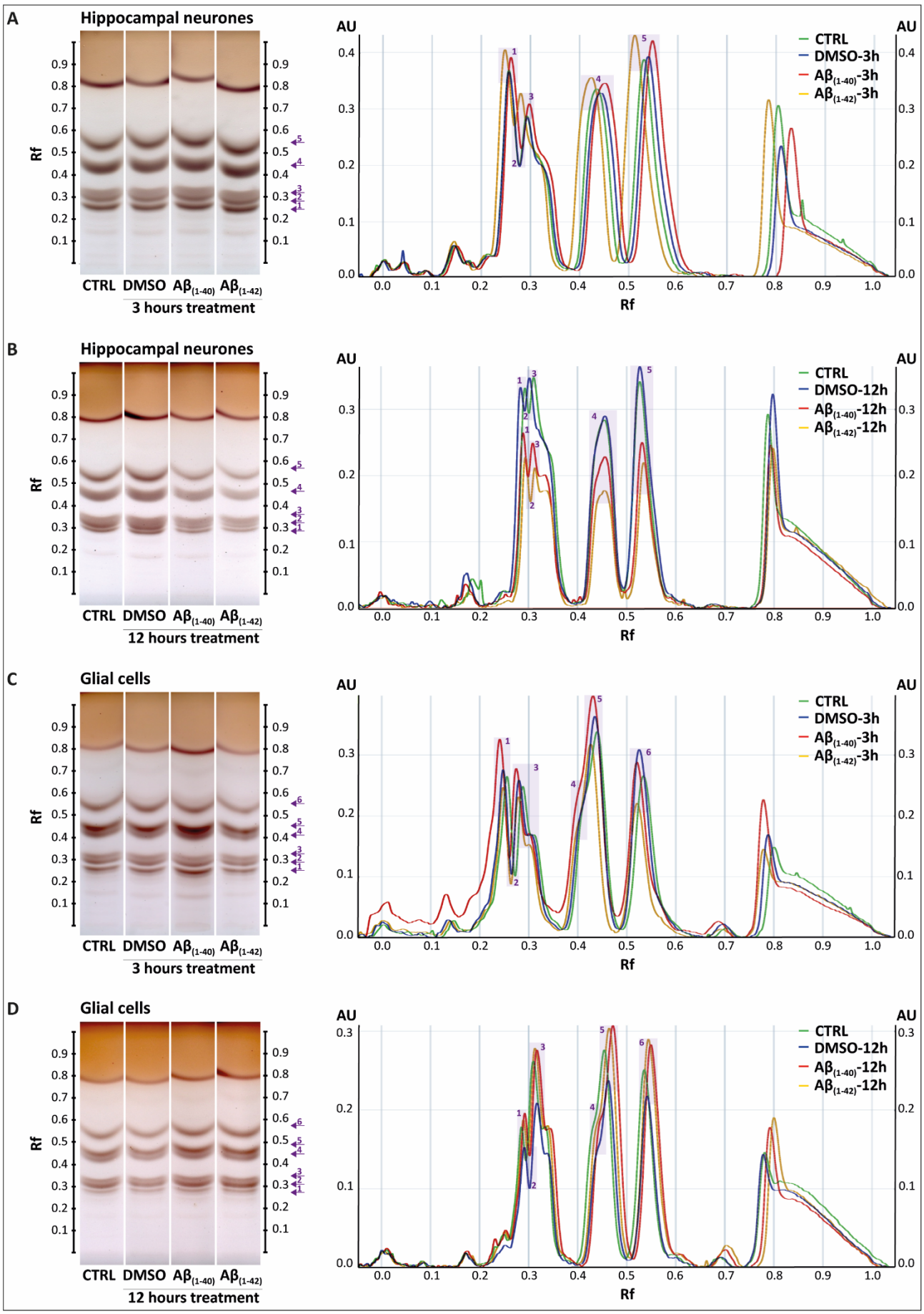

Figure S11: *HPTLC analysis based on derivatised copper (II)-sulfate images and scanning profiles of hippocampal neurones and glial cells after 3 h and 12 h of $A\beta_{(1–40)}$ or $A\beta_{(1–42)}$ treatment.*

*Derivatised copper (II)-sulfate images and scanning profiles that represent various lipid classes (sphingolipids and glycerophospholipids (1-6, purple arrow and boxes)) of control groups (CTRL and DMSO), Aβ-treated groups ($Aβ_{(1–40)}$ and $Aβ_{(1–42)}$) at two different time points of treatment (3 h and 12 h) of hippocampal neurones at DIV 12 and glial cells ((**A**–**D**), all groups, from three independent experiments (N = 3). Changes in lipid classes on band intensity in derivatised copper-sulfate silica-gel HPTLC plate images are indicated by purple arrows (1-6), corresponding to their purple boxes (1-6) showing the digital copper-sulfate derivatised scanning profiles. Hippocampal neurones showed dysregulated lipid classes of sphingolipids and glycerophospholipids (purple numbered arrows and boxes (1-5)) corresponding to the external standard (DOPC (4); DOPE (5); DOPS (1 and 2); 24:1 SM (3)) used. Glial cells showed dysregulated lipid classes of sphingolipids and glycerophospholipids (purple numbered arrows and boxes (1-6)) in accordance to our external standard (DOPC (4 and 5); DOPE (6); DOPS (1 and 2); 24:1 SM (3)) used. Separated lipid classes represented by band intensity were calibrated in arbitrary units (AU) showing the relative absorbance of specific lipid classes. The retention factor (RF) represents the relative distance the sample ran compared to the distance the solvent front ran. TopFluor LPA was used as the internal loading control (Figure S10). (**A**) After 3 h, $Aβ_{(1–40)}$- and $Aβ_{(1–42)}$-treated hippocampal neurones showed slight increases both in band-intensity changes and lipid-profile graphs from different lipid classes compared to control groups. (**B**) After 12 h, $Aβ_{(1–40)}$- and $Aβ_{(1–42)}$-treated hippocampal neurones showed a prominent decrease in different lipid classes compared to control groups. Sphingolipids and glycerophospholipids showed a higher decrease after 12h $Aβ_{(1–42)}$ compared to $Aβ_{(1–40)}$-treated neurones. (**C**) Lipid classes in glial cells showed an increase after $Aβ_{(1–40)}$ treatment, while a decrease after $Aβ_{(1–42)}$ was visible at the early time point (3 h) compared to control groups. (**D**) An increase in lipid classes after 12 h was seen for both $Aβ_{(1–40)}$- and $Aβ_{(1–42)}$-treated glial cells compared to control groups.*

Table S6: *List of retention factors (RF) and arbitrary unit (AU) of hippocampal neurones and glial cells (Figure S11).*

Retention factors (RF) and arbitrary units (AU) for the different conditions (CTRL, DMSO, Aβ(1-40) and Aβ(1-42)) after 3h and 12h treatment of 12 DIV hippocampal neurones and glial cells. Here, the RF and AU show the altered expression in different lipid classes (Figure S11, numbered arrows and boxes). Hippocampal neurons at DIV 12: purple numbered arrows and boxes refer to the following dysregulated lipid classes (sphingolipids and glycerophospholipids) of our external standards; DOPC (4); DOPE (5); DOPS (1 and 2); 24:1 SM (3). Glial cells: purple numbered arrows and boxes refer to the following dysregulated lipid classes of our external standards; DOPC (4 and 5); DOPE (6); DOPS (1 and 2); 24:1 SM (3).

Cell types	Time points	Numbered arrows/boxes	Conditions							
			CTRL		DMSO		Aβ(1-40)		Aβ(1-42)	
			RF	AU	RF	AU	RF	AU	RF	AU
Hippocampal neurones	3 hours	1	0.257	0.367	0.257	0.364	0.260	0.390	0.249	0.403
		2	0.278	0.203	0.278	0.200	0.283	0.232	0.267	0.272
		3	0.293	0.287	0.294	0.284	0.298	0.308	0.280	0.325
		4	0.435	0.336	0.443	0.328	0.451	0.346	0.424	0.355
		5	0.531	0.388	0.539	0.393	0.549	0.420	0.513	0.429
	12 hours	1	0.293	0.332	0.284	0.333	0.290	0.265	0.294	0.228
		2	0.301	0.294	0.292	0.297	0.300	0.198	0.305	0.160
		3	0.310	0.348	0.302	0.348	0.309	0.249	0.313	0.212
		4	0.455	0.284	0.456	0.290	0.456	0.229	0.455	0.178
		5	0.527	0.342	0.527	0.365	0.531	0.250	0.535	0.220
Glial cells	3 hours	1	0.256	0.265	0.248	0.276	0.241	0.326	0.248	0.247
		2	0.272	0.101	0.265	0.104	0.260	0.131	0.264	0.088
		3	0.288	0.249	0.280	0.259	0.274	0.278	0.279	0.231
		4	0.408-0.424	0.206-0.265	0.407-0.420	0.206-0.265	0.394-0.409	0.206-0.265	0.406-0.416	0.206-0.265
		5	0.440	0.339	0.435	0.364	0.431	0.397	0.427	0.318
		6	0.534	0.266	0.526	0.309	0.521	0.288	0.521	0.221
	12 hours	1	0.256	0.265	0.248	0.276	0.241	0.326	0.248	0.247
		2	0.272	0.101	0.265	0.104	0.260	0.131	0.264	0.088
		3	0.288	0.249	0.280	0.259	0.274	0.278	0.279	0.231
		4	0.408-0.424	0.206-0.265	0.407-0.420	0.206-0.265	0.394-0.409	0.206-0.265	0.406-0.416	0.206-0.265
		5	0.440	0.339	0.435	0.364	0.431	0.397	0.427	0.318
		6	0.534	0.266	0.526	0.309	0.521	0.288	0.521	0.221

Table S7: *List of target ions/MRM transitions, assignment to internal standard and mode of analysis.*
List of lipid analytes with their corresponding target ions/MRM transitions for tandem mass spectrometry (MS). Target ions/MRM transitions are assigned to their internal standard and mode of tandem MS analysis (APCI and ESI). Abbreviations: atmospheric-pressure chemical ionization (APCI), electrospray ionization (ESI), ceramide (Cer), dihydroceramide (DHCer), lactosylceramide (LacCer), monohexosylceramide (HexCer), sphingosine (So), sphinganine (Sa), sphingosine 1-phosphate (So1P), sphinganine 1-phosphate (Sa1P), sphingomyelin (SM), dihydrosphingomyelin (DHSM), sphingosylphosphorylcholine (SPC), phosphatidylcholine (PC), lysophosphatidylcholine (LPC), lysophosphatidylethanolamine (LPE), lysophosphatidylserine (LPS), lysophosphatidylglycerol (LPG). For CER, SM and (lyso-) phosphadityl-compounds, the number of carbon atoms, and the number of unsaturated bonds is given; for PC the total number of carbon atoms, as well as of unsaturated bonds, are given.

Name	Internal standard	Mode	Target ion Q1>Q3
C15:0 Cer		APCI	524.4>264.3
C12:0 Cer	>C15:0 Cer<	APCI	482.6>264.4
C14:0 Cer	>C15:0 Cer<	APCI	510.7>264.4
C16:0 Cer	>C15:0 Cer<	APCI	538.7>264.4
C18:0 Cer	>C15:0 Cer<	APCI	566.7>264.4
C18:1 Cer	>C15:0 Cer<	APCI	564.7>264.4
C20:0 Cer	>C15:0 Cer<	APCI	594.7>264.4
C22:0 Cer	>C15:0 Cer<	APCI	622.8>264.4
C24:0 Cer	>C15:0 Cer<	APCI	650.9>264.4
C24:1 Cer	>C15:0 Cer<	APCI	648.9>264.4
C12:0 DHCer	>C15:0 Cer<	APCI	484.6>266.4
C14:0 DHCer	>C15:0 Cer<	APCI	512.7>266.4
C16:0 DHCer	>C15:0 Cer<	APCI	540.7>266.4
C18:0 DHCer	>C15:0 Cer<	APCI	568.7>266.4
C18:1 DHCer	>C15:0 Cer<	APCI	566.7>266.4
C20:0 DHCer	>C15:0 Cer<	APCI	596.7>266.4
C22:0 DHCer	>C15:0 Cer<	APCI	624.8>266.4
C24:0 DHCer	>C15:0 Cer<	APCI	652.9>266.4
C24:1 DHCer	>C15:0 Cer<	APCI	650.9>266.4
C12:0 LacCer	>C15:0 Cer<	APCI	806.6>264.4
C16:0 LacCer	>C15:0 Cer<	APCI	862.7>264.4
C18:0 LacCer	>C15:0 Cer<	APCI	890.7>264.4
C22:0 LacCer	>C15:0 Cer<	APCI	946.8>264.4
C24:1 LacCer	>C15:0 Cer<	APCI	972.9>264.4
C12:0 HexCer	>C15:0 Cer<	APCI	644.6>264.4
C14:0 HexCer	>C15:0 Cer<	APCI	672.6>264.4
C16:0 HexCer	>C15:0 Cer<	APCI	700.7>264.4
C18:0 HexCer	>C15:0 Cer<	APCI	728.7>264.4
C20:0 HexCer	>C15:0 Cer<	APCI	756.7>264.4
C22:0 HexCer	>C15:0 Cer<	APCI	784.8>264.4

C24:0 HexCer	>C15:0 Cer<	APCI	812.9>264.4
d17:1 So1P		ESI	366.4>250.4
d18:1 So1P	>d17:1 So1P<	ESI	380.4>264.4
d18:0 Sa1P	>d17:1 So1P<	ESI	382.4>266.4
d17:1 So		ESI	286.4>268.4
d18:1 So	>d17:1 So<	ESI	300.4>282.4
d18:0 Sa	>d17:1 So<	ESI	302.4>284.4
SPC	>C17:0 SM<	ESI	465.4>184.1
C17:0 SM		ESI	717.5>184.1
C12:0 SM	>C17:0 SM<	ESI	647.7>184.1
C14:0 SM	>C17:0 SM<	ESI	675.7>184.1
C16:0 SM	>C17:0 SM<	ESI	703.8>184.1
C18:1 SM	>C17:0 SM<	ESI	729.8>184.1
C18:0 SM	>C17:0 SM<	ESI	731.8>184.1
C20:0 SM	>C17:0 SM<	ESI	759.9>184.1
C22:0 SM	>C17:0 SM<	ESI	797.9>184.1
C24:1 SM	>C17:0 SM<	ESI	813.9>184.1
C24:0 SM	>C17:0 SM<	ESI	815.9>184.1
C26:1 SM	>C17:0 SM<	ESI	841.9>184.1
C26:0 SM	>C17:0 SM<	ESI	843.9>184.1
C14:0 DHSM	>C17:0 SM<	ESI	677.7>184.1
C16:0 DHSM	>C17:0 SM<	ESI	705.8>184.1
C18:1 DHSM	>C17:0 SM<	ESI	731.8>184.1
C18:0 DHSM	>C17:0 SM<	ESI	733.8>184.1
C20:0 DHSM	>C17:0 SM<	ESI	761.9>184.1
C22:0 DHSM	>C17:0 SM<	ESI	799.9>184.1
C24:1 DHSM	>C17:0 SM<	ESI	815.9>184.1
C24:0 DHSM	>C17:0 SM<	ESI	817.9>184.1
C26:1 DHSM	>C17:0 SM<	ESI	843.9>184.1
C26:0 DHSM	>C17:0 SM<	ESI	845.9>184.1
28:0 PC	>34:0 PC<	ESI	678.5>184.1
30:0 PC	>34:0 PC<	ESI	706.6>184.1
30:1 PC	>34:0 PC<	ESI	704.5>184.1
32:0 PC	>34:0 PC<	ESI	734.6>184.1
32:1 PC	>34:0 PC<	ESI	732.6>184.1
34:0 PC		ESI	762.5>184.1
34:1 PC	>34:0 PC<	ESI	760.6>184.1
34:2 PC	>34:0 PC<	ESI	758.6>184.1
36:0 PC	>34:0 PC<	ESI	790.7>184.1
36:1 PC	>34:0 PC<	ESI	788.6>184.1
36:2 PC	>34:0 PC<	ESI	786.6>184.1
36:3 PC	>34:0 PC<	ESI	784.6>184.1

36:4 PC	>34:0 PC<	ESI	782.6>184.1
38:0 PC	>34:0 PC<	ESI	818.7>184.1
38:1 PC	>34:0 PC<	ESI	816.7>184.1
38:2 PC	>34:0 PC<	ESI	814.7>184.1
38:3 PC	>34:0 PC<	ESI	812.6>184.1
38:4 PC	>34:0 PC<	ESI	810.6>184.1
16:0 LPC	>17:0 LPC<	ESI	496.3>184.1
16:1 LPC	>17:0 LPC<	ESI	494.3>184.1
17:0 LPC		ESI	510.2>184.1
18:0 LPC	>17:0 LPC<	ESI	524.4>184.1
18:1 LPC	>17:0 LPC<	ESI	522.4>184.1
18:2 LPC	>17:0 LPC<	ESI	520.4>184.1
20:0 LPC	>17:0 LPC<	ESI	552.4>184.1
20:1 LPC	>17:0 LPC<	ESI	550.4>184.1
20:3 LPC	>17:0 LPC<	ESI	546.4>184.1
20:4 LPC	>17:0 LPC<	ESI	544.4>184.1
16:0 LPE	>17:1 LPE<	ESI	454.3>313.3
16:1 LPE	>17:1 LPE<	ESI	452.3>311.3
17:1 LPE		ESI	466.3>325.3
18:0 LPE	>17:1 LPE<	ESI	482.3>341.3
18:1 LPE	>17:1 LPE<	ESI	480.3>339.3
18:2 LPE	>17:1 LPE<	ESI	478.3>337.3
20:4 LPE	>17:1 LPE<	ESI	502.3>361.3
14:1 LPG	>17:1 LPG<	ESI	455.3>283.2
16:1 LPG	>17:1 LPG<	ESI	483.3>311.2
17:1 LPG		ESI	497.3>325.2
16:0 LPS	>17:1 LPS<	ESI	498.3>313.3
17:1 LPS		ESI	510.3>325.3
18:0 LPS	>17:1 LPS<	ESI	526.3>341.3
18:2 LPS	>17:1 LPS<	ESI	522.3>337.3
Lyso-PAF	>17:0 LPC<	ESI	482.3>104.2

Unpublished additional data:

4.7.1. Materials and methods

All results are presented as explained in the materials and methods section of the publication. The only variations are the samples utilised for lipid profiling, the collection method, and the processing method for tandem mass spectrometry. All the differences are explained below in separate sections.

4.7.1.1. Samples collection for lipid analysis

Conditioned media from hippocampal primary neurones (12 DIV) and conditioned media from glial cells were harvested and collected into transparent glass centrifuge tubes (Corning) after 3 h and 12 h with and without $A\beta_{(1–40)}$ and $A\beta_{(1–42)}$ treatment. The conditioned media were centrifuged for 10 min at (300× g) at 4°C, and the supernatant was collected in new glass tubes, snap frozen and stored at -80°C for further analysis.

4.7.1.2. Tandem mass spectrometry

Lipid analyses were performed using lipid chromatography coupled to tandem MS. Lipids were extracted as previously described (Sundaram et al., 2012). Briefly, 1 mL of conditioned media was directly transferred into glass centrifuge tubes. After addition of 10 µL of the internal standard (30 µM of C17-lysophosphatidylcholine (C17-LPC), C15-ceramide (C15-Cer), C17-sphingosine (C17-So), C34:0 phosphatidylcholine (PC 17:0/17:0), C17-sphingomyelin (C17-SM), C34:0 phosphatidylserine (PS 17:0/17:0), C17-lysophosphatidylserine (C17-LPS), C17-lysophosphatidylethanolamine (C17-LPE), 10 µM C17-sphingosine 1-phosphate (C17-So1P), all from Avanti Polar Lipids, Alabaster, AL, USA, and 1 mM ergosterol from Merck), 200 µL 6 N HCl, 1 mL methanol and 2 mL $CHCl_3$ were also added. Samples were vigorously vortexed for 10 min. After centrifugation at 1900× g, the lower $CHCl_3$ phase was collected. Extraction was repeated with an additional 2 mL of $CHCl_3$, and the two $CHCl_3$ phases were combined and evaporated using the SpeedVac RVC 2–25 CDplus (Christ, Osterode, Germany). Samples were resuspended in 100 µL methanol: $CHCl_3$ (4:1 v/v) and analysed using the Prominence high-performance liquid chromatography (HPLC) system (Shimadzu, Duisburg, Germany) with a 60 mm × 2 mm MultoHigh 100 RP 18 column with 3 µm particle size (CS-Chromatographie Service, Langerwehe, Germany), which was maintained at 50 °C. The mobile phase A consisted of 1% (v/v) formic acid in ddH_2O, and the mobile phase B of 100% methanol. The column was equilibrated in 10% B with a flow rate of 0.5 mL min^{-1}. The mobile phase switched to 100%

B after sample injection. The flow rate increased linearly from 0.5 mL min^{-1} at 5 min to 1.0 mL min^{-1} at 7 min and remained constant until 10 min. Subsequently, the mobile phase changed to 10% B, and the flow rate decreased linearly from 1.0 mL min^{-1} at 10 min to 0.5 mL min^{-1} at 10.5 min and remained constant until the end of the program at 11.3 min. Detection took place between 2 and 10 min. The injection volume per sample was 10 µL, and samples were cooled to 4 °C. The HPLC system was coupled to the API 2000 triple-quadrupole mass spectrometer (Sciex, Foster City, CA, USA) equipped either with an ESI or an APCI source (Table S7), both operating in positive mode under the following source parameters: source temperature 450 °C, curtain gas 40, collision gas “low”, ion spray voltage 5500, ion source gas 1 60 (APCI: 30), ion source gas 2 30 (APCI: 60). The analytical results were quantified with Analyst 1.6.2 (AB Sciex, Forster City, CA, USA) based on internal standard samples and an external standard curve.

4.7.2. Specific identification of various lipid isoforms after $A\beta_{(1–40)}$ and $A\beta_{(1–42)}$ treatment from conditioned media of hippocampal neurones and conditioned media of glial cells using tandem mass spectrometry analysis

To further explore whether $A\beta_{(1–40)}$ and $A\beta_{(1–42)}$ also influence specific sphingolipids or glycerophospholipids isoforms, we analysed the conditioned media from hippocampal neurones at DIV 12, as well as from conditioned media of glial cells at 3 h and 12 h post-treatment with $A\beta_{(1–40)}$ and $A\beta_{(1–42)}$. These samples were subsequently analysed using tandem MS. This study presents a characterisation of the altered lipid isoforms in the conditioned media of hippocampal neurones and conditioned media of glial cells following 3 h and 12 h of treatment with $A\beta_{(1–40)}$ and $A\beta_{(1–42)}$ treatment. Our focus includes sphingolipids such as Cer, DHCer, LacCer, HexCer, So, Sa, Sa1P, So1P, SPC, SM, DHSM, as well as (lyso-) glycerophospholipids such as PC, LPC, LPE, LPG, LPS, Lyso-PAF (Figure 28, Figure 29 and Figure 30). All results are presented as explained in the materials and methods section of the publication, with the only variation being the samples utilised for lipid profiling. In this instance, we used conditioned media fractions derived from primary hippocampal neurones and glial cells. This conditioned media was obtained after treating the primary hippocampal neurones and glial cells with and without $A\beta_{(1–40)}$ and $A\beta_{(1–42)}$. In this instance, we used conditioned media fractions derived from primary hippocampal neurones and glial cells. This conditioned media was obtained after treating the primary hippocampal neurones and glial cells with and without $A\beta_{(1–40)}$ and $A\beta_{(1–42)}$.

4.7.2.1. Ceramides (Cer)

Substantial changes in Cer isoforms were observed in both conditioned media from hippocampal neurones and glial cells after 3 h and 12 h $A\beta_{(1–40)}$ and $A\beta_{(1–42)}$ treatments (Figure 28). Notably, C16 Cer showed a prominent reduction after 3 h $A\beta_{(1–42)}$, while there was a substantial increase following 12 h of $A\beta_{(1–40)}$ and $A\beta_{(1–42)}$ exposure in the conditioned media of the treated neurones. C18:1 Cer, C20 Cer and C24:1 Cer showed an increase after 3 h and 12 h of $A\beta_{(1–40)}$ and $A\beta_{(1–42)}$ in conditioned media of neurones (Figure 28). Additionally, C14 Cer, C18:1 Cer, C18:0 Cer, C24:1 Cer, and C24 Cer all demonstrated an increase in the conditioned media from neurones treated with $A\beta_{(1–40)}$ and $A\beta_{(1–42)}$ after 3 h. C22 Cer only increased in the conditioned media after 3 h $A\beta_{(1–40)}$-treated neurones (Figure 28).

In the conditioned media from glial cells treated with $A\beta_{(1–40)}$ and $A\beta_{(1–42)}$, a prominent increase in C14 Cer was observed after 12h. After 12 h, conditioned media from $A\beta_{(1–40)}$-treated glial cells showed a weak reduction in C18:1 Cer, while a substantial increase was noted following 12 h of $A\beta_{(1–42)}$ treatment (Figure 28). A decrease in C24 Cer was observed after 3 h of $A\beta_{(1–40)}$ as well as after 12 h of $A\beta_{(1–40)}$ and $A\beta_{(1–42)}$ treatment in the conditioned media of the treated glial cells. Other Cer isoforms, including C16 Cer, C18:0 Cer; C20 Cer, C22 Cer and C24:1 Cer, did not show any discernible changes in the conditioned media from glial cells treated for 3 h or 12 h with $A\beta_{(1–40)}$ and $A\beta_{(1–42)}$ (Figure 28).

4.7.2.2. Dihydroceramides (DHCer)

In conditioned media of $A\beta_{(1–40)}$-treated glial cells, C16 DHCer, C20 DHCer, and C24:1 DHCer increased after 3 h of treatment. Conversely, C18:0 DHCer and C22 DHCer levels decreased in conditioned media of glial cells after 3 h of $A\beta_{(1–40)}$ treatment. After 3 h $A\beta_{(1–42)}$- and 12 h $A\beta_{(1–40)}$-treatment, a reduction in C14 DHCer was observed in the lipids of conditioned media from treated glial cells (Figure 28). After 12 h $A\beta_{(1–40)}$ treatment, C16 DHCer levels decreased, while increases in C20 DHCer, C24:1 DHCer and C24 DHCer were observed in conditioned media of glial cells. In conditioned media of glial cells, C20 DHCer and C22 DHCer showed a decline after 3 h of $A\beta_{(1–42)}$ treatment, followed by an increase after 12 h. Additionally, C24:1 DHCer increased after 3 h and 12 h $A\beta_{(1–40)}$ treatment. After 12 h $A\beta_{(1–42)}$, both C18:0 DHCer and C24:1 DHCer levels diminished in conditioned media of glial cells (Figure 28).

In conditioned media from hippocampal neurones treated with $A\beta_{(1–40)}$ and $A\beta_{(1–42)}$, a specific increase in C18:0 DHCer was observed after 3 h and 12h. Furthermore, an increase in C16 DHCer was observed in the conditioned media of neurones after 3 h $A\beta_{(1–40)}$ and after 12 h of $A\beta_{(1–40)}$ and $A\beta_{(1–42)}$ treatment (Figure 28). Conditioned media from neurones treated with $A\beta_{(1–40)}$ and $A\beta_{(1–42)}$ showed a decrease in DHCer isoforms (C14 DHCer, C22 DHCer and C24 DHCer) after 3 h and in DHCer isoforms (C20 DHCer, C24:1 DHCer, and C24 DHCer) after 12 h. Conditioned media of 3 h $A\beta_{(1–42)}$-treated neurones observed a decrease in the DHCer isoforms (C20 DHCer and C24:1) (Figure 28).

4.7.2.3. Lactosylceramides (LacCer)

Conditioned media from neurones treated with $A\beta_{(1–40)}$ and $A\beta_{(1–42)}$ exhibited a reduction in all LacCer isoforms after 3 h. After 12 h, the conditioned media from both $A\beta_{(1–40)}$- and $A\beta_{(1–42)}$-treated neurones showed a decrease in C16 LacCer and C24:1 LacCer (Figure 28). Conditioned media from $A\beta_{(1–40)}$-treated glial cells revealed a decrease after 3h and an increase after 12 h in C18:0 LacCer and C22 LacCer. For C16 LacCer, a decline was observed after 3h $A\beta_{(1–42)}$ and an increase after 12 $A\beta_{(1–40)}$ in conditioned media of glial cells. Additionally, the conditioned media from glial cells treated for 12 h with $A\beta_{(1–42)}$ demonstrated a reduction in the LacCer isoforms C22 LacCer and C24:1 LacCer, alongside an elevation in C18:0 LacCer. Furthermore, C24:1 LacCer decreased in the conditioned media of 3 h $A\beta_{(1–40)}$- and $A\beta_{(1–42)}$-treated glial cells (Figure 28).

4.7.2.4. Monohexosylceramides (HexCer)

After treatment with $A\beta_{(1–40)}$ and $A\beta_{(1–42)}$, several HexCer isoforms (C14 HexCer, C18:0 HexCer and C22 HexCer) in the conditioned media of 12 h-treated glial cells showed a substantial increase. Conversely, the conditioned media from glial cells treated for 3 h and 12 h exhibited a decrease in C24 HexCer. Notably, almost all other HexCer isoforms (C14 HexCer, C16 HexCer, C18:0 HexCer, C20 HexCer and C22 HexCer) showed a reduction in the conditioned media of 3h $A\beta_{(1–42)}$-treated glial cells. In the conditioned media of treated glial cells, a slight increase was observed in C16 HexCer after 12 h $A\beta_{(1–40)}$ and $A\beta_{(1–42)}$. Furthermore, a minor increase was seen in C14 HexCer after 3 h and C20 HexCer after 12 h in the conditioned media of $A\beta_{(1–40)}$ treated glial cells. Additionally, a minor decrease in C20 HexCer was seen in the conditioned media of 3 h $A\beta_{(1–40)}$-treated glial cells (Figure 28).

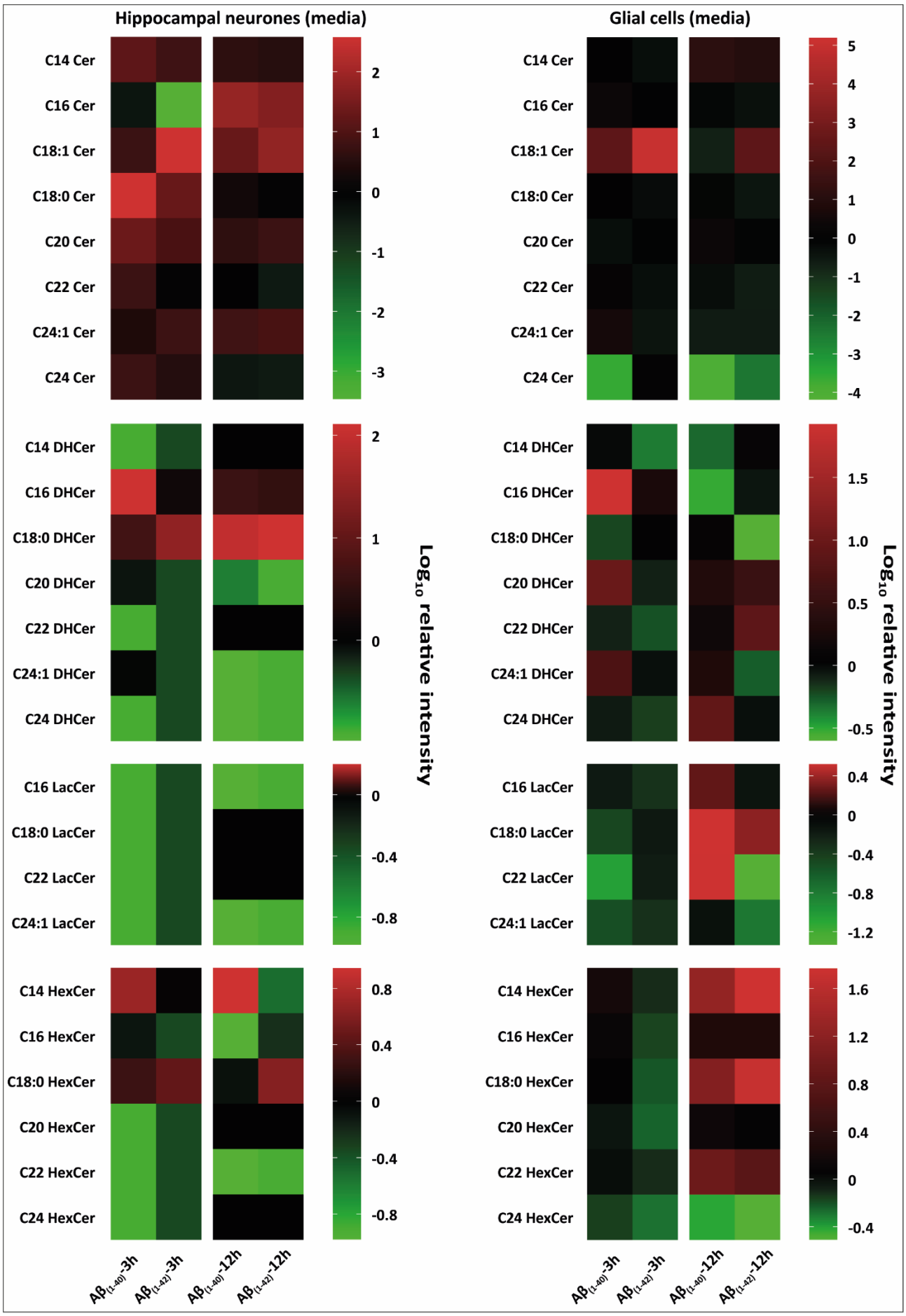
Hippocampal neurones (media)
Glial cells (media)
C14 Cer
C16 Cer
C18:1 Cer
C18:0 Cer
C20 Cer
C22 Cer
C24:1 Cer
C24 Cer
C14 DHCer
C16 DHCer
C18:0 DHCer
C20 DHCer
C22 DHCer
C24:1 DHCer
C24 DHCer
C16 LacCer
C18:0 LacCer
C22 LacCer
C24:1 LacCer
C14 HexCer
C16 HexCer
C18:0 HexCer
C20 HexCer
C22 HexCer
C24 HexCer
Log10 relative intensity
Aβ(1-40)-3h
Aβ(1-42)-3h
Aβ(1-40)-12h
Aβ(1-42)-12h

Figure 28: *Heat-map-based mass spectrometry analysis of sphingolipid classes from conditioned media of hippocampal neurones and glial cells after 3 h and 12 h Aβ treatment.*
Here, we conducted a comprehensive examination of different sphingolipid isoforms: ceramides (Cer), dihydroceramides (DHCer), lactosylceramides (LacCer), and monohexosylceramides (HexCer) after 3 h and 12 h treatment with (1 µM) $Aβ_{(1–40)}$ and (1 µM) $Aβ_{(1–42)}$ from conditioned media of hippocampal neurons at DIV 12 and conditioned media of glial cells (all groups, from three independent experiments (n = 3)). The changes of these lipid classes are shown as logarithmic (log_{10}) relative intensity (arbitrary unit); the green colour refers to a reduction, and the red colour refers to an increase of lipid levels compared to our negative control (DMSO), which was set to 0 as baseline. Both conditioned media of hippocampal neurones and conditioned media of glial cells showed an increased and reduced intensity of Cer, DHCer, LacCer, and HexCer isoforms after both 3 h and 12 h $Aβ_{(1–40)}$ and $Aβ_{(1–42)}$ treatment. Different changes in the lipid classes are shown between conditioned media of treated hippocampal neurones and glial cells. Conditioned media of Aβ-treated hippocampal neurones and conditioned media of Aβ-treated glial cells showed prominent increases and decreases in Cer, DHCer, LacCer and HexCer isoforms after 3 h and 12 h of $Aβ_{(1–40)}$ and $Aβ_{(1–42)}$ treatment. Conditioned media of Aβ-treated hippocampal neurones showed only a prominent intensity decrease of LacCer isoforms after 3 h and 12 h of $Aβ_{(1–40)}$ and $Aβ_{(1–42)}$ treatment.

After $Aβ_{(1–40)}$ and $Aβ_{(1–42)}$ treatment, HexCer isoforms (C16 HexCer, C20 HexCer and C24 HexCer) from 3 h and HexCer isoforms (C16 HexCer and C22 HexCer) from 12 h is reduced in the conditioned media of treated neurones. In contrast, conditioned media from 3 h treated neurones showed increased C18:0 HexCer for both $Aβ_{(1–40)}$ and $Aβ_{(1–42)}$ treament. C14 HexCer levels increased in the conditioned media from neurones exposed to $Aβ_{(1–40)}$ for 3 h and 12 h. After 12 h $Aβ_{(1–42)}$ treatment, we observed a reduction in C14 HexCer and an elevation in C18:0 HexCer from conditioned media of treated primary neurones (Figure 28).

4.7.2.5. Sphingosine (So) and sphingosine-1-phosphate (So1P)

Conditioned media derived from $Aβ_{(1–40)}$-and $Aβ_{(1–42)}$-treated hippocampal neurones showed a prominent increase in d18:1 So1P after 3 h followed by a decrease after 12h. In contrast, the conditioned media from glial cells treated with $Aβ_{(1–42)}$ for 3 h and $Aβ_{(1–40)}$ for 12 h showed decreased d18:1 So1P. The conditioned media of neurones showed intriguingly minor changes in d18:1 So after both 3 h and 12 h $Aβ_{(1–40)}$ and $Aβ_{(1–42)}$ treatments. Conversely, the conditioned media of treated glial cells showed an eminent increase in d18:1 So after 12 h $Aβ_{(1–40)}$ treatment, alongside a decrease after 3 h of both $Aβ_{(1–40)}$ and $Aβ_{(1–42)}$ treatments (Figure 29).

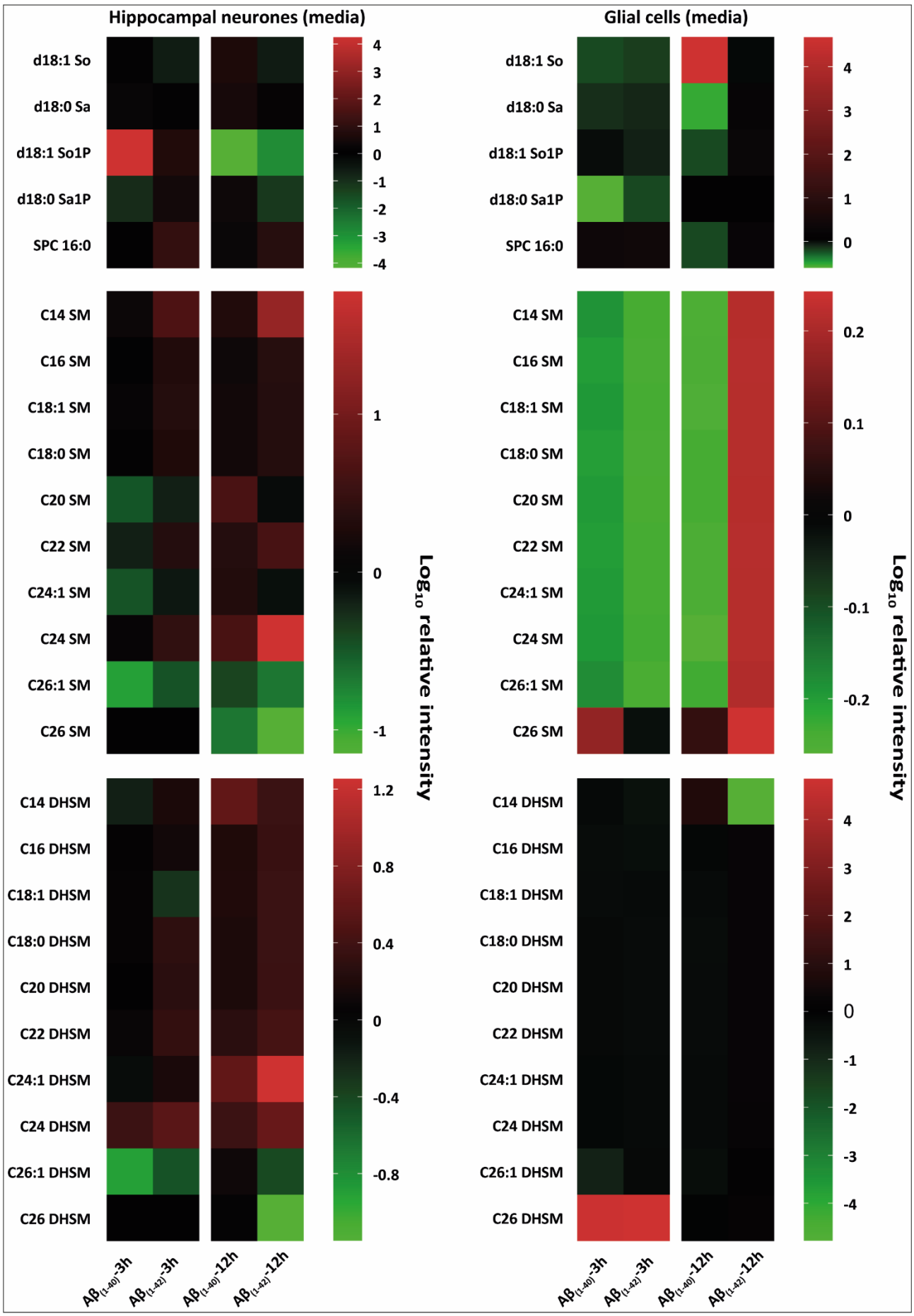
Hippocampal neurones (media)
Glial cells (media)
d18:1 So
d18:0 Sa
d18:1 So1P
d18:0 Sa1P
SPC 16:0
C14 SM
C16 SM
C18:1 SM
C18:0 SM
C20 SM
C22 SM
C24:1 SM
C24 SM
C26:1 SM
C26 SM
C14 DHSM
C16 DHSM
C18:1 DHSM
C18:0 DHSM
C20 DHSM
C22 DHSM
C24:1 DHSM
C24 DHSM
C26:1 DHSM
C26 DHSM
Aβ(1-40)-3h
Aβ(1-42)-3h
Aβ(1-40)-12h
Aβ(1-42)-12h
Log10 relative intensity

Figure 29: *Heat-map-based mass spectrometry analysis of sphingophospholipid classes from conditioned media of hippocampal neurones and glial cells after 3 h and 12 h Aβ treatment.*
Here, we examined different sphingophospholipid isoforms; sphingosine (d18:1 So), sphinganine (d18:0 Sa), sphingosine-1-phosphate (d18:1 So1P), sphinganine-1-phosphate (d18:1 Sa1P), sphingosylphosphoryl-choline (SPC (16:0)), sphingomyelines (SM) and dihydrosphingomyelines (DHSM) after 3 h and 12 h treatment with (1 µM) $Aβ_{(1–40)}$ and (1 µM) $Aβ_{(1–42)}$ from conditioned media of hippocampal neurones at DIV 12 and conditioned media of glial cells (all groups, from three independent experiments (N = 3)). Changes in these lipid classes are shown as logarithmic (log10) relative intensity (arbitrary unit); the green colour refers to a reduction, and the red colour refers to an increase in lipid levels compared to our negative control (DMSO), which was set to 0 as a baseline. Significant intensity changes in lipid classes of d18:1 So, d18:0 Sa, d18:1 So1P, d18:1 Sa1P after 3 h and 12 h $Aβ_{(1–40)}$ and $Aβ_{(1–42)}$ treatment in conditioned media of hippocampal neurones and conditioned media of glial cells were observed. Specific lipid intensity changes after $Aβ_{(1–40)}$ and $Aβ_{(1–42)}$ treatment in conditioned media of hippocampal neurones from very long fatty acid SM compared to conditioned media of Aβ-treated glial cells were detected.

4.7.2.6. Sphinganine (Sa) and sphinganine-1-phosphate (Sa1P)

A reduction in d18:0 Sa was observed in the conditioned media of glial cells after 3 h $Aβ_{(1–40)}$ and $Aβ_{(1–42)}$, as well as 12 h $Aβ_{(1–40)}$ treatment (Figure 29). In contrast, the conditioned media of hippocampal neurones showed a slight increase in d18:0 Sa after 12 h $Aβ_{(1–40)}$ treatment. Additionally, a decrease in d18:0 Sa1P was observed in the conditioned media from both 3 h $Aβ_{(1–40)}$- and 12 h $Aβ_{(1–42)}$-treated hippocampal neurones, as well as conditioned media from 3 h $Aβ_{(1–40)}$- and $Aβ_{(1–42)}$-treated glial cells. No substantial alterations were observed in d18:0 Sa1P in conditioned media after 12 h $Aβ_{(1–40)}$-and $Aβ_{(1–42)}$-treated glial cells, nor in conditioned media after 3 h $Aβ_{(1–42)}$- and 12 h $Aβ_{(1–40)}$-treated hippocampal neurones (Figure 29).

4.7.2.7. Sphingosylphosphorylcholine (SPC)

Both conditioned media from hippocampal neurones and glial cells exhibited changes in SPC 16:0 after 3 h and 12 h of treatment with $Aβ_{(1–42)}$ as well as 12 h $Aβ_{(1–40)}$ treatment. Notably, the most prominent increase in SPC 16:0 was observed in the conditioned media of neurones after 3 h and 12 h $Aβ_{(1–42)}$ treatment. In contrast, a decrease in SPC 16:0 was shown in the conditioned media of glial cells after 12 h of $Aβ_{(1–40)}$ treatment (Figure 29). No significant changes in SPC 16:0 were detected in the conditioned media from neurones after 3 h and 12 h $Aβ_{(1–40)}$ treatment. Furthermore, there were no specific alterations in SPC 16:0 in the conditioned media from glial cells treated for 3 h with either $Aβ_{(1–40)}$ or $Aβ_{(1–42)}$, as well as after 12 h of treatment with $Aβ_{(1–42)}$ (Figure 29).

4.7.2.8. Sphingomyelines (SM)

The following SM isoforms, including C14 SM, C16 SM, C18:1 SM, C18:0 SM, C20 SM, C22 SM, C24:1 SM, C24 SM, and C26:1 SM, derived from the conditioned media of glial cells, exhibited a decrease after 3 h and 12h of treatment with $A\beta_{(1–40)}$ as well as 3 h $A\beta_{(1–42)}$ treatment. Interestingly, 12 h $A\beta_{(1–42)}$ treatment increased these isoforms (Figure 29). In contrast, specific SM isoforms (C14 SM, C16 SM, C18:1 SM, C18:0 SM, C24 SM) from the conditioned media of hippocampal neurones showed an increase after both 3 h and 12 h $A\beta_{(1–42)}$ treatment (Figure 29). Both C20 SM and C24:1 SM showed an increase after 12 h $A\beta_{(1–40)}$ and a decrease after 3 h $A\beta_{(1–40)}$ and $A\beta_{(1–42)}$ in conditioned media of neurones.

Furthermore, conditioned media of neurones observed an increase in C22 SM and C24 SM after 3 h $A\beta_{(1–42)}$ and after 12 h $A\beta_{(1–40)}$ and $A\beta_{(1–42)}$ treatment. However, a reduction in C22 SM was seen in the conditioned media of neurones treated with $A\beta_{(1–40)}$ for 3 h (Figure 29). C26:1 SM showed a prominent reduction in the conditioned media of 3h and 12 h $A\beta_{(1–40)}$- and $A\beta_{(1–42)}$-treated hippocampal neurones. Similarly, C26 SM showed a pronounced decrease in the conditioned media of 12 h $A\beta_{(1–40)}$- and $A\beta_{(1–42)}$-treated hippocampal neurones. Conditioned media from 3 h $A\beta_{(1–40)}$ and 12 h $A\beta_{(1–42)}$ treated glial cells exhibited elevated levels of C26 SM, while no specific alterations were observed in the conditioned media of 3 h $A\beta_{(1–42)}$-and 12 h $A\beta_{(1–40)}$-treated glial cells. Lastly, no changes in C26 SM were detected in the conditioned media of 3h $A\beta_{(1–40)}$-and $A\beta_{(1–42)}$-treated neurones (Figure 29).

4.7.2.9. Dihydrosphingomyelines (DHSM)

The most prominent increase in DHSM levels in the conditioned media of glial cells was observed in C26 DHSM after 3 h $A\beta_{(1–40)}$ and $A\beta_{(1–42)}$ treatment. In contrast, C14 DHSM exhibited a substantial reduction after 12 h $A\beta_{(1–42)}$, with only a slight increase observed after 12 h $A\beta_{(1–40)}$ (Figure 29). Additionally, an increase in various DHSM isoforms (C14 DHSM, C16 DHSM, C18:1 DHSM, C18:0 DHSM, C20 DHSM, C22 DHSM, C24:1 DHSM, C24 DHSM) was detected in the conditioned media of hippocampal neurones after 12 h $A\beta_{(1–40)}$ and $A\beta_{(1–42)}$ treatment. Moreover, conditioned media from hippocampal neurones showed an increase in DHSM isoforms (C14 DHSM, C16 DHSM, C18:0 DHSM, C20 DHSM, C22 DHSM, C24:1 DHSM, C24 DHSM) after 3 h $A\beta_{(1–42)}$ and in C24 DHSM after 3h $A\beta_{(1–40)}$ treatment (Figure 29). However, there was a reduction in DHSM isoforms (C14 DHSM and C24:1 DHSM) after 3 h $A\beta_{(1–40)}$ treatment, and a decrease in C18:1 DHSM was observed after 3 h $A\beta_{(1–42)}$ treatment in the conditioned media of hippocampal neurones. Furthermore, conditioned media from hippocampal neurones showed a prominent decrease in C26:1

DHSM after 3h $A\beta_{(1–40)}$-and $A\beta_{(1–42)}$-treatment, alongside reductions in both C26:1 DHSM and C26 DHSM after 12 h $A\beta_{(1–42)}$ treatment (Figure 29).

4.7.2.10. Phosphatidylcholines (PC) and lysophosphatidylcholines (LPC)

A prominent increase in PC (30:1) and PC (38:0) of conditioned media from glial cells after 3 h $A\beta_{(1–40)}$- and $A\beta_{(1–42)}$-treatment. In addition to PC (38:1), several other PC isoforms (PC (28:0), PC (30:0), PC (32:0), PC (32:1), PC (34:1), PC (34:2), PC (36:0), PC (36:1), PC (36:2), PC (36:3), PC (38:2), PC (38:3) and PC (38:4)) exhibited a decrease in the conditioned media of 3 h $A\beta_{(1–40)}$- or $A\beta_{(1–42)}$-treated glial cells (Figure 30). Notably, PC (28:0) showed a decrease after 12h $A\beta_{(1–40)}$ and an increase after 12h $A\beta_{(1–42)}$ from conditioned media of treated glial cells. All other PC isoforms (PC (30:0), PC (30:1), PC (32:0), PC (32:1), PC (34:1), PC (34:2), PC (36:1), PC (36:2), PC (36:3), PC (36:4), PC (38:1), PC (38:2), PC (38:3) and PC (38:4)) showed an increase in the conditioned media after 12 h $A\beta_{(1–40)}$- or $A\beta_{(1–42)}$-treated glial cells (Figure 30).

Alterations in PC isoforms were observed in the conditioned media from hippocampal neurones after 3 h and 12 h $A\beta_{(1–40)}$ and $A\beta_{(1–42)}$ treatment. After 3h, the most prominent decrease were detected in PC isoforms (PC (28:0), PC (30:1) and PC (38:0)) with $A\beta_{(1–42)}$ treatment, while an increase in PC isoforms (PC (38:1), PC (38:2) and PC (38:3)) was seen in the conditioned media of both $A\beta_{(1–40)}$- and $A\beta_{(1–42)}$-treated hippocampal neurones (Figure 30).

After 12 h $A\beta_{(1–42)}$ treatment, there was a reduction in the following PC isoforms: PC (28:0), PC (30:0), PC (30:1), PC (32:0), PC (32:1), PC (34:1), PC (34:2), PC (36:0), PC (36:1), PC (36:2), PC (36:3), PC (38:3), and PC (38:4). In contrast, PC isoforms (PC (38:0), PC (38:1) and PC (38:2)) saw an increase after the same duration of $A\beta_{(1–42)}$ treatment in the conditioned media of hippocampal neurones (Figure 30). After both 3 h and 12 h $A\beta_{(1–40)}$ treatment, a slight elevation of PC (36:4) and PC (38:0) was detected in the conditioned media of treated hippocampal neurones (Figure 30).

We observed alterations in nearly all LPC isoforms in the conditioned media after 3 h and 12h $A\beta_{(1–40)}$- and $A\beta_{(1–42)}$- treated glial cells and hippocampal neurones. The conditioned media of hippocampal neurones showed the most prominent decrease in LPC (20:0) after 12 h $A\beta_{(1–40)}$ treatment, as well as in LPC (20:3) after 3 h $A\beta_{(1–40)}$ and $A\beta_{(1–42)}$ treatment (Figure 30). Conversely, conditioned media from neurones demonstrated a substantial

increase in several LPC isoforms (LPC (18:2), LPC (20:1), LPC (20:3) and LPC (20:4)) after 12 h $A\beta_{(1–40)}$ treatment, as well as in LPC isoforms (LPC (18:2) and PC (20:1)) after 3 h $A\beta_{(1–40)}$ and $A\beta_{(1–42)}$ treatment (Figure 30). Additionally, LPC (20:0) and LPC (20:4) showed a reduction in the conditioned media after 3 h $A\beta_{(1–40)}$-treated neurones. Other LPC isoforms (LPC (16:0), LPC (16:1), LPC (18:0), LPC (18:1)) showed a modest increase in the conditioned media of hippocampal neurones after 12 h $A\beta_{(1–40)}$ treatment (Figure 30). Conditioned media of glial cells revealed a prominent increase in LPC (20:0) and LPC (20:1) after 3 h $A\beta_{(1–40)}$ and $A\beta_{(1–42)}$, while a decrease was observed in LPC (16:0) after 3 h $A\beta_{(1–40)}$ and $A\beta_{(1–42)}$ as well as in LPC (18:1) after 3h $A\beta_{(1–40)}$ treatment. Additionally, LPC (20:1) showed an elevation in the conditioned media after 12h $A\beta_{(1–40)}$-and $A\beta_{(1–42)}$-treated glial cells (Figure 30).

4.7.2.11. Lysophosphatidylethanolamine (LPE)

An increase in LPE isoforms (LPE (16:1), LPE (18:0), LPE (18:1) and LPE (18:2)) was shown in conditioned media after 3 h $A\beta_{(1–42)}$-treated hippocampal neurones. Additionally, an increase in conditioned media of hippocampal neurones after 3h $A\beta_{(1–40)}$ in LPE (18:0) and after 12 h $A\beta_{(1–40)}$ in LPE (20:4) was observed. Notably, LPE (20:4) revealed a slight decrease after 3 h $A\beta_{(1–40)}$ treatment and a prominent reduction after 12 h $A\beta_{(1–42)}$ treatment in conditioned media of hippocampal neurones (Figure 30). LPE (18:2) showed a prominent reduction after 3 h $A\beta_{(1–40)}$ as well as 12 h $A\beta_{(1–40)}$ and $A\beta_{(1–42)}$ treatment in conditioned media of hippocampal neurones. Furthermore, all other LPE isoforms (LPE (16:0), LPE (16:1), LPE (18:1), LPE (18:2), and LPE (20:4)) exhibited a decrease in conditioned media after 12 h $A\beta_{(1–42)}$-treated neurones, whereas LPE (18:0) and LPE (18:2) showed a prominent reduction in conditioned media after 12 h $A\beta_{(1–40)}$-treated neurones (Figure 30).

Furthermore, an increase was observed in the following LPE isoforms (LPE (16:0), LPE (18:1), LPE (18:2), and LPE (20:4)) after 3 h $A\beta_{(1–40)}$ treatment, as well as in LPE isoforms (LPE (16:1), LPE (18:0) and LPE (20:4)) after 3 h $A\beta_{(1–42)}$ treatment in the conditioned media of glial cells. However, there was a slight reduction in LPE (16:1) after 3h $A\beta_{(1–40)}$ and in LPE (18:2) after 3 h $A\beta_{(1–42)}$ in the conditioned media of glial cells (Figure 30). After 12 h $A\beta_{(1–40)}$ and $A\beta_{(1–42)}$ treatment, the conditioned media from glial cells exhibited a prominent decrease in LPE isoforms (LPE (16:1) and LPE (18:0)), while LPE isoforms (LPE (16:0) and LPE (18:2) showed an increase. Additionally, there was reduction in LPE (18:1) after 12 h $A\beta_{(1–42)}$ treatment, as well as an increase in LPE (20:4) after 12 h $A\beta_{(1–40)}$ treatment (Figure 30).

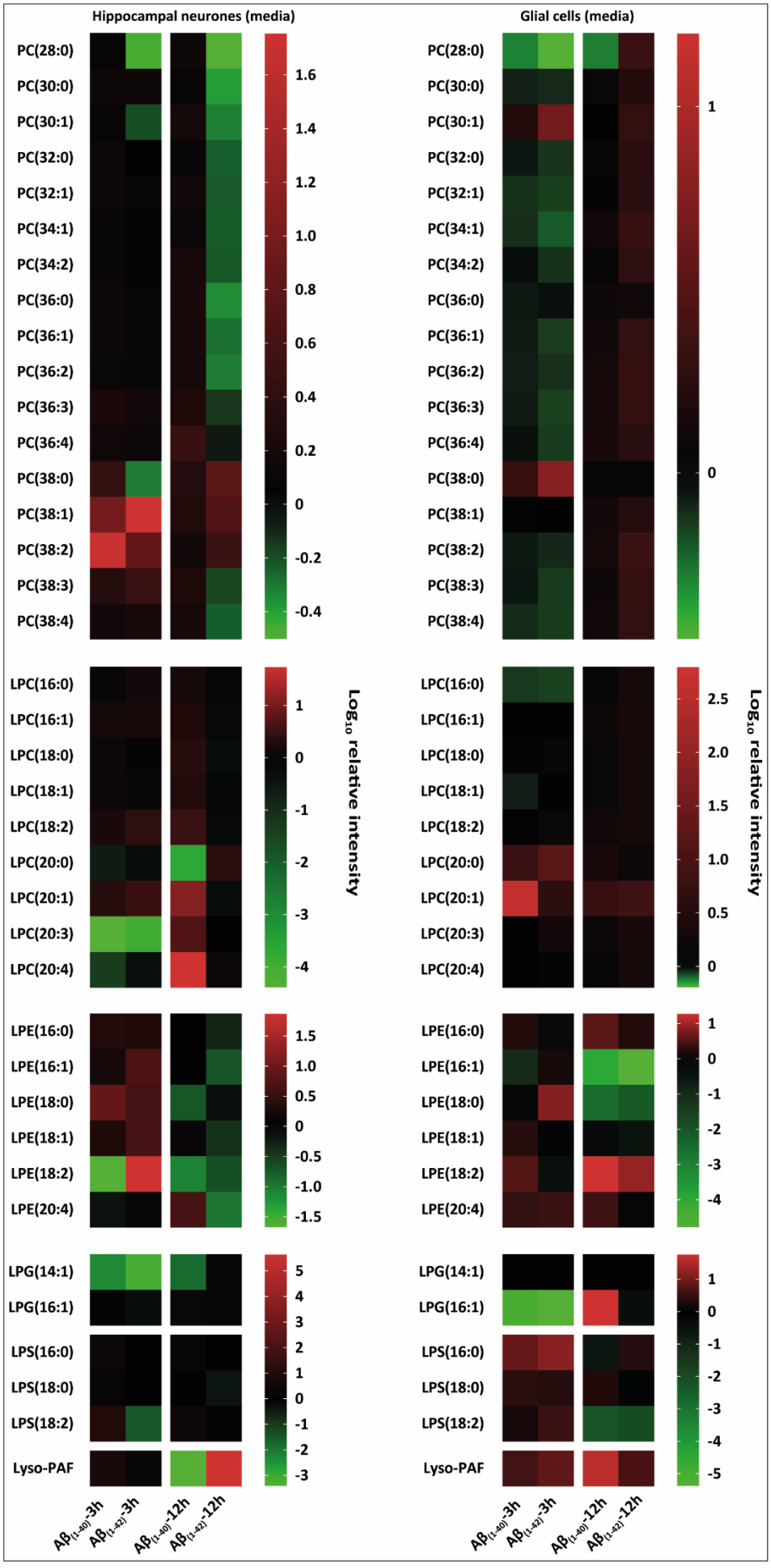
Hippocampal neurones (media)
Glial cells (media)
PC(28:0)
PC(30:0)
PC(30:1)
PC(32:0)
PC(32:1)
PC(34:1)
PC(34:2)
PC(36:0)
PC(36:1)
PC(36:2)
PC(36:3)
PC(36:4)
PC(38:0)
PC(38:1)
PC(38:2)
PC(38:3)
PC(38:4)
1.6
1.4
1.2
1.0
0.8
0.6
0.4
0.2
0
-0.2
-0.4
1
0
LPC(16:0)
LPC(16:1)
LPC(18:0)
LPC(18:1)
LPC(18:2)
LPC(20:0)
LPC(20:1)
LPC(20:3)
LPC(20:4)
1
0
-1
-2
-3
-4
2.5
2.0
1.5
1.0
0.5
0
Log10 relative intensity
LPE(16:0)
LPE(16:1)
LPE(18:0)
LPE(18:1)
LPE(18:2)
LPE(20:4)
1.5
1.0
0.5
0
-0.5
-1.0
-1.5
1
0
-1
-2
-3
-4
LPG(14:1)
LPG(16:1)
LPS(16:0)
LPS(18:0)
LPS(18:2)
Lyso-PAF
5
4
3
2
1
0
-1
-2
-3
-4
-5
Aβ(1-40)-3h
Aβ(1-42)-3h
Aβ(1-40)-12h
Aβ(1-42)-12h

Figure 30: *Heat map-based mass spectrometry analysis of glycerophospholipid classes from conditioned media of hippocampal neurones and glial cells after 3 h and 12 h Aβ treatment.*
Here, we examined different glycerophospholipids isoforms: phosphatidylcholine (PC), lysophosphatidylcholine (LPC), lysophosphatidylethanolamine (LPE), lysophosphatidylglycerol (LPG), lysophosphatidylserine (LPS), and lyso-platelet-activating factor (lyso-PAF) after 3 h and 12 h treatment with (1 µM) $Aβ_{(1–40)}$ and (1 µM) $Aβ_{(1–42)}$ from conditioned media of hippocampal neurones at DIV 12 and conditioned media of glial cells (all groups, from three independent experiments (N = 3)). Changes in these lipid classes are shown as logarithmic (log_{10}) relative intensity (arbitrary unit); the green colour refers to a reduction, and the red colour refers to an increase in lipid levels compared to our negative control (DMSO), which was set to 0 as baseline. Conditioned media of hippocampal neurones and conditioned media of glial cells showed a prominent decrease and increase in intensity changes after 3 h and 12 h $Aβ_{(1–40)}$ and $Aβ_{(1–42)}$ treatment from PC, LPC, and LPE isoforms. Also, LPG, LPS isoforms and lyso-PAF showed specific changes after 3 h and 12 h $Aβ_{(1–40)}$ and $Aβ_{(1–42)}$ treatment in both conditioned media of hippocampal neurones and glial cells.

4.7.2.12. Lysophosphatidylglycerol (LPG)

LPG (14:1) showed a prominent reduction after 3 h $Aβ_{(1–40)}$ and $Aβ_{(1–42)}$ in conditioned media of hippocampal neurones. In contrast, a similar effect was observed for LPG (16:1) in conditioned media of treated glial cells. After 12 h, $Aβ_{(1–40)}$ treatment resulted in a decrease in LPG (14:1) levels in the conditioned media from neurones, while LPG (16:1) levels increased in the conditioned media of treated glial cells (Figure 30). No notable changes were observed in LPG (14:1) levels in the conditioned media of glial cells after 3 h and 12 h for both $Aβ_{(1–40)}$ and $Aβ_{(1–42)}$ treatment. Additionally, there was no specific alteration in LPG (16:1) levels in the conditioned media from neurones after 3h or 12 h for either Aβ treatment (Figure 30).

4.7.2.13. Lysophosphatidylserine (LPS)

LPS (18:2) exhibited an increase in conditioned media after 3 h $Aβ_{(1–40)}$- and $Aβ_{(1–42)}$-treated glial cells, as well as in conditioned media after 3 h $Aβ_{(1–40)}$-treated hippocampal neurones. However, a decrease in LPS (18:2) was observed in conditioned media after 3 h $Aβ_{(1–42)}$-treated hippocampal neurons and in conditioned media after 12h $Aβ_{(1–40)}$- and $Aβ_{(1–42)}$-treated glial cells(Figure 30). An increase in LPS (16:0) and LPS (18:0) was observed in conditioned media after 3 h $Aβ_{(1–40)}$- and $Aβ_{(1–42)}$-treated glial cells. LPS (16:0) was reduced in conditioned media after 12 h $Aβ_{(1–40)}$-treated glial cells, while LPS (16:0) after 12 h $Aβ_{(1–42)}$ treatment and LPS (18:0) after 12 h $Aβ_{(1–40)}$ treatment showed an increase in conditioned media of glial cells. Additionally, conditioned media from hippocampal neurones indicated a slight reduction in LPS (18:0) after 12 h $Aβ_{(1–42)}$ treatment (Figure 30).

4.7.2.14. Lyso-platelet-activating factor (Lyso-PAF)

Lyso-PAF showed a prominent increase in the conditioned media after 12 h $A\beta_{(1–42)}$-treated hippocampal neurones, as well as in conditioned media of glial cells after 3 h and 12 h, for both $A\beta_{(1–40)}$ and $A\beta_{(1–42)}$ treatment (Figure 30). Conversely, a prominent decrease in lyso-PAF was observed in the conditioned media after 12 h $A\beta_{(1–40)}$-treated hippocampal neurones (Figure 30). Additionally, the conditioned media of hippocampal neurones showed a weak enhancement in lyso-PAF levels after 3h $A\beta_{(1–40)}$ treatment (Figure 30).

5. Discussion

It is widely recognised that Aβ species may play a role in Aβ pathology associated with AD and other amyloid-related disorders (Findeis, 2007; Sadigh-Eteghad et al., 2015). Additionally, Aβ-induced toxicity, which leads to impairment in neuroplasticity and neuroinflammation, could enhance our understanding of AD. While several studies investigated the biochemical properties of Aβ, the precise pathological role of both $Aβ_{(1–40)}$ and $Aβ_{(1–42)}$ species on lipid homeostasis in hippocampal neurones and glial cells remains unclear (Cai et al., 2023; Chemuru et al., 2016; Hu et al., 2009; Klementieva et al., 2017; Takahashi et al., 2004). Nevertheless, current FDA-approved therapeutic drugs primarily address neurological behaviour and psychological symptoms, merely slowing down the progression of the disease (Therapeutics Search | ALZFORUM; Varadharajan et al., 2023). Herein, I would like to briefly mention Lecanemab (Leqembi®), a new monoclonal Aβ antibody which is FDA-approved and has received conditional approval in the European Union for treating mild cognitive impairment (memory and thinking problems) or mild dementia due to early AD (European Medicines Agency, 2024; Kim et al., 2025; van Dyck et al., 2023). This drug is also under revision for subcutaneous autoinjection in patients, which makes the patient's life more convenient (Eisai co. Ltd. & Biogen Inc., 2025). However, this drug only slows down the disease progression and does not cure or prevent the disorder. Considering the challenges associated with ineffective drug development, it is essential to investigate alternative mechanisms of AD that go beyond the conventional focus of the Aβ and Tau pathology (Morris et al., 2014).

Considering these findings, this thesis explores the pathological role of various Aβ species using both cellular (physiological and pathological) models and an AD transgenic mouse model. Additionally, we conducted preliminary testing of a potential novel synthetic N,N-tryptamine compound, such as DET, both *in vitro* and *in vivo,* concerning AD pathology. Our qualitative research focussed on the neuropathological characterisation of various Aβ-specific aggregations, neuroplasticity and neuroinflammation across various brain regions of the AD mice. Complementing this, we also performed quantitative research using various cellular and *in vivo* techniques. For the first time, we demonstrated that lipid profiles altered after Aβ treatment, even before synaptic loss became apparent (Van Bulck et al., 2022). The exogenous addition of Aβ species to primary brain cells revealed time-dependent impacts on active synapse values and lipid alterations. Treatment with pathological concentrations of $Aβ_{(1–40)}$ and $Aβ_{(1–42)}$ exhibited a species-dependent influence on the integrity of (extra-) cellular lipids in various brain cells (Van Bulck et al., 2022).

Furthermore, we provided initial evidence that DET administration might have a potential therapeutic effect on AD. However, it is important to note the significant limitations present in our study. Nonetheless, the current data offers preliminary insight into understanding early pathological patterns of AD (e.g., adult neurogenesis, lipid alterations and synaptic loss) and the potential for novel drugs to prevent or address AD-related disorders.

5.1. Qualitative analysis of neuropathological effects in AD models

5.1.1. Characterisation of Aβ aggregation and associated neuroinflammation

APP proteins, which have been described to play a crucial role in neuronal processes such as neurite growth, neuronal adhesion, synapto- and axongenesis, are key players in the development and maintenance of the nervous system (Baumkötter et al., 2014). The mature APP, consisting of 770 amino acids, and its cleavage fragments are crucial for determining the neuropathological role in AD (Kang et al., 1987; Müller & Zheng, 2012; Price et al., 1998). The use of specific antibodies to recognise specialised epitopes in APP and its cleavage fragments holds great promise in better understanding the Aβ pathology in genetically modified AD animal models. Various Aβ antibodies, which recognise specific epitopes of APP, have been widely used for the detection of APP and its Aβ cleavage peptide forms (Gouras et al., 2015; Gouras et al., 2010; Gouras et al., 2000; Klementieva et al., 2017; Roos et al., 2021; Takahashi et al., 2004; Takahashi et al., 2013; Tampellini et al., 2007; Willén et al., 2017).

Our studies observed that the Tg mice model exhibited specific $A\beta_{(1–42)}$-aggregates in the cortex starting at 4 months of age, while the entorhinal cortex and hippocampus showed such aggregates beginning at 9 months. Notably, in the hippocampus, Aβ plaque deposition (Aβ, C99, APP and sAPPα) was already detected in 4-month-old Tg mice. This observation aligns with previous research done by Ordóñez-Gutiérrez and colleagues, which noted early Aβ plaque deposition in Tg mice as young as 3 months. (Ordóñez-Gutiérrez et al., 2015). In contrast, other studies using different Aβ detection techniques in the same mouse model found that the earliest Aβ plaque deposition occurred at 4 months in the cortex and 6 months in the hippocampus (Jackson et al., 2013; Minkeviciene et al., 2008). These discrepancies in the research highlight the importance of the investigated methodologies and neuronal changes in Aβ pathology.

Moreover, exploring the size and number of specific $A\beta_{(1–42)}$ plaques across ageing could give us a better understanding of how these aggregates evolve within various brain regions.

However, we did not measure or quantify the size and number of $A\beta_{(1–42)}$ plaques due to issues with the mice population, the COVID-19 crisis and the research interests of Dr. Ana Perez Castillo's laboratory. Further investigation is necessary to clarify this matter. However, the observed regional differences in Aβ burden and Aβ density are influenced by the brain region and AD mice utilised in each study (Hanspal & Gillotin, 2022; Minkeviciene et al., 2009). Notably, our observation from Aβ fibrils and fibrillar oligomers may be more dispersed in the 9-12 months Tg mice compared to the distinct $A\beta_{(1–42)}$ plaques and Aβ plaques deposition. Our observations complement the earlier findings (Hanspal & Gillotin, 2022; Minkeviciene et al., 2009), suggesting a shift in Aβ deposition over time.

Lastly, the consistent findings of plaque-associated gliosis in the cortex and hippocampus of younger Tg mice reinforce the idea that Aβ accumulation might be linked to neuroinflammatory processes, a narrative supported by numerous studies (Jackson et al., 2013; Malm et al., 2007; Minkeviciene et al., 2008). The connection between early and later stages of Aβ aggregation and its impact on gliosis emphasises the specific dynamics of AD progression. Furthermore, studies demonstrated that several structural characteristics of Aβ and its aggregation forms could promote neuroinflammation (Chen et al., 2017; LaRocca et al., 2021).

5.1.2. Impaired neurogenesis and neuroinflammation

Alteration in adult neurogenesis is an early event in Familial AD observed in Tg mice, beginning at 2 months in both subventricular and subgranular zones (Demars et al., 2010). These observations align with our findings, suggesting that the proliferation of cells and neuroplasticity in the cortex and hippocampus might be diminished in Tg mice starting at 2 months. Another study indicates that progenitor cell proliferation is almost abolished by 6 months of age (Faure et al., 2011) and is consistent with our finding of a potential reduction in adult neurogenesis in subventricular and subgranular zones in our Tg mice. Furthermore, It has been reported that depletion of neurogenesis can lead to cognitive impairment in Tg mice (Hollands et al., 2017). Impaired neurogenesis has also been shown to increase hyperphosphorylated Tau levels in the hippocampus, while no effect was seen on oligomeric Aβ levels in the entorhinal cortex of Tg mice (Hollands et al., 2017).

To enhance our understanding of the mechanisms driving these changes, we are the first to describe a possible alteration of RELN expression concerning specific $A\beta_{(1–42)}$- and microglia-positive cells in the entorhinal cortex and hippocampus of ageing Tg mice

compared to WT littermates. Previous studies have established that the entorhinal cortex is an essential brain region directly linked to the hippocampus and is one of the earliest regions affected by AD (Gómez-Isla et al., 1996; Thal et al., 2000a; Witter, 2007). RELN, when studied in association with Aβ, has been found to have diminished expression in both mice and human AD brains (Botella-López et al., 2010; Cuchillo-Ibáñez et al., 2013; Cuchillo-Ibañez et al., 2016; Kocherhans et al., 2010). It has also been reported that Aβ interacts with layer II entorhinal cortical neurones, which are positive for RELN and are among the first to be impaired in AD (Kobro-Flatmoen et al., 2016). Furthermore, our Tg mice model has not yet explored the characterisation of $A\beta_{(1–42)}$ and neuroinflammation (e.g., microgliosis (Iba1) on neuroplasticity (e.g., RELN). This examination could provide critical insight into how disruptions in adult neurogenesis and RELN expression may contribute to the progression of cognitive deficits in AD.

The present study is subject to several pitfalls related to the available animal cohort and the experimental methodologies employed by the research group of Dr. Ana Perez Castillo's laboratory at that time. Additionally, the lockdown and restrictions resulting from the COVID-19 pandemic in Spain significantly disrupted experiments and limited access to research facilities. These problems caused incomplete datasets in our research findings. Furthermore, eradicating the mice colony due to viral infection in the research animal facility in Spain led to limited tissue samples and insufficient quantitative data sets. Therefore, further research is needed to validate the impaired neurogenesis related to neuroinflammation in this Tg mouse model. Future investigations should include an expanded sample size and incorporate supplementary analysis, such as protein and RNA quantitation across various age groups of these mice. This analysis could elucidate the underlying molecular mechanisms involved in neuroinflammation and neurogenesis, thereby better understanding the neurodegenerative ageing processes. Furthermore, conducting more detailed confocal imaging will be essential to deepen our understanding of the interrelationships among Iba1-$A\beta_{(1–42)}$, RELN-$A\beta_{(1–42)}$ and RELN-Iba1 positive cells. This might give us a better understanding of how neuroinflammation influences neurogenesis over time in the Aβ pathology.

5.1.3. Adult neurogenesis using neurospheres

We are the first to describe a potential application of neurospheres derived from the subventricular zone of normal-aged and Tg mice at approximately 16 months. Our findings

might suggest that adult neurogenesis and NSC differentiation of adult neurospheres may be affected when exposed to the pathological concentration of human $A\beta_{(1–40)}$ and $A\beta_{(1–42)}$.

Previous neurospheres research has shown that NSC can be isolated from adult mice from 1 to 18 months. Although, older mice exhibit a decrease in the number of neurospheres and an extended maturation time for these neurospheres (Daynac et al., 2016; Deshpande et al., 2019; Maslov et al., 2004; Radecki & Samanta, 2022; Wang et al., 2022). Only two studies have specifically investigated neurospheres derived from mice with the same APP/PSEN-1 mutation, utilising samples from embryonic stage 15 or 3-month-old mice (Esteve et al., 2022; Ghate et al., 2014). Both studies demonstrated the impact of Aβ concentration on adult neurogenesis (Esteve et al., 2022; Ghate et al., 2014). While our data may indicate the neurotrophic effect of $A\beta_{(1–40)}$ treatment on neurospheres from 16-month-old Tg, this observation requires further investigation.

As previously described, our study has several notable pitfalls arising from challenges with our mice colony and the experimental data yield. These limitations should be carefully considered to guide future research in the field. Our protocol for collecting neurospheres and characterising their phenotypes from older mice likely proposed a more effective *in vitro* approach for investigating adult neurogenesis in AD. However, it is essential to consider the disadvantages, advantages, and limitations associated with translating adult neurogenesis into human AD (da Silva Siqueira et al., 2021; Gillotin et al., 2021; Salta et al., 2023; Seki, 2020).

This study should be repeated with additional experimental datasets and human-derived AD cellular models to validate our previous findings. A recent review has highlighted the development and exploration of various three-dimensional human-derived AD cellular models, including spheroids, organoids, and assembloids, to investigate disease progression, specific disease phenotypes, and cellular and molecular mechanisms in AD (Cerneckis et al., 2023). These models might offer a promising alternative for enhancing the screening of diagnostics and therapeutic tools for AD. Also, these advanced three-dimensional models could better mimic human AD pathology.

5.2. Quantitative analysis of Aβ-induced neuropathology in mice brain cells

Here, we demonstrated for the first time that lipid profiles alter after post-treatment of Aβ species and before the appearance of synaptic loss in distinct Aβ-treated primary brain cells,

utilising various quantitative cellular approaches (Van Bulck et al., 2022). Our findings indicate that the exogenous administration of human Aβ species to primary neurones affects the yield of active synapses and induces lipid alterations in a time-dependent manner. Furthermore, we showed that treatment with $Aβ_{(1–40)}$ and $Aβ_{(1–42)}$ affects the integrity of cellular lipids in glial cells and hippocampal neurones, exhibiting in both species- and time-dependent variations (Van Bulck et al., 2022). In addition, extracellular lipid from glial cells and hippocampal neurones showed a similar alteration tendency after treatment with $Aβ_{(1–40)}$ and $Aβ_{(1–42)}$.

5.2.1. Synaptic loss is a late event in AD

Aβ buildup leads to synaptic dysfunctions, which are closely associated with cognitive impairments and represent an early pathological event in AD. The accumulation of extracellular Aβ is believed to play a regulatory role in synaptic activity and plasticity of neuronal membranes (Gouras et al., 2010; Tampellini, 2015). Consequently, investigating the loss of synaptic integrity due to the depletion of synaptic proteins on synaptic membranes can be efficiently conducted *in vitro* by exposing neurones to various Aβ peptides. In the brain of individuals with AD, the predominant types of Aβ peptides are $Aβ_{(1–40)}$ and $Aβ_{(1–42)}$, with $Aβ_{(1–42)}$ considered to be more detrimental than $Aβ_{(1–40)}$ (Bate & Williams, 2010; Fu et al., 2017; Willén et al., 2017). Our research indicated that a 12 h exposure to human Aβ species resulted in synaptic loss; however, we found no significant difference in synaptic loss between $Aβ_{(1–40)}$ and $Aβ_{(1–42)}$ in cultured hippocampal neurones. Notably, after 12 h treatment, both Aβ species induced synaptic loss, while a 3 h exposure did not affect active synapses with either Aβ variant (Van Bulck et al., 2022).

The influence of various Aβ species on synapse alterations is contingent upon their concentration and aggregated forms (Willén et al., 2017). Moreover, the effect of Aβ species at synaptic sites highly depends on the choice of pre- and postsynaptic markers for analysis (Willén et al., 2017). The synaptic loss we observed is closely associated with the strong binding affinity of Aβ to specific glutamatergic presynaptic (Vglut-1) and postsynaptic (PSD-95) proteins (Almeida et al., 2005; El-Husseini et al., 2000; Sokolow et al., 2012). Both *in vitro* and *in vivo* studies have shown downregulation of glutamatergic transmission in WT and AD transgenic hippocampal neurones, correlating with this solid binding affinity of Aβ for presynaptic proteins (Du et al., 2020; Rodriguez-Perdigon et al., 2016; Sokolow et al., 2012). Additionally, different Aβ-aggregated forms can lead to abnormalities of postsynaptic proteins such as PSD-95, which is crucial for synapse maturation, synaptic stability, and

synaptic plasticity (Almeida et al., 2005; El-Husseini et al., 2000). Furthermore, Fu and his colleagues (Fu et al., 2017) strongly implicated that $A\beta_{(1–42)}$ oligomers exhibit an elevated level of neurotoxicity, while monomers exhibit the least neurotoxic effect (~20%) on neuronal cells, with no noticeable difference between $A\beta_{(1–40)}$ and $A\beta_{(1–42)}$.

Our findings concerning primary hippocampal neurones align with these previous studies. Notably, prior to the onset of synaptic loss, $A\beta_{(1–40)}$ and $A\beta_{(1–42)}$ exert distinct effects on cellular lipid composition (Van Bulck et al., 2022). Furthermore, changes in lipid classes, such as levels of cholesterol and sphingolipids, can affect the activity of membrane-associated proteins such as APP, β-secretase and γ-secretase (Chan et al., 2012; Grimm et al., 2005). Therefore, the potential impact of investigating human Aβ species on various lipid classes, including sphingolipids, sphingophospholipids, and glycerophospholipids, as well as their different isoforms, are essential in understanding other risk-related biomarkers in AD.

However, further investigations are essential to clarify the specific effect of these lipid alterations on neurological disorders such as AD. The impact of physiological concentrations and species of Aβ on lipid profile changes in physiological and AD-related models needs to be further elucidated. Additionally, it is important to examine the biochemical aggregation states, their concentrations at synapses, and their effects on lipid homeostasis. Previous studies have shown that maintaining the native, physiological confirmation of Aβ peptides is crucial in preventing alteration in AD pathology (Benseny-Cases et al., 2012; Klementieva et al., 2017; Roos et al., 2021; Tampellini et al., 2010). Understanding which Aβ species, aggregation forms and concentrations significantly disrupt lipid homeostasis in AD will enhance our insight into the Aβ hypothesis, which remains a topic of debate (recently reviewed in (Kepp et al., 2023)). Moreover, a better understanding of these lipid alterations could lead to potential new diagnostic and therapeutic strategies for addressing various neurological disorders, including AD.

5.2.2. Alterations in lipid homeostasis: an early event in AD

Previous research identified alterations in various lipid classes associated with AD pathogenesis. However, the precise relationship between AD and lipid metabolism remains unclear. Despite this, growing evidence suggests that lipids, alongside other risk factors, could serve as a valuable fluid biomarker for AD diagnostics (Agarwal & Khan, 2020;

Ceccom et al., 2014). Still, the specific lipid isoforms that are dysregulated on both cellular and extracellular levels require further investigation.

Our novel findings indicated that changes in lipid content within hippocampal neurones occur prior to synapse loss and are independent of the Aβ species. Furthermore, we have demonstrated for the first time that early alterations in the lipid profiles of glial cells manifest after exposure to Aβ species (Van Bulck et al., 2022). This early response is likely attributable to the dynamic nature of phospholipid remodelling at the pre- and postsynaptic sites within the synaptosome membranes of neurones (Bennett et al., 2013; Cazzaniga et al., 2011; Lewis et al., 2017; Riganti et al., 2016).

The synaptosomes exhibit a definite membranous lipid composition (e.g., ceramides, sphingomyelins, and phospholipids), which is essential for the specific internal regulation of synapse formation. Any disruption caused by toxic factors such as Aβ can lead to alterations in the structural lipid integrity of the synaptosome, resulting in impaired synaptic transmission and subsequent synaptic loss (Bennett et al., 2013; Cazzaniga et al., 2011; Lewis et al., 2017; Riganti et al., 2016). However, the specific context of synaptosomes to Aβ species remains fertile ground for further research and exploration.

Additionally, Aβ, particularly the $A\beta_{(1–42)}$ species, significantly influences the elasticity of neuronal membranes of the hippocampal neurones during the ageing process (Ungureanu et al., 2016). Different aggregation forms of Aβ, such as oligomers, protofibrils, and fibrils, likely interact with neurones in distinct ways, leading to varying degrees of disruption in membrane elasticity. This disruption in membrane elasticity underlines the critical role of neuronal membrane elasticity in sustaining proper brain function (Ungureanu et al., 2016). Although our study did not investigate the various aggregation forms, we presumed that we commenced with monomeric Aβ species, as previously reported (Klementieva et al., 2017; Willén et al., 2017). Consequently, exploring the relationship between altered lipid classes, specific Aβ species, and their aggregation states would be crucial in the following research phase.

The analysis of extracellular lipid composition from the media of conditioned glial cells and hippocampal neurones aligns with our earlier results, which showed early changes in various lipid classes of interest. Notably, research has shown that changes in lipid classes can be detected in both CSF and plasma from patients and mouse models of AD, although these

studies have revealed various result outcomes (Barupal et al., 2019; Koal et al., 2015; Mielke et al., 2010; Tan et al., 2020; Varma et al., 2018). A related study highlighted that characterising lipids in brain extracellular vesicles offers a more accurate AD reflection in the extracellular fluids (Su et al., 2021). More recently, investigations focussing on mice in the early stages of AD have revealed significant alterations in specific lipid classes, such as sphingolipids and (lyso-) glycerophospholipids, in both plasma and brain samples (Ferré-González et al., 2024). Despite these advancements, the influence of various major Aβ species on extracellular fluid has not yet been investigated. Consequently, our findings represent the first detailed description of lipid alterations in brain cells and their conditioned media following treatment with specific human Aβ species. With these results, we aim to encourage further exploration and discussion of the diverse lipid classes in extracellular fluid and their relationship to the brain lipidome. These endeavours may ultimately contribute to identifying potential and more accurate AD biomarkers.

5.2.2.1. Alterations in sphingolipids

Our findings indicate that glial cells exhibit elevated levels of ceramides, particularly C14 Cer, after early Aβ treatment (Van Bulck et al., 2022). This elevated level might suggest that 3 h $A\beta_{(1\text{-}40)}$ and $A\beta_{(1\text{-}42)}$ treatment can inhibit the glucosylceramide synthase in glial cells, leading to an accumulation in C14 Cer due to increased ceramide synthase activity. A recent study has explained this increase in C14 Cer for astrocytes and microglia cells after specifically inhibiting glucosylceramide synthesis (McInnis et al., 2023). However, our study did not differentiate between these glial cell types derived from induced pluripotent stem cells, nor did we inhibit the glucosylceramide synthesis. Additionally, we observed that hippocampal neurones exhibit an early decrease after $A\beta_{(1–40)}$ and an early increase after $A\beta_{(1–42)}$. We are the first to report these changes in C14 Cer in both hippocampal neurones and glial cells upon Aβ treatment (Van Bulck et al., 2022).

In general, ceramides are crucial in maintaining structural function and fluidity of cell membranes (Kaltenegger et al., 2021; Pinto et al., 2011). They are vital for cell growth, differentiation, apoptosis, and the cellular response to stress signals. Glial cells produce more ceramides than neurones; however, neurones exhibit greater sensitivity to fluctuations in ceramide levels (McInnis et al., 2023). This sensitivity is reflected in the observed difference in the alteration of Cer for both our cellular and extracellular Cer isoforms. A recent study has noted similar trends between neurones and various types of glial cells (McInnis et al., 2023). Moreover, alteration in C14 Cer may affect the mitochondrial integrity, neuronal

development, and synaptic plasticity in hippocampal neurones following early Aβ exposure. Recent research indicates that ablation of CerS5 and CerS6, enzymes responsible for producing C14 Cer and C16 Cer in neurones, could protect against mitochondrial dysfunction after exposure to oxidative stress (Amatruda et al., 2025; McInnis et al., 2023). CerS6 has been reported to be downregulated in both mild and severe AD (Katsel et al., 2007). Mitochondrial dysfunction and oxidative stress have been associated with Aβ pathology in MDD and AD (Hait & Maiti, 2017; Kao et al., 2020; Kim et al., 2015). Although the $A\beta_{(1–42)}$-induced neuronal accumulation of Cer (e.g., C18 Cer and C24 Cer) has been described in oxidative stress-induced abnormalities in hippocampal neurones *in vitro* (Cutler et al., 2004), this aligns with our findings of toxicity induced by $A\beta_{(1–42)}$ at 3 h and 12 h. Notably, our 3 h treatment with $A\beta_{(1–40)}$ may indicate mitochondrial dysfunction due to oxidative stress for the first time. Further experiments are needed to elucidate this effect.

Our research might indicate that a 3 h $A\beta_{(1–42)}$ treatment may enhance the activity of nSMase. Although, previous research has shown this potential effect on nSMase activity following exposure to $A\beta_{(1–42)}$ (Grimm et al., 2005; Lee et al., 2014). Conversely, our findings might suggest that a 3 h $A\beta_{(1–40)}$ treatment may inhibit this activity. However, detailed lipid isoforms profiling following Aβ exposure and assessment of nSMase activity will provide further clarity on this matter.

Furthermore, inhibiting nSMase in Aβ-activated astrocytes has been found to suppress the production of NF-κB signalling and pro-inflammatory cytokines, including TNF-α, IL-1*β* and IL-6 (Jana & Pahan, 2010). Suppression of these neuroinflammatory processes can reduce Cer levels, which protect neuronal cells from apoptosis (Jana & Pahan, 2010). A similar effect may be suggested in C14 Cer and C24 Cer after 12 h Aβ species treatment. Additionally, a study reported that astrocyte mitochondrial fragmentation occurs following $A\beta_{(1–42)}$ stimulation, resulting in elevated Cer levels (Kong et al., 2018). Nevertheless, the specific C14 Cer concerning mitochondrial dysfunction, neuronal development, neuroinflammation, and synaptic dysfunction within the context of Aβ pathology requires further investigation. However, previous studies have shown that a high concentration of Cer can induce apoptosis or lead to development problems in hippocampal neurones (de Wit et al., 2020; Schwarz & Futerman, 1997).

Additionally, alterations in Cer isoforms have been proposed to play a role in pro- and anti-inflammatory responses by inhibiting ceramide synthase or glucosylceramide synthase in

glial cells (McInnis et al., 2023). Consequently, our data may indirectly contribute to these changes in inflammatory signalling because of toxic Aβ treatment. Short-term exposure to Aβ species may act as an inhibitor of glucosylceramide synthase, which may trigger pro-inflammatory signalling. In contrast, prolonged Aβ treatment might function as a ceramide synthase inhibitor, leading to an enhanced anti-inflammatory response in glial cells. However, in the conditioned media of glial cells, a decrease in C24 Cer is observed due to Aβ-induced inhibition of ceramide synthase, while C18:1 Cer may show increased levels. The aggregation status of Aβ could be a contributing factor to this effect. Further experiments are necessary to explore the relationship between inflammatory signalling, Cer isoforms (e.g., C14 Cer, C18:1 Cer, and C24 Cer), and Aβ species in these brain cells. Also, separating different types of glial cells may be crucial for a better understanding of these lipid alterations within each cell type and their extracellular environment.

Moreover, both types of brain cells demonstrate an early reduction in dihydroceramide, specifically C20 DHCer and C22 DHCer (Van Bulck et al., 2022). The conditioned media from these brain cells exhibited similar alterations in specific dihydroceramides. Consequently, the variations in lipid levels induced by Aβ may stem from the inflammatory responses and activated apoptotic-survival pathways initiated by oxidative stress (Jazvinšćak Jembrek et al., 2015).

Additionally, hippocampal neurones or glial cells exhibit a differential expression of glycosylated Cer, with specific isoforms showing decreased levels (e.g., C16 HexCer and C20 HexCer) and others demonstrating increased quantities (e.g., C16 HexCer, C22 HexCer, C24 HexCer, C16 LacCer, C18 LacCer and C24:1 LacCer) (Van Bulck et al., 2022). Furthermore, analysis of conditioned media from hippocampal neurones and glial cells indicates a reduction in levels of specific glycosylated Cer (e.g., C16 HexCer, C20 HexCer, C24 HexCer, C16 LacCer and C24:1 LacCer), alongside an elevation in levels of C14 HexCer and C18:0 HexCer in conditioned media from hippocampal neurones or glial cells. The implications of glycosylated Cer in neuronal growth and survival have been extensively addressed in prior research (Chao et al., 2019; Mayo et al., 2014; Olsen & Faergeman, 2017; Pannu et al., 2005). Alterations in these lipid isoforms due to Aβ may reflect the activation of neuroinflammatory processes, which could lead to mitochondrial fragmentation and neurite disruption (Kong et al., 2018; Zhang, L. et al., 2018). The morphological disruption of neurites has been characterised, with evidence suggesting that the extent of the disruption is contingent upon Aβ concentration, Aβ species and their aggregation forms

(Mokhtar et al., 2013; Salvadores et al., 2020; Wei et al., 2010). In AD, dystrophic neurites are often found near amyloid plaques. It has been established that pre-fibrillar Aβ forms are closely linked to this disruption (Gouras et al., 2010; Klementieva et al., 2017; Roos et al., 2021; Takahashi et al., 2013). These neurites exhibit degeneration features, such as swelling and the presence of proteins typically associated with axons, indicating a breakdown of normal neuronal polarity (Morita & Sobue, 2009). This phenomenon may suggest that Aβ deposition disrupts the normal structural lipid integrity of neurites, leading to their degeneration or retraction. Our data may contribute to some evidence of disruption in the lipid integrity of neurites after Aβ-induced toxicity. However, the effect of these Aβ species on lipid alteration remains inadequately understood. Our findings may enhance our understanding of possible neurite disruption manifested through lipid changes in neuronal cells. Nevertheless, further investigation is needed to examine the lipid alteration following exposure to specific Aβ aggregation forms while focussing on specific regions within these neuronal cells.

Another potential mechanism underlying alterations in glycosylated Cer may be attributed to Aβ-induced toxicity directed at the enzymes responsible for the synthesis and degradation of these glycosylated Cer. A gene expression analysis revealed a significant reduction in enzymes such as UGCG across all stages of AD, while CGT levels were found to increase in the severe stage of AD. Furthermore, β4GALNT6 exhibited a progressive decline throughout AD (Katsel et al., 2007). Additional research has suggested that the variations in glycosylated ceramide could be closely associated with late-onset AD genetic risk factor, ATP-binding cassette subfamily A 7 (Dehghan et al., 2022). Moreover, the accumulation of glycosylated Cer may be linked to Aβ-induced toxicity within the lysosome compartments. Lysosomes play a vital role in the degradation of accumulated glycosylated Cer. Deficiency in lysosomal enzymes such as GALC and GCase has been implicated in disorders that confer an elevated risk of dementia (Indellicato & Trinchera, 2019; Spratley et al., 2016).

5.2.2.2. Alterations in sphingophospholipids

In glial cells, sphingomyelin (C26 SM) levels were downregulated, whereas hippocampal neurones were elevated (Van Bulck et al., 2022). Additionally, sphingomyelin (C26 SM) exhibited upregulation in the conditioned media of glial cells, while it was downregulated in the conditioned media of hippocampal neurones. These changes are a direct effect of Aβ-induced toxicity, a complex process that involves multiple factors. $A\beta_{(1-40)}$, $A\beta_{(1-42)}$, and Aβ-islet amyloid polypeptide concentrations have been implicated in nSMase-mediated

apoptosis activity, which subsequently leads to neuronal cell death and Aβ-induced oxidative stress. The oligomeric isoforms of $A\beta_{(1-42)}$ and $A\beta_{(1-40)}$ species alter ceramide levels, potentially explaining the increase in nSMase and decrease in cellular SM activity (Grimm et al., 2005; He et al., 2010; Malaplate-Armand et al., 2006; Qi et al., 2005; Zhang et al., 2009). Additionally, it has been shown that $A\beta_{(1-42)}$, unlike $A\beta_{(1-40)}$, directly activates nSMase through a γ-secretase-dependent mechanism, resulting in elevated levels of Cer and possibly reduced levels of SM (Michno et al., 2018). Moreover, the accumulation of Aβ, particularly Aβ oligomers, can elevate the aSMase, which reduces So1P activity and increases Cer levels. This Aβ-induced toxicity may contribute to neuronal death in AD, a condition with intricate pathophysiology (He et al., 2010). Research indicated that glial cells have an increased expression of Cer and SMase in cases of cerebral amyloid angiopathy (de Wit et al., 2017). This observation could help explain our cellular and extracellular lipid profile alterations after $A\beta_{(1-40)}$ and $A\beta_{(1-42)}$ treatment of glial cells and hippocampal neurones.

Furthermore, we discovered novel findings that d18:1 So1P was upregulated after 3 h $A\beta_{(1-40)}$ and 12 h $A\beta_{(1-42)}$ treatment in glial cells and after 12 h $A\beta_{(1-42)}$ in hippocampal neurones (Van Bulck et al., 2022). We observed an early upregulation of extracellular lipids, particularly d18:1 So1P and d18 Sa1P, in conditioned media of hippocampal neurones, while conditioned media of glial cells exhibited a downregulation of these lipids after $A\beta_{(1-40)}$ treatment. Research has linked *in vitro* and *in vivo* Aβ-induced toxicity in glial cells and hippocampal neurones to elevated So1P levels (Czubowicz et al., 2015; Zhong et al., 2019).

Additionally, we demonstrated that glial cells and hippocampal neurones showed a downregulation of SPC (16:0), Sa (d18:0 Sa), and Sa1P (d18:0 Sa1P) after $A\beta_{(1-40)}$ and $A\beta_{(1-42)}$ treatment (Van Bulck et al., 2022). It is plausible that the aggregation of toxic Aβ species, stimulated by β-secretase mediated pathways and the activity of anti-inflammatory responses in neuronal cells, contributes to these observed downregulations (Park & Lee, 2019; Yi et al., 2011).

Another mechanism contributing to alterations in sphingophospholipids may involve the regulatory effect of key enzymes, such as SMS, SphK, and SPL, in the context of Aβ-induced toxicity. Evidence suggests that alterations in the expression of SphK and SPL are correlated with the presence of amyloid deposits within the entorhinal cortex of AD (Ceccom et al., 2014). Another study on SMS deficiency indicates that this deficiency may mitigate

the inflammatory response after ischemic stroke (Xue et al., 2019). Consequently, our finding may suggest that higher levels of C26 SM following exposure to $A\beta_{(1-40)}$ in neurones may indicate a reduced aggregation propensity compared to $A\beta_{(1-42)}$ and possessing anti-inflammatory activity. These factors may ultimately influence the pro-survival or pro-apoptotic dynamics within these cells, which could be a potential area of further research. It has been documented that $A\beta_{(1-42)}$ exhibits a higher tendency for aggregation, and its pre-fibrillary forms demonstrated enhanced structural stability compared to $A\beta_{(1-40)}$ (Coalier et al., 2013; Masters & Selkoe, 2012).

5.2.2.3. Alterations in lysoglycerophospholipids

Treatment with $A\beta_{(1-40)}$ and $A\beta_{(1-42)}$ resulted in an early increase of specific phospholipid isoforms in hippocampal neurones as well as in lysophospholipids in glial cells and hippocampal neurones. We also confirmed that, after either a 3 h or 12 h Aβ treatment, (lyso-) glycerophospholipids (PC (38:0), LPC (20:0), all LPE, LPG, LPE (18:1), LPS (18:2), and Lyso-PAF) were specifically reduced or elevated in Aβ-treated hippocampal neurones and glial cells (Van Bulck et al., 2022). Additionally, we verified that extracellular lipid of Aβ-treated hippocampal neurones and glial cells showed a specific reduction in (lyso-) glycerophospholipids (almost all PC, LPC (16:0), LPC (18:2), LPC (20:0), LPC (20:3), LPC (20:4), all LPE, all LPG, LPS (16:0), LPS (18:2) and Lyso-PAF) as well as a specific upregulation in (lyso-) glycerophospholipids (almost all PC, LPC (16:0), LPC (18:2), LPC (20:0), LPC (20:1), LPC (20:3), LPC (20:4), all LPE, all LPG, LPS (16:0), LPS (18:2) and Lyso-PAF) after either 3 h or 12 h Aβ treatment.

The changes in glycerophospholipid have been linked to synapse-mediated Aβ toxicity and the hyperactivity of cPLA2 in neuro-inflammatory reactions (Moses et al., 2006; Sundaram et al., 2012). It has been demonstrated that inhibiting cPLA2 activity can significantly mitigate $A\beta_{(1-42)}$ toxicity (Sanchez-Mejia et al., 2008). Moreover, $A\beta_{(1-42)}$ is capable of activating cPLA2, which hydrolyses arachidonic acid from specific glycerophospholipids; this process is a critical step in $A\beta_{(1-42)}$ neurotoxicity (Kita et al., 2006; Sanchez-Mejia et al., 2008). Previous research has also highlighted the role of cPLA2 in both soluble oligomeric forms of $A\beta_{(1-40)}$ and $A\beta_{(1-42)}$ at similar concentrations (Kriem et al., 2005). While we initially presumed our Aβ species were monomeric from the onset of treatment, as noted in prior research (Klementieva et al., 2017; Willén et al., 2017). Further investigations should explore the Aβ aggregations associated with these lipid isoform changes. Additionally, the observed lipid alterations may relate to the impact of Aβ toxicity on LPLAT, an enzyme responsible for

converting lysophospholipids into phospholipids. The early alterations in PC (38:0) might be associated with increased LPLAT activity, driven by soluble oligomeric Aβ forms previously observed in AD (Ross et al., 1998). Furthermore, it has been shown that lyso-PAF can accumulate due to $A\beta_{(1-42)}$ (Ryan et al., 2009), and our data indicate a similar effect following $A\beta_{(1-42)}$-induced toxicity. In conclusion, to our knowledge, we are the first to utilise both Aβ species to demonstrate their effect on various lipid isoforms changes in healthy brain cells from mice.

5.3. Qualitative and quantitative analysis of N,N-Diethyltryptamine

Previous studies and those conducted in Dr. Ana Perez Castillo's laboratory in Madrid, Spain, and by others have explored various psychedelic N,N-tryptamines, such as DMT, DET (Perez Castillo et al., 2018 (Patent No. US11723894B2)), DPT, and 5-MeO-DMT (Fontanilla et al., 2009; Lima da Cruz et al., 2018; Morales-Garcia et al., 2020; Szabo et al., 2014; Szabo et al., 2016; Winter, 1969). These studies have demonstrated the capacity of N,N-tryptamines (such as DMT, DPT, 5-MeO-DMT and DET) to prevent neuroinflammatory responses and enhance adult neurogenesis in neurological and psychiatric disorders (Fontanilla et al., 2009; Lima da Cruz et al., 2018; Morales-Garcia et al., 2020; Szabo et al., 2014; Szabo et al., 2016; Winter, 1969). Moreover, research from Dr. Ana Perez Castillo's laboratory has indicated, through experiments with neuroblastoma cell lines featuring WT APP or Swedish APP mutation, that DET could be a promising candidate for *in vivo* validation in AD (unpublished data). However, further research is needed to fully understand the potential of DET in AD.

Despite the limited existing knowledge on DET, previous research conducted in the late 20th century primarily focussed on its psychotogenic effect and the retrieval of the pharmacological properties from tissue and plasma samples through various administration routes (Böszörményi et al., 1959; Cohen & Vogel, 1972; Szara & Hearst, 1962; Szara et al., 1966). Nevertheless, a substantial amount of information has been documented based on observation, interviews, and the personal experiences of researchers within the field of psychedelics, as detailed in the book by Shulgin et al. (1997) (TIHKAL: The Continuation). To enhance our study, we utilised an MAO inhibitor (CLQ) to prevent the metabolisation of DET, thereby bypassing the MAO degradation pathway and ensuring the bioavailability of DET (Huszti & Borsy, 1964; Moriya et al., 2019; Tittarelli et al., 2015).

Due to the beneficial effects of these tryptamines and the inconsistencies found in the literature, we are the first to empirically describe the impact of DET on *in vitro* and *in vivo* models of AD pathology. We cannot make a definitive statement regarding the *in vitro* effect of DET due to a lack of statistical evaluations. Consequently, we can only suggest that DET may potentially influence the promotion of NSC differentiation into more mature neurones, even after Aβ treatment. Nonetheless, our *in vivo* experiment with DET in Tg mice could pave the way for further research into its potential applications in neurological disorders.

5.3.1. Revealing the neurogenic effect of N,N-Diethyltryptamine in vivo

In this study, we integrate MRI analysis with MRS to explore the effects of DET administration on metabolic and biochemical alterations in the brain of WT and Tg mice with AD for the first time. Our findings also indicate that DET does not affect the improvement of axonal damage and demyelination in various brain regions of WT and Tg mice. Furthermore, we demonstrate that DET had no initial effect on the accumulation of macromolecules, such as Aβ plaques, or on adult neurogenesis *in vivo*. This lack of impact may be attributed to the age of the mice used in the experiment design and the dosage of DET. Therefore, it is essential to investigate younger mice before the onset of cognitive impairment and to examine different dosages of DET. Research indicated that cognitive functions and behaviours decline occur between 6 and 10 months and deteriorate further with age (Minkeviciene et al., 2008). In the behavioural tests, Tg mice at 10 months cannot recall the location of an escape platform in the Morris water maze, and by 15 months, they struggle even to learn the platform's location (Minkeviciene et al., 2008). Additionally, adult neurogenesis starts to decline at 2 months and is nearly abolished by 6 months in these Tg mice (Demars et al., 2010; Faure et al., 2011). Our findings may suggest the necessity for further research in this area, particularly concerning the effects of DET on younger mice and varying dosages.

5.3.1.1. Exploring the neuroprotective potential of N,N-Diethyltryptamine: implication for brain atrophy and Aβ accumulation

Our voxel-based morphometry analysis using T2-weighted imaging and MT analysis revealed no significant alteration in atrophy or accumulation of macromolecules, such as Aβ plaques, in various brain regions when comparing vehicle-treated controls to DET-treated mice. The MT value reflects the relative ratio of free water molecules to macromolecules bound to water molecules (Esteras et al., 2012). Alterations in the MT ratio can occur during neuroinflammation and may be associated with neuronal loss, the accumulation of Aβ

plaques, neurofibrillary tangles, and gliosis (Esteras et al., 2012; Ridha et al., 2007). These findings may suggest that DET does not induce any neuroinflammatory response at the dosage administered *in vivo*. Despite the positive effect of DET on the neuroblastoma cell lines featuring WT APP or Swedish APP mutation (unpublished data from Dr. Ana Perez Castillo's laboratory). However, further investigation is necessary to explore the effects of DET on the reduction of neuronal loss and Aβ aggregation, neurofibrillary tangles, and gliosis in these Tg mice. These alterations could be accomplished by employing microscopic and molecular techniques to assess the brain for signs of neuronal loss, Aβ aggregation, neurofibrillary tangles, and gliosis after DET treatment in WT and Tg mice.

We propose a novel hypothesis that DET may stimulate the differentiation and proliferation of NSC and potentially influence Aβ aggregation in the subventricular areas of both WT and Tg mice. Research conducted at Dr. Ana Perez Castillo's laboratory has shown that DMT, a natural compound structurally similar to DET, positively affects neurogenesis by promoting the proliferation and differentiation of NSC. *In vivo* studies indicate that DMT enhances spatial learning and memory tasks (Morales-Garcia et al., 2020). Furthermore, *in vitro* investigations have demonstrated that DET can encourage adult neurogenesis by inducing the differentiation of NSC into neurones (Perez Castillo et al., 2018 (Patent No. US11723894B2).

In our investigation of 12-month-old mice, histological analyses revealed prominent Aβ accumulation in the brain; however, we noted no significant alterations in the MT metric values when comparing WT and Tg groups. Prior findings by Esteras and colleagues (Esteras et al., 2012) have documented that MT values can indicate AD histopathological changes. Conversely, studies conducted by Delatour (Delatour et al., 2006) and Liang (Liang et al., 2017), using T2-weighted imaging alongside histopathological evaluations, identified atrophy changes across both whole brain and regional brain volumes in various age groups of mice exhibiting a similar APP/PSEN-1 mutation. This atrophy is hypothesised to correlate with Aβ burden (Delatour et al., 2006; Huang et al., 2016).

Despite these precedents, our study did not reveal any significant correlations between structural changes in brain regions and Aβ accumulation. The absence of observed structural alterations may be attributable to factors such as the specific age of the mice, duration of treatment, and DET dosage. Moreover, it has been observed that astrocytic loss and hippocampal atrophy in AD mice occur in proximity to Aβ plaque formation (Huang et

al., 2016). Astrocytic loss, a common feature of AD, is believed to contribute to the progression of the disease, while hippocampal atrophy is associated with memory loss (Heneka et al., 2015; Ries & Sastre, 2016). In contrast, neuronal loss appears to be less pronounced in the hippocampus than alterations in synaptic integrity (Huang et al., 2016). In addition, a longitudinal study reported no brain atrophy, suggesting that the observed difference in anatomical structural volume may stem from the developmental status of the mouse brain rather than the neuropathological process associated with Aβ accumulation (Lau et al., 2008). These findings align with our data, which also failed to demonstrate notable structural volumetric changes.

Additionally, a recent report indicated no brain atrophy in 12-month-old mice bearing the APP/PSEN-1 mutation; however, the noted decrease in neuronal density within the cortex was not reflected in the MRI morphometry analysis (Kuhla et al., 2017). The observed increase in glial activation associated with neuronal loss may elucidate the apparent discrepancy regarding the absence of detectable atrophy through MRI (Manaye et al., 2007). Although our assessment indicated elevated glial activation surrounding Aβ aggregation starting from 4 months of age. The implications of neuronal loss warrant further investigation to fully understand the results of our MRI data regarding undetectable brain atrophy.

The duration and age of experimental mice may be critical factors contributing to the lack of significant volumetric changes observed in our MRI analyses. Furthermore, discrepancies in the current literature surrounding MRI volumetric alterations appear to be primarily influenced by specific mouse strains utilised and the age of the subjects in various experimental settings (Delatour et al., 2006; Lau et al., 2008; Liang et al., 2017). Consequently, we advocate for additional histopathological and biochemical examinations of WT and Tg brain regions subjected to either vehicle or DET treatment in further research endeavours.

5.3.1.2. Exploring the neuroplasticity implications of N,N-Diethyltryptamine on the white matter integrity

DTI scans are a powerful approach for examining the impairment of white matter integrity by assessing the direction of water diffusivity. This method is crucial in identifying anatomical changes before they become apparent in structural MRI (Shu et al., 2013; Zerbi et al., 2013). However, interpreting altered diffusivity in neurobiological mechanisms is not straightforward and highly depends on the local fibre architecture (Madden et al., 2009). Therefore, axialdiff

and radialdiff should not be interpreted separately without considering FA and MD. An increase in FA generally indicates a higher degree of white matter integrity, as regions of white matter with prominent structural integrity tend to impose greater directional restriction on the diffusion of water molecules in the brain (Madden et al., 2009).

Our data did not demonstrate any influence of DET on white matter integrity across different brain regions in both WT and Tg mice. However, the hippocampus exhibited a significant decrease in axialdiff and MD, with radialdiff remaining unchanged between vehicle-treated WT and Tg mice. This suggests a notable increase in axonal damage while indicating no alterations in demyelination within the hippocampus of vehicle-treated Tg compared to vehicle-treated WT. Furthermore, a reduction in axialdiff may imply degeneration of axonal structural density, while the increase in radialdiff may lead to demyelination (Song et al., 2004; Song et al., 2002). Our observation is consistent with this previous research. Contrarily, another study reported an opposite effect, with increases in axialdiff and FA in the hippocampus, cortex and corpus callosum (Qin et al., 2013). At the same time, the thalamus displayed a significant increase in FA. Additionally, a significant decrease in radialdiff was seen in the hippocampus (Qin et al., 2013).

Moreover, research by Zerbi and his colleagues (Zerbi et al., 2013) indicated a decrease in all DTI parameters in the corpus callosum. However, the hippocampus showed an increase in MD and radialdiff, alongside a decrease in FA, whereas various other brain regions, including the cerebral cortex, exhibited a decline in axialdiff (Zerbi et al., 2013). In a recent study that aligns with our findings, it was reported that there was a decrease in axialdiff and FA, an increase in radialdiff, and no difference in MD was observed (Zhou et al., 2019). Therefore, relying solely on DTI measurements, without correlating them with other MRI and biochemical analyses, could lead to a limited understanding of the effects of DET on white matter integrity. Further research is necessary to investigate the brain regions after the post-mortem of these treated mice through various biochemical analyses.

5.3.2. Revealing the neurogenic effect of N,N-diethyltryptamine on brain metabolic changes in vivo

We presented metabolic profiles for 7 out of 27 molecules in the hippocampus, providing a comprehensive overview of the brain metabolic landscape. Among the 7 analysed molecules, we identified 3 individual metabolites (inositol, NAA and taurine), 2 metabolite complexes (NAA + NAAG and Glu + Gln), and 2 lipids/macromolecules complexes (GPC +

PCh and MM09 + Lip09) in both vehicle-treated and DET-treated WT and Tg mice. Notably, we did not observe any significant changes in these molecules; however, we did find slight alterations in inositol, NAA, NAA + NAAG, Glu + Gln, and MM09 + Lip09 in WT and Tg mice after DET treatment. Previous studies have demonstrated that MRS can effectively characterise specific metabolic profiles after non-treatment and treatment in WT mice compared to Tg mice harbouring the APP/PSEN-1 mutation. In summary, these studies showed a reduction in NAA and Glu levels in Tg mice compared to WT (Chen et al., 2012; Esteras et al., 2012; Kuhla et al., 2017; Liang et al., 2017; Marjanska et al., 2005; Marjańska et al., 2014; Shen et al., 2018; Westman et al., 2009). Additionally, we will discuss our findings regarding each metabolite, lipid and macromolecule from MRS in the context of existing literature in Tg mice with a similar APP/PSEN-1 mutation and the relationship to neuroinflammation and Aβ aggregation in AD.

Inositol, a naturally occurring sugar-like metabolite in the brain, regulates various biochemical pathways and can be altered in neurological pathologies (López-Gambero et al., 2020). Free-inositol acts as an osmolyte in astrocytes, providing essential cellular defence against external or metabolic stress and thereby modulating the neuronal and glial activity in the brain. In AD, inositol isomers have been shown to have a significant potential in reducing toxic Aβ aggregation and stabilising soluble forms of Aβ-induced toxicity (McLaurin et al., 1998; McLaurin et al., 2000). *In vivo* studies have shown that specific inositol isoforms may reduce astrogliosis, ameliorate synaptic regulation, decrease Aβ aggregation and mitigate neuronal damage, resulting in improved cognitive abilities in AD (Aytan et al., 2013; Dorr et al., 2012; McLaurin et al., 2006; Morrone et al., 2020). Thus, we might propose that DET acts as a neuromodulator, helping to diminish Aβ peptide aggregation and promoting an anti-inflammatory response. These mechanisms might play a vital role in alleviating cognitive deficits related to memory impairment. However, further investigations are necessary to clarify these effects, which could help understand better their implications in neurodegenerative disorders. Additionally, Dr. Ana Perez Castillo's laboratory in Spain has demonstrated that DET prevents neuronal cell death and reduces glial activity in a cellular model of Parkinson's disease (Perez Castillo et al., 2018 (Patent No. US11723894B2)). Further research is needed to elaborate on this in AD pathology.

NAA is a potential inhibitor of protein aggregation and an important marker for neuronal viability and axonal density. Besides this, NAAG is synthesised in neurones and subsequently converted to NAA in astrocytes (Moffett et al., 2007). Previous studies

involving similar age groups of mice demonstrated a reduction in NAA levels in Tg harbouring a similar APP/PSEN-1 mutation compared to WT (Jansen et al., 2013; Kuhla et al., 2017). In contrast, our observations revealed a slight increase in both NAA and NAA + NAAG levels, alongside a decrease solely in DET-treated Tg mice, which was even lower than in vehicle- and DET-treated WT. This finding may indicate that DET treatment in Tg mice inhibits Aβ peptide aggregation.

Furthermore, taurine, a well-known amino acid, has been shown to impact neuronal differentiation, arborization, and formation of synapses (Hernández-Benítez et al., 2013). Previous research has indicated that taurine administration may have an antidepressant effect (Song et al., 2024). Additionally, taurine has been associated with targeting Aβ while enhancing cognitive function in models of AD (Jang et al., 2017). However, it has been observed that taurine levels decline in ageing-related processes and after treatment with donepezil, an acetylcholinesterase inhibitor used to address the symptomatic effects of AD, such as memory loss and confusion (Barbiera et al., 2022; Westman et al., 2009). Moreover, depressive-like systems have been linked to AD pathology, as well as the treatment involving N,N-tryptamines (Amani et al., 2019; Bai et al., 2021; Borbély et al., 2022; Szabó et al., 2021). Unfortunately, our results indicated no significant upregulation or downregulation in taurine levels after DET treatment. Consequently, DET treatment may not affect neuronal plasticity, depressive-like symptoms, or cognitive functions. However, it is important to investigate how DET might influence neuronal plasticity and whether it could improve cognitive impairment, as this aspect was not clarified in this present research.

Glu and Gln produce overlapping resonances called Glx, representing glutamatergic neurotransmission (Senaratne et al., 2009). The Glx signal combines glutamine and glutamate, with glutamate being the predominant component and the major excitatory neurotransmitter in the central nervous system (Fayed et al., 2011; Westman et al., 2009). We observed a slight decrease in Glx levels in vehicle-treated Tg compared to vehicle-treated WT. However, after DET treatment, this decrease was abolished, resulting in neuronal activity levels comparable to those of WT. Other studies have reported a similar reduction in neuronal activity in the Glu peak of Tg mice compared to WT (Chen et al., 2012; Liang et al., 2017; Marjanska et al., 2005; Shen et al., 2018), while an increase was noted after donepezil treatment (Westman et al., 2009). Furthermore, research has indicated that Glx, Glu levels and NAA were decreased in AD patients compared to those with MCI, as well as compared to healthy individuals (Fayed et al., 2011).

GPC and PCh, which reflect the choline resonance signal, serve as markers for membrane density and integrity, linking them to the synthesis and degradation of phospholipids (Senaratne et al., 2009; Westman et al., 2009). Choline is a critical component of the phosphatidylcholine in cell membranes. Any alteration due to a deficiency in acetylcholine production, particularly in neurological disorders, can increase free choline (Mohan et al., 2010; Wurtman et al., 1985). We showed no alteration in WT and Tg, even after DET treatment, indicating no impact on membrane density and integrity of phospholipids in the brain. However, our lipid study on cellular (Van Bulck et al., 2022) and extracellular lipids has implicated that specific phospholipids isoforms are dysregulated due to Aβ-induced toxicity. Contrarily, previous studies have indicated either an increase or no change in choline levels in Tg mice, which bear a similar APP/PSEN-1 mutation, compared to WT (Esteras et al., 2012; Marjanska et al., 2005). In 2009, Westman and his colleagues (Westman et al., 2009) reported an elevation in choline levels after donepezil treatment, while Marjańska in 2014 (Marjańska et al., 2014) found no significant difference in choline levels between Tg compared WT. Notably, we are the first to report no change in choline levels in this AD model after vehicle or DET treatment.

Lip09 and MM09 were successfully quantified in our MRS analysis. However, the origin and biological relevance of the spectra peaks associated with macromolecules and lipid resonance remains poorly defined. Previous research suggests that the peaks corresponding to MM09 and Lip09 spectra peaks may indicate levels of thymosin β4 (Kauppinen et al., 1992a; Kauppinen et al., 1992b). Thymosin β4 is a peptide expressed in microglia and has been implicated in neuroprotective and anti-inflammatory responses. Additionally, thymosin β4 plays a role in various biological processes, including cell proliferation and differentiation, axonal integrity, neurite outgrowth and autophagy. These processes often become dysregulated in neurological disorders (Kim et al., 2023; Paulussen et al., 2009; Xiong et al., 2012), and our findings could potentially lead to new insights and treatment possibilities.

Our findings indicated an increase in both WT and Tg mice after DET treatment, suggesting that DET may exert a neurotrophic effect that could enhance neuronal cell differentiation, proliferation, neuronal outgrowth, and an anti-inflammatory effect. These observations might align with the previous work of Dr. Ana Perez Castillo's laboratory in Spain (Perez Castillo et al., 2018 (Patent No. US11723894B2)).

Furthermore, MM09 has been observed to be downregulated with ageing (Ryan et al., 2018). In contrast, prior research has indicated a positive effect on the levels of Lip09 and MM09 after the immune stimulus in WT mice, while an adverse effect was noted in Tg mice, which harbour a similar APP/PSEN-1 mutation (Pardon et al., 2016). This finding is consistent with our observations; however, we noted a slight decline in vehicle-treated Tg compared to their WT littermates, which may be associated with the destruction of microglia surrounding the plaques in our 12-month-old Tg cohort. A key difference between our study and that conducted by Pardon and his colleagues (Pardon et al., 2016) is the absence of an external inflammatory stimulus in our experimental design and the differing age groups of the mice utilised. These factors are crucial for understanding their impact on microglial morphology and phenotypical activation, which are linked to Aβ aggregation in AD (Chen et al., 2012; Cherry et al., 2014; Guo et al., 2022). Nevertheless, MM09 and Lip09 show great potential to serve as functional markers for assessing microglia responses within *in vivo* studies, highlighting the practical implications of our research. Further investigation is necessary to understand better the neurobiological responses associated with these macromolecules and lipid resonances.

The discrepancy observed in the literature concerning these metabolites primarily stems from the variation in the brain regions evaluated using MRI and MRS, as well as subtle differences in the genetic backgrounds, which can lead to significant phenotypical variability (Doetschman, 2009), as evidenced by our findings. Furthermore, it is essential to repeat the investigation with additional controls, such as DET alone and including mice that do not receive any vehicle treatment. Additionally, it would be beneficial to explore alternative routes of administration and various concentrations, which could lead to potential new insights and discoveries. The metabolic pathways of DET should also be examined more thoroughly due to the scarcity of information available in the literature and the earlier studies on DET from the 20th century (Böszörményi et al., 1959; Cohen & Vogel, 1972; Szara & Hearst, 1962; Szara et al., 1966). Moreover, increasing experimental sample sizes and conducting a more detailed examination of molecular effects concerning inflammation, lipid homeostasis, adult neurogenesis, and improvements in BPSD associated with AD would be advantageous.

5.4. Conclusion

In this study, we uncovered for the first time that lipid dysfunction occurs as an early event before synaptic loss occurs in Aβ-induced toxicity, utilising various quantitative methods. While lipid alterations depend on the specific Aβ species, variations among human Aβ species do not influence synaptic loss. In addition to this novel finding, the limitations of our research have potential implications for characterising a new therapeutic agent. We employed an unique qualitative *in vitro* AD model alongside quantitative *in vivo* analysis using the AD-Tg model, which carries the APP/PSEN-1 mutation. Nonetheless, we observed no significant impact after DET treatment in our MRI and MRS spectra. Further exploration into the effects of DET and its pathways in both BPSD and AD-related disorders could provide valuable insights. Such research can enhance our understanding and provide valuable insights for innovative diagnostic and therapeutic strategies for those complex conditions. This pursuit not only aims to advance scientific knowledge but also seeks to improve the lives of those affected by these challenging disorders.

References

Aaldijk, E., & Vermeiren, Y. (2022). The role of serotonin within the microbiota-gut-brain axis in the development of Alzheimer's disease: A narrative review. *Ageing Res Rev*, *75*, 101556. https://doi.org/10.1016/j.arr.2021.101556

Acquarone, E., Argyrousi, E. K., Arancio, O., Watterson, D. M., & Roy, S. M. (2024). The 5HT2b Receptor in Alzheimer's Disease: Increased Levels in Patient Brains and Antagonist Attenuation of Amyloid and Tau Induced Dysfunction. *J Alzheimers Dis*, *98*(4), 1349-1360. https://doi.org/10.3233/JAD-240063

Afshar, S., Shahidi, S., Rohani, A. H., Asl, S. S., & Komaki, A. (2019). Protective effects of 5-$HT_{(1A)}$ receptor antagonist and 5-$HT_{(2A)}$ receptor agonist on the biochemical and histological features in a rat model of Alzheimer's disease. *J Chem Neuroanat*, *96*, 140-147. https://doi.org/10.1016/j.jchemneu.2019.01.008

Afshar, S., Shahidi, S., Rohani, A. H., Komaki, A., & Asl, S. S. (2018). The effect of NAD-299 and TCB-2 on learning and memory, hippocampal BDNF levels and amyloid plaques in Streptozotocin-induced memory deficits in male rats. *Psychopharmacology (Berl)*, *235*(10), 2809-2822. https://doi.org/10.1007/s00213-018-4973-x

Agarwal, M., & Khan, S. (2020). Plasma Lipids as Biomarkers for Alzheimer's Disease: A Systematic Review. *Cureus*, *12*(12). https://doi.org/10.7759/cureus.12008

Alaamery, M., Albesher, N., Aljawini, N., Alsuwailm, M., Massadeh, S., Wheeler, M. A., Chao, C.-C., & Quintana, F. J. (2021). Role of sphingolipid metabolism in neurodegeneration. *J Neurochem*, *158*(1), 25-35. https://doi.org/10.1111/jnc.15044

Alarcon-Gil, J., Sierra-Magro, A., Morales-Garcia, J. A., Sanz-SanCristobal, M., Alonso-Gil, S., Cortes-Canteli, M., Niso-Santano, M., Martinez-Chacon, G., Fuentes, J. M., Santos, A., & Perez-Castillo, A. (2022). Neuroprotective and Anti-Inflammatory Effects of Linoleic Acid in Models of Parkinson's Disease: The Implication of Lipid Droplets and Lipophagy. *Cells*, *11*(15). https://doi.org/10.3390/cells11152297

Almeida, C. G., Tampellini, D., Takahashi, R. H., Greengard, P., Lin, M. T., Snyder, E. M., & Gouras, G. K. (2005). Beta-amyloid accumulation in APP mutant neurons reduces PSD-95 and GluR1 in synapses. *Neurobiol Dis*, *20*(2), 187-198. https://doi.org/10.1016/j.nbd.2005.02.008

Alzheimer's Disease Research Models | ALZFORUM. Retrieved 2025/02/20 from https://www.alzforum.org/research-models/alzheimers-disease

Amani, M., Shokouhi, G., & Salari, A.-A. (2019). Minocycline prevents the development of depression-like behavior and hippocampal inflammation in a rat model of Alzheimer's disease. *Psychopharmacology (Berl)*, *236*(4), 1281-1292. https://doi.org/10.1007/s00213-018-5137-8

Amatruda, M., Marechal, D., Gacias, M., Wentling, M., Turpin-Nolan, S., Morstein, J., Moniruzzaman, M., Brüning, J. C., Haughey, N. J., Trauner, D. H., & Casaccia, P. (2025). Neuroprotective effect of neuron-specific deletion of the C16 ceramide synthetic enzymes in an animal model of multiple sclerosis. *Glia*, *73*(2), 271-290. https://doi.org/10.1002/glia.24631

Amor, S., Peferoen, L. A. N., Vogel, D. Y. S., Breur, M., van der Valk, P., Baker, D., & van Noort, J. M. (2014). Inflammation in neurodegenerative diseases – an update. *Immunology*, *142*(2), 151-166. https://doi.org/10.1111/imm.12233

Araújo, A. M., Carvalho, F., Bastos, M. D. L., Guedes de Pinho, P., & Carvalho, M. (2015). The hallucinogenic world of tryptamines: an updated review. *Arch Toxicol*, *89*(8), 1151-1173. https://doi.org/10.1007/s00204-015-1513-x

Area-Gomez, E., de Groof, A., Bonilla, E., Montesinos, J., Tanji, K., Boldogh, I., Pon, L., & Schon, E. A. (2018). A key role for MAM in mediating mitochondrial dysfunction in Alzheimer disease. *Cell Death Dis*, *9*(3), 335. https://doi.org/10.1038/s41419-017-0215-0

Area-Gomez, E., de Groof, A. J. C., Boldogh, I., Bird, T. D., Gibson, G. E., Koehler, C. M., Yu, W. H., Duff, K. E., Yaffe, M. P., Pon, L. A., & Schon, E. A. (2009). Presenilins Are Enriched in Endoplasmic Reticulum Membranes Associated with Mitochondria. *Am J Pathol*, *175*(5), 1810-1816. https://doi.org/10.2353/ajpath.2009.090219

Arjona, A. A., Pooler, A. M., Lee, R. K., & Wurtman, R. J. (2002). Effect of a 5-HT(2C) serotonin agonist, dexnorfenfluramine, on amyloid precursor protein metabolism in guinea pigs. *Brain Res*, *951*(1), 135-140. https://doi.org/10.1016/s0006-8993(02)03153-0

Asghar, S., Mushtaq, N., Ahmed, A., Anwar, L., Munawar, R., & Akhtar, S. (2024). Potential of Tryptamine Derivatives as Multi-Target Directed Ligands for Alzheimer's Disease: AChE, MAO-B, and COX-2 as Molecular Targets. *Molecules*, *29*(2), 490. https://doi.org/10.3390/molecules29020490

Aytan, N., Choi, J.-K., Carreras, I., Kowall, N. W., Jenkins, B. G., & Dedeoglu, A. (2013). Combination therapy in a transgenic model of Alzheimer's disease. *Exp Neurol*, *250*, 228-238. https://doi.org/10.1016/j.expneurol.2013.10.001

Babcock, K. R., Page, J. S., Fallon, J. R., & Webb, A. E. (2021). Adult Hippocampal Neurogenesis in Aging and Alzheimer's Disease. *Stem Cell Reports*, *16*(4), 681-693. https://doi.org/10.1016/j.stemcr.2021.01.019

Bai, Y., Li, M., Zhou, Y., Ma, L., Qiao, Q., Hu, W., Li, W., Wills, Z. P., & Gan, W.-B. (2017). Abnormal dendritic calcium activity and synaptic depotentiation occur early in a mouse model of Alzheimer's disease. *Mol Neurodegener*, *12*(1), 86. https://doi.org/10.1186/s13024-017-0228-2

Bai, Y., Liu, D., Zhang, H., Wang, Y., Wang, D., Cai, H., Wen, H., Yuan, G., An, H., Wang, Y., Shi, T., & Wang, Z. (2021). N-salicyloyl tryptamine derivatives as potential therapeutic agents for Alzheimer's disease with neuroprotective effects. *Bioorg Chem*, *115*, 105255. https://doi.org/10.1016/j.bioorg.2021.105255

Barbiera, A., Sorrentino, S., Fard, D., Lepore, E., Sica, G., Dobrowolny, G., Tamagnone, L., & Scicchitano, B. M. (2022). Taurine Administration Counteracts Aging-Associated Impingement of Skeletal Muscle Regeneration by Reducing Inflammation and Oxidative Stress. *Antioxidants (Basel)*, *11*(5), 1016. https://doi.org/10.3390/antiox11051016

Barker, S. A., McIlhenny, E. H., & Strassman, R. (2012). A critical review of reports of endogenous psychedelic N, N-dimethyltryptamines in humans: 1955-2010. *Drug Test Anal*, *4*(7-8), 617-635. https://doi.org/10.1002/dta.422

Barnes, D. A., Galloway, D. A., Hoener, M. C., Berry, M. D., & Moore, C. S. (2021). TAAR1 Expression in Human Macrophages and Brain Tissue: A Potential Novel Facet of MS Neuroinflammation. *Int J Mol Sci*, *22*(21), 11576. https://doi.org/10.3390/ijms222111576

Barupal, D. K., Baillie, R., Fan, S., Saykin, A. J., Meikle, P. J., Arnold, M., Nho, K., Fiehn, O., Kaddurah-Daouk, R., & Alzheimer's Disease Neuroimaging Initiative-the Alzheimer Disease Metabolomics Consortium. (2019). Sets of coregulated serum lipids are associated with Alzheimer's disease pathophysiology. *Alzheimers Dement (Amst)*, *11*(1), 619-627. https://doi.org/10.1016/j.dadm.2019.07.002

Bate, C., & Williams, A. (2010). Amyloid-β_{1-40} Inhibits Amyloid-β_{1-42} Induced Activation of Cytoplasmic Phospholipase A_2 and Synapse Degeneration. *J Alzheimers Dis*, *21*(3), 985-993. https://doi.org/10.3233/JAD-2010-100528

Baumkötter, F., Schmidt, N., Vargas, C., Schilling, S., Weber, R., Wagner, K., Fiedler, S., Klug, W., Radzimanowski, J., Nickolaus, S., Keller, S., Eggert, S., Wild, K., & Kins, S. (2014). Amyloid Precursor Protein Dimerization and Synaptogenic Function Depend on Copper Binding to the Growth Factor-Like Domain. *J Neurosci*, *34*(33), 11159-11172. https://doi.org/10.1523/JNEUROSCI.0180-14.2014

Benilova, I., Karran, E., & De Strooper, B. (2012). The toxic Aβ oligomer and Alzheimer's disease: an emperor in need of clothes. *Nat Neurosci*, *15*(3), 349-357. https://doi.org/10.1038/nn.3028

Bennett, S. A. L., Valenzuela, N., Xu, H., Franko, B., Fai, S., & Figeys, D. (2013). Using neurolipidomics to identify phospholipid mediators of synaptic (dys)function in Alzheimer's Disease. *Front Physiol*, *4*, 168. https://doi.org/10.3389/fphys.2013.00168

Benseny-Cases, N., Klementieva, O., & Cladera, J. (2012). In vitroOligomerization and Fibrillogenesis of Amyloid-beta Peptides. In Harris, J. R. (Ed.), *Protein Aggregation and Fibrillogenesis in Cerebral and Systemic Amyloid Disease* (Vol. 65, pp. 53-74). Springer Netherlands. https://doi.org/10.1007/978-94-007-5416-4_3

Bilousova, T., Miller, C. A., Poon, W. W., Vinters, H. V., Corrada, M., Kawas, C., Hayden, E. Y., Teplow, D. B., Glabe, C., Albay, R., 3rd, Cole, G. M., Teng, E., & Gylys, K. H. (2016). Synaptic Amyloid-beta Oligomers Precede p-Tau and Differentiate High Pathology Control Cases. *Am J Pathol*, *186*(1), 185-198. https://doi.org/10.1016/j.ajpath.2015.09.018

Bohár, Z., Toldi, J., Fülöp, F., & Vécsei, L. (2015). Changing the Face of Kynurenines and Neurotoxicity: Therapeutic Considerations *Int J Mol Sci*, *16*(5), 9772-9793. https://doi.org/10.3390/ijms16059772

Bonda, D. J., Mailankot, M., Stone, J. G., Garrett, M. R., Staniszewska, M., Castellani, R. J., Siedlak, S. L., Zhu, X., Lee, H.-G., Perry, G., Nagaraj, R. H., & Smith, M. A. (2010). Indoleamine 2,3-dioxygenase and 3-hydroxykynurenine modifications are found in the neuropathology of Alzheimer's disease. *Redox Rep*, *15*(4), 161-168. https://doi.org/10.1179/174329210X12650506623645

Borbély, E., Varga, V., Szögi, T., Schuster, I., Bozsó, Z., Penke, B., & Fülöp, L. (2022). Impact of Two Neuronal Sigma-1 Receptor Modulators, PRE084 and DMT, on Neurogenesis and Neuroinflammation in an $A\beta_{1-42}$-Injected, Wild-Type Mouse Model of AD. *Int J Mol Sci*, *23*(5). https://doi.org/10.3390/ijms23052514

Böszörményi, Z., Dér, P., & Nagy, T. (1959). Observations on the Psychotogenic Effect of N-N Diethyltryptamine, a New Tryptamine Derivative. *J Ment Sci*, *105*(438), 171-181. https://doi.org/10.1192/bjp.105.438.171

Botella-López, A., Cuchillo-Ibáñez, I., Cotrufo, T., Mok, S. S., Li, Q.-X., Barquero, M.-S., Dierssen, M., Soriano, E., & Sáez-Valero, J. (2010). β-amyloid controls altered Reelin expression and processing in Alzheimer's disease. *Neurobiol Dis*, *37*(3), 682-691. https://doi.org/10.1016/j.nbd.2009.12.006

Botto, R., Callai, N., Cermelli, A., Causarano, L., & Rainero, I. (2022). Anxiety and depression in Alzheimer's disease: a systematic review of pathogenetic mechanisms and relation to cognitive decline. *Neurol Sci*, *43*(7), 4107-4124. https://doi.org/10.1007/s10072-022-06068-x

Brothers, H. M., Gosztyla, M. L., & Robinson, S. R. (2018). The Physiological Roles of Amyloid-β Peptide Hint at New Ways to Treat Alzheimer's Disease. *Front Aging Neurosci*, *10*, 118. https://doi.org/10.3389/fnagi.2018.00118

Buga, A. M., Ciobanu, O., Bădescu, G. M., Bogdan, C., Weston, R., Slevin, M., Di Napoli, M., & Popa-Wagner, A. (2016). Up-regulation of serotonin receptor 2B mRNA and protein in the peri-infarcted area of aged rats and stroke patients. *Oncotarget*, *7*(14), 17415-17430. https://doi.org/10.18632/oncotarget.8277

Busceti, C. L., Di Pietro, P., Riozzi, B., Traficante, A., Biagioni, F., Nisticò, R., Fornai, F., Battaglia, G., Nicoletti, F., & Bruno, V. (2015). 5-HT(2C) serotonin receptor blockade prevents tau protein hyperphosphorylation and corrects the defect in hippocampal synaptic plasticity caused by a combination of environmental stressors in mice. *Pharmacol Res*, *99*, 258-268. https://doi.org/10.1016/j.phrs.2015.06.017

Cai, D., Zhong, M., Wang, R., Netzer, W. J., Shields, D., Zheng, H., Sisodia, S. S., Foster, D. A., Gorelick, F. S., Xu, H., & Greengard, P. (2006). Phospholipase D1 corrects impaired βAPP trafficking and neurite outgrowth in familial Alzheimer's disease-linked presenilin-1 mutant neurons. *Proc Natl Acad Sci U S A*, *103*(6), 1936-1940. https://doi.org/10.1073/pnas.0510710103

Cai, W., Li, L., Sang, S., Pan, X., & Zhong, C. (2023). Physiological Roles of β-amyloid in Regulating Synaptic Function: Implications for AD Pathophysiology. *Neurosci Bull*, *39*(8), 1289-1308. https://doi.org/10.1007/s12264-022-00985-9

Cameron, L. P., Benson, C. J., Dunlap, L. E., & Olson, D. E. (2018). Effects of N, N-Dimethyltryptamine on Rat Behaviors Relevant to Anxiety and Depression. *ACS Chem Neurosci*, *9*(7), 1582-1590. https://doi.org/10.1021/acschemneuro.8b00134

Campo, C. G., Sinagra, M., Verrier, D., Manzoni, O. J., & Chavis, P. (2009). Reelin Secreted by GABAergic Neurons Regulates Glutamate Receptor Homeostasis. *PLoS ONE*, *4*(5), e5505. https://doi.org/10.1371/journal.pone.0005505

Cassano, T., Calcagnini, S., Carbone, A., Bukke, V. N., Orkisz, S., Villani, R., Romano, A., Avolio, C., & Gaetani, S. (2019). Pharmacological Treatment of Depression in Alzheimer's Disease: A Challenging Task. *Front Pharmacol*, *10*, 1067. https://doi.org/10.3389/fphar.2019.01067

Cazzaniga, E., Bulbarelli, A., Lonati, E., Orlando, A., Re, F., Gregori, M., & Masserini, M. (2011). Abeta Peptide Toxicity is Reduced After Treatments Decreasing Phosphatidylethaolamine Content in Differentiated Neuroblastoma Cells. *Neurochem Res*, *36*(5), 863-869. https://doi.org/10.1007/s11064-011-0415-4

Ceccom, J., Loukh, N., Lauwers-Cances, V., Touriol, C., Nicaise, Y., Gentil, C., Uro-Coste, E., Pitson, S., Maurage, C. A., Duyckaerts, C., Cuvillier, O., & Delisle, M. B. (2014). Reduced sphingosine kinase-1 and enhanced sphingosine 1-phosphate lyase expression demonstrate deregulated sphingosine 1-phosphate signaling in Alzheimer's disease. *Acta Neuropathol Commun*, *2*, 12. https://doi.org/10.1186/2051-5960-2-12

Cenini, G., Hebisch, M., Iefremova, V., Flitsch, L. J., Breitkreuz, Y., Tanzi, R. E., Kim, D. Y., Peitz, M., & Brüstle, O. (2021). Dissecting Alzheimer's disease pathogenesis in human 2D and 3D models. *Mol Cell Neurosci*, *110*, 103568. https://doi.org/10.1016/j.mcn.2020.103568

Centeno, E. G. Z., Cimarosti, H., & Bithell, A. (2018). 2D versus 3D human induced pluripotent stem cell-derived cultures for neurodegenerative disease modelling. *Mol Neurodegener*, *13*(1), 27. https://doi.org/10.1186/s13024-018-0258-4

Cerneckis, J., Bu, G., & Shi, Y. (2023). Pushing the boundaries of brain organoids to study Alzheimer's disease. *Trends Mol Med*, *29*(8), 659-672. https://doi.org/10.1016/j.molmed.2023.05.007

Chakraborty, S., Lennon, J. C., Malkaram, S. A., Zeng, Y., Fisher, D. W., & Dong, H. (2019). Serotonergic system, cognition, and BPSD in Alzheimer's disease. *Neurosci Lett*, *704*, 36-44. https://doi.org/10.1016/j.neulet.2019.03.050

Chalbot, S., Zetterberg, H., Blennow, K., Fladby, T., Grundke-Iqbal, I., & Iqbal, K. (2009). Cerebrospinal Fluid Secretory Ca^{2+}-Dependent Phospholipase A_2 Activity Is Increased in Alzheimer Disease *Clin Chem*, *55*(12), 2171-2179. https://doi.org/10.1373/clinchem.2009.130286

Chan, R. B., Oliveira, T. G., Cortes, E. P., Honig, L. S., Duff, K. E., Small, S. A., Wenk, M. R., Shui, G., & Di Paolo, G. (2012). Comparative Lipidomic Analysis of Mouse and Human Brain with Alzheimer Disease. *J Biol Chem*, *287*(4), 2678-2688. https://doi.org/10.1074/jbc.M111.274142

Chao, C.-C., Gutiérrez-Vázquez, C., Rothhammer, V., Mayo, L., Wheeler, M. A., Tjon, E. C., Zandee, S. E. J., Blain, M., de Lima, K. A., Takenaka, M. C., Avila-Pacheco, J., Hewson, P., Liu, L., Sanmarco, L. M., Borucki, D. M., Lipof, G. Z., Trauger, S. A., Clish, C. B., Antel, J. P., Prat, A., & Quintana, F. J. (2019). Metabolic Control of Astrocyte Pathogenic Activity via cPLA2-MAVS. *Cell*, *179*(7), 1483-1498 e1422. https://doi.org/10.1016/j.cell.2019.11.016

Chemuru, S., Kodali, R., & Wetzel, R. (2016). C-Terminal Threonine Reduces $A\beta_{43}$ Amyloidogenicity Compared with $A\beta_{42}$. *J Mol Biol*, *428*(2 Pt A), 274-291. https://doi.org/10.1016/j.jmb.2015.06.008

Chen, G.-F., Xu, T.-H., Yan, Y., Zhou, Y.-R., Jiang, Y., Melcher, K., & Xu, H. E. (2017). Amyloid beta: structure, biology and structure-based therapeutic development. *Acta Pharmacol Sin*, *38*(9), 1205-1235. https://doi.org/10.1038/aps.2017.28

Chen, S.-Q., Cai, Q., Shen, Y.-Y., Wang, P.-J., Teng, G.-J., Zhang, W., & Zang, F.-C. (2012). Age-related changes in brain metabolites and cognitive function in APP/PS1 transgenic mice. *Behav Brain Res*, *235*(1), 1-6. https://doi.org/10.1016/j.bbr.2012.07.016

Cheng, D., Lei, Z.-G., Chu, K., Lam, O. J. H., Chiang, C. Y., & Zhang, Z.-J. (2024). N, N-Dimethyltryptamine, a natural hallucinogen, ameliorates Alzheimer's disease by restoring neuronal Sigma-1 receptor-mediated endoplasmic reticulum-mitochondria crosstalk. *Alzheimers Res Ther*, *16*(1), 95. https://doi.org/10.1186/s13195-024-01462-3

Cherry, J. D., Olschowka, J. A., & O'Banion, M. K. (2014). Neuroinflammation and M2 microglia: the good, the bad, and the inflamed. *J Neuroinflammation*, *11*(1), 98. https://doi.org/10.1186/1742-2094-11-98

Chin, J., Massaro, C. M., Palop, J. J., Thwin, M. T., Yu, G.-Q., Bien-Ly, N., Bender, A., & Mucke, L. (2007). Reelin Depletion in the Entorhinal Cortex of Human Amyloid Precursor Protein Transgenic Mice and Humans with Alzheimer's Disease. *J Neurosci*, *27*(11), 2727-2733. https://doi.org/10.1523/JNEUROSCI.3758-06.2007

Chintapaludi, S. R., Uyar, A., Jackson, H. M., Acklin, C. J., Wang, X., Sasner, M., Carter, G. W., & Howell, G. R. (2020). Staging Alzheimer's Disease in the Brain and Retina of B6.APP/PS1 Mice by Transcriptional Profiling. *J Alzheimers Dis*, *73*(4), 1421-1434. https://doi.org/10.3233/JAD-190793

Choi, S. H., Kim, Y. H., Quinti, L., Tanzi, R. E., & Kim, D. Y. (2016). 3D culture models of Alzheimer's disease: a road map to a "cure-in-a-dish". *Mol Neurodegener*, *11*(1), 75. https://doi.org/10.1186/s13024-016-0139-7

Christensen, M. C., Schmidt, S. N., & Grande, I. (2023). Effectiveness of vortioxetine in patients with major depressive disorder and early-stage dementia: The MEMORY study. *J Affect Disord*, *338*, 423-431. https://doi.org/10.1016/j.jad.2023.06.024

Cirrito, J. R., Disabato, B. M., Restivo, J. L., Verges, D. K., Goebel, W. D., Sathyan, A., Hayreh, D., D'Angelo, G., Benzinger, T., Yoon, H., Kim, J., Morris, J. C., Mintun, M. A., & Sheline, Y. I. (2011). Serotonin signaling is associated with lower amyloid-β levels and plaques in transgenic mice and humans. *Proc Natl Acad Sci U S A*, *108*(36), 14968-14973. https://doi.org/10.1073/pnas.1107411108

Coalier, K. A., Paranjape, G. S., Karki, S., & Nichols, M. R. (2013). Stability of early-stage amyloid-β(1–42) aggregation species. *Biochim Biophys Acta*, *1834*(1), 65-70. https://doi.org/10.1016/j.bbapap.2012.08.017

Cohen, I., & Vogel, W. H. (1972). Determination and physiological disposition of dimethyltryptamine and diethyltryptamine in rat brain, liver and plasma. *Biochem Pharmacol*, *21*(8), 1214-1216. https://doi.org/10.1016/0006-2952(72)90119-0

Connor, T. J., Starr, N., O'Sullivan, J. B., & Harkin, A. (2008). Induction of indolamine 2,3-dioxygenase and kynurenine 3-monooxygenase in rat brain following a systemic inflammatory challenge: A role for IFN-γ? *Neurosci Lett*, *441*(1), 29-34. https://doi.org/10.1016/j.neulet.2008.06.007

Cornell, J., Salinas, S., Huang, H.-Y., & Zhou, M. (2022). Microglia regulation of synaptic plasticity and learning and memory. *Neural Regen Res*, *17*(4), 705-716. https://doi.org/10.4103/1673-5374.322423

Correia, A. S., Cardoso, A., & Vale, N. (2021). Highlighting Immune System and Stress in Major Depressive Disorder, Parkinson's, and Alzheimer's Diseases, with a Connection with Serotonin. *Int J Mol Sci*, *22*(16), 8525. https://doi.org/10.3390/ijms22168525

Correia, A. S., & Vale, N. (2021). Antidepressants in Alzheimer's Disease: A Focus on the Role of Mirtazapine. *Pharmaceuticals (Basel)*, *14*(9), 930. https://doi.org/10.3390/ph14090930

Cozzi, N. V., Gopalakrishnan, A., Anderson, L. L., Feih, J. T., Shulgin, A. T., Daley, P. F., & Ruoho, A. E. (2009). Dimethyltryptamine and other hallucinogenic tryptamines exhibit substrate behavior at the serotonin uptake transporter and the vesicle monoamine transporter. *J Neural Transm (Vienna)*, *116*(12), 1591-1599. https://doi.org/10.1007/s00702-009-0308-8

Cuchillo-Ibáñez, I., Balmaceda, V., Botella-López, A., Rabano, A., Avila, J., & Sáez-Valero, J. (2013). Beta-Amyloid Impairs Reelin Signaling. *PLoS ONE*, *8*(8), e72297. https://doi.org/10.1371/journal.pone.0072297

Cuchillo-Ibañez, I., Mata-Balaguer, T., Balmaceda, V., Arranz, J. J., Nimpf, J., & Sáez-Valero, J. (2016). The β-amyloid peptide compromises Reelin signaling in Alzheimer's disease. *Sci Rep*, *6*(1), 31646. https://doi.org/10.1038/srep31646

Cudalbu, C., Behar, K. L., Bhattacharyya, P. K., Bogner, W., Borbath, T., de Graaf, R. A., Gruetter, R., Henning, A., Juchem, C., Kreis, R., Lee, P., Lei, H., Marjańska, M., Mekle, R., Murali-Manohar, S., Považan, M., Rackayová, V., Simicic, D., Slotboom, J., Soher, B. J., Starčuk, Z., Jr., Starčuková, J., Tkáč, I., Williams, S., Wilson, M., Wright, A. M., Xin, L., & Mlynárik, V. (2021). Contribution of macromolecules to brain ^{1}H MR spectra: Experts' consensus recommendations. *NMR Biomed*, *34*(5), e4393. https://doi.org/10.1002/nbm.4393

Cumbo, E., Adair, M., Åström, D. O., & Christensen, M. C. (2022). Effectiveness of vortioxetine in patients with major depressive disorder and comorbid Alzheimer's disease in routine clinical practice: An analysis of a post-marketing surveillance study in South Korea. *Front Aging Neurosci*, *14*, 1037816. https://doi.org/10.3389/fnagi.2022.1037816

Cumbo, E., Cumbo, S., Torregrossa, S., & Migliore, D. (2019). Treatment Effects of Vortioxetine on Cognitive Functions in Mild Alzheimer's Disease Patients with Depressive Symptoms: A 12 Month, Open-Label, Observational Study. *J Prev Alzheimers Dis*, *6*(3), 192-197. https://doi.org/10.14283/jpad.2019.24

Cutler, R. G., Kelly, J., Storie, K., Pedersen, W. A., Tammara, A., Hatanpaa, K., Troncoso, J. C., & Mattson, M. P. (2004). Involvement of oxidative stress-induced abnormalities in ceramide and cholesterol

metabolism in brain aging and Alzheimer's disease. *Proc Natl Acad Sci U S A*, *101*(7), 2070-2075. https://doi.org/10.1073/pnas.0305799101

Cutuli, D., Giacovazzo, G., Decandia, D., & Coccurello, R. (2022). Alzheimer's disease and depression in the elderly: A trajectory linking gut microbiota and serotonin signaling. *Front Psychiatry*, *13*, 1010169. https://doi.org/10.3389/fpsyt.2022.1010169

Czubowicz, K., Cieślik, M., Pyszko, J., Strosznajder, J. B., & Strosznajder, R. P. (2015). Sphingosine-1-Phosphate and Its Effect on Glucose Deprivation/Glucose Reload Stress: From Gene Expression to Neuronal Survival. *Mol Neurobiol*, *51*(3), 1300-1308. https://doi.org/10.1007/s12035-014-8807-5

D'Angelo, G., Capasso, S., Sticco, L., & Russo, D. (2013). Glycosphingolipids: synthesis and functions. *FEBS J*, *280*(24), 6338-6353. https://doi.org/10.1111/febs.12559

D'Avanzo, C., Aronson, J., Kim, Y. H., Choi, S. H., Tanzi, R. E., & Kim, D. Y. (2015). Alzheimer's in 3D culture: Challenges and perspectives. *Bioessays*, *37*(10), 1139-1148. https://doi.org/10.1002/bies.201500063

da Silva Siqueira, L., Majolo, F., da Silva, A. P. B., da Costa, J. C., & Marinowic, D. R. (2021). Neurospheres: a potential in vitro model for the study of central nervous system disorders. *Mol Biol Rep*, *48*(4), 3649-3663. https://doi.org/10.1007/s11033-021-06301-4

Dakic, V., Minardi Nascimento, J., Costa Sartore, R., Maciel, R. D. M., de Araujo, D. B., Ribeiro, S., Martins-de-Souza, D., & Rehen, S. K. (2017). Short term changes in the proteome of human cerebral organoids induced by 5-MeO-DMT. *Sci Rep*, *7*(1), 12863. https://doi.org/10.1038/s41598-017-12779-5

Darmoise, A., Maschmeyer, P., & Winau, F. (2010). Chapter 2 - The Immunological Functions of Saposins. In Alt, F. W. (Ed.), *Advances in Immunology* (Vol. 105, pp. 25-62). Academic Press. https://doi.org/10.1016/s0065-2776(10)05002-9

Daynac, M., Morizur, L., Chicheportiche, A., Mouthon, M. A., & Boussin, F. D. (2016). Age-related neurogenesis decline in the subventricular zone is associated with specific cell cycle regulation changes in activated neural stem cells. *Sci Rep*, *6*(1), 21505. https://doi.org/10.1038/srep21505

Dayon, L., Núñez Galindo, A., Wojcik, J., Cominetti, O., Corthésy, J., Oikonomidi, A., Henry, H., Kussmann, M., Migliavacca, E., Severin, I., Bowman, G. L., & Popp, J. (2018). Alzheimer disease pathology and the cerebrospinal fluid proteome. *Alzheimers Res Ther*, *10*(1), 66. https://doi.org/10.1186/s13195-018-0397-4

de Ménorval, M. A., Mir, L. M., Fernández, M. L., & Reigada, R. (2012). Effects of Dimethyl Sulfoxide in Cholesterol-Containing Lipid Membranes: A Comparative Study of Experiments In Silico and with Cells. *PLoS ONE*, *7*(7), e41733. https://doi.org/10.1371/journal.pone.0041733

De Strooper, B. (2010). Proteases and Proteolysis in Alzheimer Disease: A Multifactorial View on the Disease Process. *Physiol Rev*, *90*(2), 465-494. https://doi.org/10.1152/physrev.00023.2009

De Strooper, B., Vassar, R., & Golde, T. (2010). The secretases: enzymes with therapeutic potential in Alzheimer disease. *Nat Rev Neurol*, *6*(2), 99-107. https://doi.org/10.1038/nrneurol.2009.218

de Wit, N. M., Mol, K., Rodríguez-Lorenzo, S., de Vries, H. E., & Kooij, G. (2020). The Role of Sphingolipids and Specialized Pro-Resolving Mediators in Alzheimer's Disease. *Front Immunol*, *11*, 620348. https://doi.org/10.3389/fimmu.2020.620348

de Wit, N. M., Snkhchyan, H., den Hoedt, S., Wattimena, D., de Vos, R., Mulder, M. T., Walter, J., Martinez-Martinez, P., Hoozemans, J. J., Rozemuller, A. J., & de Vries, H. E. (2017). Altered Sphingolipid Balance in Capillary Cerebral Amyloid Angiopathy. *J Alzheimers Dis*, *60*(3), 795-807. https://doi.org/10.3233/JAD-160551

Dehghan, A., Pinto, R. C., Karaman, I., Huang, J., Durainayagam, B. R., Ghanbari, M., Nazeer, A., Zhong, Q., Liggi, S., Whiley, L., Mustafa, R., Kivipelto, M., Solomon, A., Ngandu, T., Kanekiyo, T., Aikawa, T., Radulescu, C. I., Barnes, S. J., Graça, G., Chekmeneva, E., Camuzeaux, S., Lewis, M. R., Kaluarachchi, M. R., Ikram, M. A., Holmes, E., Tzoulaki, I., Matthews, P. M., Griffin, J. L., & Elliott, P. (2022). Metabolome-wide association study on *ABCA7* indicates a role of ceramide metabolism in Alzheimer's disease. *Proc Natl Acad Sci U S A*, *119*(43), e2206083119. https://doi.org/10.1073/pnas.2206083119

Delatour, B., Guégan, M., Volk, A., & Dhenain, M. (2006). In vivo MRI and histological evaluation of brain atrophy in APP/PS1 transgenic mice. *Neurobiol Aging*, *27*(6), 835-847. https://doi.org/10.1016/j.neurobiolaging.2005.04.011

Demars, M., Hu, Y.-S., Gadadhar, A., & Lazarov, O. (2010). Impaired neurogenesis is an early event in the etiology of familial Alzheimer's disease in transgenic mice. *J Neurosci Res*, *88*(10), 2103-2117. https://doi.org/10.1002/jnr.22387

Deshpande, K., Saatian, B., Martirosian, V., Lin, M., Julian, A., & Neman, J. (2019). Isolation of Neural Stem Cells from Whole Brain Tissues of Adult Mice. *Curr Protoc Stem Cell Biol*, *49*(1), e80. https://doi.org/10.1002/cpsc.80

Dhakal, S., & Macreadie, I. (2021). Potential contributions of trace amines in Alzheimer's disease and therapeutic prospects. *Neural Regen Res*, *16*(7), 1394-1396. https://doi.org/10.4103/1673-5374.300985

Dodge, J. C., Tamsett, T. J., Treleaven, C. M., Taksir, T. V., Piepenhagen, P., Sardi, S. P., Cheng, S. H., & Shihabuddin, L. S. (2022). Glucosylceramide synthase inhibition reduces ganglioside GM3 accumulation, alleviates amyloid neuropathology, and stabilizes remote contextual memory in a mouse model of Alzheimer's disease. *Alzheimers Res Ther*, *14*(1), 19. https://doi.org/10.1186/s13195-022-00966-0

Doetschman, T. (2009). Influence of Genetic Background on Genetically Engineered Mouse Phenotypes. In Wurst, W. & Kühn, R. (Eds.), *Gene Knockout Protocols: Second Edition* (Vol. 530, pp. 423-433). Humana Press. https://doi.org/10.1007/978-1-59745-471-1_23

Doody, R. S., Demirovic, J., Ballantyne, C. M., Chan, W., Barber, R., Powell, S., Pavlik, V., & Texas Alzheimer's Disease Research and Care Consortium. (2015). Lipoprotein-associated phospholipase A2, homocysteine, and Alzheimer's disease. *Alzheimers Dement (Amst)*, *1*(4), 464-471. https://doi.org/10.1016/j.dadm.2015.08.001

Dorninger, F., Moser, A. B., Kou, J., Wiesinger, C., Forss-Petter, S., Gleiss, A., Hinterberger, M., Jungwirth, S., Fischer, P., & Berger, J. (2018). Alterations in the Plasma Levels of Specific Choline Phospholipids in Alzheimer's Disease Mimic Accelerated Aging. *J Alzheimers Dis*, *62*(2), 841-854. https://doi.org/10.3233/JAD-171036

Dorr, A., Sahota, B., Chinta, L. V., Brown, M. E., Lai, A. Y., Ma, K., Hawkes, C. A., McLaurin, J., & Stefanovic, B. (2012). Amyloid-β-dependent compromise of microvascular structure and function in a model of Alzheimer's disease *Brain*, *135*(10), 3039-3050. https://doi.org/10.1093/brain/aws243

Drummond, E., & Wisniewski, T. (2017). Alzheimer's disease: experimental models and reality. *Acta Neuropathol*, *133*(2), 155-175. https://doi.org/10.1007/s00401-016-1662-x

Du, X., Li, J., Li, M., Yang, X., Qi, Z., Xu, B., Liu, W., Xu, Z., & Deng, Y. (2020). Research progress on the role of type I vesicular glutamate transporter (VGLUT1) in nervous system diseases. *Cell Biosci*, *10*(1), 26. https://doi.org/10.1186/s13578-020-00393-4

Durakoglugil, M. S., Chen, Y., White, C. L., Kavalali, E. T., & Herz, J. (2009). Reelin signaling antagonizes β-amyloid at the synapse. *Proc Natl Acad Sci U S A*, *106*(37), 15938-15943. https://doi.org/10.1073/pnas.0908176106

Eisai co. Ltd., & Biogen Inc. (2025). *FDA Accepts LEQEMBI® (lecanemab-irmb) Biologics License Application for Subcutaneous Maintenance Dosing for the Treatment of Early Alzheimer's Disease*. Retrieved 2025/02/20 from https://www.prnewswire.com/news-releases/fda-accepts-leqembi-lecanemab-irmb-biologics-license-application-for-subcutaneous-maintenance-dosing-for-the-treatment-of-early-alzheimers-disease-302349842.html

Eisele, A., Hill-Strathy, M., Michels, L., & Rauen, K. (2020). Magnetic Resonance Spectroscopy following Mild Traumatic Brain Injury: A Systematic Review and Meta-Analysis on the Potential to Detect Posttraumatic Neurodegeneration. *Neurodegener Dis*, *20*(1), 2-11. https://doi.org/10.1159/000508098

El-Husseini, A. E., Schnell, E., Chetkovich, D. M., Nicoll, R. A., & Bredt, D. S. (2000). PSD-95 involvement in maturation of excitatory synapses. *Science*, *290*(5495), 1364-1368. https://www.ncbi.nlm.nih.gov/pubmed/11082065

Esteras, N., Alquézar, C., Bartolomé, F., Antequera, D., Barrios, L., Carro, E., Cerdán, S., & Martin-Requero, A. (2012). Systematic Evaluation of Magnetic Resonance Imaging and Spectroscopy Techniques for Imaging a Transgenic Model of Alzheimer's Disease (AβPP/PS1). *J Alzheimers Dis*, *30*(2), 337-353. https://doi.org/10.3233/JAD-2012-111967

Esteve, D., Molina-Navarro, M. M., Giraldo, E., Martínez-Varea, N., Blanco-Gandia, M.-C., Rodríguez-Arias, M., García-Verdugo, J. M., Viña, J., & Lloret, A. (2022). Adult Neural Stem Cell Migration Is Impaired in a Mouse Model of Alzheimer's Disease. *Mol Neurobiol*, *59*(2), 1168-1182. https://doi.org/10.1007/s12035-021-02620-6

European Medicines Agency. (2024, 2024/11/14). *Leqembi recommended for treatment of early Alzheimer's disease | European Medicines Agency (EMA)*. Retrieved 2025/02/20 from https://www.ema.europa.eu/en/news/leqembi-recommended-treatment-early-alzheimers-disease

Fabbretti, E., Antognolli, G., & Tongiorgi, E. (2021). Amyloid-β Impairs Dendritic Trafficking of Golgi-Like Organelles in the Early Phase Preceding Neurite Atrophy: Rescue by Mirtazapine. *Front Mol Neurosci*, *14*, 661728. https://doi.org/10.3389/fnmol.2021.661728

Faria, M. C., Gonçalves, G. S., Rocha, N. P., Moraes, E. N., Bicalho, M. A., Gualberto Cintra, M. T., Jardim de Paula, J., Jose Ravic de Miranda, L. F., Clayton de Souza Ferreira, A., Teixeira, A. L., Gomes, K. B., Carvalho, M. D. G., & Sousa, L. P. (2014). Increased plasma levels of BDNF and inflammatory markers in Alzheimer's disease. *J Psychiatr Res*, *53*, 166-172. https://doi.org/10.1016/j.jpsychires.2014.01.019

Farooqui, A. A., Horrocks, L. A., & Farooqui, T. (2000a). Deacylation and reacylation of neural membrane glycerophospholipids. *J Mol Neurosci*, *14*(3), 123-135. https://doi.org/10.1385/jmn:14:3:123

Farooqui, A. A., Horrocks, L. A., & Farooqui, T. (2000b). Glycerophospholipids in brain: their metabolism, incorporation into membranes, functions, and involvement in neurological disorders. *Chem Phys Lipids*, *106*(1), 1-29. https://doi.org/10.1016/s0009-3084(00)00128-6

Faure, A., Verret, L., Bozon, B., El Tannir El Tayara, N., Ly, M., Kober, F., Dhenain, M., Rampon, C., & Delatour, B. (2011). Impaired neurogenesis, neuronal loss, and brain functional deficits in the

APPxPS1-Ki mouse model of Alzheimer's disease. *Neurobiol Aging*, *32*(3), 407-418. https://doi.org/10.1016/j.neurobiolaging.2009.03.009

Fayed, N., Modrego, P. J., Rojas-Salinas, G., & Aguilar, K. (2011). Brain Glutamate Levels Are Decreased in Alzheimer's Disease: A Magnetic Resonance Spectroscopy Study. *Am J Alzheimers Dis Other Demen*, *26*(6), 450-456. https://doi.org/10.1177/1533317511421780

Ferré-González, L., Balaguer, Á., Roca, M., Ftara, A., Lloret, A., & Cháfer-Pericás, C. (2024). Plasma lipidomics in early APP/PS1 female mouse model and its relationship with brain: Is it affected by the estrous cycle? *Alzheimers Res Ther*, *16*(1), 183. https://doi.org/10.1186/s13195-024-01549-x

Ferreira, S. T., & Klein, W. L. (2011). The Aβ oligomer hypothesis for synapse failure and memory loss in Alzheimer's disease. *Neurobiol Learn Mem*, *96*(4), 529-543. https://doi.org/10.1016/j.nlm.2011.08.003

Ferrón, S. R., Andreu-Agulló, C., Mira, H., Sánchez, P., Marqués-Torrejón, M. A., & Fariñas, I. (2007). A combined *ex/in vivo* assay to detect effects of exogenously added factors in neural stem cells. *Nat Protoc*, *2*(4), 849-859. https://doi.org/10.1038/nprot.2007.104

Figley, C. R., Uddin, M. N., Wong, K., Kornelsen, J., Puig, J., & Figley, T. D. (2021). Potential Pitfalls of Using Fractional Anisotropy, Axial Diffusivity, and Radial Diffusivity as Biomarkers of Cerebral White Matter Microstructure. *Front Neurosci*, *15*, 799576. https://doi.org/10.3389/fnins.2021.799576

Findeis, M. A. (2007). The role of amyloid β peptide 42 in Alzheimer's disease. *Pharmacol Ther*, *116*(2), 266-286. https://doi.org/10.1016/j.pharmthera.2007.06.006

Folsom, T. D., & Fatemi, S. H. (2013). The involvement of Reelin in neurodevelopmental disorders. *Neuropharmacology*, *68*, 122-135. https://doi.org/10.1016/j.neuropharm.2012.08.015

Fontanilla, D., Johannessen, M., Hajipour, A. R., Cozzi, N. V., Jackson, M. B., & Ruoho, A. E. (2009). The Hallucinogen N,N-Dimethyltryptamine (DMT) Is an Endogenous Sigma-1 Receptor Regulator. *Science*, *323*(5916), 934-937. https://doi.org/10.1126/science.1166127

Forlenza, O. V., Mendes, C. T., Marie, S. K. N., & Gattaz, W. F. (2007). Inhibition of phospholipase A2 reduces neurite outgrowth and neuronal viability. *Prostaglandins Leukot Essent Fatty Acids*, *76*(1), 47-55. https://doi.org/10.1016/j.plefa.2006.10.002

Förster, E., Zhao, S., & Frotscher, M. (2006). Laminating the hippocampus. *Nat Rev Neurosci*, *7*(4), 259-267. https://doi.org/10.1038/nrn1882

Frisardi, V., Panza, F., Seripa, D., Farooqui, T., & Farooqui, A. A. (2011). Glycerophospholipids and glycerophospholipid-derived lipid mediators: A complex meshwork in Alzheimer's disease pathology. *Prog Lipid Res*, *50*(4), 313-330. https://doi.org/10.1016/j.plipres.2011.06.001

Fu, L., Sun, Y., Guo, Y., Chen, Y., Yu, B., Zhang, H., Wu, J., Yu, X., Kong, W., & Wu, H. (2017). Comparison of neurotoxicity of different aggregated forms of Aβ40, Aβ42 and Aβ43 in cell cultures. *J Pept Sci*, *23*(3), 245-251. https://doi.org/10.1002/psc.2975

Fukunaga, K., & Moriguchi, S. (2017). Stimulation of the Sigma-1 Receptor and the Effects on Neurogenesis and Depressive Behaviors in Mice. In Smith, S. B. & Su, T.-P. (Eds.), *Sigma Receptors: Their Role in Disease and as Therapeutic Targets* (Vol. 964, pp. 201-211). Springer International Publishing. https://doi.org/10.1007/978-3-319-50174-1_14

Gao, C., Jiang, J., Tan, Y., & Chen, S. (2023). Microglia in neurodegenerative diseases: mechanism and potential therapeutic targets. *Signal Transduct Target Ther*, *8*(1), 359. https://doi.org/10.1038/s41392-023-01588-0

Gao, L., Zhang, Y., Sterling, K., & Song, W. (2022). Brain-derived neurotrophic factor in Alzheimer's disease and its pharmaceutical potential. *Transl Neurodegener*, *11*(1), 4. https://doi.org/10.1186/s40035-022-00279-0

Garcia-Alloza, M., Robbins, E. M., Zhang-Nunes, S. X., Purcell, S. M., Betensky, R. A., Raju, S., Prada, C., Greenberg, S. M., Bacskai, B. J., & Frosch, M. P. (2006). Characterization of amyloid deposition in the APPswe/PS1dE9 mouse model of Alzheimer disease. *Neurobiol Dis*, *24*(3), 516-524. https://doi.org/10.1016/j.nbd.2006.08.017

Garcia-Miralles, M., Ooi, J., Ferrari Bardile, C., Tan, L. J., George, M., Drum, C. L., Lin, R. Y., Hayden, M. R., & Pouladi, M. A. (2016). Treatment with the MAO-A inhibitor clorgyline elevates monoamine neurotransmitter levels and improves affective phenotypes in a mouse model of Huntington disease. *Exp Neurol*, *278*, 4-10. https://doi.org/10.1016/j.expneurol.2016.01.019

Garcia-Romeu, A., Darcy, S., Jackson, H., White, T., & Rosenberg, P. (2022). Psychedelics as Novel Therapeutics in Alzheimer's Disease: Rationale and Potential Mechanisms. In Barrett, F. S. & Preller, K. H. (Eds.), *Disruptive Psychopharmacology* (Vol. 56, pp. 287-317). Springer International Publishing. https://doi.org/10.1007/7854_2021_267

Ghate, P. S., Sidhar, H., Carlson, G. A., & Giri, R. K. (2014). Development of a novel cellular model of Alzheimer's disease utilizing neurosphere cultures derived from B6C3-Tg(APPswe,PSEN1dE9)85Dbo/J embryonic mouse brain. *SpringerPlus*, *3*(1), 161. https://doi.org/10.1186/2193-1801-3-161

Gillotin, S., Sahni, V., Lepko, T., Hanspal, M. A., Swartz, J. E., Alexopoulou, Z., & Marshall, F. H. (2021). Targeting impaired adult hippocampal neurogenesis in ageing by leveraging intrinsic mechanisms regulating Neural Stem Cell activity. *Ageing Res Rev*, *71*, 101447. https://doi.org/10.1016/j.arr.2021.101447

Glenner, G. G., & Wong, C. W. (1984). Alzheimer's disease: initial report of the purification and characterization of a novel cerebrovascular amyloid protein. *Biochem Biophys Res Commun*, *120*(3), 885-890. https://doi.org/10.1016/s0006-291x(84)80190-4

Gold, B. T., Johnson, N. F., Powell, D. K., & Smith, C. D. (2012). White matter integrity and vulnerability to Alzheimer's disease: Preliminary findings and future directions. *Biochim Biophys Acta*, *1822*(3), 416-422. https://doi.org/10.1016/j.bbadis.2011.07.009

Gómez-Isla, T., Price, J. L., McKeel, D. W., Jr., Morris, J. C., Growdon, J. H., & Hyman, B. T. (1996). Profound Loss of Layer II Entorhinal Cortex Neurons Occurs in Very Mild Alzheimer's Disease. *J Neurosci*, *16*(14), 4491-4500. https://doi.org/10.1523/JNEUROSCI.16-14-04491.1996

Gouras, G. K., Olsson, T. T., & Hansson, O. (2015). β-amyloid Peptides and Amyloid Plaques in Alzheimer's Disease. *Neurotherapeutics*, *12*(1), 3-11. https://doi.org/10.1007/s13311-014-0313-y

Gouras, G. K., Tampellini, D., Takahashi, R. H., & Capetillo-Zarate, E. (2010). Intraneuronal β-amyloid accumulation and synapse pathology in Alzheimer's disease. *Acta Neuropathol*, *119*(5), 523-541. https://doi.org/10.1007/s00401-010-0679-9

Gouras, G. K., Tsai, J., Naslund, J., Vincent, B., Edgar, M., Checler, F., Greenfield, J. P., Haroutunian, V., Buxbaum, J. D., Xu, H., Greengard, P., & Relkin, N. R. (2000). Intraneuronal Aβ42 Accumulation in Human Brain. *Am J Pathol*, *156*(1), 15-20. https://doi.org/10.1016/s0002-9440(10)64700-1

Griebel, G., Stemmelin, J., Lopez-Grancha, M., Boulay, D., Boquet, G., Slowinski, F., Pichat, P., Beeské, S., Tanaka, S., Mori, A., Fujimura, M., & Eguchi, J. (2019). The selective GSK3 inhibitor, SAR502250,

displays neuroprotective activity and attenuates behavioral impairments in models of neuropsychiatric symptoms of Alzheimer's disease in rodents. *Sci Rep*, *9*(1), 18045. https://doi.org/10.1038/s41598-019-54557-5

Grimm, M. O. W., Grimm, H. S., Pätzold, A. J., Zinser, E. G., Halonen, R., Duering, M., Tschäpe, J.-A., De Strooper, B., Müller, U., Shen, J., & Hartmann, T. (2005). Regulation of cholesterol and sphingomyelin metabolism by amyloid-β and presenilin. *Nat Cell Biol*, *7*(11), 1118-1123. https://doi.org/10.1038/ncb1313

Guillemin, G. J., Brew, B. J., Noonan, C. E., Takikawa, O., & Cullen, K. M. (2005). Indoleamine 2,3 dioxygenase and quinolinic acid Immunoreactivity in Alzheimer's disease hippocampus. *Neuropathol Appl Neurobiol*, *31*(4), 395-404. https://doi.org/10.1111/j.1365-2990.2005.00655.x

Gulbins, E., Palmada, M., Reichel, M., Lüth, A., Böhmer, C., Amato, D., Müller, C. P., Tischbirek, C. H., Groemer, T. W., Tabatabai, G., Becker, K. A., Tripal, P., Staedtler, S., Ackermann, T. F., van Brederode, J., Alzheimer, C., Weller, M., Lang, U. E., Kleuser, B., Grassmé, H., & Kornhuber, J. (2013). Acid sphingomyelinase-ceramide system mediates effects of antidepressant drugs. *Nat Med*, *19*(7), 934-938. https://doi.org/10.1038/nm.3214

Gulbins, E., Walter, S., Becker, K. A., Halmer, R., Liu, Y., Reichel, M., Edwards, M. J., Müller, C. P., Fassbender, K., & Kornhuber, J. (2015). A central role for the acid sphingomyelinase/ceramide system in neurogenesis and major depression. *J Neurochem*, *134*(2), 183-192. https://doi.org/10.1111/jnc.13145

Guo, S., Wang, H., & Yin, Y. (2022). Microglia Polarization From M1 to M2 in Neurodegenerative Diseases. *Front Aging Neurosci*, *14*, 815347. https://doi.org/10.3389/fnagi.2022.815347

Guo, T., Zhang, D., Zeng, Y., Huang, T. Y., Xu, H., & Zhao, Y. (2020). Molecular and cellular mechanisms underlying the pathogenesis of Alzheimer's disease. *Mol Neurodegener*, *15*(1), 40. https://doi.org/10.1186/s13024-020-00391-7

Haass, C., Kaether, C., Thinakaran, G., & Sisodia, S. (2012). Trafficking and Proteolytic Processing of APP. *Cold Spring Harb Perspect Med*, *2*(5), a006270. https://doi.org/10.1101/cshperspect.a006270

Hait, N. C., & Maiti, A. (2017). The Role of Sphingosine-1-Phosphate and Ceramide-1-Phosphate in Inflammation and Cancer. *Mediators Inflamm*, *2017*, 4806541. https://doi.org/10.1155/2017/4806541

Hamm, H. E. (1998). The Many Faces of G Protein Signaling. *J Biol Chem*, *273*(2), 669-672. https://doi.org/10.1074/jbc.273.2.669

Hamon, M., & Blier, P. (2013). Monoamine neurocircuitry in depression and strategies for new treatments. *Prog Neuropsychopharmacol Biol Psychiatry*, *45*, 54-63. https://doi.org/10.1016/j.pnpbp.2013.04.009

Han, X., Holtzman, D. M., McKeel, D. W. J., Kelley, J., & Morris, J. C. (2002). Substantial sulfatide deficiency and ceramide elevation in very early Alzheimer's disease: potential role in disease pathogenesis. *J Neurochem*, *82*(4), 809-818. https://doi.org/10.1046/j.1471-4159.2002.00997.x

Hannon, J., & Hoyer, D. (2008). Molecular biology of 5-HT receptors. *Behav Brain Res*, *195*(1), 198-213. https://doi.org/10.1016/j.bbr.2008.03.020

Hanspal, M. A., & Gillotin, S. (2022). A new age in understanding adult hippocampal neurogenesis in Alzheimer's disease. *Neural Regen Res*, *17*(12), 2615-2618. https://doi.org/10.4103/1673-5374.339472

Harayama, T., Eto, M., Shindou, H., Kita, Y., Otsubo, E., Hishikawa, D., Ishii, S., Sakimura, K., Mishina, M., & Shimizu, T. (2014). Lysophospholipid Acyltransferases Mediate Phosphatidylcholine Diversification to

Achieve the Physical Properties Required In Vivo. *Cell Metab*, *20*(2), 295-305. https://doi.org/10.1016/j.cmet.2014.05.019

Haruki, H., Hovius, R., Pedersen, M. G., & Johnsson, K. (2016). Tetrahydrobiopterin Biosynthesis as a Potential Target of the Kynurenine Pathway Metabolite Xanthurenic Acid. *J Biol Chem*, *291*(2), 652-657. https://doi.org/10.1074/jbc.C115.680488

Harvey, B. K., Richie, C. T., Hoffer, B. J., & Airavaara, M. (2011). Transgenic animal models of neurodegeneration based on human genetic studies. *J Neural Transm (Vienna)*, *118*(1), 27-45. https://doi.org/10.1007/s00702-010-0476-6

Hatami, A., Monjazeb, S., Milton, S., & Glabe, C. G. (2017). Familial Alzheimer's Disease Mutations within the Amyloid Precursor Protein Alter the Aggregation and Conformation of the Amyloid-beta Peptide. *J Biol Chem*, *292*(8), 3172-3185. https://doi.org/10.1074/jbc.M116.755264

Hayashi, M. K., Tang, C., Verpelli, C., Narayanan, R., Stearns, M. H., Xu, R.-M., Li, H., Sala, C., & Hayashi, Y. (2009). The Postsynaptic Density Proteins Homer and Shank Form a Polymeric Network Structure. *Cell*, *137*(1), 159-171. https://doi.org/10.1016/j.cell.2009.01.050

He, X., Huang, Y., Li, B., Gong, C.-X., & Schuchman, E. H. (2010). Deregulation of sphingolipid metabolism in Alzheimer's disease. *Neurobiol Aging*, *31*(3), 398-408. https://doi.org/10.1016/j.neurobiolaging.2008.05.010

Hendricksen, M., Thomas, A. J., Ferrier, I. N., Ince, P., & O'Brien, J. T. (2004). Neuropathological Study of the Dorsal Raphe Nuclei in Late-Life Depression and Alzheimer's Disease With and Without Depression. *Am J Psychiatry*, *161*(6), 1096-1102. https://doi.org/10.1176/appi.ajp.161.6.1096

Heneka, M. T., Carson, M. J., El Khoury, J., Landreth, G. E., Brosseron, F., Feinstein, D. L., Jacobs, A. H., Wyss-Coray, T., Vitorica, J., Ransohoff, R. M., Herrup, K., Frautschy, S. A., Finsen, B., Brown, G. C., Verkhratsky, A., Yamanaka, K., Koistinaho, J., Latz, E., Halle, A., Petzold, G. C., Town, T., Morgan, D., Shinohara, M. L., Perry, V. H., Holmes, C., Bazan, N. G., Brooks, D. J., Hunot, S., Joseph, B., Deigendesch, N., Garaschuk, O., Boddeke, E., Dinarello, C. A., Breitner, J. C., Cole, G. M., Golenbock, D. T., & Kummer, M. P. (2015). Neuroinflammation in Alzheimer's disease. *Lancet Neurol*, *14*(4), 388-405. https://doi.org/10.1016/S1474-4422(15)70016-5

Heras-Sandoval, D., Ferrera, P., & Arias, C. (2012). Amyloid-β Protein Modulates Insulin Signaling in Presynaptic Terminals. *Neurochem Res*, *37*(9), 1879-1885. https://doi.org/10.1007/s11064-012-0800-7

Hernández-Benítez, R., Vangipuram, S. D., Ramos-Mandujano, G., Lyman, W. D., & Pasantes-Morales, H. (2013). Taurine Enhances the Growth of Neural Precursors Derived from Fetal Human Brain and Promotes Neuronal Specification. *Dev Neurosci*, *35*(1), 40-49. https://doi.org/10.1159/000346900

Hernández-Sapiéns, M. A., Reza-Zaldívar, E. E., Márquez-Aguirre, A. L., Gómez-Pinedo, U., Matias-Guiu, J., Cevallos, R. R., Mateos-Díaz, J. C., Sánchez-González, V. J., & Canales-Aguirre, A. A. (2022). Presenilin mutations and their impact on neuronal differentiation in Alzheimer's disease. *Neural Regen Res*, *17*(1), 31-37. https://doi.org/10.4103/1673-5374.313016

Hishikawa, D., Hashidate, T., Shimizu, T., & Shindou, H. (2014). Diversity and function of membrane glycerophospholipids generated by the remodeling pathway in mammalian cells. *J Lipid Res*, *55*(5), 799-807. https://doi.org/10.1194/jlr.R046094

Hoe, H.-S., Lee, K. J., Carney, R. S., Lee, J., Markova, A., Lee, J.-Y., Howell, B. W., Hyman, B. T., Pak, D. T., Bu, G., & Rebeck, G. W. (2009). Interaction of Reelin with Amyloid Precursor Protein Promotes Neurite Outgrowth. *J Neurosci*, *29*(23), 7459-7473. https://doi.org/10.1523/JNEUROSCI.4872-08.2009

Hollands, C., Tobin, M. K., Hsu, M., Musaraca, K., Yu, T.-S., Mishra, R., Kernie, S. G., & Lazarov, O. (2017). Depletion of adult neurogenesis exacerbates cognitive deficits in Alzheimer's disease by compromising hippocampal inhibition. *Mol Neurodegener*, *12*(1), 64. https://doi.org/10.1186/s13024-017-0207-7

Holtzman, D. M., Morris, J. C., & Goate, A. M. (2011). Alzheimer's Disease: The Challenge of the Second Century. *Sci Transl Med*, *3*(77), 77sr71. https://doi.org/10.1126/scitranslmed.3002369

Hong, S., Beja-Glasser, V. F., Nfonoyim, B. M., Frouin, A., Li, S., Ramakrishnan, S., Merry, K. M., Shi, Q., Rosenthal, A., Barres, B. A., Lemere, C. A., Selkoe, D. J., & Stevens, B. (2016). Complement and microglia mediate early synapse loss in Alzheimer mouse models. *Science*, *352*(6286), 712-716. https://doi.org/10.1126/science.aad8373

Hong, S., Ostaszewski, B. L., Yang, T., O'Malley, T. T., Jin, M., Yanagisawa, K., Li, S., Bartels, T., & Selkoe, D. J. (2014). Soluble Aβ Oligomers Are Rapidly Sequestered from Brain ISF In Vivo and Bind GM1 Ganglioside on Cellular Membranes. *Neuron*, *82*(2), 308-319. https://doi.org/10.1016/j.neuron.2014.02.027

Hoyer, D., Clarke, D. E., Fozard, J. R., Hartig, P. R., Martin, G. R., Mylecharane, E. J., Saxena, P. R., & Humphrey, P. P. (1994). International Union of Pharmacology classification of receptors for 5-hydroxytryptamine (Serotonin). *Pharmacol Rev*, *46*(2), 157-203. https://www.ncbi.nlm.nih.gov/pubmed/7938165

Hu, X., Crick, S. L., Bu, G., Frieden, C., Pappu, R. V., & Lee, J. M. (2009). Amyloid seeds formed by cellular uptake, concentration, and aggregation of the amyloid-beta peptide. *Proc Natl Acad Sci U S A*, *106*(48), 20324-20329. https://doi.org/10.1073/pnas.0911281106

Huang, H., Nie, S., Cao, M., Marshall, C., Gao, J., Xiao, N., Hu, G., & Xiao, M. (2016). Characterization of AD-like phenotype in aged APPSwe/PS1dE9 mice. *Age (Dordr)*, *38*(4), 303-322. https://doi.org/10.1007/s11357-016-9929-7

Hulshof, L. A., Frajmund, L. A., van Nuijs, D., van der Heijden, D. C. N., Middeldorp, J., & Hol, E. M. (2022). Both male and female APPswe/PSEN1dE9 mice are impaired in spatial memory and cognitive flexibility at 9 months of age. *Neurobiol Aging*, *113*, 28-38. https://doi.org/10.1016/j.neurobiolaging.2021.12.009

Hussain, G., Wang, J., Rasul, A., Anwar, H., Imran, A., Qasim, M., Zafar, S., Kamran, S. K. S., Razzaq, A., Aziz, N., Ahmad, W., Shabbir, A., Iqbal, J., Baig, S. M., & Sun, T. (2019). Role of cholesterol and sphingolipids in brain development and neurological diseases. *Lipids Health Dis*, *18*(1), 26. https://doi.org/10.1186/s12944-019-0965-z

Huszti, Z., & Borsy, J. (1964). The effect of diethyltryptamine and its derivatives on monoamine oxidase. *Biochem Pharmacol*, *13*(8), 1151-1156. https://doi.org/10.1016/0006-2952(64)90116-9

Ikeguchi, K., & Kuroda, A. (1995). Mianserin, a 5-HT_2 receptor antagonist, in the treatment of delirium: an open study. *Eur J Neurol*, *1*(3), 261-266. https://doi.org/10.1111/j.1468-1331.1995.tb00082.x

Indellicato, R., & Trinchera, M. (2019). The Link between Gaucher Disease and Parkinson's Disease Sheds Light on Old and Novel Disorders of Sphingolipid Metabolism. *Int J Mol Sci*, *20*(13), 3304. https://doi.org/10.3390/ijms20133304

Iwata, N., Tsubuki, S., Takaki, Y., Shirotani, K., Lu, B., Gerard, N. P., Gerard, C., Hama, E., Lee, H.-J., & Saido, T. C. (2001). Metabolic Regulation of Brain Aβ by Neprilysin. *Science*, *292*(5521), 1550-1552. https://doi.org/10.1126/science.1059946

Izco, M., Martínez, P., Corrales, A., Fandos, N., García, S., Insua, D., Montañes, M., Pérez-Grijalba, V., Rueda, N., Vidal, V., Martínez-Cué, C., Pesini, P., & Sarasa, M. (2014). Changes in the brain and plasma Aβ peptide levels with age and its relationship with cognitive impairment in the APPswe/PS1dE9 mouse model of Alzheimer's disease. *Neuroscience*, *263*, 269-279. https://doi.org/10.1016/j.neuroscience.2014.01.003

Jackson, H. M., Soto, I., Graham, L. C., Carter, G. W., & Howell, G. R. (2013). Clustering of transcriptional profiles identifies changes to insulin signaling as an early event in a mouse model of Alzheimer's disease. *BMC Genomics*, *14*(1), 831. https://doi.org/10.1186/1471-2164-14-831

Jana, A., & Pahan, K. (2004). Fibrillar Amyloid-β Peptides Kill Human Primary Neurons via NADPH Oxidase-mediated Activation of Neutral Sphingomyelinase: IMPLICATIONS FOR ALZHEIMER'S DISEASE. *J Biol Chem*, *279*(49), 51451-51459. https://doi.org/10.1074/jbc.M404635200

Jana, A., & Pahan, K. (2010). Fibrillar Amyloid-β-Activated Human Astroglia Kill Primary Human Neurons via Neutral Sphingomyelinase: Implications for Alzheimer's Disease. *J Neurosci*, *30*(38), 12676-12689. https://doi.org/10.1523/JNEUROSCI.1243-10.2010

Jang, H., Lee, S., Choi, S. L., Kim, H. Y., Baek, S., & Kim, Y. (2017). Taurine Directly Binds to Oligomeric Amyloid-β and Recovers Cognitive Deficits in Alzheimer Model Mice. In Lee, D., Schaffer, S.W., Park, E., Kim, H.W. (Ed.), *Taurine 10* (Vol. 975, pp. 233-241). Springer Netherlands. https://doi.org/10.1007/978-94-024-1079-2_21

Jankowsky, J. L., Fadale, D. J., Anderson, J., Xu, G. M., Gonzales, V., Jenkins, N. A., Copeland, N. G., Lee, M. K., Younkin, L. H., Wagner, S. L., Younkin, S. G., & Borchelt, D. R. (2004). Mutant presenilins specifically elevate the levels of the 42 residue β-amyloid peptide in vivo: evidence for augmentation of a 42-specific γ secretase *Hum Mol Genet*, *13*(2), 159-170. https://doi.org/10.1093/hmg/ddh019

Jankowsky, J. L., Slunt, H. H., Ratovitski, T., Jenkins, N. A., Copeland, N. G., & Borchelt, D. R. (2001). Co-expression of multiple transgenes in mouse CNS: a comparison of strategies. *Biomol Eng*, *17*(6), 157-165. https://doi.org/10.1016/s1389-0344(01)00067-3

Jansen, D., Zerbi, V., Janssen, C. I. F., Dederen, P. J. W. C., Mutsaers, M. P. C., Hafkemeijer, A., Janssen, A. L., Nobelen, C. L., Veltien, A., Asten, J. J., Heerschap, A., & Kiliaan, A. J. (2013). A Longitudinal Study of Cognition, Proton MR Spectroscopy and Synaptic and Neuronal Pathology in Aging Wild-type and AβPPswe-PS1dE9 Mice. *PLoS ONE*, *8*(5), e63643. https://doi.org/10.1371/journal.pone.0063643

Jazvinšćak Jembrek, M., Hof, P. R., & Šimić, G. (2015). Ceramides in Alzheimer's Disease: Key Mediators of Neuronal Apoptosis Induced by Oxidative Stress and Aβ Accumulation. *Oxid Med Cell Longev*, *2015*, 346783. https://doi.org/10.1155/2015/346783

Johansson, P., Almqvist, E. G., Wallin, A., Johansson, J. O., Andreasson, U., Blennow, K., Zetterberg, H., & Svensson, J. (2015). Cerebrospinal fluid substance P concentrations are elevated in patients with Alzheimer's disease. *Neurosci Lett*, *609*, 58-62. https://doi.org/10.1016/j.neulet.2015.10.006

Johnson, M. W., Hendricks, P. S., Barrett, F. S., & Griffiths, R. R. (2019). Classic psychedelics: An integrative review of epidemiology, therapeutics, mystical experience, and brain network function. *Pharmacol Ther*, *197*, 83-102. https://doi.org/10.1016/j.pharmthera.2018.11.010

Joshi, A., Wang, D.-H., Watterson, S., McClean, P. L., Behera, C. K., Sharp, T., & Wong-Lin, K. (2020). Opportunities for multiscale computational modelling of serotonergic drug effects in Alzheimer's disease. *Neuropharmacology*, *174*, 108118. https://doi.org/10.1016/j.neuropharm.2020.108118

Jurkowski, M. P., Bettio, L., E, K. W., Patten, A., Yau, S.-Y., & Gil-Mohapel, J. (2020). Beyond the Hippocampus and the SVZ: Adult Neurogenesis Throughout the Brain. *Front Cell Neurosci*, *14*, 576444. https://doi.org/10.3389/fncel.2020.576444

Kaltenegger, M., Kremser, J., Frewein, M. P. K., Ziherl, P., Bonthuis, D. J., & Pabst, G. (2021). Intrinsic lipid curvatures of mammalian plasma membrane outer leaflet lipids and ceramides. *Biochim Biophys Acta Biomembr*, *1863*(11), 183709. https://doi.org/10.1016/j.bbamem.2021.183709

Kamphuis, W., Orre, M., Kooijman, L., Dahmen, M., & Hol, E. M. (2012). Differential cell proliferation in the cortex of the APPswePS1dE9 Alzheimer's disease mouse model. *Glia*, *60*(4), 615-629. https://doi.org/10.1002/glia.22295

Kang, J., Lemaire, H.-G., Unterbeck, A., Salbaum, J. M., Masters, C. L., Grzeschik, K.-H., Multhaup, G., Beyreuther, K., & Müller-Hill, B. (1987). The precursor of Alzheimer's disease amyloid A4 protein resembles a cell-surface receptor. *Nature*, *325*(6106), 733-736. https://doi.org/10.1038/325733a0

Kao, Y.-C., Ho, P.-C., Tu, Y.-K., Jou, I.-M., & Tsai, K.-J. (2020). Lipids and Alzheimer's Disease. *Int J Mol Sci*, *21*(4), 1505. https://doi.org/10.3390/ijms21041505

Karaca, I., Tamboli, I. Y., Glebov, K., Richter, J., Fell, L. H., Grimm, M. O., Haupenthal, V. J., Hartmann, T., Gräler, M. H., van Echten-Deckert, G., & Walter, J. (2014). Deficiency of Sphingosine-1-phosphate Lyase Impairs Lysosomal Metabolism of the Amyloid Precursor Protein. *J Biol Chem*, *289*(24), 16761-16772. https://doi.org/10.1074/jbc.M113.535500

Katsel, P., Li, C., & Haroutunian, V. (2007). Gene Expression Alterations in the Sphingolipid Metabolism Pathways during Progression of Dementia and Alzheimer's Disease: A Shift Toward Ceramide Accumulation at the Earliest Recognizable Stages of Alzheimer's Disease? *Neurochem Res*, *32*(4-5), 845-856. https://doi.org/10.1007/s11064-007-9297-x

Katsuyama, Y., & Terashima, T. (2009). Developmental anatomy of *reeler* mutant mouse. *Dev Growth Differ*, *51*(3), 271-286. https://doi.org/10.1111/j.1440-169X.2009.01102.x

Kauppinen, R. A., Kokko, H., & Williams, S. R. (1992a). Detection of Mobile Proteins by Proton Nuclear Magnetic Resonance Spectroscopy in the Guinea Pig Brain Ex Vivo and Their Partial Purification. *J Neurochem*, *58*(3), 967-974. https://doi.org/10.1111/j.1471-4159.1992.tb09350.x

Kauppinen, R. A., Nissinen, T., Kärkkäinen, A.-M., Pirttilä, T. R. M., Palvimo, J., Kokko, H., & Williams, S. R. (1992b). Detection of thymosin beta 4 in situ in a guinea pig cerebral cortex preparation using 1H NMR spectroscopy. *J Biol Chem*, *267*(14), 9905-9910. https://doi.org/10.1016/S0021-9258(19)50178-8

Kaur, S., DasGupta, G., & Singh, S. (2019). Altered Neurochemistry in Alzheimer's Disease: Targeting Neurotransmitter Receptor Mechanisms and Therapeutic Strategy. *Neurophysiology*, *51*(4), 293-309. https://doi.org/10.1007/s11062-019-09823-7

Kawarabayashi, T., Shoji, M., Younkin, L. H., Wen-Lang, L., Dickson, D. W., Murakami, T., Matsubara, E., Abe, K., Ashe, K. H., & Younkin, S. G. (2004). Dimeric Amyloid β Protein Rapidly Accumulates in Lipid Rafts followed by Apolipoprotein E and Phosphorylated Tau Accumulation in the Tg2576 Mouse Model of Alzheimer's Disease. *J Neurosci*, *24*(15), 3801-3809. https://doi.org/10.1523/JNEUROSCI.5543-03.2004

Kepp, K. P., Robakis, N. K., Høilund-Carlsen, P. F., Sensi, S. L., & Vissel, B. (2023). The amyloid cascade hypothesis: an updated critical review. *Brain*, *146*(10), 3969-3990. https://doi.org/10.1093/brain/awad159

Kern, R., Joseleau-Petit, D., Chattopadhyay, M. K., & Richarme, G. (2001). Chaperone-like properties of lysophospholipids. *Biochem Biophys Res Commun*, *289*(5), 1268-1274. https://doi.org/10.1006/bbrc.2001.6093

Kilkus, J. P., Goswami, R., Dawson, S. A., Testai, F. D., Berdyshev, E. V., Han, X., & Dawson, G. (2008). Differential regulation of sphingomyelin synthesis and catabolism in oligodendrocytes and neurons. *J Neurochem*, *106*(4), 1745-1757. https://doi.org/10.1111/j.1471-4159.2008.05490.x

Kim, B.-H., Kim, S., Nam, Y., Park, Y. H., Shin, S. M., & Moon, M. (2025). Second-generation anti-amyloid monoclonal antibodies for Alzheimer's disease: current landscape and future perspectives. *Transl Neurodegener*, *14*(1), 6. https://doi.org/10.1186/s40035-025-00465-w

Kim, G. H., Kim, J. E., Rhie, S. J., & Yoon, S. (2015). The Role of Oxidative Stress in Neurodegenerative Diseases. *Exp Neurobiol*, *24*(4), 325-340. https://doi.org/10.5607/en.2015.24.4.325

Kim, S., Choi, J., & Kwon, J. (2023). Thymosin Beta 4 Protects Hippocampal Neuronal Cells against PrP (106-126) via Neurotrophic Factor Signaling. *Molecules*, *28*(9), 3920. https://doi.org/10.3390/molecules28093920

Kim, Y., Kim, C., Jang, H. Y., & Mook-Jung, I. (2016). Inhibition of Cholesterol Biosynthesis Reduces γ-Secretase Activity and Amyloid-β Generation. *J Alzheimers Dis*, *51*(4), 1057-1068. https://doi.org/10.3233/JAD-150982

Kita, Y., Ohto, T., Uozumi, N., & Shimizu, T. (2006). Biochemical properties and pathophysiological roles of cytosolic phospholipase A_2s. *Biochim Biophys Acta*, *1761*(11), 1317-1322. https://doi.org/10.1016/j.bbalip.2006.08.001

Kitaichi, Y., Inoue, T., Nakagawa, S., Boku, S., & Koyama, T. (2012). Effects of combined treatment with clorgyline and selegiline on extracellular noradrenaline and serotonin levels. *Acta Neuropsychiatr*, *24*(6), 369-373. https://doi.org/10.1111/j.1601-5215.2012.00652.x

Kitazawa, M., Medeiros, R., & Laferla, F. M. (2012). Transgenic Mouse Models of Alzheimer Disease: Developing a Better Model as a Tool for Therapeutic Interventions. *Curr Pharm Des*, *18*(8), 1131-1147. https://doi.org/10.2174/138161212799315786

Klein, C., Patte-Mensah, C., Taleb, O., Bourguignon, J. J., Schmitt, M., Bihel, F., Maitre, M., & Mensah-Nyagan, A.-G. (2013). The neuroprotector kynurenic acid increases neuronal cell survival through neprilysin induction. *Neuropharmacology*, *70*, 254-260. https://doi.org/10.1016/j.neuropharm.2013.02.006

Klein, C., Roussel, G., Brun, S., Rusu, C., Patte-Mensah, C., Maitre, M., & Mensah-Nyagan, A.-G. (2018). 5-HIAA induces neprilysin to ameliorate pathophysiology and symptoms in a mouse model for Alzheimer's disease. *Acta Neuropathol Commun*, *6*(1), 136. https://doi.org/10.1186/s40478-018-0640-z

Klementieva, O., Willén, K., Martinsson, I., Israelsson, B., Engdahl, A., Cladera, J., Uvdal, P., & Gouras, G. K. (2017). Pre-plaque conformational changes in Alzheimer's disease-linked Aβ and APP. *Nat Commun*, *8*, 14726. https://doi.org/10.1038/ncomms14726

Koal, T., Klavins, K., Seppi, D., Kemmler, G., & Humpel, C. (2015). Sphingomyelin SM(d18:1/18:0) is Significantly Enhanced in Cerebrospinal Fluid Samples Dichotomized by Pathological Amyloid-β_{42},

Tau, and Phospho-Tau-181 Levels. *J Alzheimers Dis*, *44*(4), 1193-1201. https://doi.org/10.3233/JAD-142319

Kobro-Flatmoen, A., Nagelhus, A., & Witter, M. P. (2016). Reelin-immunoreactive neurons in entorhinal cortex layer II selectively express intracellular amyloid in early Alzheimer's disease. *Neurobiol Dis*, *93*, 172-183. https://doi.org/10.1016/j.nbd.2016.05.012

Kocherhans, S., Madhusudan, A., Doehner, J., Breu, K. S., Nitsch, R. M., Fritschy, J. M., & Knuesel, I. (2010). Reduced Reelin Expression Accelerates Amyloid-β Plaque Formation and Tau Pathology in Transgenic Alzheimer's Disease Mice. *J Neurosci*, *30*(27), 9228-9240. https://doi.org/10.1523/JNEUROSCI.0418-10.2010

Kong, J.-N., Zhu, Z., Itokazu, Y., Wang, G., Dinkins, M. B., Zhong, L., Lin, H.-P., Elsherbini, A., Leanhart, S., Jiang, X., Qin, H., Zhi, W., Spassieva, S. D., & Bieberich, E. (2018). Novel function of ceramide for regulation of mitochondrial ATP release in astrocytes. *J Lipid Res*, *59*(3), 488-506. https://doi.org/10.1194/jlr.M081877

Korshavn, K. J., Satriano, C., Lin, Y., Zhang, R., Dulchavsky, M., Bhunia, A., Ivanova, M. I., Lee, Y.-H., La Rosa, C., Lim, M. H., & Ramamoorthy, A. (2017). Reduced Lipid Bilayer Thickness Regulates the Aggregation and Cytotoxicity of Amyloid-β. *J Biol Chem*, *292*(11), 4638-4650. https://doi.org/10.1074/jbc.M116.764092

Kozlowska, U., Nichols, C., Wiatr, K., & Figiel, M. (2022). From psychiatry to neurology: Psychedelics as prospective therapeutics for neurodegenerative disorders. *J Neurochem*, *162*(1), 89-108. https://doi.org/10.1111/jnc.15509

Kriem, B., Sponne, I., Fifre, A., Malaplate-Armand, C., Lozac'h-Pillot, K., Koziel, V., Yen-Potin, F. T., Bihain, B., Oster, T., Olivier, J.-L., & Pillot, T. (2005). Cytosolic phospholipase A_2 mediates neuronal apoptosis induced by soluble oligomers of the amyloid-β peptide. *Faseb j*, *19*(1), 85-87. https://doi.org/10.1096/fj.04-1807fje

Krstic, D., Rodriguez, M., & Knuesel, I. (2012). Regulated Proteolytic Processing of Reelin through Interplay of Tissue Plasminogen Activator (tPA), ADAMTS-4, ADAMTS-5, and Their Modulators. *PLoS ONE*, *7*(10), e47793. https://doi.org/10.1371/journal.pone.0047793

Kuhla, A., Rühlmann, C., Lindner, T., Polei, S., Hadlich, S., Krause, B. J., Vollmar, B., & Teipel, S. J. (2017). APPswe/PS1dE9 mice with cortical amyloid pathology show a reduced NAA/Cr ratio without apparent brain atrophy: A MRS and MRI study. *Neuroimage Clin*, *15*, 581-586. https://doi.org/10.1016/j.nicl.2017.06.009

Kuhn, P.-H., Wang, H., Dislich, B., Colombo, A., Zeitschel, U., Ellwart, J. W., Kremmer, E., Roßner, S., & Lichtenthaler, S. F. (2010). ADAM10 is the physiologically relevant, constitutive α-secretase of the amyloid precursor protein in primary neurons. *Embo j*, *29*(17), 3020-3032. https://doi.org/10.1038/emboj.2010.167

Kumar, A., Singh, A., & Ekavali. (2015). A review on Alzheimer's disease pathophysiology and its management: an update. *Pharmacol Rep*, *67*(2), 195-203. https://doi.org/10.1016/j.pharep.2014.09.004

Lacor, P. N., Buniel, M. C., Chang, L., Fernandez, S. J., Gong, Y., Viola, K. L., Lambert, M. P., Velasco, P. T., Bigio, E. H., Finch, C. E., Krafft, G. A., & Klein, W. L. (2004). Synaptic Targeting by Alzheimer's-Related Amyloid β Oligomers. *J Neurosci*, *24*(45), 10191-10200. https://doi.org/10.1523/JNEUROSCI.3432-04.2004

Lacor, P. N., Buniel, M. C., Furlow, P. W., Clemente, A. S., Velasco, P. T., Wood, M., Viola, K. L., & Klein, W. L. (2007). Aβ Oligomer-Induced Aberrations in Synapse Composition, Shape, and Density Provide a Molecular Basis for Loss of Connectivity in Alzheimer's Disease. *J Neurosci*, *27*(4), 796-807. https://doi.org/10.1523/JNEUROSCI.3501-06.2007

Lacor, P. N., Grayson, D. R., Auta, J., Sugaya, I., Costa, E., & Guidotti, A. (2000). Reelin secretion from glutamatergic neurons in culture is independent from neurotransmitter regulation. *Proc Natl Acad Sci U S A*, *97*(7), 3556-3561. https://doi.org/10.1073/pnas.97.7.3556

Lalonde, R., Kim, H. D., Maxwell, J. A., & Fukuchi, K. (2005). Exploratory activity and spatial learning in 12-month-old APP_{695}SWE/co + *PS1*/ΔE9 mice with amyloid plaques. *Neurosci Lett*, *390*(2), 87-92. https://doi.org/10.1016/j.neulet.2005.08.028

Lane-Donovan, C., Philips, G. T., Wasser, C. R., Durakoglugil, M. S., Masiulis, I., Upadhaya, A., Pohlkamp, T., Coskun, C., Kotti, T., Steller, L., Hammer, R. E., Frotscher, M., Bock, H. H., & Herz, J. (2015). Reelin protects against amyloid beta toxicity in vivo. *Sci Signal*, *8*(384), ra67. https://doi.org/10.1126/scisignal.aaa6674

LaRocca, T. J., Cavalier, A. N., Roberts, C. M., Lemieux, M. R., Ramesh, P., Garcia, M. A., & Link, C. D. (2021). Amyloid beta acts synergistically as a pro-inflammatory cytokine. *Neurobiol Dis*, *159*, 105493. https://doi.org/10.1016/j.nbd.2021.105493

Lau, J. C., Lerch, J. P., Sled, J. G., Henkelman, R. M., Evans, A. C., & Bedell, B. J. (2008). Longitudinal neuroanatomical changes determined by deformation-based morphometry in a mouse model of Alzheimer's disease. *Neuroimage*, *42*(1), 19-27. https://doi.org/10.1016/j.neuroimage.2008.04.252

Lauretti, E., Dincer, O., & Praticò, D. (2020). Glycogen synthase kinase-3 signaling in Alzheimer's disease. *Biochim Biophys Acta Mol Cell Res*, *1867*(5), 118664. https://doi.org/10.1016/j.bbamcr.2020.118664

Lecanu, L., & Papadopoulos, V. (2013). Modeling Alzheimer's disease with non-transgenic rat models. *Alzheimers Res Ther*, *5*(3), 17. https://doi.org/10.1186/alzrt171

Lee, I.-S., Jung, K., Kim, I.-S., & Park, K. I. (2013). Amyloid-β oligomers regulate the properties of human neural stem cells through GSK-3β signaling. *Exp Mol Med*, *45*(11), e60. https://doi.org/10.1038/emm.2013.125

Lee, J.-C., Simonyi, A., Sun, A. Y., & Sun, G. Y. (2011). Phospholipases A_2 and neural membrane dynamics: implications for Alzheimer's disease. *J Neurochem*, *116*(5), 813-819. https://doi.org/10.1111/j.1471-4159.2010.07033.x

Lee, J. K., Jin, H. K., Park, M. H., Kim, B.-R., Lee, P. H., Nakauchi, H., Carter, J. E., He, X., Schuchman, E. H., & Bae, J.-S. (2014). Acid sphingomyelinase modulates the autophagic process by controlling lysosomal biogenesis in Alzheimer's disease. *J Exp Med*, *211*(8), 1551-1570. https://doi.org/10.1084/jem.20132451

Lewis, K. T., Maddipati, K. R., Naik, A. R., & Jena, B. P. (2017). Unique Lipid Chemistry of Synaptic Vesicle and Synaptosome Membrane Revealed Using Mass Spectrometry. *ACS Chem Neurosci*, *8*(6), 1163-1169. https://doi.org/10.1021/acschemneuro.7b00030

Leysen, J. E. (2004). 5-HT2 Receptors. *Curr Drug Targets CNS Neurol Disord*, *3*(1), 11-26. https://doi.org/10.2174/1568007043482598

Liang, S., Huang, J., Liu, W., Jin, H., Li, L., Zhang, X., Nie, B., Lin, R., Tao, J., Zhao, S., Shan, B., & Chen, L. (2017). Magnetic resonance spectroscopy analysis of neurochemical changes in the atrophic

hippocampus of APP/PS1 transgenic mice. *Behav Brain Res*, *335*, 26-31. https://doi.org/10.1016/j.bbr.2017.08.005

Lima da Cruz, R. V., Moulin, T. C., Petiz, L. L., & Leão, R. N. (2018). A Single Dose of 5-MeO-DMT Stimulates Cell Proliferation, Neuronal Survivability, Morphological and Functional Changes in Adult Mice Ventral Dentate Gyrus. *Front Mol Neurosci*, *11*, 312. https://doi.org/10.3389/fnmol.2018.00312

Liu, G.-H., Ding, Z., & Izpisua Belmonte, J. C. (2012). iPSC technology to study human aging and aging-related disorders. *Curr Opin Cell Biol*, *24*(6), 765-774. https://doi.org/10.1016/j.ceb.2012.08.014

Liu, J.-L., Fan, Y.-G., Yang, Z.-S., Wang, Z.-Y., & Guo, C. (2018). Iron and Alzheimer's Disease: From Pathogenesis to Therapeutic Implications. *Front Neurosci*, *12*, 632. https://doi.org/10.3389/fnins.2018.00632

Liu, Y., Yoo, M.-J., Savonenko, A., Stirling, W., Price, D. L., Borchelt, D. R., Mamounas, L., Lyons, W. E., Blue, M. E., & Lee, M. K. (2008). Amyloid Pathology Is Associated with Progressive Monoaminergic Neurodegeneration in a Transgenic Mouse Model of Alzheimer's Disease. *J Neurosci*, *28*(51), 13805-13814. https://doi.org/10.1523/JNEUROSCI.4218-08.2008

Lopez-Font, I., Iborra-Lazaro, G., Sánchez-Valle, R., Molinuevo, J. L., Cuchillo-Ibañez, I., & Sáez-Valero, J. (2019). CSF-ApoER2 fragments as a read-out of reelin signaling: Distinct patterns in sporadic and autosomal-dominant Alzheimer disease. *Clin Chim Acta*, *490*, 6-11. https://doi.org/10.1016/j.cca.2018.12.012

López-Gambero, A. J., Sanjuan, C., Serrano-Castro, P. J., Suárez, J., & Rodríguez de Fonseca, F. (2020). The Biomedical Uses of Inositols: A Nutraceutical Approach to Metabolic Dysfunction in Aging and Neurodegenerative Diseases. *Biomedicines*, *8*(9), 295. https://doi.org/10.3390/biomedicines8090295

Lorke, D. E., Lu, G., Cho, E., & Yew, D. T. (2006). Serotonin 5-HT_{2A} and 5-HT_6 receptors in the prefrontal cortex of Alzheimer and normal aging patients. *BMC Neurosci*, *7*(1), 36. https://doi.org/10.1186/1471-2202-7-36

Lu, J., Zhang, C., Lv, J., Zhu, X., Jiang, X., Lu, W., Lu, Y., Tang, Z., Wang, J., & Shen, X. (2021). Antiallergic drug desloratadine as a selective antagonist of $5HT_{2A}$ receptor ameliorates pathology of Alzheimer's disease model mice by improving microglial dysfunction. *Aging Cell*, *20*(1), e13286. https://doi.org/10.1111/acel.13286

Ly, C., Greb, A. C., Cameron, L. P., Wong, J. M., Barragan, E. V., Wilson, P. C., Burbach, K. F., Soltanzadeh Zarandi, S. S., Sood, A., Paddy, M. R., Duim, W. C., Dennis, M. Y., McAllister, A. K., Ori-McKenney, K. M., Gray, J. A., & Olson, D. E. (2018). Psychedelics Promote Structural and Functional Neural Plasticity. *Cell Rep*, *23*(11), 3170-3182. https://doi.org/10.1016/j.celrep.2018.05.022

Ly, P. T. T., Wu, Y., Zou, H., Wang, R., Zhou, W., Kinoshita, A., Zhang, M., Yang, Y., Cai, F., Woodgett, J., & Song, W. (2013). Inhibition of GSK3β-mediated BACE1 expression reduces Alzheimer-associated phenotypes. *J Clin Invest*, *123*(1), 224-235. https://doi.org/10.1172/JCI64516

Madden, D. J., Bennett, I. J., & Song, A. W. (2009). Cerebral White Matter Integrity and Cognitive Aging: Contributions from Diffusion Tensor Imaging. *Neuropsychol Rev*, *19*(4), 415-435. https://doi.org/10.1007/s11065-009-9113-2

Maitre, M., Klein, C., Patte-Mensah, C., & Mensah-Nyagan, A.-G. (2020). Tryptophan metabolites modify brain Aβ peptide degradation: A role in Alzheimer's disease? *Prog Neurobiol*, *190*, 101800. https://doi.org/10.1016/j.pneurobio.2020.101800

Malaplate-Armand, C., Florent-Béchard, S., Youssef, I., Koziel, V., Sponne, I., Kriem, B., Leininger-Muller, B., Olivier, J.-L., Oster, T., & Pillot, T. (2006). Soluble oligomers of amyloid-β peptide induce neuronal apoptosis by activating a cPLA$_2$-dependent sphingomyelinase-ceramide pathway. *Neurobiol Dis*, *23*(1), 178-189. https://doi.org/10.1016/j.nbd.2006.02.010

Malm, T. M., Iivonen, H., Goldsteins, G., Keksa-Goldsteine, V., Ahtoniemi, T., Kanninen, K., Salminen, A., Auriola, S., Van Groen, T., Tanila, H., & Koistinaho, J. (2007). Pyrrolidine Dithiocarbamate Activates Akt and Improves Spatial Learning in APP/PS1 Mice without Affecting β-Amyloid Burden. *J Neurosci*, *27*(14), 3712-3721. https://doi.org/10.1523/JNEUROSCI.0059-07.2007

Manaye, K. F., Wang, P. C., O'Neil, J. N., Huang, S. Y., Xu, T., Lei, D.-L., Tizabi, Y., Ottinger, M. A., Ingram, D. K., & Mouton, P. R. (2007). Neuropathological quantification of dtg APP/PS1: neuroimaging, stereology, and biochemistry. *AGE*, *29*(2), 87-96. https://doi.org/10.1007/s11357-007-9035-y

Marjanska, M., Curran, G. L., Wengenack, T. M., Henry, P.-G., Bliss, R. L., Poduslo, J. F., Jack, C. R. J., Uğurbil, K., & Garwood, M. (2005). Monitoring disease progression in transgenic mouse models of Alzheimer's disease with proton magnetic resonance spectroscopy. *Proc Natl Acad Sci U S A*, *102*(33), 11906-11910. https://doi.org/10.1073/pnas.0505513102

Marjańska, M., Weigand, S. D., Preboske, G., Wengenack, T. M., Chamberlain, R., Curran, G. L., Poduslo, J. F., Garwood, M., Kobayashi, D., Lin, J. C., & Jack, C. R. J. (2014). Treatment effects in a transgenic mouse model of Alzheimer's disease: a magnetic resonance spectroscopy study after passive immunization. *Neuroscience*, *259*, 94-100. https://doi.org/10.1016/j.neuroscience.2013.11.052

Maslov, A. Y., Barone, T. A., Plunkett, R. J., & Pruitt, S. C. (2004). Neural Stem Cell Detection, Characterization, and Age-Related Changes in the Subventricular Zone of Mice. *J Neurosci*, *24*(7), 1726-1733. https://doi.org/10.1523/JNEUROSCI.4608-03.2004

Masters, C. L., & Selkoe, D. J. (2012). Biochemistry of Amyloid β-Protein and Amyloid Deposits in Alzheimer Disease. *Cold Spring Harb Perspect Med*, *2*(6), a006262. https://doi.org/10.1101/cshperspect.a006262

Matsuzaki, K. (2020). Aβ–ganglioside interactions in the pathogenesis of Alzheimer's disease. *Biochim Biophys Acta Biomembr*, *1862*(8), 183233. https://doi.org/10.1016/j.bbamem.2020.183233

Mawuenyega, K. G., Sigurdson, W., Ovod, V., Munsell, L., Kasten, T., Morris, J. C., Yarasheski, K. E., & Bateman, R. J. (2010). Decreased Clearance of CNS β-Amyloid in Alzheimer's Disease. *Science*, *330*(6012), 1774. https://doi.org/10.1126/science.1197623

Mayo, L., Trauger, S. A., Blain, M., Nadeau, M., Patel, B., Alvarez, J. I., Mascanfroni, I. D., Yeste, A., Kivisäkk, P., Kallas, K., Ellezam, B., Bakshi, R., Prat, A., Antel, J. P., Weiner, H. L., & Quintana, F. J. (2014). Regulation of astrocyte activation by glycolipids drives chronic CNS inflammation. *Nat Med*, *20*(10), 1147-1156. https://doi.org/10.1038/nm.3681

McInnis, J. J., Sood, D., Guo, L., Dufault, M. R., Garcia, M., Passaro, R., Gao, G., Zhang, B., & Dodge, J. C. (2023). Unravelling neuronal and glial differences in ceramide composition, synthesis, and sensitivity to toxicity. *bioRxiv*, 2023.2012.2006.569570. https://doi.org/10.1101/2023.12.06.569570

McLaurin, J., Franklin, T., Chakrabartty, A., & Fraser, P. E. (1998). Phosphatidylinositol and inositol involvement in alzheimer amyloid-β fibril growth and arrest. *J Mol Biol*, *278*(1), 183-194. https://doi.org/10.1006/jmbi.1998.1677

McLaurin, J., Golomb, R., Jurewicz, A., Antel, J. P., & Fraser, P. E. (2000). Inositol Stereoisomers Stabilize an Oligomeric Aggregate of Alzheimer Amyloid β Peptide and Inhibit Aβ-induced Toxicity. *J Biol Chem*, *275*(24), 18495-18502. https://doi.org/10.1074/jbc.M906994199

McLaurin, J., Kierstead, M. E., Brown, M. E., Hawkes, C. A., Lambermon, M. H., Phinney, A. L., Darabie, A. A., Cousins, J. E., French, J. E., Lan, M. F., Chen, F., Wong, S. S., Mount, H. T., Fraser, P. E., Westaway, D., & St George-Hyslop, P. (2006). Cyclohexanehexol inhibitors of Aβ aggregation prevent and reverse Alzheimer phenotype in a mouse model. *Nat Med*, *12*(7), 801-808. https://doi.org/10.1038/nm1423

Meneses, A., Nieto-Vera, R., & Anaya-Jiménez, R. M. (2018). 5-$HT_{2A/2B/2C}$ Receptors, Memory and Therapeutic Targets. In Guiard, B., Di Giovanni, G. (Ed.), *5-HT2A Receptors in the Central Nervous System* (Vol. 32, pp. 259-271). Springer International Publishing. https://doi.org/10.1007/978-3-319-70474-6_11

Mi, Z., Abrahamson, E. E., Ryu, A. Y., Fish, K. N., Sweet, R. A., Mufson, E. J., & Ikonomovic, M. D. (2017). Loss of precuneus dendritic spines immunopositive for spinophilin is related to cognitive impairment in early Alzheimer's disease. *Neurobiol Aging*, *55*, 159-166. https://doi.org/10.1016/j.neurobiolaging.2017.01.022

Michno, W., Kaya, I., Nyström, S., Guerard, L., Nilsson, K. P. R., Hammarström, P., Blennow, K., Zetterberg, H., & Hanrieder, J. (2018). Multimodal Chemical Imaging of Amyloid Plaque Polymorphism Reveals Aβ Aggregation Dependent Anionic Lipid Accumulations and Metabolism. *Anal Chem*, *90*(13), 8130-8138. https://doi.org/10.1021/acs.analchem.8b01361

Mielke, M. M., Haughey, N. J., Bandaru, V. V. R., Schech, S., Carrick, R., Carlson, M. C., Mori, S., Miller, M. I., Ceritoglu, C., Brown, T., Albert, M., & Lyketsos, C. G. (2010). Plasma ceramides are altered in mild cognitive impairment and predict cognitive decline and hippocampal volume loss. *Alzheimers Dement*, *6*(5), 378-385. https://doi.org/10.1016/j.jalz.2010.03.014

Minkeviciene, R., Ihalainen, J., Malm, T., Matilainen, O., Keksa-Goldsteine, V., Goldsteins, G., Iivonen, H., Leguit, N., Glennon, J., Koistinaho, J., Banerjee, P., & Tanila, H. (2008). Age-related decrease in stimulated glutamate release and vesicular glutamate transporters in APP/PS1 transgenic and wild-type mice. *J Neurochem*, *105*(3), 584-594. https://doi.org/10.1111/j.1471-4159.2007.05147.x

Minkeviciene, R., Rheims, S., Dobszay, M. B., Zilberter, M., Hartikainen, J., Fülöp, L., Penke, B., Zilberter, Y., Harkany, T., Pitkänen, A., & Tanila, H. (2009). Amyloid β-Induced Neuronal Hyperexcitability Triggers Progressive Epilepsy. *J Neurosci*, *29*(11), 3453-3462. https://doi.org/10.1523/JNEUROSCI.5215-08.2009

Moffett, J. R., Ross, B., Arun, P., Madhavarao, C. N., & Namboodiri, A. M. A. (2007). N-Acetylaspartate in the CNS: from neurodiagnostics to neurobiology. *Prog Neurobiol*, *81*(2), 89-131. https://doi.org/10.1016/j.pneurobio.2006.12.003

Mohan, S., Verma, A., Lim, C. C. T., Hui, F., & Kumar, S. (2010). Lipid Resonance on In Vivo Proton MR Spectroscopy: Value of Other Metabolites in Differential Diagnosis. *Neuroradiol J*, *23*(3), 269-278. https://doi.org/10.1177/197140091002300302

Mokhtar, S. H., Bakhuraysah, M. M., Cram, D. S., & Petratos, S. (2013). The Beta-Amyloid Protein of Alzheimer's Disease: Communication Breakdown by Modifying the Neuronal Cytoskeleton. *Int J Alzheimers Dis*, *2013*(1), 910502. https://doi.org/10.1155/2013/910502

Morales-Garcia, J. A., Alonso-Gil, S., Gil, C., Martinez, A., Santos, A., & Perez-Castillo, A. (2015). Phosphodiesterase 7 Inhibition Induces Dopaminergic Neurogenesis in Hemiparkinsonian Rats. *Stem Cells Transl Med*, *4*(6), 564-575. https://doi.org/10.5966/sctm.2014-0277

Morales-Garcia, J. A., Calleja-Conde, J., Lopez-Moreno, J. A., Alonso-Gil, S., Sanz-SanCristobal, M., Riba, J., & Perez-Castillo, A. (2020). N,N-dimethyltryptamine compound found in the hallucinogenic tea ayahuasca, regulates adult neurogenesis in vitro and in vivo. *Transl Psychiatry*, *10*(1), 331. https://doi.org/10.1038/s41398-020-01011-0

Morales-García, J. A., de la Fuente Revenga, M., Alonso-Gil, S., Rodríguez-Franco, M. I., Feilding, A., Perez-Castillo, A., & Riba, J. (2017). The alkaloids of *Banisteriopsis caapi*, the plant source of the Amazonian hallucinogen Ayahuasca, stimulate adult neurogenesis *in vitro*. *Sci Rep*, *7*(1), 5309. https://doi.org/10.1038/s41598-017-05407-9

Morales-Garcia, J. A., Echeverry-Alzate, V., Alonso-Gil, S., Sanz-SanCristobal, M., Lopez-Moreno, J. A., Gil, C., Martinez, A., Santos, A., & Perez-Castillo, A. (2017). Phosphodiesterase7 Inhibition Activates Adult Neurogenesis in Hippocampus and Subventricular Zone In Vitro and In Vivo. *Stem Cells*, *35*(2), 458-472. https://doi.org/10.1002/stem.2480

Morales-Garcia, J. A., Luna-Medina, R., Alfaro-Cervello, C., Cortes-Canteli, M., Santos, A., Garcia-Verdugo, J. M., & Perez-Castillo, A. (2011). Peroxisome proliferator-activated receptor γ ligands regulate neural stem cell proliferation and differentiation in vitro and in vivo. *Glia*, *59*(2), 293-307. https://doi.org/10.1002/glia.21101

Morales-Garcia, J. A., Luna-Medina, R., Alonso-Gil, S., Sanz-Sancristobal, M., Palomo, V., Gil, C., Santos, A., Martinez, A., & Perez-Castillo, A. (2012). Glycogen synthase kinase 3 inhibition promotes adult hippocampal neurogenesis in vitro and in vivo. *ACS Chem Neurosci*, *3*(11), 963-971. https://doi.org/10.1021/cn300110c

Morel, E., Chamoun, Z., Lasiecka, Z. M., Chan, R. B., Williamson, R. L., Vetanovetz, C., Dall'Armi, C., Simoes, S., Point Du Jour, K. S., McCabe, B. D., Small, S. A., & Di Paolo, G. (2013). Phosphatidylinositol-3-phosphate regulates sorting and processing of amyloid precursor protein through the endosomal system. *Nat Commun*, *4*(1), 2250. https://doi.org/10.1038/ncomms3250

Morita, T., & Sobue, K. (2009). Specification of Neuronal Polarity Regulated by Local Translation of CRMP2 and Tau via the mTOR-p70S6K Pathway. *J Biol Chem*, *284*(40), 27734-27745. https://doi.org/10.1074/jbc.M109.008177

Moriya, Y., Kogame, A., Tagawa, Y., Morohashi, A., Kondo, T., Asahi, S., & Benet, L. Z. (2019). The Enhancement of Subcutaneous First-Pass Metabolism Causes Nonlinear Pharmacokinetics of TAK-448 after a Single Subcutaneous Administration to Rats. *Drug Metab Dispos*, *47*(9), 1004-1012. https://doi.org/10.1124/dmd.119.087148

Morley, J. E., Farr, S. A., Banks, W. A., Johnson, S. N., Yamada, K. A., & Xu, L. (2010). A Physiological Role for Amyloid-β Protein: Enhancement of Learning and Memory. *J Alzheimers Dis*, *19*(2), 441-449. https://doi.org/10.3233/JAD-2010-1230

Morley, J. E., Farr, S. A., Nguyen, A. D., & Xu, F. (2019). What is the Physiological Function of Amyloid-Beta Protein? *J Nutr Health Aging*, *23*(3), 225-226. https://doi.org/10.1007/s12603-019-1162-5

Morris, G. P., Clark, I. A., & Vissel, B. (2014). Inconsistencies and Controversies Surrounding the Amyloid Hypothesis of Alzheimer's Disease. *Acta Neuropathol Commun*, *2*, 135. https://doi.org/10.1186/s40478-014-0135-5

Morrone, C. D., Bazzigaluppi, P., Beckett, T. L., Hill, M. E., Koletar, M. M., Stefanovic, B., & McLaurin, J. (2020). Regional differences in Alzheimer's disease pathology confound behavioural rescue after amyloid-β attenuation. *Brain*, *143*(1), 359-373. https://doi.org/10.1093/brain/awz371

Moses, G. S., Jensen, M. D., Lue, L.-F., Walker, D. G., Sun, A. Y., Simonyi, A., & Sun, G. Y. (2006). Secretory PLA2-IIA: a new inflammatory factor for Alzheimer's disease. *J Neuroinflammation*, *3*(1), 28. https://doi.org/10.1186/1742-2094-3-28

Müller, U. C., & Zheng, H. (2012). Physiological Functions of APP Family Proteins. *Cold Spring Harb Perspect Med*, *2*(2), a006288. https://doi.org/10.1101/cshperspect.a006288

Myers, A., & McGonigle, P. (2019). Overview of Transgenic Mouse Models for Alzheimer's Disease. *Curr Protoc Neurosci*, *89*(1), e81. https://doi.org/10.1002/cpns.81

Nagai, F., Nonaka, R., & Satoh Hisashi Kamimura, K. (2007). The effects of non-medically used psychoactive drugs on monoamine neurotransmission in rat brain. *Eur J Pharmacol*, *559*(2-3), 132-137. https://doi.org/10.1016/j.ejphar.2006.11.075

Nardai, S., László, M., Szabó, A., Alpár, A., Hanics, J., Zahola, P., Merkely, B., Frecska, E., & Nagy, Z. (2020). N,N-dimethyltryptamine reduces infarct size and improves functional recovery following transient focal brain ischemia in rats. *Exp Neurol*, *327*, 113245. https://doi.org/10.1016/j.expneurol.2020.113245

Nau, F. J., Yu, B., Martin, D., & Nichols, C. D. (2013). Serotonin 5-HT_{2A} Receptor Activation Blocks TNF-α Mediated Inflammation *In Vivo*. *PLoS ONE*, *8*(10), e75426. https://doi.org/10.1371/journal.pone.0075426

Naumann, N., Alpár, A., Ueberham, U., Arendt, T., & Gärtner, U. (2010). Transgenic expression of human wild-type amyloid precursor protein decreases neurogenesis in the adult hippocampus. *Hippocampus*, *20*(8), 971-979. https://doi.org/10.1002/hipo.20693

Nhan, H. S., Chiang, K., & Koo, E. H. (2015). The multifaceted nature of amyloid precursor protein and its proteolytic fragments: friends and foes. *Acta Neuropathol*, *129*(1), 1-19. https://doi.org/10.1007/s00401-014-1347-2

Ni, R. (2021). Magnetic Resonance Imaging in Animal Models of Alzheimer's Disease Amyloidosis. *Int J Mol Sci*, *22*(23), 12768. https://doi.org/10.3390/ijms222312768

Nichols, D. E., & Nichols, C. D. (2008). Serotonin receptors. *Chem Rev*, *108*(5), 1614-1641. https://doi.org/10.1021/cr078224o

Nichols, E., Steinmetz, J. D., Vollset, S. E., Fukutaki, K., Chalek, J., Abd-Allah, F., Abdoli, A., Abualhasan, A., Abu-Gharbieh, E., Akram, T. T., Al Hamad, H., Alahdab, F., Alanezi, F. M., Alipour, V., Almustanyir, S., Amu, H., Ansari, I., Arabloo, J., Ashraf, T., Astell-Burt, T., Ayano, G., Ayuso-Mateos, J. L., Baig, A. A., Barnett, A., Barrow, A., Baune, B. T., Béjot, Y., Bezabhe, W. M. M., Bezabih, Y. M., Bhagavathula, A. S., Bhaskar, S., Bhattacharyya, K., Bijani, A., Biswas, A., Bolla, S. R., Boloor, A., Brayne, C., Brenner, H., Burkart, K., Burns, R. A., Cámera, L. A., Cao, C., Carvalho, F., Castro-de-Araujo, L. F. S., Catalá-López, F., Cerin, E., Chavan, P. P., Cherbuin, N., Chu, D.-T., Costa, V. M., Couto, R. A. S., Dadras, O., Dai, X., Dandona, L., Dandona, R., De la Cruz-Góngora, V., Dhamnetiya, D., Dias da Silva, D., Diaz, D., Douiri, A., Edvardsson, D., Ekholuenetale, M., El Sayed, I., El-Jaafary, S. I., Eskandari, K., Eskandarieh, S., Esmaeilnejad, S., Fares, J., Faro, A., Farooque, U., Feigin, V. L., Feng, X., Fereshtehnejad, S.-M., Fernandes, E., Ferrara, P., Filip, I., Fillit, H., Fischer, F., Gaidhane, S., Galluzzo, L., Ghashghaee, A., Ghith, N., Gialluisi, A., Gilani, S. A., Glavan, I.-R., Gnedovskaya, E. V., Golechha, M., Gupta, R., Gupta, V. B., Gupta, V. K., Haider, M. R., Hall, B. J., Hamidi, S., Hanif, A.,

Hankey, G. J., Haque, S., Hartono, R. K., Hasaballah, A. I., Hasan, M. T., Hassan, A., Hay, S. I., Hayat, K., Hegazy, M. I., Heidari, G., Heidari-Soureshjani, R., Herteliu, C., Househ, M., Hussain, R., Hwang, B.-F., Iacoviello, L., Iavicoli, I., Ilesanmi, O. S., Ilic, I. M., Ilic, M. D., Irvani, S. S. N., Iso, H., Iwagami, M., Jabbarinejad, R., Jacob, L., Jain, V., Jayapal, S. K., Jayawardena, R., Jha, R. P., Jonas, J. B., Joseph, N., Kalani, R., Kandel, A., Kandel, H., Karch, A., Kasa, A. S., Kassie, G. M., Keshavarz, P., Khan, M. A. B., Khatib, M. N., Khoja, T. A. M., Khubchandani, J., Kim, M. S., Kim, Y. J., Kisa, A., Kisa, S., Kivimäki, M., Koroshetz, W. J., Koyanagi, A., Kumar, G. A., Kumar, M., Lak, H. M., Leonardi, M., Li, B., Lim, S. S., Liu, X., Liu, Y., Logroscino, G., Lorkowski, S., Lucchetti, G., Lutzky Saute, R., Magnani, F. G., Malik, A. A., Massano, J., Mehndiratta, M. M., Menezes, R. G., Meretoja, A., Mohajer, B., Mohamed Ibrahim, N., Mohammad, Y., Mohammed, A., Mokdad, A. H., Mondello, S., Moni, M. A. A., Moniruzzaman, M., Mossie, T. B., Nagel, G., Naveed, M., Nayak, V. C., Neupane Kandel, S., Nguyen, T. H., Oancea, B., Otstavnov, N., Otstavnov, S. S., Owolabi, M. O., Panda-Jonas, S., Pashazadeh Kan, F., Pasovic, M., Patel, U. K., Pathak, M., Peres, M. F. P., Perianayagam, A., Peterson, C. B., Phillips, M. R., Pinheiro, M., Piradov, M. A., Pond, C. D., Potashman, M. H., Pottoo, F. H., Prada, S. I., Radfar, A., Raggi, A., Rahim, F., Rahman, M., Ram, P., Ranasinghe, P., Rawaf, D. L., Rawaf, S., Rezaei, N., Rezapour, A., Robinson, S. R., Romoli, M., Roshandel, G., Sahathevan, R., Sahebkar, A., Sahraian, M. A., Sathian, B., Sattin, D., Sawhney, M., Saylan, M., Schiavolin, S., Seylani, A., Sha, F., Shaikh, M. A., Shaji, K. S., Shannawaz, M., Shetty, J. K., Shigematsu, M., Shin, J. I., Shiri, R., Silva, D. A. S., Silva, J. P., Silva, R., Singh, J. A., Skryabin, V. Y., Skryabina, A. A., Smith, A. E., Soshnikov, S., Spurlock, E. E., Stein, D. J., Sun, J., Tabarés-Seisdedos, R., Thakur, B., Timalsina, B., Tovani-Palone, M. R., Tran, B. X., Tsegaye, G. W., Valadan Tahbaz, S., Valdez, P. R., Venketasubramanian, N., Vlassov, V., Vu, G. T., Vu, L. G., Wang, Y.-P., Wimo, A., Winkler, A. S., Yadav, L., Yahyazadeh Jabbari, S. H., Yamagishi, K., Yang, L., Yano, Y., Yonemoto, N., Yu, C., Yunusa, I., Zadey, S., Zastrozhin, M. S., Zastrozhina, A., Zhang, Z.-J., Murray, C. J. L., & Vos, T. (2022). Estimation of the global prevalence of dementia in 2019 and forecasted prevalence in 2050: an analysis for the Global Burden of Disease Study 2019. *The Lancet Public Health*, *7*(2), e105-e125. https://doi.org/10.1016/S2468-2667(21)00249-8

Nilsson, P., Saito, T., & Saido, T. C. (2014). New Mouse Model of Alzheimer's. *ACS Chem Neurosci*, *5*(7), 499-502. https://doi.org/10.1021/cn500105p

Nitsch, R. M., Deng, M., Growdon, J. H., & Wurtman, R. J. (1996). Serotonin 5-HT2a and 5-HT2c Receptors Stimulate Amyloid Precursor Protein Ectodomain Secretion. *J Biol Chem*, *271*(8), 4188-4194. https://doi.org/10.1074/jbc.271.8.4188

Niu, Z., Zhang, Z., Zhao, W., & Yang, J. (2018). Interactions between amyloid β peptide and lipid membranes. *Biochim Biophys Acta Biomembr*, *1860*(9), 1663-1669. https://doi.org/10.1016/j.bbamem.2018.04.004

Niu, Z., Zhao, W., Zhang, Z., Xiao, F., Tang, X., & Yang, J. (2014). The Molecular Structure of Alzheimer β-Amyloid Fibrils Formed in the Presence of Phospholipid Vesicles. *Angew Chem Int Ed Engl*, *53*(35), 9294-9297. https://doi.org/10.1002/anie.201311106

Nixon, G. F., Mathieson, F. A., & Hunter, I. (2008). The multi-functional role of sphingosylphosphorylcholine. *Prog Lipid Res*, *47*(1), 62-75. https://doi.org/10.1016/j.plipres.2007.11.001

Novo, M., Freire, S., & Al-Soufi, W. (2018). Critical aggregation concentration for the formation of early Amyloid-β (1–42) oligomers. *Sci Rep*, *8*(1), 1783. https://doi.org/10.1038/s41598-018-19961-3

Oddo, S., Caccamo, A., Smith, I. F., Green, K. N., & LaFerla, F. M. (2006). A Dynamic Relationship between Intracellular and Extracellular Pools of Aβ. *Am J Pathol*, *168*(1), 184-194. https://doi.org/10.2353/ajpath.2006.050593

Olsen, A. S. B., & Faergeman, N. J. (2017). Sphingolipids: membrane microdomains in brain development, function and neurological diseases. *Open Biol*, *7*(5), 170069. https://doi.org/10.1098/rsob.170069

Olson, D. E. (2022). Biochemical Mechanisms Underlying Psychedelic-Induced Neuroplasticity. *Biochemistry*, *61*(3), 127-136. https://doi.org/10.1021/acs.biochem.1c00812

Onos, K. D., Uyar, A., Keezer, K. J., Jackson, H. M., Preuss, C., Acklin, C. J., O'Rourke, R., Buchanan, R., Cossette, T. L., Sukoff Rizzo, S. J., Soto, I., Carter, G. W., & Howell, G. R. (2019). Enhancing face validity of mouse models of Alzheimer's disease with natural genetic variation. *PLoS Genet*, *15*(5), e1008155. https://doi.org/10.1371/journal.pgen.1008155

Ordóñez-Gutiérrez, L., Antón, M., & Wandosell, F. (2015). Peripheral Amyloid Levels Present Gender Differences Associated with Aging in AβPP/PS1 Mice. *J Alzheimers Dis*, *44*(4), 1063-1068. https://doi.org/10.3233/JAD-141158

Pannu, R., Singh, A. K., & Singh, I. (2005). A Novel Role of Lactosylceramide in the Regulation of Tumor Necrosis Factor α-mediated Proliferation of Rat Primary Astrocytes IMPLICATIONS FOR ASTROGLIOSIS FOLLOWING NEUROTRAUMA. *J Biol Chem*, *280*(14), 13742-13751. https://doi.org/10.1074/jbc.M411959200

Papaspyropoulos, A., Tsolaki, M., Foroglou, N., & Pantazaki, A. A. (2020). Modeling and Targeting Alzheimer's Disease With Organoids. *Front Pharmacol*, *11*, 396. https://doi.org/10.3389/fphar.2020.00396

Pardon, M. C., Yanez Lopez, M., Yuchun, D., Marjańska, M., Prior, M., Brignell, C., Parhizkar, S., Agostini, A., Bai, L., Auer, D. P., & Faas, H. M. (2016). Magnetic Resonance Spectroscopy discriminates the response to microglial stimulation of wild type and Alzheimer's disease models. *Sci Rep*, *6*(1), 19880. https://doi.org/10.1038/srep19880

Park, M. K., & Lee, C. H. (2019). Role of Sphingosylphosphorylcholine in Tumor and Tumor Microenvironment. *Cancers (Basel)*, *11*(11), 1696. https://doi.org/10.3390/cancers11111696

Parrott, J. M., & O'Connor, J. C. (2015). Kynurenine 3-monooxygenase: an influential mediator of neuropathology. *Front Psychiatry*, *6*, 116. https://doi.org/10.3389/fpsyt.2015.00116

Paulussen, M., Landuyt, B., Schoofs, L., Luyten, W., & Arckens, L. (2009). Thymosin beta 4 mRNA and peptide expression in phagocytic cells of different mouse tissues. *Peptides*, *30*(10), 1822-1832. https://doi.org/10.1016/j.peptides.2009.07.010

Pearson, H. A., & Peers, C. (2006). Physiological roles for amyloid β peptides. *J Physiol*, *575*(1), 5-10. https://doi.org/10.1113/jphysiol.2006.111203

Pera, M., Larrea, D., Guardia-Laguarta, C., Montesinos, J., Velasco, K. R., Agrawal, R. R., Xu, Y., Chan, R. B., Di Paolo, G., Mehler, M. F., Perumal, G. S., Macaluso, F. P., Freyberg, Z. Z., Acin-Perez, R., Enriquez, J. A., Schon, E. A., & Area-Gomez, E. (2017). Increased localization of APP-C99 in mitochondria-associated ER membranes causes mitochondrial dysfunction in Alzheimer disease. *Embo j*, *36*(22), 3356-3371. https://doi.org/10.15252/embj.201796797

Perez-Tur, J., Froelich, S., Prihar, G., Crook, R., Baker, M., Duff, K., Wragg, M., Busfield, F., Lendon, C., & Clark, R. F. (1995). A mutation in Alzheimer's disease destroying a splice acceptor site in the presenilin-1 gene. *Neuroreport*, *7*(1), 297-301. https://www.ncbi.nlm.nih.gov/pubmed/8742474

Pilozzi, A., Foster, S., Mischoulon, D., Fava, M., & Huang, X. (2023). A Brief Review on the Potential of Psychedelics for Treating Alzheimer's Disease and Related Depression. *Int J Mol Sci*, *24*(15), 12513. https://doi.org/10.3390/ijms241512513

Pimenova, A. A., Thathiah, A., De Strooper, B., & Tesseur, I. (2014). Regulation of Amyloid Precursor Protein Processing by Serotonin Signaling. *PLoS ONE*, *9*(1), e87014. https://doi.org/10.1371/journal.pone.0087014

Pinto, S. N., Silva, L. C., Futerman, A. H., & Prieto, M. (2011). Effect of ceramide structure on membrane biophysical properties: the role of acyl chain length and unsaturation. *Biochim Biophys Acta*, *1808*(11), 2753-2760. https://doi.org/10.1016/j.bbamem.2011.07.023

Platten, M., Nollen, E. A. A., Röhrig, U. F., Fallarino, F., & Opitz, C. A. (2019). Tryptophan metabolism as a common therapeutic target in cancer, neurodegeneration and beyond. *Nat Rev Drug Discov*, *18*(5), 379-401. https://doi.org/10.1038/s41573-019-0016-5

Plemel, J. R., Michaels, N. J., Weishaupt, N., Caprariello, A. V., Keough, M. B., Rogers, J. A., Yukseloglu, A., Lim, J., Patel, V. V., Rawji, K. S., Jensen, S. K., Teo, W., Heyne, B., Whitehead, S. N., Stys, P. K., & Yong, V. W. (2018). Mechanisms of lysophosphatidylcholine-induced demyelination: A primary lipid disrupting myelinopathy. *Glia*, *66*(2), 327-347. https://doi.org/10.1002/glia.23245

Polini, B., Ricardi, C., Bertolini, A., Carnicelli, V., Rutigliano, G., Saponaro, F., Zucchi, R., & Chiellini, G. (2023). T1AM/TAAR1 System Reduces Inflammatory Response and β-Amyloid Toxicity in Human Microglial HMC3 Cell Line. *Int J Mol Sci*, *24*(14), 11569. https://doi.org/10.3390/ijms241411569

Polter, A. M., & Li, X. (2011). Glycogen synthase kinase-3 is an intermediate modulator of serotonin neurotransmission. *Front Mol Neurosci*, *4*, 31. https://doi.org/10.3389/fnmol.2011.00031

Price, D. L., Sisodia, S. S., & Borchelt, D. R. (1998). Genetic Neurodegenerative Diseases: The Human Illness and Transgenic Models. *Science*, *282*(5391), 1079-1083. https://doi.org/10.1126/science.282.5391.1079

Puglielli, L., Ellis, B. C., Saunders, A. J., & Kovacs, D. M. (2003). Ceramide Stabilizes β-Site Amyloid Precursor Protein-cleaving Enzyme 1 and Promotes Amyloid β-Peptide Biogenesis. *J Biol Chem*, *278*(22), 19777-19783. https://doi.org/10.1074/jbc.M300466200

Pujadas, L., Rossi, D., Andrés, R., Teixeira, C. M., Serra-Vidal, B., Parcerisas, A., Maldonado, R., Giralt, E., Carulla, N., & Soriano, E. (2014). Reelin delays amyloid-beta fibril formation and rescues cognitive deficits in a model of Alzheimer's disease. *Nat Commun*, *5*, 3443. https://doi.org/10.1038/ncomms4443

Qi, X.-L., Xiu, J., Shan, K.-R., Xiao, Y., Gu, R., Liu, R.-Y., & Guan, Z.-Z. (2005). Oxidative stress induced by beta-amyloid peptide$_{1–42}$ is involved in the altered composition of cellular membrane lipids and the decreased expression of nicotinic receptors in human SH-SY5Y neuroblastoma cells. *Neurochem Int*, *46*(8), 613-621. https://doi.org/10.1016/j.neuint.2005.02.007

Qin, Y.-Y., Li, M.-W., Zhang, S., Zhang, Y., Zhao, L.-Y., Lei, H., Oishi, K., & Zhu, W.-Z. (2013). In vivo quantitative whole-brain diffusion tensor imaging analysis of APP/PS1 transgenic mice using voxel-based and atlas-based methods. *Neuroradiology*, *55*(8), 1027-1038. https://doi.org/10.1007/s00234-013-1195-0

Quinville, B. M., Deschenes, N. M., Ryckman, A. E., & Walia, J. S. (2021). A Comprehensive Review: Sphingolipid Metabolism and Implications of Disruption in Sphingolipid Homeostasis. *Int J Mol Sci*, *22*(11), 5793. https://doi.org/10.3390/ijms22115793

Radecki, D. Z., & Samanta, J. (2022). Isolation and culture of neural stem cells from adult mouse subventricular zone for genetic and pharmacological treatments with proliferation analysis. *STAR Protoc*, *3*(1), 101153. https://doi.org/10.1016/j.xpro.2022.101153

Rajendran, L., & Annaert, W. (2012). Membrane Trafficking Pathways in Alzheimer's Disease. *Traffic*, *13*(6), 759-770. https://doi.org/10.1111/j.1600-0854.2012.01332.x

Ramos-Moreno, T., Galazo, M. J., Porrero, C., Martínez-Cerdeño, V., & Clascá, F. (2006). Extracellular matrix molecules and synaptic plasticity: immunomapping of intracellular and secreted Reelin in the adult rat brain. *Eur J Neurosci*, *23*(2), 401-422. https://doi.org/10.1111/j.1460-9568.2005.04567.x

Ranjan, V. D., Qiu, L., Tan, E. K., Zeng, L., & Zhang, Y. (2018). Modelling Alzheimer's disease: Insights from *in vivo* to *in vitro* three-dimensional culture platforms. *J Tissue Eng Regen Med*, *12*(9), 1944-1958. https://doi.org/10.1002/term.2728

Reddy, A. P., Sawant, N., Morton, H., Kshirsagar, S., Bunquin, L. E., Yin, X., & Reddy, P. H. (2021). Selective serotonin reuptake inhibitor citalopram ameliorates cognitive decline and protects against amyloid beta-induced mitochondrial dynamics, biogenesis, autophagy, mitophagy and synaptic toxicities in a mouse model of Alzheimer's disease. *Hum Mol Genet*, *30*(9), 789-810. https://doi.org/10.1093/hmg/ddab091

Reitz, C., & Mayeux, R. (2014). Alzheimer disease: Epidemiology, diagnostic criteria, risk factors and biomarkers. *Biochem Pharmacol*, *88*(4), 640-651. https://doi.org/10.1016/j.bcp.2013.12.024

Research Models Search | ALZFORUM. Retrieved 2025/02/20 from https://www.alzforum.org/research-models/search?species%5B%5D=319&diseases%5B%5D=145&genes%5B%5D=33501&genes%5B%5D=33521&genes%5B%5D=33531&types=&keywords-entry=&keywords=#resultsfiles/16/search.html

Riba, J., Valle, M., Urbano, G., Yritia, M., Morte, A., & Barbanoj, M. J. (2003). Human Pharmacology of Ayahuasca: Subjective and Cardiovascular Effects, Monoamine Metabolite Excretion, and Pharmacokinetics. *J Pharmacol Exp Ther*, *306*(1), 73-83. https://doi.org/10.1124/jpet.103.049882

Rickli, A., Moning, O. D., Hoener, M. C., & Liechti, M. E. (2016). Receptor interaction profiles of novel psychoactive tryptamines compared with classic hallucinogens. *Eur Neuropsychopharmacol*, *26*(8), 1327-1337. https://doi.org/10.1016/j.euroneuro.2016.05.001

Ridha, B. H., Symms, M. R., Tozer, D. J., Stockton, K. C., Frost, C., Siddique, M. M., Lewis, E. B., MacManus, D. G., Boulby, P. A., Barker, G. J., Rossor, M. N., Fox, N. C., & Tofts, P. S. (2007). Magnetization transfer ratio in Alzheimer disease: comparison with volumetric measurements. *AJNR Am J Neuroradiol*, *28*(5), 965-970. https://www.ncbi.nlm.nih.gov/pubmed/17494679

Ries, M., & Sastre, M. (2016). Mechanisms of Aβ Clearance and Degradation by Glial Cells. *Front Aging Neurosci*, *8*, 160. https://doi.org/10.3389/fnagi.2016.00160

Riganti, L., Antonucci, F., Gabrielli, M., Prada, I., Giussani, P., Viani, P., Valtorta, F., Menna, E., Matteoli, M., & Verderio, C. (2016). Sphingosine-1-Phosphate (S1P) Impacts Presynaptic Functions by Regulating Synapsin I Localization in the Presynaptic Compartment. *J Neurosci*, *36*(16), 4624-4634. https://doi.org/10.1523/JNEUROSCI.3588-15.2016

Rodriguez-Perdigon, M., Tordera, R. M., Gil-Bea, F. J., Gerenu, G., Ramirez, M. J., & Solas, M. (2016). Down-regulation of glutamatergic terminals (VGLUT1) driven by Aβ in Alzheimer's disease. *Hippocampus*, *26*(10), 1303-1312. https://doi.org/10.1002/hipo.22607

Roos, T. T., Garcia, M. G., Martinsson, I., Mabrouk, R., Israelsson, B., Deierborg, T., Kobro-Flatmoen, A., Tanila, H., & Gouras, G. K. (2021). Neuronal spreading and plaque induction of intracellular Aβ and its disruption of Aβ homeostasis. *Acta Neuropathol*, *142*(4), 669-687. https://doi.org/10.1007/s00401-021-02345-9

Ross, B. M., Moszczynska, A., Erlich, J., & Kish, S. J. (1998). Phospholipid-Metabolizing Enzymes in Alzheimer's Disease: Increased Lysophospholipid Acyltransferase Activity and Decreased Phospholipase A_2 Activity. *J Neurochem*, *70*(2), 786-793. https://doi.org/10.1046/j.1471-4159.1998.70020786.x

Ruan, L., Kang, Z., Pei, G., & Le, Y. (2009). Amyloid Deposition and Inflammation in APPswe/PS1dE9 Mouse Model of Alzheimers Disease. *Curr Alzheimer Res*, *6*(6), 531-540. https://doi.org/10.2174/156720509790147070

Rutherford, C., Childs, S., Ohotski, J., McGlynn, L., Riddick, M., MacFarlane, S., Tasker, D., Pyne, S., Pyne, N. J., Edwards, J., & Palmer, T. M. (2013). Regulation of cell survival by sphingosine-1-phosphate receptor $S1P_1$ via reciprocal ERK-dependent suppression of Bim and PI-3-kinase/protein kinase C-mediated upregulation of Mcl-1. *Cell Death Dis*, *4*(11), e927. https://doi.org/10.1038/cddis.2013.455

Ryan, M. C., Kochunov, P., Sherman, P. M., Rowland, L. M., Wijtenburg, S. A., Acheson, A., Hong, L. E., Sladky, J., & McGuire, S. (2018). Miniature pig magnetic resonance spectroscopy model of normal adolescent brain development. *J Neurosci Methods*, *308*, 173-182. https://doi.org/10.1016/j.jneumeth.2018.08.008

Ryan, S. D., Whitehead, S. N., Swayne, L. A., Moffat, T. C., Hou, W., Ethier, M., Bourgeois, A. J. G., Rashidian, J., Blanchard, A. P., Fraser, P. E., Park, D. S., Figeys, D., & Bennett, S. A. L. (2009). Amyloid-β_{42} signals tau hyperphosphorylation and compromises neuronal viability by disrupting alkylacylglycerophosphocholine metabolism. *Proc Natl Acad Sci U S A*, *106*(49), 20936-20941. https://doi.org/10.1073/pnas.0905654106

Saavedra, J. M., & Axelrod, J. (1972). Psychotomimetic N-Methylated Tryptamines: Formation in Brain in vivo and in vitro. *Science*, *175*(4028), 1365-1366. https://doi.org/10.1126/science.175.4028.1365

Sadigh-Eteghad, S., Sabermarouf, B., Majdi, A., Talebi, M., Farhoudi, M., & Mahmoudi, J. (2015). Amyloid-Beta: A Crucial Factor in Alzheimer's Disease. *Med Princ Pract*, *24*(1), 1-10. https://doi.org/10.1159/000369101

Salta, E., Lazarov, O., Fitzsimons, C. P., Tanzi, R., Lucassen, P. J., & Choi, S. H. (2023). Adult hippocampal neurogenesis in Alzheimer's disease: A roadmap to clinical relevance. *Cell Stem Cell*, *30*(2), 120-136. https://doi.org/10.1016/j.stem.2023.01.002

Salvadores, N., Gerónimo-Olvera, C., & Court, F. A. (2020). Axonal Degeneration in AD: The Contribution of Aβ and Tau. *Front Aging Neurosci*, *12*, 581767. https://doi.org/10.3389/fnagi.2020.581767

Sanchez-Mejia, R. O., Newman, J. W., Toh, S., Yu, G.-Q., Zhou, Y., Halabisky, B., Cissé, M., Scearce-Levie, K., Cheng, I. H., Gan, L., Palop, J. J., Bonventre, J. V., & Mucke, L. (2008). Phospholipase A_2 reduction ameliorates cognitive deficits in a mouse model of Alzheimer's disease. *Nat Neurosci*, *11*(11), 1311-1318. https://doi.org/10.1038/nn.2213

Sanchez-Varo, R., Mejias-Ortega, M., Fernandez-Valenzuela, J. J., Nuñez-Diaz, C., Caceres-Palomo, L., Vegas-Gomez, L., Sanchez-Mejias, E., Trujillo-Estrada, L., Garcia-Leon, J. A., Moreno-Gonzalez, I., Vizuete, M., Vitorica, J., Baglietto-Vargas, D., & Gutierrez, A. (2022). Transgenic Mouse Models of

Alzheimer's Disease: An Integrative Analysis. *Int J Mol Sci*, *23*(10). https://doi.org/10.3390/ijms23105404

Sasaguri, H., Nilsson, P., Hashimoto, S., Nagata, K., Saito, T., De Strooper, B., Hardy, J., Vassar, R., Winblad, B., & Saido, T. C. (2017). APP mouse models for Alzheimer's disease preclinical studies. *Embo j*, *36*(17), 2473-2487. https://doi.org/10.15252/embj.201797397

Sato, Y., Kobayashi, D., Kohno, T., Kidani, Y., Prox, J., Becker-Pauly, C., & Hattori, M. (2016). Determination of cleavage site of Reelin between its sixth and seventh repeat and contribution of meprin metalloproteases to the cleavage. *J Biochem*, *159*(3), 305-312. https://doi.org/10.1093/jb/mvv102

Sayo, A., Konishi, H., Kobayashi, M., Kano, K., Kobayashi, H., Hibi, H., Aoki, J., & Kiyama, H. (2019). GPR34 in spinal microglia exacerbates neuropathic pain in mice. *J Neuroinflammation*, *16*(1), 82. https://doi.org/10.1186/s12974-019-1458-8

Schipke, C. G., Heuser, I., & Peters, O. (2011). Antidepressants act on glial cells: SSRIs and serotonin elicit astrocyte calcium signaling in the mouse prefrontal cortex. *J Psychiatr Res*, *45*(2), 242-248. https://doi.org/10.1016/j.jpsychires.2010.06.005

Schmidt, V., Carlo, A.-S., & Willnow, T. E. (2014). Apolipoprotein E receptor pathways in Alzheimer disease. *Wiley Interdiscip Rev Syst Biol Med*, *6*(3), 255-270. https://doi.org/10.1002/wsbm.1262

Schwarcz, R., Bruno, J. P., Muchowski, P. J., & Wu, H.-Q. (2012). Kynurenines in the mammalian brain: when physiology meets pathology. *Nat Rev Neurosci*, *13*(7), 465-477. https://doi.org/10.1038/nrn3257

Schwarz, A., & Futerman, A. H. (1997). Distinct Roles for Ceramide and Glucosylceramide at Different Stages of Neuronal Growth. *J Neurosci*, *17*(9), 2929-2938. https://doi.org/10.1523/JNEUROSCI.17-09-02929.1997

Schwarz, A., Rapaport, E., Hirschberg, K., & Futerman, A. H. (1995). A Regulatory Role for Sphingolipids in Neuronal Growth
INHIBITION OF SPHINGOLIPID SYNTHESIS AND DEGRADATION HAVE OPPOSITE EFFECTS ON AXONAL BRANCHING. *J Biol Chem*, *270*(18), 10990-10998. https://doi.org/10.1074/jbc.270.18.10990

Seki, T. (2020). Understanding the Real State of Human Adult Hippocampal Neurogenesis From Studies of Rodents and Non-human Primates. *Front Neurosci*, *14*, 839. https://doi.org/10.3389/fnins.2020.00839

Senaratne, R., Milne, A. M., MacQueen, G. M., & Hall, G. B. C. (2009). Increased choline-containing compounds in the orbitofrontal cortex and hippocampus in euthymic patients with bipolar disorder: A proton magnetic resonance spectroscopy study. *Psychiatry Res*, *172*(3), 205-209. https://doi.org/10.1016/j.pscychresns.2008.07.007

Sethi, J., Van Bulck, M., Suhail, A., Safarzadeh, M., Perez-Castillo, A., & Pan, G. (2020). A label-free biosensor based on graphene and reduced graphene oxide dual-layer for electrochemical determination of beta-amyloid biomarkers. *Mikrochim Acta*, *187*(5), 288. https://doi.org/10.1007/s00604-020-04267-x

Sheline, Y. I., West, T., Yarasheski, K., Swarm, R., Jasielec, M. S., Fisher, J. R., Ficker, W. D., Yan, P., Xiong, C., Frederiksen, C., Grzelak, M. V., Chott, R., Bateman, R. J., Morris, J. C., Mintun, M. A., Lee, J.-M., & Cirrito, J. R. (2014). An Antidepressant Decreases CSF Aβ Production in Healthy Individuals and in Transgenic AD Mice. *Sci Transl Med*, *6*(236), 236re234. https://doi.org/10.1126/scitranslmed.3008169

Shen, Z., Lei, J., Li, X., Wang, Z., Bao, X., & Wang, R. (2018). Multifaceted assessment of the APP/PS1 mouse model for Alzheimer's disease: Applying MRS, DTI, and ASL. *Brain Res*, *1698*, 114-120. https://doi.org/10.1016/j.brainres.2018.08.001

Shin, M.-K., Choi, M.-S., Chae, H.-J., Kim, J.-W., Kim, H.-G., & Kim, K.-L. (2019). Ganglioside GQ1b ameliorates cognitive impairments in an Alzheimer's disease mouse model, and causes reduction of amyloid precursor protein. *Sci Rep*, *9*(1), 8512. https://doi.org/10.1038/s41598-019-44739-6

Shindou, H., Hishikawa, D., Nakanishi, H., Harayama, T., Ishii, S., Taguchi, R., & Shimizu, T. (2007). A Single Enzyme Catalyzes Both Platelet-activating Factor Production and Membrane Biogenesis of Inflammatory Cells

CLONING AND CHARACTERIZATION OF ACETYL-CoA:LYSO-PAF ACETYLTRANSFERASE. *J Biol Chem*, *282*(9), 6532-6539. https://doi.org/10.1074/jbc.M609641200

Shinohara, M., Shinohara, M., Zhao, J., Fu, Y., Liu, C.-C., Kanekiyo, T., & Bu, G. (2019). 5-HT3 Antagonist Ondansetron Increases apoE Secretion by Modulating the LXR-ABCA1 Pathway. *Int J Mol Sci*, *20*(6), 1488. https://doi.org/10.3390/ijms20061488

Shu, X., Qin, Y.-Y., Zhang, S., Jiang, J.-J., Zhang, Y., Zhao, L.-Y., Shan, D., & Zhu, W.-Z. (2013). Voxel-Based Diffusion Tensor Imaging of an APP/PS1 Mouse Model of Alzheimer's Disease. *Mol Neurobiol*, *48*(1), 78-83. https://doi.org/10.1007/s12035-013-8418-6

Sinha, J. K., Trisal, A., Ghosh, S., Gupta, S., Singh, K. K., Han, S. S., Mahapatra, M., Abomughaid, M. M., Abomughayedh, A. M., Almutary, A. G., Iqbal, D., Bhaskar, R., Mishra, P. C., Jha, S. K., Jha, N. K., & Singh, A. K. (2024). Psychedelics for alzheimer's disease-related dementia: Unveiling therapeutic possibilities and pathways. *Ageing Res Rev*, *96*, 102211. https://doi.org/10.1016/j.arr.2024.102211

Smalheiser, N. R., Costa, E., Guidotti, A., Impagnatiello, F., Auta, J., Lacor, P., Kriho, V., & Pappas, G. D. (2000). Expression of reelin in adult mammalian blood, liver, pituitary pars intermedia, and adrenal chromaffin cells. *Proc Natl Acad Sci U S A*, *97*(3), 1281-1286. https://doi.org/10.1073/pnas.97.3.1281

Soares, J. M., Marques, P., Alves, V., & Sousa, N. (2013). A hitchhiker's guide to diffusion tensor imaging. *Front Neurosci*, *7*, 31. https://doi.org/10.3389/fnins.2013.00031

Sokolow, S., Luu, S. H., Nandy, K., Miller, C. A., Vinters, H. V., Poon, W. W., & Gylys, K. H. (2012). Preferential accumulation of amyloid-beta in presynaptic glutamatergic terminals (VGluT1 and VGluT2) in Alzheimer's disease cortex. *Neurobiol Dis*, *45*(1), 381-387. https://doi.org/10.1016/j.nbd.2011.08.027

Solas, M., Van Dam, D., Janssens, J., Ocariz, U., Vermeiren, Y., De Deyn, P. P., & Ramirez, M. J. (2021). 5-HT_7 receptors in Alzheimer's disease. *Neurochem Int*, *150*, 105185. https://doi.org/10.1016/j.neuint.2021.105185

Song, S.-K., Kim, J. H., Lin, S.-J., Brendza, R. P., & Holtzman, D. M. (2004). Diffusion tensor imaging detects age-dependent white matter changes in a transgenic mouse model with amyloid deposition. *Neurobiol Dis*, *15*(3), 640-647. https://doi.org/10.1016/j.nbd.2003.12.003

Song, S.-K., Sun, S.-W., Ramsbottom, M. J., Chang, C., Russell, J., & Cross, A. H. (2002). Dysmyelination Revealed through MRI as Increased Radial (but Unchanged Axial) Diffusion of Water. *Neuroimage*, *17*(3), 1429-1436. https://doi.org/10.1006/nimg.2002.1267

Song, Y., Cho, J.-H., Kim, H., Eum, Y.-J., Cheong, E.-N., Choi, S., Park, J.-H., Tak, S., Park, B., Sohn, J.-H., Cho, G., & Cheong, C. (2024). Association Between Taurine Level in the Hippocampus and Major Depressive Disorder in Young Women: A Proton Magnetic Resonance Spectroscopy Study at 7T. *Biol Psychiatry*, *95*(5), 465-472. https://doi.org/10.1016/j.biopsych.2023.08.025

Sonnino, S., & Prinetti, A. (2016). The role of sphingolipids in neuronal plasticity of the brain. *J Neurochem*, *137*(4), 485-488. https://doi.org/10.1111/jnc.13589

Sosa, L. J., Cáceres, A., Dupraz, S., Oksdath, M., Quiroga, S., & Lorenzo, A. (2017). The physiological role of the amyloid precursor protein as an adhesion molecule in the developing nervous system. *J Neurochem*, *143*(1), 11-29. https://doi.org/10.1111/jnc.14122

Spratley, S. J., Hill, C. H., Viuff, A. H., Edgar, J. R., Skjødt, K., & Deane, J. E. (2016). Molecular Mechanisms of Disease Pathogenesis Differ in Krabbe Disease Variants. *Traffic*, *17*(8), 908-922. https://doi.org/10.1111/tra.12404

Sreenivasamurthy, S., Laul, M., Zhao, N., Kim, T., & Zhu, D. (2023). Current progress of cerebral organoids for modeling Alzheimer's disease origins and mechanisms. *Bioeng Transl Med*, *8*(2), e10378. https://doi.org/10.1002/btm2.10378

Su, H., Rustam, Y. H., Masters, C. L., Makalic, E., McLean, C. A., Hill, A. F., Barnham, K. J., Reid, G. E., & Vella, L. J. (2021). Characterization of brain-derived extracellular vesicle lipids in Alzheimer's disease. *J Extracell Vesicles*, *10*(7), e12089. https://doi.org/10.1002/jev2.12089

Sugo, T., Tachimoto, H., Chikatsu, T., Murakami, Y., Kikukawa, Y., Sato, S., Kikuchi, K., Nagi, T., Harada, M., Ogi, K., Ebisawa, M., & Mori, M. (2006). Identification of a lysophosphatidylserine receptor on mast cells. *Biochem Biophys Res Commun*, *341*(4), 1078-1087. https://doi.org/10.1016/j.bbrc.2006.01.069

Sundaram, J. R., Chan, E. S., Poore, C. P., Pareek, T. K., Cheong, W. F., Shui, G., Tang, N., Low, C.-M., Wenk, M. R., & Kesavapany, S. (2012). Cdk5/p25-Induced Cytosolic PLA2-Mediated Lysophosphatidylcholine Production Regulates Neuroinflammation and Triggers Neurodegeneration. *J Neurosci*, *32*(3), 1020-1034. https://doi.org/10.1523/JNEUROSCI.5177-11.2012

Sung, P.-S., Lin, P.-Y., Liu, C.-H., Su, H.-C., & Tsai, K.-J. (2020). Neuroinflammation and Neurogenesis in Alzheimer's Disease and Potential Therapeutic Approaches. *Int J Mol Sci*, *21*(3), 701. https://doi.org/10.3390/ijms21030701

Szabo, A., Kovacs, A., Frecska, E., & Rajnavolgyi, E. (2014). Psychedelic N,N-Dimethyltryptamine and 5-Methoxy-N,N-Dimethyltryptamine Modulate Innate and Adaptive Inflammatory Responses through the Sigma-1 Receptor of Human Monocyte-Derived Dendritic Cells. *PLoS ONE*, *9*(8), e106533. https://doi.org/10.1371/journal.pone.0106533

Szabo, A., Kovacs, A., Riba, J., Djurovic, S., Rajnavolgyi, E., & Frecska, E. (2016). The Endogenous Hallucinogen and Trace Amine N,N-Dimethyltryptamine (DMT) Displays Potent Protective Effects against Hypoxia via Sigma-1 Receptor Activation in Human Primary iPSC-Derived Cortical Neurons and Microglia-Like Immune Cells. *Front Neurosci*, *10*, 423. https://doi.org/10.3389/fnins.2016.00423

Szabó, Í., Varga, V. É., Dvorácskó, S., Farkas, A. E., Körmöczi, T., Berkecz, R., Kecskés, S., Menyhárt, Á., Frank, R., Hantosi, D., Cozzi, N. V., Frecska, E., Tömböly, C., Krizbai, I. A., Bari, F., & Farkas, E. (2021). N,N-Dimethyltryptamine attenuates spreading depolarization and restrains neurodegeneration by sigma-1 receptor activation in the ischemic rat brain. *Neuropharmacology*, *192*, 108612. https://doi.org/10.1016/j.neuropharm.2021.108612

Szara, S., & Hearst, E. (1962). THE 6-HYDROXYLATION OF TRYPTAMINE DERIVATIVES: A WAY OF PRODUCING PSYCHOACTIVE METABOLITES. *Annals of the New York Academy of Sciences*, *96*(1), 134-141. https://doi.org/10.1111/j.1749-6632.1962.tb50108.x

Szara, S., Rockland, L. H., Rosenthal, D., & Handlon, J. H. (1966). Psychological Effects and Metabolism of N,N-diethyltryptamine in Man. *Arch Gen Psychiatry*, *15*(3), 320-329. https://doi.org/10.1001/archpsyc.1966.01730150096014

Takahashi, H., Sekino, Y., Tanaka, S., Mizui, T., Kishi, S., & Shirao, T. (2003). Drebrin-Dependent Actin Clustering in Dendritic Filopodia Governs Synaptic Targeting of Postsynaptic Density-95 and Dendritic Spine Morphogenesis. *J Neurosci*, *23*(16), 6586-6595. https://doi.org/10.1523/JNEUROSCI.23-16-06586.2003

Takahashi, R. H., Almeida, C. G., Kearney, P. F., Yu, F., Lin, M. T., Milner, T. A., & Gouras, G. K. (2004). Oligomerization of Alzheimer's β-Amyloid within Processes and Synapses of Cultured Neurons and Brain. *J Neurosci*, *24*(14), 3592-3599. https://doi.org/10.1523/JNEUROSCI.5167-03.2004

Takahashi, R. H., Capetillo-Zarate, E., Lin, M. T., Milner, T. A., & Gouras, G. K. (2013). Accumulation of Intraneuronal β-Amyloid 42 Peptides Is Associated with Early Changes in Microtubule-Associated Protein 2 in Neurites and Synapses. *PLoS ONE*, *8*(1), e51965. https://doi.org/10.1371/journal.pone.0051965

Takahashi, R. H., Milner, T. A., Li, F., Nam, E. E., Edgar, M. A., Yamaguchi, H., Beal, M. F., Xu, H., Greengard, P., & Gouras, G. K. (2002). Intraneuronal Alzheimer Aβ42 Accumulates in Multivesicular Bodies and Is Associated with Synaptic Pathology. *Am J Pathol*, *161*(5), 1869-1879. https://doi.org/10.1016/s0002-9440(10)64463-x

Tampellini, D. (2015). Synaptic activity and Alzheimer's disease: a critical update. *Front Neurosci*, *9*, 423. https://doi.org/10.3389/fnins.2015.00423

Tampellini, D., Capetillo-Zarate, E., Dumont, M., Huang, Z., Yu, F., Lin, M. T., & Gouras, G. K. (2010). Effects of Synaptic Modulation on β-Amyloid, Synaptophysin, and Memory Performance in Alzheimer's Disease Transgenic Mice. *J Neurosci*, *30*(43), 14299-14304. https://doi.org/10.1523/JNEUROSCI.3383-10.2010

Tampellini, D., Magrané, J., Takahashi, R. H., Li, F., Lin, M. T., Almeida, C. G., & Gouras, G. K. (2007). Internalized Antibodies to the Aβ Domain of APP Reduce Neuronal Aβ and Protect against Synaptic Alterations. *J Biol Chem*, *282*(26), 18895-18906. https://doi.org/10.1074/jbc.M700373200

Tan, S. T., Ramesh, T., Toh, X. R., & Nguyen, L. N. (2020). Emerging roles of lysophospholipids in health and disease. *Prog Lipid Res*, *80*, 101068. https://doi.org/10.1016/j.plipres.2020.101068

Terry, A. V., Jr., Buccafusco, J. J., & Bartoszyk, G. D. (2005). Selective serotonin 5-HT_{2A} receptor antagonist EMD 281014 improves delayed matching performance in young and aged rhesus monkeys. *Psychopharmacology (Berl)*, *179*(4), 725-732. https://doi.org/10.1007/s00213-004-2114-1

Thal, D. R., Rüb, U., Schultz, C., Sassin, I., Ghebremedhin, E., Del Tredici, K., Braak, E., & Braak, H. (2000a). Sequence of Aβ-Protein Deposition in the Human Medial Temporal Lobe. *J Neuropathol Exp Neurol*, *59*(8), 733-748. https://doi.org/10.1093/jnen/59.8.733

Thal, D. R., Schultz, C., Dehghani, F., Yamaguchi, H., Braak, H., & Braak, E. (2000b). Amyloid β-protein (Aβ)-containing astrocytes are located preferentially near N-terminal-truncated Aβ deposits in the human entorhinal cortex. *Acta Neuropathol*, *100*(6), 608-617. https://doi.org/10.1007/s004010000242

Thathiah, A., Horré, K., Snellinx, A., Vandewyer, E., Huang, Y., Ciesielska, M., De Kloe, G., Munck, S., & De Strooper, B. (2013). β-arrestin 2 regulates Aβ generation and γ-secretase activity in Alzheimer's disease. *Nat Med*, *19*(1), 43-49. https://doi.org/10.1038/nm.3023

Therapeutics Search | ALZFORUM. Retrieved 2025/02/20 from https://www.alzforum.org/therapeutics/search?fda_statuses%5B%5D=184&target_types=&therapy_types=&conditions%5B%5D=145&keywords-entry=&keywords=#resultsfiles/4/search.html

Tian, X.-L., Yu, L.-H., Li, W.-Q., Hu, Y., Yin, M., & Wang, Z.-J. (2015). Activation of 5-HT_{2C} Receptor Promotes the Expression of Neprilysin in U251 Human Glioma Cells. *Cell Mol Neurobiol*, *35*(3), 425-432. https://doi.org/10.1007/s10571-014-0138-6

Tittarelli, R., Mannocchi, G., Pantano, F., & Romolo, F. S. (2015). Recreational Use, Analysis and Toxicity of Tryptamines. *Curr Neuropharmacol*, *13*(1), 26-46. https://doi.org/10.2174/1570159X13666141210222409

Toledo, E. M., & Inestrosa, N. C. (2010). Activation of Wnt signaling by lithium and rosiglitazone reduced spatial memory impairment and neurodegeneration in brains of an APPswe/PSEN1ΔE9 mouse model of Alzheimer's disease. *Mol Psychiatry*, *15*(3), 272-285, 228. https://doi.org/10.1038/mp.2009.72

Tourino, M. C., de Oliveira, E. M., Bellé, L. P., Knebel, F. H., Albuquerque, R. C., Dörr, F. A., Okada, S. S., Migliorini, S., Soares, I. S., & Campa, A. (2013). Tryptamine and dimethyltryptamine inhibit indoleamine 2,3 dioxygenase and increase the tumor-reactive effect of peripheral blood mononuclear cells. *Cell Biochem Funct*, *31*(5), 361-364. https://doi.org/10.1002/cbf.2980

Tracey, T. J., Steyn, F. J., Wolvetang, E. J., & Ngo, S. T. (2018). Neuronal Lipid Metabolism: Multiple Pathways Driving Functional Outcomes in Health and Disease. *Front Mol Neurosci*, *11*, 10. https://doi.org/10.3389/fnmol.2018.00010

Tseng, W.-L., Chen, T.-H., Huang, C.-C., Huang, Y.-H., Yeh, C.-F., Tsai, H.-J., Lee, H.-Y., Kao, C.-Y., Lin, S.-W., Liao, H.-R., Cheng, J.-C., & Tseng, C.-P. (2014). Impaired thrombin generation in Reelin-deficient mice: a potential role of plasma Reelin in hemostasis. *J Thromb Haemost*, *12*(12), 2054-2064. https://doi.org/10.1111/jth.12736

Ungureanu, A.-A., Benilova, I., Krylychkina, O., Braeken, D., De Strooper, B., Van Haesendonck, C., Dotti, C. G., & Bartic, C. (2016). Amyloid beta oligomers induce neuronal elasticity changes in age-dependent manner: a force spectroscopy study on living hippocampal neurons. *Sci Rep*, *6*, 25841. https://doi.org/10.1038/srep25841

Van Bulck, M., Brandt, N., Claus, R. A., Gräler, M., & Bräuer, A. U. (2022). Aβ-Induced Alterations in Membrane Lipids Occur before Synaptic Loss Appears. *Int J Mol Sci*, *23*(4), 2300. https://doi.org/10.3390/ijms23042300

Van Bulck, M., Sierra-Magro, A., Alarcon-Gil, J., Perez-Castillo, A., & Morales-Garcia, J. A. (2019). Novel Approaches for the Treatment of Alzheimer's and Parkinson's Disease. *Int J Mol Sci*, *20*(3), 719. https://doi.org/10.3390/ijms20030719

van der Flier, W. M., Pijnenburg, Y. A., Fox, N. C., & Scheltens, P. (2011). Early-onset versus late-onset Alzheimer's disease: the case of the missing APOE ε4 allele. *Lancet Neurol*, *10*(3), 280-288. https://doi.org/10.1016/S1474-4422(10)70306-9

van Dyck, C. H., Swanson, C. J., Aisen, P., Bateman, R. J., Chen, C., Gee, M., Kanekiyo, M., Li, D., Reyderman, L., Cohen, S., Froelich, L., Katayama, S., Sabbagh, M., Vellas, B., Watson, D., Dhadda, S., Irizarry, M., Kramer, L. D., & Iwatsubo, T. (2023). Lecanemab in Early Alzheimer's Disease. *N Engl J Med*, *388*(1), 9-21. https://doi.org/10.1056/NEJMoa2212948

Vance, J. E. (2014). MAM (mitochondria-associated membranes) in mammalian cells: lipids and beyond. *Biochim Biophys Acta*, *1841*(4), 595-609. https://doi.org/10.1016/j.bbalip.2013.11.014

Vandamme, T. F. (2014). Use of rodents as models of human diseases. *J Pharm Bioallied Sci*, *6*(1), 2-9. https://doi.org/10.4103/0975-7406.124301

Varadharajan, A., Davis, A. D., Ghosh, A., Jagtap, T., Xavier, A., Menon, A. J., Roy, D., Gandhi, S., & Gregor, T. (2023). Guidelines for pharmacotherapy in Alzheimer's disease - A primer on FDA-approved drugs. *J Neurosci Rural Pract*, *14*(4), 566-573. https://doi.org/10.25259/JNRP_356_2023

Vargas, M. V., Dunlap, L. E., Dong, C., Carter, S. J., Tombari, R. J., Jami, S. A., Cameron, L. P., Patel, S. D., Hennessey, J. J., Saeger, H. N., McCorvy, J. D., Gray, J. A., Tian, L., & Olson, D. E. (2023). Psychedelics promote neuroplasticity through the activation of intracellular 5-HT2A receptors. *Science*, *379*(6633), 700-706. https://doi.org/10.1126/science.adf0435

Varma, V. R., Oommen, A. M., Varma, S., Casanova, R., An, Y., Andrews, R. M., O'Brien, R., Pletnikova, O., Troncoso, J. C., Toledo, J., Baillie, R., Arnold, M., Kastenmueller, G., Nho, K., Doraiswamy, P. M., Saykin, A. J., Kaddurah-Daouk, R., Legido-Quigley, C., & Thambisetty, M. (2018). Brain and blood metabolite signatures of pathology and progression in Alzheimer disease: A targeted metabolomics study. *PLoS Med*, *15*(1), e1002482. https://doi.org/10.1371/journal.pmed.1002482

Velasco, S., Kedaigle, A. J., Simmons, S. K., Nash, A., Rocha, M., Quadrato, G., Paulsen, B., Nguyen, L., Adiconis, X., Regev, A., Levin, J. Z., & Arlotta, P. (2019). Individual brain organoids reproducibly form cell diversity of the human cerebral cortex. *Nature*, *570*(7762), 523-527. https://doi.org/10.1038/s41586-019-1289-x

Venkateswaran, A., Laffitte, B. A., Joseph, S. B., Mak, P. A., Wilpitz, D. C., Edwards, P. A., & Tontonoz, P. (2000). Control of cellular cholesterol efflux by the nuclear oxysterol receptor LXRα. *Proc Natl Acad Sci U S A*, *97*(22), 12097-12102. https://doi.org/10.1073/pnas.200367697

Verstraelen, P., Barriga, G. G.-D., Verschuuren, M., Asselbergh, B., Nuydens, R., Larsen, P. H., Timmermans, J. P., & De Vos, W. H. (2020). Systematic Quantification of Synapses in Primary Neuronal Culture. *Iscience*, *23*(9), 101542. https://doi.org/10.1016/j.isci.2020.101542

Vertes, R. P. (1991). A PHA-L analysis of ascending projections of the dorsal raphe nucleus in the rat. *J Comp Neurol*, *313*(4), 643-668. https://doi.org/10.1002/cne.903130409

Vertes, R. P., Fortin, W. J., & Crane, A. M. (1999). Projections of the median raphe nucleus in the rat. *J Comp Neurol*, *407*(4), 555-582. https://www.ncbi.nlm.nih.gov/pubmed/10235645

Vidal, B., Sebti, J., Verdurand, M., Fieux, S., Billard, T., Streichenberger, N., Troakes, C., Newman-Tancredi, A., & Zimmer, L. (2016). Agonist and antagonist bind differently to 5-HT_{1A} receptors during Alzheimer's disease: A post-mortem study with PET radiopharmaceuticals. *Neuropharmacology*, *109*, 88-95. https://doi.org/10.1016/j.neuropharm.2016.05.009

Walsh, D. M., Klyubin, I., Fadeeva, J. V., Cullen, W. K., Anwyl, R., Wolfe, M. S., Rowan, M. J., & Selkoe, D. J. (2002). Naturally secreted oligomers of amyloid β protein potently inhibit hippocampal long-term potentiation *in vivo*. *Nature*, *416*(6880), 535-539. https://doi.org/10.1038/416535a

Walsh, D. M., & Selkoe, D. J. (2004). Deciphering the Molecular Basis of Memory Failure in Alzheimer's Disease. *Neuron*, *44*(1), 181-193. https://doi.org/10.1016/j.neuron.2004.09.010

Wang, B., & Tontonoz, P. (2019). Phospholipid Remodeling in Physiology and Disease. *Annu Rev Physiol*, *81*(1), 165-188. https://doi.org/10.1146/annurev-physiol-020518-114444

Wang, C., Haas, M., Yeo, S. K., Sebti, S., Fernández, Á. F., Zou, Z., Levine, B., & Guan, J.-L. (2022). Enhanced autophagy in $Becn1^{F121A/F121A}$ knockin mice counteracts aging-related neural stem cell exhaustion and dysfunction. *Autophagy*, *18*(2), 409-422. https://doi.org/10.1080/15548627.2021.1936358

Watson, J., Brough, S., Coldwell, M. C., Gager, T., Ho, M., Hunter, A. J., Jerman, J., Middlemiss, D. N., Riley, G. J., & Brown, A. M. (1998). Functional effects of the muscarinic receptor agonist, xanomeline, at 5-HT_1 and 5-HT_2 receptors. *Br J Pharmacol*, *125*(7), 1413-1420. https://doi.org/10.1038/sj.bjp.0702201

Weeber, E. J., Beffert, U., Jones, C., Christian, J. M., Förster, E., Sweatt, J. D., & Herz, J. (2002). Reelin and ApoE Receptors Cooperate to Enhance Hippocampal Synaptic Plasticity and Learning. *J Biol Chem*, *277*(42), 39944-39952. https://doi.org/10.1074/jbc.M205147200

Wei, W., Nguyen, L. N., Kessels, H. W., Hagiwara, H., Sisodia, S., & Malinow, R. (2010). Amyloid beta from axons and dendrites reduces local spine number and plasticity. *Nat Neurosci*, *13*(2), 190-196. https://doi.org/10.1038/nn.2476

Westman, E., Spenger, C., Öberg, J., Reyer, H., Pahnke, J., & Wahlund, L.-O. (2009). *In vivo* ^{1}H-magnetic resonance spectroscopy can detect metabolic changes in APP/PS1 mice after donepezil treatment. *BMC Neurosci*, *10*(1), 33. https://doi.org/10.1186/1471-2202-10-33

Wheeler, D., Knapp, E., Bandaru, V. V. R., Wang, Y., Knorr, D., Poirier, C., Mattson, M. P., Geiger, J. D., & Haughey, N. J. (2009). Tumor necrosis factor-α-induced neutral sphingomyelinase-2 modulates synaptic plasticity by controlling the membrane insertion of NMDA receptors. *J Neurochem*, *109*(5), 1237-1249. https://doi.org/10.1111/j.1471-4159.2009.06038.x

Widner, B., Leblhuber, F., Walli, J., Tilz, G. P., Demel, U., & Fuchs, D. (2000). Tryptophan degradation and immune activation in Alzheimer's disease. *J Neural Transm (Vienna)*, *107*(3), 343-353. https://doi.org/10.1007/s007020050029

Willén, K., Sroka, A., Takahashi, R. H., & Gouras, G. K. (2017). Heterogeneous Association of Alzheimer's Disease-Linked Amyloid-β and Amyloid-β Protein Precursor with Synapses. *J Alzheimers Dis*, *60*(2), 511-524. https://doi.org/10.3233/JAD-170262

Williams, T. L., & Serpell, L. C. (2011). Membrane and surface interactions of Alzheimer's Aβ peptide – insights into the mechanism of cytotoxicity. *FEBS J*, *278*(20), 3905-3917. https://doi.org/10.1111/j.1742-4658.2011.08228.x

Winter, J. C. (1969). Behavioral effects of N,N-diethyltryptamine: absence of antagonism by xylamidine tosylate. *J Pharmacol Exp Ther*, *169*(1), 7-16. https://www.ncbi.nlm.nih.gov/pubmed/5306645

Witter, M. P. (2007). The perforant path: projections from the entorhinal cortex to the dentate gyrus. *Prog Brain Res*, *163*, 43-61. https://doi.org/10.1016/S0079-6123(07)63003-9

Wu, W., Du, S., Shi, W., Liu, Y., Hu, Y., Xie, Z., Yao, X., Liu, Z., Ma, W., Xu, L., Ma, C., & Zhong, Y. (2019). Inhibition of Rac1-dependent forgetting alleviates memory deficits in animal models of Alzheimer's disease. *Protein Cell*, *10*(10), 745-759. https://doi.org/10.1007/s13238-019-0641-0

Wu, W., Nicolazzo, J. A., Wen, L., Chung, R., Stankovic, R., Bao, S. S., Lim, C. K., Brew, B. J., Cullen, K. M., & Guillemin, G. J. (2013). Expression of Tryptophan 2,3-Dioxygenase and Production of Kynurenine Pathway Metabolites in Triple Transgenic Mice and Human Alzheimer's Disease Brain. *PLoS ONE*, *8*(4), e59749. https://doi.org/10.1371/journal.pone.0059749

Wurtman, R. J., Blusztajn, J. K., & Maire, J. C. (1985). "Autocannibalism" of choline-containing membrane phospholipids in the pathogenesis of Alzheimer's disease—A hypothesis. *Neurochem Int*, *7*(2), 369-372. https://doi.org/10.1016/0197-0186(85)90127-5

Xian, X., Pohlkamp, T., Durakoglugil, M. S., Wong, C. H., Beck, J. K., Lane-Donovan, C., Plattner, F., & Herz, J. (2018). Reversal of ApoE4-induced recycling block as a novel prevention approach for Alzheimer's disease. *Elife*, *7*, e40048. https://doi.org/10.7554/eLife.40048

Xiong, Y., Mahmood, A., Meng, Y., Zhang, Y., Zhang, Z. G., Morris, D. C., & Chopp, M. (2012). Neuroprotective and neurorestorative effects of thymosin β4 treatment following experimental traumatic brain injury. *Ann N Y Acad Sci*, *1270*(1), 51-58. https://doi.org/10.1111/j.1749-6632.2012.06683.x

Xue, J., Yu, Y., Zhang, X., Zhang, C., Zhao, Y., Liu, B., Zhang, L., Wang, L., Chen, R., Gao, X., Jiao, P., Song, G., Jiang, X.-C., & Qin, S. (2019). Sphingomyelin Synthase 2 Inhibition Ameliorates Cerebral Ischemic Reperfusion Injury Through Reducing the Recruitment of Toll-Like Receptor 4 to Lipid Rafts. *J Am Heart Assoc*, *8*(22), e012885. https://doi.org/10.1161/JAHA.119.012885

Yan, P., Hu, X., Song, H., Yin, K., Bateman, R. J., Cirrito, J. R., Xiao, Q., Hsu, F. F., Turk, J. W., Xu, J., Hsu, C. Y., Holtzman, D. M., & Lee, J.-M. (2006). Matrix Metalloproteinase-9 Degrades Amyloid-β Fibrils *in Vitro* and Compact Plaques *in Situ*. *J Biol Chem*, *281*(34), 24566-24574. https://doi.org/10.1074/jbc.M602440200

Yanagisawa, K., Odaka, A., Suzuki, N., & Ihara, Y. (1995). GM1 ganglioside–bound amyloid β–protein (Aβ): A possible form of preamyloid in Alzheimer's disease. *Nat Med*, *1*(10), 1062-1066. https://doi.org/10.1038/nm1095-1062

Yi, H., Lee, S. J., Lee, J., Myung, C.-S., Park, W.-K., Lim, H.-J., Lee, G. H., Kong, J. Y., & Cho, H. (2011). Sphingosylphosphorylcholine Attenuated β–Amyloid Production by Reducing BACE1 Expression and Catalysis in PC12 Cells. *Neurochem Res*, *36*(11), 2083-2090. https://doi.org/10.1007/s11064-011-0532-0

Yin, F. (2023). Lipid metabolism and Alzheimer's disease: clinical evidence, mechanistic link and therapeutic promise. *FEBS J*, *290*(6), 1420-1453. https://doi.org/10.1111/febs.16344

Yin, K.-J., Cirrito, J. R., Yan, P., Hu, X., Xiao, Q., Pan, X., Bateman, R., Song, H., Hsu, F.-F., Turk, J., Xu, J., Hsu, C. Y., Mills, J. C., Holtzman, D. M., & Lee, J.-M. (2006). Matrix Metalloproteinases Expressed by Astrocytes Mediate Extracellular Amyloid-β Peptide Catabolism. *J Neurosci*, *26*(43), 10939-10948. https://doi.org/10.1523/JNEUROSCI.2085-06.2006

Yokoyama, M., Kobayashi, H., Tatsumi, L., & Tomita, T. (2022). Mouse Models of Alzheimer's Disease. *Front Mol Neurosci*, *15*, 912995. https://doi.org/10.3389/fnmol.2022.912995

Yu, D., Fan, W., Wu, P., Deng, J., Liu, J., Niu, Y., Li, M., & Deng, J. (2014). Characterization of hippocampal Cajal-Retzius cells during development in a mouse model of Alzheimer's disease (Tg2576). *Neural Regen Res*, *9*(4), 394-401. https://doi.org/10.4103/1673-5374.128243

Yu, D., Tao, B.-B., Yang, Y.-Y., Du, L.-S., Yang, S.-S., He, X.-J., Zhu, Y.-W., Yan, J.-K., & Yang, Q. (2015). The IDO Inhibitor Coptisine Ameliorates Cognitive Impairment in a Mouse Model of Alzheimer's Disease. *J Alzheimers Dis*, *43*(1), 291-302. https://doi.org/10.3233/JAD-140414

Yu, R. K., Tsai, Y.-T., Ariga, T., & Yanagisawa, M. (2011). Structures, Biosynthesis, and Functions of Gangliosides-an Overview. *J Oleo Sci*, *60*(10), 537-544. https://doi.org/10.5650/jos.60.537

Yuede, C. M., Wallace, C. E., Davis, T. A., Gardiner, W. D., Hettinger, J. C., Edwards, H. M., Hendrix, R. D., Doherty, B. M., Yuede, K. M., Burstein, E. S., & Cirrito, J. R. (2021). Pimavanserin, a $5HT_{2A}$ receptor inverse agonist, rapidly suppresses Aβ production and related pathology in a mouse model of Alzheimer's disease. *J Neurochem*, *156*(5), 658-673. https://doi.org/10.1111/jnc.15260

Zamolodchikov, D., Chen, Z.-L., Conti, B. A., Renné, T., & Strickland, S. (2015). Activation of the factor XII-driven contact system in Alzheimer's disease patient and mouse model plasma. *Proc Natl Acad Sci U S A*, *112*(13), 4068-4073. https://doi.org/10.1073/pnas.1423764112

Zerbi, V., Kleinnijenhuis, M., Fang, X., Jansen, D., Veltien, A., Van Asten, J., Timmer, N., Dederen, P. J., Kiliaan, A. J., & Heerschap, A. (2013). Gray and white matter degeneration revealed by diffusion in an Alzheimer mouse model. *Neurobiol Aging*, *34*(5), 1440-1450. https://doi.org/10.1016/j.neurobiolaging.2012.11.017

Zha, Q., Ruan, Y., Hartmann, T., Beyreuther, K., & Zhang, D. (2004). GM1 ganglioside regulates the proteolysis of amyloid precursor protein. *Mol Psychiatry*, *9*(10), 946-952. https://doi.org/10.1038/sj.mp.4001509

Zhang, H., Ben Zablah, Y., Zhang, H., Liu, A., Gugustea, R., Lee, D., Luo, X., Meng, Y., Li, S., Zhou, C., Xin, T., & Jia, Z. (2022a). Inhibition of Rac1 in ventral hippocampal excitatory neurons improves social recognition memory and synaptic plasticity. *Front Aging Neurosci*, *14*, 914491. https://doi.org/10.3389/fnagi.2022.914491

Zhang, H., Jiang, X., Ma, L., Wei, W., Li, Z., Chang, S., Wen, J., Sun, J., & Li, H. (2022b). Role of Aβ in Alzheimer's-related synaptic dysfunction. *Front Cell Dev Biol*, *10*, 964075. https://doi.org/10.3389/fcell.2022.964075

Zhang, L., Trushin, S., Christensen, T. A., Tripathi, U., Hong, C., Geroux, R. E., Howell, K. G., Poduslo, J. F., & Trushina, E. (2018). Differential effect of amyloid beta peptides on mitochondrial axonal trafficking depends on their state of aggregation and binding to the plasma membrane. *Neurobiol Dis*, *114*, 1-16. https://doi.org/10.1016/j.nbd.2018.02.003

Zhang, Q., Yang, C., Liu, T., Liu, L., Li, F., Cai, Y., Lv, K., Li, X., Gao, J., Sun, D., Xu, H., Yang, Q., & Fan, X. (2018). Citalopram restores short-term memory deficit and non-cognitive behaviors in APP/PS1 mice while halting the advance of Alzheimer's disease-like pathology. *Neuropharmacology*, *131*, 475-486. https://doi.org/10.1016/j.neuropharm.2017.12.021

Zhang, S., Zhang, M., Cai, F., & Song, W. (2013). Biological function of Presenilin and its role in AD pathogenesis. *Transl Neurodegener*, *2*(1), 15. https://doi.org/10.1186/2047-9158-2-15

Zhang, Y., Ranta, F., Tang, C., Shumilina, E., Mahmud, H., Föller, M., Ullrich, S., Häring, H.-U., & Lang, F. (2009). Sphingomyelinase dependent apoptosis following treatment of pancreatic beta-cells with amyloid peptides Aß$_{1-42}$ or IAPP. *Apoptosis*, *14*(7), 878-889. https://doi.org/10.1007/s10495-009-0364-4

Zhao, X., Zhang, S., Sanders, A. R., & Duan, J. (2023). Brain Lipids and Lipid Droplet Dysregulation in Alzheimer's Disease and Neuropsychiatric Disorders. *Complex Psychiatry*, *9*(1-4), 154-171. https://doi.org/10.1159/000535131

Zhong, G., Guo, J., Pang, C., Su, D., Tang, C., Jing, L., Zhang, F., He, P., Yan, Y., Chen, Z., Liu, J., & Jiang, N. (2023). Novel AP2238-clorgiline hybrids as multi-target agents for the treatment of Alzheimer's disease: Design, synthesis, and biological evaluation. *Bioorg Chem*, *130*, 106224. https://doi.org/10.1016/j.bioorg.2022.106224

Zhong, L., Jiang, X., Zhu, Z., Qin, H., Dinkins, M. B., Kong, J.-N., Leanhart, S., Wang, R., Elsherbini, A., Bieberich, E., Zhao, Y., & Wang, G. (2019). Lipid transporter Spns2 promotes microglia pro-inflammatory activation in response to amyloid-beta peptide. *Glia*, *67*(3), 498-511. https://doi.org/10.1002/glia.23558

Zhou, C., Sun, X., Hu, Y., Song, J., Dong, S., Kong, D., Wang, Y., Hua, X., Han, J., Zhou, Y., Jin, G., Yang, X., Shi, H., Zhang, Z., & Hua, F. (2019). Genomic deletion of TLR2 induces aggravated white matter

damage and deteriorated neurobehavioral functions in mouse models of Alzheimer's disease. *Aging (Albany NY)*, *11*(17), 7257-7273. https://doi.org/10.18632/aging.102260

Ziegler, A. B., & Tavosanis, G. (2019). Glycerophospholipids - Emerging players in neuronal dendrite branching and outgrowth. *Dev Biol*, *451*(1), 25-34. https://doi.org/10.1016/j.ydbio.2018.12.009

Zschoche, A., Fürst, W., Schwarzmann, G., & Sanhoff, K. (1994). Hydrolysis of lactosylceramide by human galactosylceramidase and GM1-β-galactosidase in a detergent-free system and its stimulation by sphingolipid activator proteins, *sap*-B and *sap*-C Activator proteins stimulate lactosylceramide hydrolysis. *Eur J Biochem*, *222*(1), 83-90. https://doi.org/10.1111/j.1432-1033.1994.tb18844.x

Zucchi, R., Chiellini, G., Scanlan, T. S., & Grandy, D. K. (2006). Trace amine-associated receptors and their ligands. *Br J Pharmacol*, *149*(8), 967-978. https://doi.org/10.1038/sj.bjp.0706948

Żukowska, J., Moss, S. J., Subramanian, V., & Acharya, K. R. (2024). Molecular basis of selective amyloid-β degrading enzymes in Alzheimer's disease. *FEBS J*, *291*(14), 2999-3029. https://doi.org/10.1111/febs.16939

Zwilling, D., Huang, S.-Y., Sathyasaikumar, K. V., Notarangelo, F. M., Guidetti, P., Wu, H.-Q., Lee, J., Truong, J., Andrews-Zwilling, Y., Hsieh, E. W., Louie, J. Y., Wu, T., Scearce-Levie, K., Patrick, C., Adame, A., Giorgini, F., Moussaoui, S., Laue, G., Rassoulpour, A., Flik, G., Huang, Y., Muchowski, J. M., Masliah, E., Schwarcz, R., & Muchowski, P. J. (2011). Kynurenine 3-Monooxygenase Inhibition in Blood Ameliorates Neurodegeneration. *Cell*, *145*(6), 863-874. https://doi.org/10.1016/j.cell.2011.05.020

Citation of patent

Perez Castillo, A., Morales-Garcia, J.A., Riba, J. (2018). Combination product for the treatment of neurological and/or psychiatric disorders. Patent No. US11723894B2. New York, NY (US), Terran Biosciences Inc.

Acknowledgement

I would like to first express my sincere gratitude to Prof. Dr. Anja Bräuer for giving me the indispensable opportunity to conduct and complete my doctoral work at the University of Oldenburg. I am grateful for your mentorship, endless forbearance and the enriching environment you implemented for my academic and professional growth. Your encouragement, good research environment and professional guidance gave me improved confidence, especially during COVID-19 times and after the conflict management with the Spanish research unit. I also extend my sincere gratitude to PD Dr. Peter Sörös. I am genuinely thankful that you jumped on the train at the final phase of my dissertation without hesitation. Your warm-hearted and solid background left a deep impression on me. Thanks for your constructive and efficient feedback on the MRI data. Your help further enables me to reach my dissertation goal.

Second, I would like to thank all the research staff of the Anatomy research group. Your warm-hearted welcome, tremendous support and constructive advice have made my time in and outside the lab both enjoyable and impeccable. A special thanks goes to Dr. Nicola Brandt for her professional guidance in statistics, endless support, discussions and patience. Your expertise and supervision have been a game changer during my research journey. Further, I would like to extend my appreciation to Dr. Isabel Groß, Anne Gläser, and Jennifer Sevecke-rave for their willingness to share their knowledge and for providing seamless support in the lab. Your collaborative spirit and enjoyable moments together have enormously enriched the work environment. I would also like to thank Ciberned for their financial support. I would also like to express my gratitude to all the members of BBDiag for giving me the great opportunity to join this wonderful European project. Your contribution has not gone unnoticed, and your inspirational, creative and professional expertise in and outside the field of Alzheimer's and diagnostics has significantly contributed to enriching my career goals. Being part of this community has shaped my friends for life.

Next, I want to express my devout appreciation to all my friends. Your persistent encouragement, sports activities and delightful moments have crafted resplendent memories in my life. I especially appreciate the opportunity to express my gratitude to Dr. Yaoyu Chen and Sang Ngoc Ngo for our shared enjoyment, lifelong friendship and cherished memories. To Dr. Yaoya Chen, with whom I have shared work and life experiences over the past few years, I am delighted to witness your opportunity to proceed with your professional and personal life in China with your girlfriend. To Sang Ngoc Ngo, I

want to express my thanks for all the incredible adventures we have had and those still awaiting us. I would like to extend a special appreciation to my badminton fiends, Yaoya, Sang, Kumarah, Daryl and Jing. Our joyful and pleasant badminton games, game nights and delicious food evenings with stunning moments to cherish. In addition, I would like to express my thanks to Dr. Hamad Koochakikelardeh for the pleasant food evenings and spontaneous weekend getaways. Furthermore, I would like to thank Dr. Jessica Janson for her support and the memorable moments during Christmas and birthdays. I wish all of you the best in pursuing your future endeavours.

Further, I would like to express my deepest gratitude to my family. Without your undeviating support, I would never be able to persist in my career goals where I stand today. The physical distance has shaped and marked me. However, your persistent support has been a continuous presence in my life journey. Despite this, I deeply regret not being able to attend both sad and happy moments, especially when my little nephew saw the light of his life for the first time. Your endless patience and understanding have been a provenance of driving spirit for me.

Lastly, I would like to sincerely express my beloved gratitude to my girlfriend, Srijita Chanda. Our paths crossed during the COVID-19 pandemic, and we could not believe that fate would bring us together. I am grateful to witness your happiness in pursuing a career in Europe, which will bring us even closer and more genuinely thrilling experiences together. Your tremendous patience and persistent support have played an enormous role in my personal growth and our future goals. Therefore, I sincerely desire that we can remain life partners in our future.

Curriculum vitae

Michiel Van Bulck

Tel: (+32) 494786437

Email: michiel.van.bulck@uni-oldenburg.de / mivbulck@outlook.com

Address: Volksstraat 2A 0302, 2830 Willebroek, Belgium

Heideweg 20, 26160 Bad Zwischenahn, Germany

Research experience

2024 – present **Career transition and professional development**

2021 – 2024 **Experimental Ophthalmology Laboratory**

Research associate, Oldenburg, Germany

Research topic: Development, characterization and application of modified substrates based on hair keratin and collagen for reconstruction of the corneal and conjunctival ocular surface.

2019 – 2020 **Research Group Anatomy, School for Medicine and Health Science, Carl von Ossietzky University Oldenburg**

Research intern, Oldenburg, Germany

Research topic: "Synaptic stability and lipid homeostasis after amyloid-beta stimulation in various brain cells"[1]

2017 – 2020 **The Network Center for Biomedical Research in Neurodegenerative Diseases (CIBERNED)**

Marie Skłodowska-Curie early stage researcher, Madrid, Spain

Research topic: "Preclinical validation of blood biomarkers for early diagnostic tool in Alzheimer disease"[3]

2019 **School of Computing, Electronics & Mathematics, Faculty of Science and Engineering, University of Plymouth**

Research intern, Plymouth, Devon, PL4 8AA, United Kingdom

Research topic: "Developing Biosensors for Alzheimer's disease biomarker detection in blood plasma samples"[2]

2015 – 2016 **Experimental Dementia Research Unit, Biomedical Centre (BMC), Lund University**

Research intern, Lund, Sweden

Research dissertation: "Effect of beta-amyloid on synapse modulation in Alzheimer's disease"

2015	**Esperite N.V. (Cryo-Save Labs, The Cell Factory, R&D unit)** *Research intern, Niel, Belgium* Research dissertation: "Developing a clinical grade (GMP) 3D *in vitro* potency test for culturing mesenchymal stem cells"
2015	**Laboratory for industrial medicine, toxicology and forensic analysis, Sonic Healthcare (AML)** *Research intern, Antwerp, Belgium* Research dissertation: "Urinary Benzodiazepines and metabolites using liquid chromatography tandem mass spectrometry"

Education

2021 – 2025	**PhD student at the faculty of medicine and health science at the Carl von Ossietzky Universität Oldenburg** Research Group Anatomy, School for Medicine and Health Science, Carl von Ossietzky University Oldenburg, Germany
2017 – 2021	**PhD Student in Molecular Biosciences (transferred to Carl von Ossietzky Universität Oldenburg)** Department of Experimental Models of Human Disease, CIBERNED, Institute for Biomedical Research A. Sols (CSIC-UAM), Madrid, Spain
2013 – 2016	**Master of Science in Biomedical Sciences** Vrije Universiteit Brussel (VUB), Faculty Medicine & Pharmacy, Belgium
2010 – 2014	**Bachelor of Science in Biomedical Sciences** Vrije Universiteit Brussel (VUB), Faculty Medicine & Pharmacy, Belgium

Publications

1. ***Van Bulck, M.***; Brandt, N.; Claus, R.A.; Gräler, M.; Bräuer, A.U. Aβ-Induced Alterations in Membrane Lipids Occur before Synaptic Loss Appears. Int. J. Mol. Sci. 2022, 23, 2300. https://doi.org/10.3390/ijms23042300
2. Sethi, J., ***Van Bulck, M.***, Suhail, A. et al. A label-free biosensor based on graphene and reduced graphene oxide dual-layer for electrochemical determination of beta-amyloid biomarkers. Microchim Acta 187, 288 (2020). https://doi.org/10.1007/s00604-020-04267-x

3. ***Van Bulck, M.***; Sierra-Magro, A.; Alarcon-Gil, J.; Perez-Castillo, A.; Morales-Garcia, J.A. Novel Approaches for the Treatment of Alzheimer's and Parkinson's Disease. *Int. J. Mol. Sci.* 2019, *20*, 719. https://doi.org/10.3390/ijms20030719

Fellowship

2017 – 2020 **Marie Skłodowska-Curie fellowship**

Project: Blood Biomarker-based Diagnostic Tools for Early-stage Alzheimer's Disease (BBDiag)

http://bbdiag-itn-etn.eu/

Skill and expertise

- Neurodegenerative diseases (e.g. Alzheimer's disease)
- Extracellular vesicles
- Biomaterials and Bio-scaffold
  - Hydrogels
  - Keratin films
  - Plastic compressed collagen gels
- Bio-fluids (urine and blood)
- Biomarkers discovery and developing biosensors
- Cell cultures
  - Primary cell linages
  - Stem cells
  - Neurospheres
  - Tumor cell lines
- High-throughput methods: HPTLC, HPLC and tandem mass spectrometry
- Research GxP compliance: GMP, GLP, GCP
- Western blot, immunohistochemistry, immunohistochemistry
- Imaging analysis:
  - Confocal imaging
  - Magnetic resonance imaging
  - Magnetic resonance spectroscopy
- Animal experiments: Non-invasive sample collection and treatment methods

Extra career experiences (conferences)

2020 **30th Alzheimer Europe Conference: Dementia in a changing world**

Virtual Event

Co-organiser of live session of BBDiag symposium on this conference

ISTAART Professional Interest Area Scientific Sessions and Business Meetings

Virtual Event

The Alzheimer's Association International Conference® (2020)

Virtual Event

Poster presentation: "Influence of amyloid-beta isoforms in different *in vitro* models" (Van Bulck M., Gräler M., Pérez Castillo Ana M., Bräuer A.)

2018 **11th FENS Forum of Neuroscience**

Berlin, Germany

China-Europe Alzheimer's Disease Symposium: Biomarkers and early diagnosis

Beijing, China

Presentation: "New insight in fluid-based biomarkers of preclinical Alzheimer's disease models"

Adult Neurogenesis (Abcam)

Dresden, Germany

VI CiiiEN - International Congress on Research and Innovation in Neurodegenerative Diseases

Santiago de Compostela, Spain

Poster presentation: "Neurogenesis analysis in transgenic model of Alzheimer'sdisease." (Van Bulck M, Sierra Magro A, Morales García Jose A, Alonso Gil S, Sanz San-Cristóbal M, Alarcón-Gil J, Pérez Castillo Ana M.)

2016 **20th Mosa Conference- International Student Research Conference**

Maastricht, Netherlands

Poster presentation: "Effect of beta-amyloid on synapse modulation in Alzheimer's disease" (Van Bulck M., Martinsson I., Willén K., Oxana Klementieva O., Isrealsson B., Svanbergsson A., Gouras GK.)

Declaration of this dissertation

I hereby declare that I have written this work independently and have not utilised any sources or resources other than those explicitly specified. I confirm that this work, in its entirety and in part, has not been submitted to any other university for assessment in a doctoral procedure. Furthermore, I have adhered to the principles of good scientific practice as outlined by the Carl Von Ossietzky University of Oldenburg. Additionally, I confirm that no commercial recruitment or consulting services (including doctoral coaching) have been utilised.

Oldenburg, 24/06/2025 (Michiel Van Bulck)